TECHNICAL REPORT EL-84-9

(2)

AN ANALYSIS OF SHORT- TO MEDIUM-RANGE SEISMIC ATTENUATION TESTS USING A MULTILAYERED VISCOELASTIC SEISMIC PROPAGATION MODEL

by

Ben L. Carnes, Jerry R. Lundien

Environmental Laboratory

DEPARTMENT OF THE ARMY
Waterways Experiment Station, Corps of Engineers
PO Box 631
Vicksburg, Mississippi 39180-0631

November 1984
Final Report

DEPARTMENT OF THE AIR FORCE
Headquarters, Ballistic Missile Office
Norton Air Force Base, California 92409

US Army Ballistic Missile Defense Systems Command
Huntsville, Alabama 35807

DEPARTMENT OF THE ARMY
US Army Corps of Engineers
Washington, DC 20314-1000

MIPR No. FY7653-83-00010, MIPR No. W31RPD-33-V062
and DA Project No. 4A762730AT42

Destroy this report when no longer needed. Do not return it to the originator.

The findings in this report are not to be construed as an official Department of the Army position unless so designated by other authorized documents.

The contents of this report are not to be used for advertising, publication, or promotional purposes. Citation of trade names does not constitute an official endorsement or approval of the use of such commercial products.

Unclassified

SECURITY CLASSIFICATION OF THIS PAGE (When Data Entered)

REPORT DOCUMENTATION PAGE

READ INSTRUCTIONS BEFORE COMPLETING FORM

1. REPORT NUMBER: Technical Report EL-84-9	2. GOVT ACCESSION NO. AD-A149 701
3. RECIPIENT'S CATALOG NUMBER	
4. TITLE (and Subtitle): AN ANALYSIS OF SHORT- TO MEDIUM-RANGE SEISMIC ATTENUATION TESTS USING A MULTILAYERED VISCOELASTIC SEISMIC PROPAGATION MODEL	5. TYPE OF REPORT & PERIOD COVERED: Final report
	6. PERFORMING ORG. REPORT NUMBER
7. AUTHOR(s): Ben L. Carnes, Jerry R. Lundien	8. CONTRACT OR GRANT NUMBER(s)
9. PERFORMING ORGANIZATION NAME AND ADDRESS: US Army Engineer Waterways Experiment Station, Environmental Laboratory, PO Box 631, Vicksburg, Mississippi 39180-0631	10. PROGRAM ELEMENT, PROJECT, TASK AREA & WORK UNIT NUMBERS: MIPR No. FY7653-83-00010; MIPR No. W31RPD-33-V062; DA Project NO. 4A762730AT42
11. CONTROLLING OFFICE NAME AND ADDRESS: Department of the Air Force, Headquarters, Ballistic Missile Office, Norton Air Force Base, California 92409, US Army Ballistic Missile Defense Systems Command, Huntsville, Alabama 35807, and DEPARTMENT OF THE ARMY, US Army Corps of Engineers, Washington, DC 20314-1000	12. REPORT DATE: November 1984 13. NUMBER OF PAGES: 216 15. SECURITY CLASS. (of this report): Unclassified
14. MONITORING AGENCY NAME & ADDRESS(if different from Controlling Office)	15a. DECLASSIFICATION/DOWNGRADING SCHEDULE

16. DISTRIBUTION STATEMENT (of this Report)

Approved for public release; distribution unlimited.

17. DISTRIBUTION STATEMENT (of the abstract entered in Block 20, if different from Report)

18. SUPPLEMENTARY NOTES

Available from National Technical Information Service, 5285 Port Royal Road, Springfield, Virginia 22161.

19. KEY WORDS (Continue on reverse side if necessary and identify by block number)

Seismic waves--computer programs (LC)
Seismic coefficient method (WES)
Rayleigh waves (LC)
WES seismic propagation model

20. ABSTRACT (Continue on reverse side if necessary and identify by block number)

This study was conducted to provide a database from which to draw conclusive results on the efficiencies of seismic wave propagation in natural terrain and the resolution and fidelity of multiple frequency signals, and to supplement data for validation of theoretical models of seismic wave propagation. An extensive test program was conducted at White Sands Missile Range, New Mexico, using an electrohydraulic vibrator, an impulse loader, and a vehicle as sources

(Continued)

DD FORM 1 JAN 73 1473 EDITION OF 1 NOV 65 IS OBSOLETE

Unclassified

SECURITY CLASSIFICATION OF THIS PAGE (When Data Entered)

20. ABSTRACT (Continued).

of seismic waves over a 5-m to 1-km range and using explosive seismic sources over a 1- to 10-km range.

The results are presented for discrete frequency vibration tests (1-120 Hz), tone burst tests (1-120 Hz), random noise vibration tests, and background noise tests for vehicle, impulse, and explosive tests. Analysis of data has been performed to correlate frequency, amplitude, range, and other signal characteristics with model predictions and to modify model coefficients to produce better predictions for future tests.

This study relates the dispersion and attenuation of seismic waves, frequency resolution, and wind and background noise to the refinement of the WES seismic propagation model.

SUMMARY

This study was conducted to provide a database from which to draw conclusive results on the efficiencies of seismic wave propagation in natural terrain and the resolution and fidelity of multiple frequency signals, and to supplement data for validation of theoretical models of seismic wave propagation. An extensive test program was conducted at White Sands Missile Range, New Mexico, using an electrohydraulic vibrator, an impulse loader, and a vehicle as sources of seismic waves over a 5-m to 1-km range and using explosive seismic sources over a 1- to 10-km range.

The results are presented for discrete frequency vibration tests (1-120 Hz), tone burst tests (1-120 Hz), random noise vibration tests, and background noise tests as well for vehicle, impulse, and explosive tests. Analysis of data has been performed to correlate frequency, amplitude, range, and other signal characteristics with model predictions and to modify model coefficients to produce better predictions for future tests.

The main conclusions of this study are:

a. Seismic signals are dispersed and selectively attenuated such that very low (2- to 3-Hz) signals predominate in the 4- to 10-km range, while at nearer ranges (less than 4 km) signal frequencies to above 100 Hz are measurable.

b. The frequency resolution of seismic signals measured out to 10 km is below 0.5 Hz, but is dependent on the length of the record and the stability of the source.

c. Wind noise creates problems in making accurate seismic measurements over long ranges (up to 10 km) for wind speeds above 8 m/sec.

d. Electrical noise can cause distortions in measured data even when attempts are made to remove this noise with filters.

e. The WES seismic model is shown to be accurate in concept for defining surface wave propagation characteristics and for making predictions of time and frequency domain signal amplitudes.

f. Rayleigh waves at low frequency travel much faster than at high frequency (i.e., dispersion); the 2- to 3-Hz component is controlled primarily by the characteristics of deep, high-velocity layers and the 100- to 200-Hz components are controlled primarily by the characteristics of the slower velocity near surface layers.

g. Signals measured in a rock outcrop indicate that the layers of soil above bedrock attenuate the seismic wave and do not cause a focusing effect.

PREFACE

The study reported herein was conducted by the US Army Engineer Waterways Experiment Station (WES) during Fiscal Year 1983. The study was funded by the Ballistic Missile Office, Norton Air Force Base, California, under MIPR No. FY7653-83-00010; the Ballistic Missile Defense System Command, Huntsville, Alabama, under MIPR No. W31RPD-33-V062; and the US Army Corps of Engineers under DA Project No. 4A762730AT42, "Terrain Operations Simulations," Task B/E3, "Analytical Techniques for the Design and Application of Sensors."

The study was conducted under the general supervision of Dr. John Harrison, Chief of the Environmental Laboratory, and Mr. Bob O. Benn, Chief of the Environmental Systems Division, and under the direct supervision of Mr. Jerry R. Lundien, Chief of the Battlefield Environment Group (BEG). This study was conducted by Dr. Ben L. Carnes of the BEG. Dr. Carnes and Mr. Lundien prepared this report.

Acknowledgment is made to Mr. Erwin Baylot of the BEG for his assistance in predictions and analysis with the WES Seismic Model. Mr. Billy T. Helmuth of the BEG assisted in conducting the fieldwork and in preparing the figures and plates. In addition, Messrs. M. B. Savage and Wallace Guy of the Instrumentation Services Division (ISD) assisted in the field data measurements. Mr. George Smith of the ISD performed the signal processing and analysis. Messrs. S. S. Cooper, T. B. Kean, and 2LT S. G. Sanders of the Geotechnical Laboratory were responsible for the Seismic Refraction Study and assisted in the field data measurements.

Commander and Director of the WES during the conduct of the study and preparation of this report was COL Tilford C. Creel, CE. Technical Director was Mr. F. R. Brown.

This report should be cited as follows:

Carnes, B. L., and Lundien, J. R. 1984. "An Analysis of Short- to Medium-Range Seismic Attenuation Tests Using a Multilayered Viscoelastic Seismic Propagation Model," Technical Report EL-84-9, US Army Engineer Waterways Experiment Station, Vicksburg, Miss.

CONTENTS

LIST OF TABLES

LIST OF PLATES

AN ANALYSIS OF SHORT- TO MEDIUM-RANGE SEISMIC ATTENUATION TESTS USING A MULTILAYERED VISCOELASTIC SEISMIC PROPAGATION MODEL

PART I: INTRODUCTION

Background

1. The components of Rayleigh waves are commonly used as the energy conveyance which activates seismic sensors. The amount of energy generated by a target of military interest such as a vehicle, military equipment, or a specific military operation or activity is site dependent, and the effect of terrain on Rayleigh wave propagation is known to be substantial. However, little is known about the relative quantitative effects of specific terrain parameters on this phenomenon. In addition, little is known about the propagation/attenuation of Rayleigh waves over long ranges, even if the terrain is relatively homogeneous (Williams 1981). In an effort to characterize Rayleigh wave propagation and attenuation under such conditions, the US Army Engineer Waterways Experiment Station (WES) was requested to participate in an extensive seismic test program. This program coupled model calculations with field testing to enable both mathematical and empirical analyses of wave propagation and attenuation over large areas.

2. A mathematical model developed at WES predicts microseismic signals in various terrain materials (Lundien and Nikodem 1973). The model has been adapted to run on an IBM 4331 computer recently installed in the Environmental Systems Division, Environmental Laboratory, WES, and the model was used for modeling and predicting the seismic test site. Predictions are made rapidly and efficiently with the computer model and, as field data are processed, the model is tuned to refine its calculations. When the model is refined by comparison with measured data, the model can be used to study the effects of other terrain parameters on the individual facets of Rayleigh wave generation and propagation phenomena and the most sensitive parameters can be identified. This flexible tool can provide an effective means of predicting seismic signals in areas where few data have been measured.

Objectives

3. The objectives of this study were to:

   a. Determine the relative efficiencies with which seismic signals propagate from impulsive and continuous wave sources in natural terrain.

   b. Determine the resolution and fidelity of multiple frequency signals propagating in natural terrain.

   c. Supplement an existing database that in turn will be used to validate theoretical models of seismic wave propagation in natural terrain.

   d. Provide a database in a form that can be related to various military programs concerned with the correlation of seismic information for detection, classification, and deception purposes.

Scope

4. In this study an extensive amount of seismic data were collected, processed, and compared to model calculations. Analysis is limited to calculation of transfer functions and spectral densities and comparison of the same parameters used in the model. Many other calculations and algorithms were not applied because of limitations in the scope of work, but can be done in the future when other applications warrant. In no way is the analysis of the data set presented in this report complete. Many of the wide-ranging analytical techniques appropriate for use with these data are still under development.

PART II: DESCRIPTION OF EQUIPMENT

Mechanical-Source Specifications

Vibrator

5. The WES electrohydraulic vibrator is a portable self-contained, trailer-mounted unit (Figure 1). It has a 680-kg inertial mass that is excited by an electrohydraulic ram. The system is capable of ±0.91 metric ton peak force output in the frequency range from 15 to 150 Hz. A variety of forcing functions may be used, including steady-state sine, swept sine, tone burst, and random excitation.

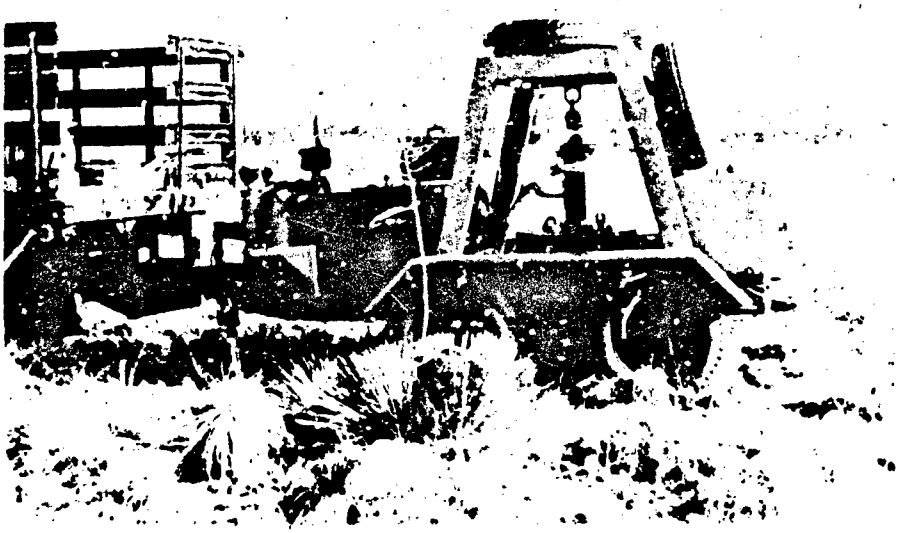

Figure 1. WES electrohydraulic vibrator

6. The vibrator hydraulic power supply is driven by a 30-hp, four-cylinder gasoline engine, and the hydraulic pump can provide up to 1.58 ℓ/sec at a service pressure of 2,109 kPa. Intercoolers are included in the hydraulic system so that the vibrator can be operated continuously in ambient temperatures between -4° and +52° C.

7. In order to provide a clean wave form and to balance loads on the electrohydraulic ram, the inertial mass is supported by two 5.9-cm-diam air bags. Approximately 4.2-Pa air bag pressure is required to suspend the inertial mass. The air bag system is quite compliant within the ±0.8-cm stroke of the ram, so there is minimal variation in peak force output during shaking.

The electrohydraulic ram is equipped with a linear variable differential transformer for static positioning of the inertial mass and for positive feedback control during shaking. The electronic vibrator control unit compares the command signal to the vibrator with the feedback position signal and automatically regulates the ram servovalve to produce the desired wave form. With this system it is possible to produce virtually constant force output from 15 to 150 Hz; however, the soil on which it is emplaced affects the actual field output, as can be seen in Figure 2. The vibrator base plate is 11.8 cm in diameter, so that the maximum peak dynamic pressure applied to the soil at 0.91 metric ton-force output is on the order of 2.0 Pa.*

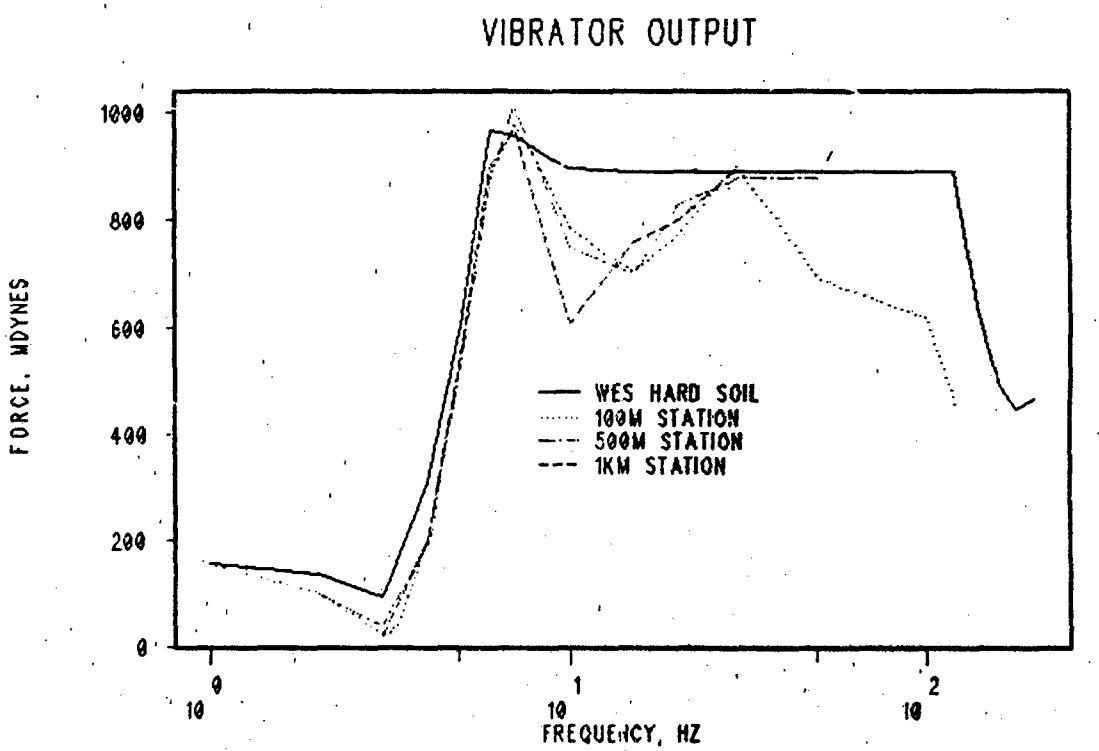

Figure 2. WES electrohydraulic vibrator output for calibration tests at WES and at each test site

Impactor

8. The impactor, or impulse loader, is a Dyna Source portable seismic energy source made by EG&G Geometrics. The system uses ambient air pressure

* Internal Memorandum, 1983, S. S. Cooper, Geotechnical Laboratory, US Army Engineer Waterways Experiment Station, Vicksburg, Miss.

to increase the downward velocity of a falling mass (39-kg solid steel piston). The system uses a small gasoline engine to power the vacuum pump/air compressor which both pressurizes and evacuates air from the cylinder. In operating the impactor, the piston is first forced to the top of the cylinder where it is automatically latched into position. The air below the piston is then evacuated. When ready, the operator pushes a firing knob which allows the piston to fall 1.8 m (accelerated by gravity and air pressure). The piston strikes an anvil at the base of the cylinder, and energy is transferred into the ground. The vacuum in the cylinder prevents the piston from rebounding and produces a single-cycle impulsive load. The impactor is shown in Figure 3.

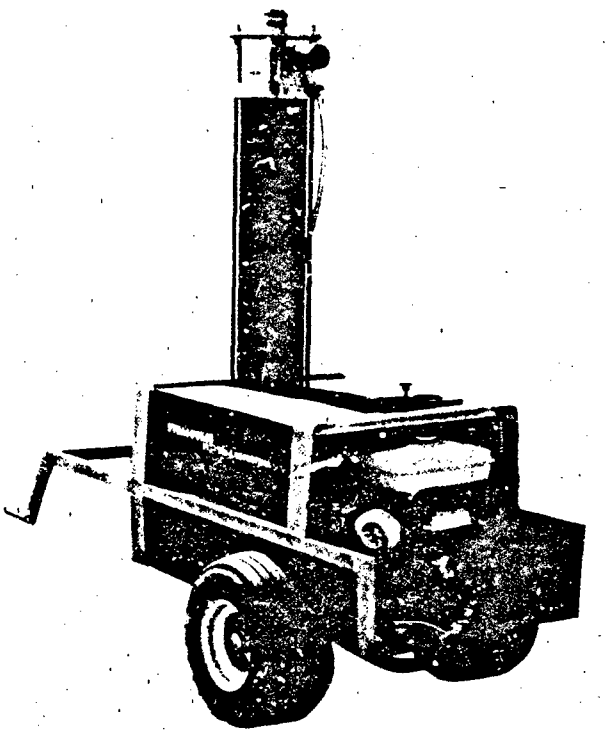

Figure 3. Photograph of impactor

Vehicle

9. The M-35 truck used in these tests was a standard M-35 base with a shop van shell mounted on it (Figure 4). The M-35 has tandem axles, each with dual wheels (total of 10 wheels on the ground, counting front) and weighs 7 metric tons in the van configuration (Field Manual 55-15)(Headquarters, Department of the Army 1968). This vehicle can be seen in Figure 4.

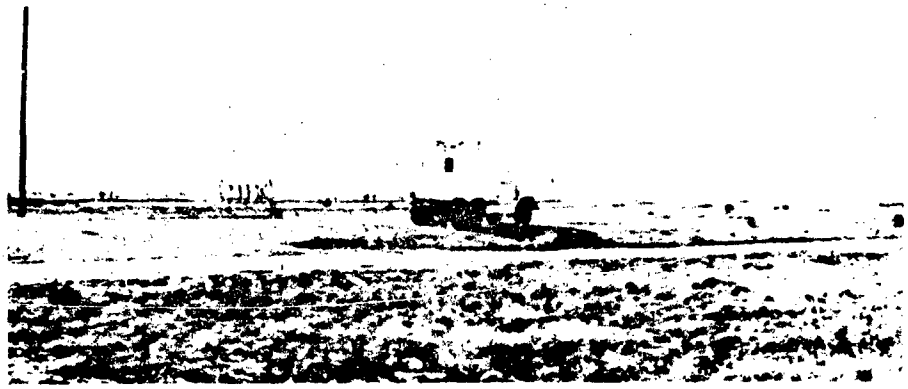

Figure 4. M-35 truck with van body

Explosive-Source Specifications

10. The explosive used in the seismic attenuation tests (SAT) at White Sands Missile Range, New Mexico, was ammonium nitrate/fuel oil (ANFO), which is a combination of prilled ammonium nitrate with about 6 percent by weight of fuel oil (diesel fuel) as a sensitizer. The ANFO explosion makes a good seismic source with characteristics similar to those of TNT. It is safe and easy to use because of its relative insensitivity to temperature and shock. Explosive charges are described further in the subsection "Explosive-source tests," Part III.

Sensor Specifications

11. The seismic refraction geophones used in the test program were Mark Products Model L-10, a standard vertical geophone used for seismic refraction. The Model L-10 has a natural frequency of 8.0 Hz.

12. The geophones used in the seismic tests are Geospace HS-10-1 calibrated vertical geophones with a natural frequency of 1 Hz, a response of 1-200 Hz, damped at 70 percent of critical, and a sensitivity of 2.95 V/cm/sec. The triaxial (three mutually perpendicular velocities) geophone was a Mark Products Model L-4C-3D with a natural frequency of 1 Hz, damped 70 percent of critical, a response of 1-200 Hz and greater, and a sensitivity of 2.35 V/cm/sec.

13. The microphone used in the tests was a Bruel and Kjaer (B&K) Model 4921 outdoor microphone unit with a frequency range of 10-20,000 Hz and

a dynamic range of 140 db. This unit has a built-in electrostatic calibrator giving 90-db sound pressure level at 1000 Hz.

Instrumentation Specifications

Systems

14. The array instrumentation system operates from a commercial 120-V AC power source that could not be provided by a portable generator because of the noise it would produce in the array area. The portable source instrumentation system was moved to each new source location and was positioned with the same orientation to the source at each location. The source instrumentation system, which was housed in the van seen in Figure 5a, is shown in Figure 5b. This system was generator powered for convenience. A schematic of the basic analog instrumentation system is shown in Figure 6. Both systems described above were similar to the schematic, except the array system included a microphone added to the input as well as a low-pass filter between the amplifier and the recorder. The lateral geophone system was battery powered and had only three channels. It was a completely self-contained system with amplifier and analog tape recorder. Its geophone frequency response is 1-200 Hz; its natural frequency was 1 Hz with a sensitivity of 2.35 V/cm/sec.

Recorders

15. Signals from the array geophone system were recorded on a Sangamo Model 3500 14-track analog tape recorder, recording at 3-3/4 in. (9.5 cm)/sec, FM mode, which gives a frequency response of DC to 1250 Hz. This recorder requires 120 V AC power. The source geophone recorder was a Racal Model STORE 7DS seven-channel analog tape recorder operated in FM mode at 3-3/4 in./sec (DC to 1250-Hz frequency response). This recorder was powered by a portable generator operating on 115 V AC.

Amplifiers

16. The array system employed Ithaca Model 456 amplifiers with a bandwidth of 1-100,000 Hz and 100-db gain range in 1-db steps, operated from a 120-V AC power source. The source system amplifiers were WES-made units, with a bandwidth of DC to 5000 Hz and a continuous gain range from 0 to 60 db, and require 12-V DC power.

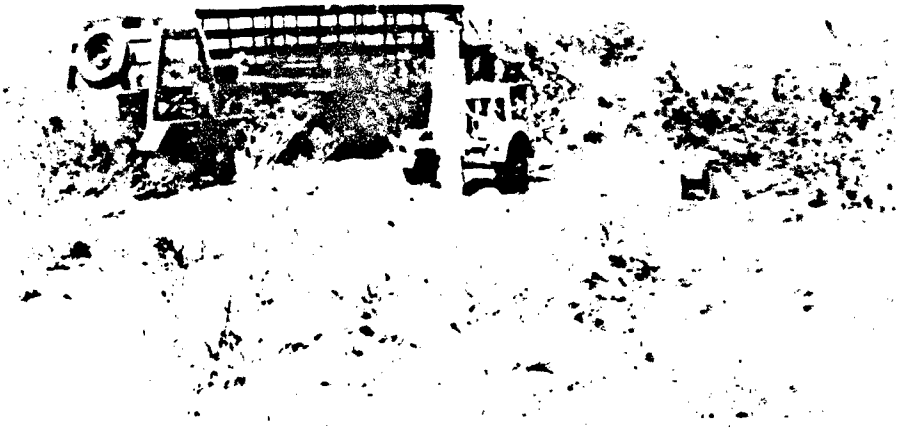

a. View of 1-km site showing vibrator, impactor, and instrumentation van

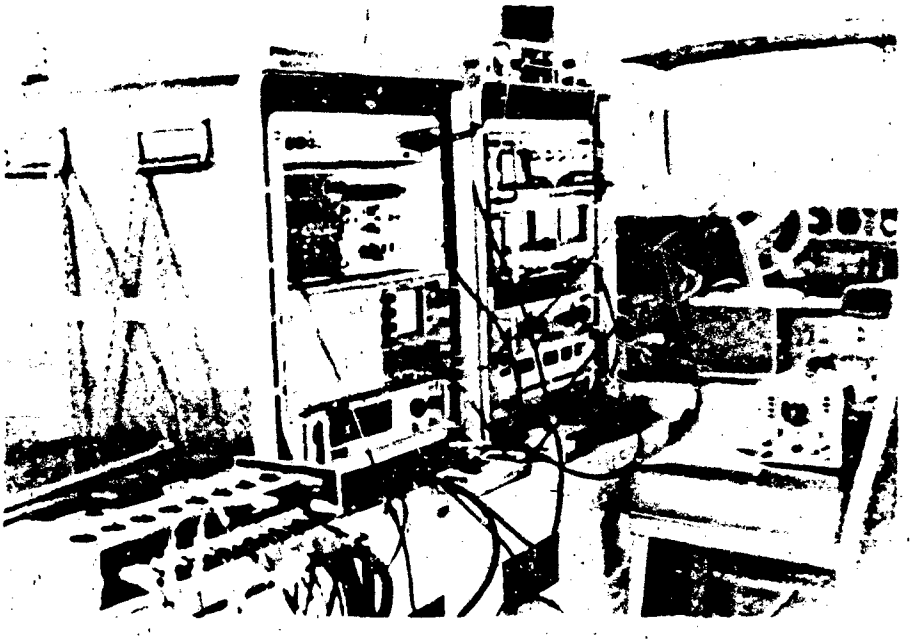

b. View of the source instrumentation system

Figure 5. Photographs of seismic sources and instrumentation

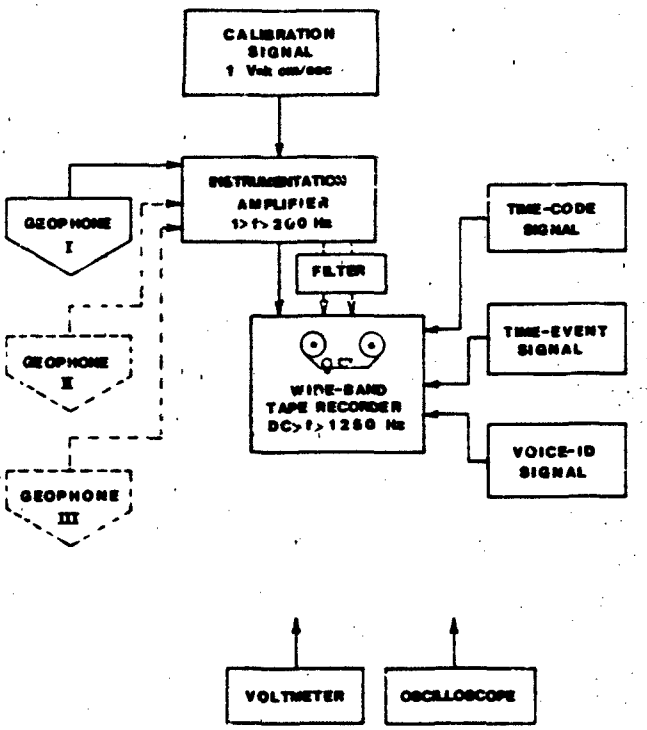

Figure 6. Schematic of typical analog recording system

Filters

17. The array system used Krohn-Hite Model 3323 filters which have the options for low-pass or band-pass operation. These filters have a frequency range of 0.01 to 100,000 Hz and an attenuation rate of 24 db per octave outside the pass-band. The source geophones were not filtered since the signals were quite strong at the source compared to background noise. The filters were, as a rule of thumb, set (low-pass) at a frequency 10 Hz above the highest frequency of interest. This kept the filters from affecting data of interest, since a point of 5 Hz below the filter setting will lose approximately 2 db of gain. (Actual filter values used for each test are listed in Table 3.)

Calibration

18. Substitution sine-wave calibrations were used as an alternate input to the amplifiers during system calibration. The sine-wave calibration signal was monitored with a precision voltmeter and frequency counter. The sine-wave calibration voltage was compared to the known geophone sensitivities to calculate the recording system sensitivity in velocity units. A time standard,

IRIG B, was recorded on both tape recorders for time of day and common timing on both tape recorders.

19. Calibration of all geophone channels was accomplished with a substitution sine-wave signal input to the amplifier. The sine wave was measured with an accurate voltmeter and proportioned to a velocity value by knowing the sensitivity of each geophone. The amplifier output was connected to the Krohn-Hite filters, which were connected to the tape recorder. A 30-Hz sine wave was selected as the calibration frequency.

20. During calibration, the smallest setting was selected on each amplifier, approximately 15 db, with the remote gain control. An input signal of 125 mV root mean square (RMS) amplitude was applied to each amplifier simultaneously, through the Krohn-Hite filter, set at 140-Hz low pass and on to the tape recorder. The 125-mV RMS signal amplified with a net gain of +12 db gives 0.5-V RMS on the tape recorder. One minute of 30-Hz signal was recorded. On several calibrations, a sine-wave sweep from 1 Hz to 200 Hz was also recorded.

21. Each geophone channel was filtered before being recorded by the Krohn-Hite filters. Each unit held two separate filter circuits, and two cascaded low-pass filters were used on each geophone channel. This gave an attenuation above the corner frequency of 48 db per octave. The corner frequency was adjusted for each test, with a rule of thumb that the corner frequency be above the vibrator driver frequency by 10 Hz.

22. The amplifier gain was adjusted for each test such that the input to the tape recorder during a test would be less than 1 V RMS. All geophone amplifiers were set to provide the 1-V RMS maximum input for each test with the use of the remote gain control.

23. The B&K microphone channel was calibrated using a built-in signal and electrostatic calibrator mounted directly on the microphone. The calibration frequency was 1000 Hz, and the signal was 90-db sound pressure level. No filtering was used on the B&K microphone signal.

Spectrum analyzer

24. The spectrum analyzer was used with the array instrumentation system to make field determinations as to what and how background noise data could be filtered from actual test signals. It was also used to determine during testing if various input frequencies were present in the signals, and what frequencies were dominant in impulse and explosive tests. The spectrum

analyzer used was a Hewlett-Packard 3582, which has a frequency response of DC to 20,000 Hz and a dynamic range of 70 db.

PART III: DESCRIPTION OF TEST PROGRAM

25. Upon identification of objectives and scope by the sponsor, an extensive test plan was devised which included proper and sufficient tests to accomplish the objectives; the test plan is presented in its entirety in Appendix A. The first activity was to select a site and conduct a preliminary site characterization. The basic site requirements were: reasonable uniformity in subsurface conditions over 10 km, flat to rolling topography, depth to water table at least 42 m, and seismic profile beginning at 427 m/sec down to 6 m, 900-1370 m/sec between 6 m and 42 m, and ±1500 m/sec below 42 m. The site requirements are described further in Appendixes A and B. After consideration of numerous sites within the continental United States, two potential sites were selected, based on available data. One was near the Oscuro gate in the northeast area of the US Army White Sands Missile Range (WSMR), New Mexico. The second was near the Trinity site in the northwest area of WSMR. The Oscuro site was the most desirable because of low background noise. During preliminary site characterization tests, however, a layer of rock with compression wave velocity on the order of 3000 m/sec was found within 10 m of the surface, and the site was deemed unusable for the tests because the shallow rock layer did not meet the requirements. The second site was verified as being usable, with several seismic refraction lines (included in Appendix B) in correlation with previous data taken in the same area.* The site, although seismically compatible with test requirements (see Appendix B), did pose some operational problems with periodic increases in background noise from construction activity in the area for DIRECT COURSE, a major weapons test.

26. The second preliminary activity for this test program was to calibrate and check the seismic sources at the WES. The vibrator and the impactor were both tested at the WES in preliminary tests to determine operating characteristics in the planned modes of use. The vibrator was tested over the expected frequency range; these preliminary data are shown in Figure 2. The

---

* Internal Memorandum, "Operation DICETHROW," 1975, S. S. Cooper, Geotechnical Laboratory, US Army Engineer Waterways Experiment Station, Vicksburg, Miss.

impactor was also tested and showed a clean impulse load. Preliminary results were used in developing plans and procedures for extracting needed data from the field tests.

Test Site

27. The SAT program was conducted near the Trinity site at the WSMR. The test course layout began near WSMR Route 13 and went north, passing just west of Trinity and ending near Beck (see site location map, Figure 7). The test line passed about 1.0 km west of the Trinity center. Calculations from weapons test data reveal that the Trinity event, a 19-kiloton nuclear weapon detonated on a 30-m tower (Rooke, Carnes, and Davis 1974), would produce permanent displacement or damage to the substrate out to a maximum distance of 300 m (Carnes 1974). Thus, the test line was located a sufficient distance to be in undisturbed material.

28. The general surface conditions at the SAT site were relatively flat to rolling, covered by sparse vegetation consisting of creosote brush, desert grass, cactus, and yucca which varied from 10 to 35 percent (average) over the test site. The site soil was a silty sand near the surface that gradually graded coarser with depth. It was difficult to travel cross-country over the site because the sand was loose in some areas and accumulated around the vegetation in others. Photographs of the site are shown in Figure 8. The test site lies in the Jornada del Muerto Basin of the Mexican Highland Section of the Basin and Range Province, which is characterized by a series of fault blocks forming asymmetric ridges or mountains and broad intervening basins. This basin has an overburden of alluvial material containing sand and rock fragments, generally grading coarser with depth.*

Site Documentation

Seismic refraction tests

29. The seismic refraction data from both the preliminary and the site characterization tests were obtained using a portable 24-channel seismograph.

---

* Internal Memorandum, 1983, S. S. Cooper, Geotechnical Laboratory, US Army Engineer Waterways Experiment Station, Vicksburg, Miss.

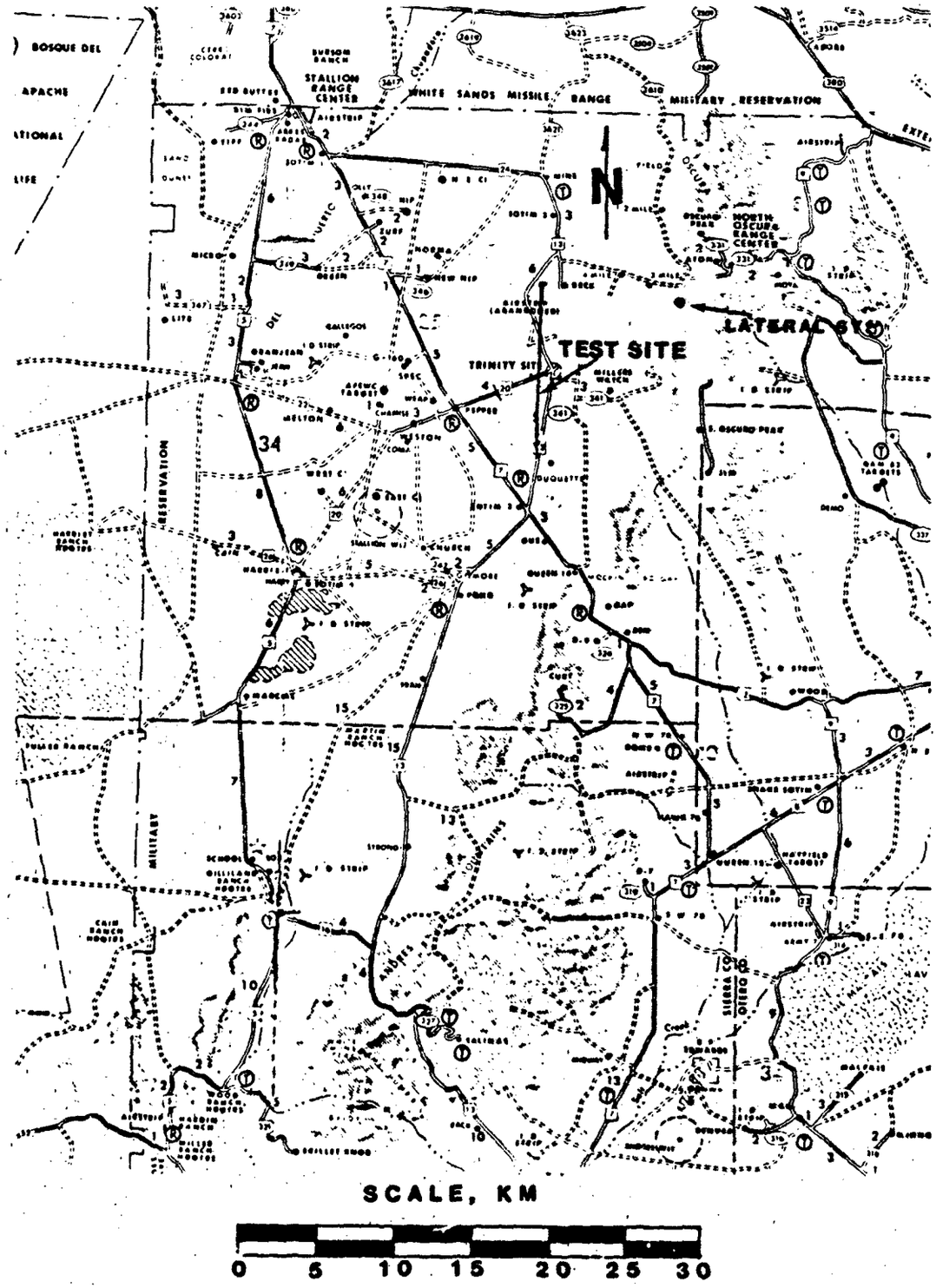

Figure 7. Site location map. The lateral geophone system location is marked.

a. View of array, looking east, showing B&K microphone

b. View of 10-km location looking north

Figure 8. Photographs of site

This seismograph produces a permanent record on oscillograph paper. A total of 23 vertical, velocity-type geophones were used in the conduct of the tests. The geophones were emplaced in a straight line along the surface of the ground at 50-m intervals. The seismic source was a 2-kg explosive charge detonated 50 m from one end geophone and repeated at the opposite end. This resulted in two seismic traverses (forward and reverse), 366 m in length, and delineation of substrate down to a minimum depth of 90 m, in accordance with Engineer Manual (EM) 1110-1-1802 (Headquarters, Department of the Army 1979).

30. Data obtained from the surface refraction seismic tests consist of the time required for a compression wave to travel from a seismic source to points of measurement. The data are plotted as time versus distance from which compression wave velocities and depths to interfaces can be computed by using conventional seismology equations (EM 1110-1-1802). These data and techniques are discussed in detail in Appendix B. Shear wave velocities were not determined for these tests. Since the refraction test lines were too short to determine shear wave velocities from explosions while using vertical geophones, empirical relationships derived from previous test programs were used to estimate the shear wave velocities for input to the theoretical model.

Environmental data

31. Quantitative environmental data describing the surface and substrate conditions included soil wet density, soil moisture content, ground cone index, soil type, soil grain size, distribution, surface topography, vegetation type and density, surface load-response characteristics, and meteorological conditions. The data listed below for the site are summarized in Table 1.

32. Soils. Soil samples representative of the surface were obtained for laboratory analysis by digging to a 30-cm depth. These samples were tested in the WES soil laboratory for moisture content and grain size distribution.

33. Cone index. Cone index is a measure of soil strength measured with a 1.25-sq-cm cone and expressed herein in kilopascals. It is determined by measuring the force needed to move a cone penetrometer vertically into the ground at a constant rate (the maximum reading available on the hand cone penetrometer is 750). Cone index data were taken at the array and at the 0.1-km, 4.0-km, and 10.0-km test locations, near the sources and the vehicle path.

34. Topography. The topography of the site is shown on US Geological Survey topographic map no. N13-7 (Tularosa), Series V502, scale 1:250,000. However, for purposes of this program, the most important topographic data come from an engineering survey along the test line. This was accomplished using a laser-type electronic distance measuring (EDM) system that measures both horizontal and vertical distance between points. In addition to the site profile, profiles of each vertical track were measured upon completion of the tests. It should be noted that these track profiles represent an instantaneous example of the degree of roughness that prevails on a particular vehicle run.

35. Meteorological conditions. A meteorological station was established at the site for the duration of the tests. Measurements of air and ground temperature, wind speed and direction, solar insolation, relative humidity, and precipitation were made continuously and recorded automatically every 30 min. The data were recorded on a cassette and then transferred to a computer for reduction and processing.

Seismic Wave Attenuation Tests

Mechanical-source tests

36. Seismic wave attenuation tests were conducted using several mechanical seismic sources, including a vibrator, an impact source, and an M-35 truck. The tests were conducted in the layout shown in Figure 9. An array of calibrated sensors, including one three-dimensional geophone, five vertical geophones, and one outdoor microphone unit, were emplaced at the beginning point of the test line to comprise the array sensor system. The three sources were employed individually at 0.1 km, 0.5 km, and 1.0 km, but no data were collected at ranges longer than 1 km with these sources since measurable signals were at the level of background noise or less for ranges of 2 km and beyond. Emplaced at each source location were four vertical geophones and one outdoor microphone unit to measure close-in attenuation, signal variation between locations, and background noise. In addition, a load cell was used to measure force applied to the ground by the vibrator, and an accelerometer was used to measure impactor acceleration, from which ground loading was calculated.

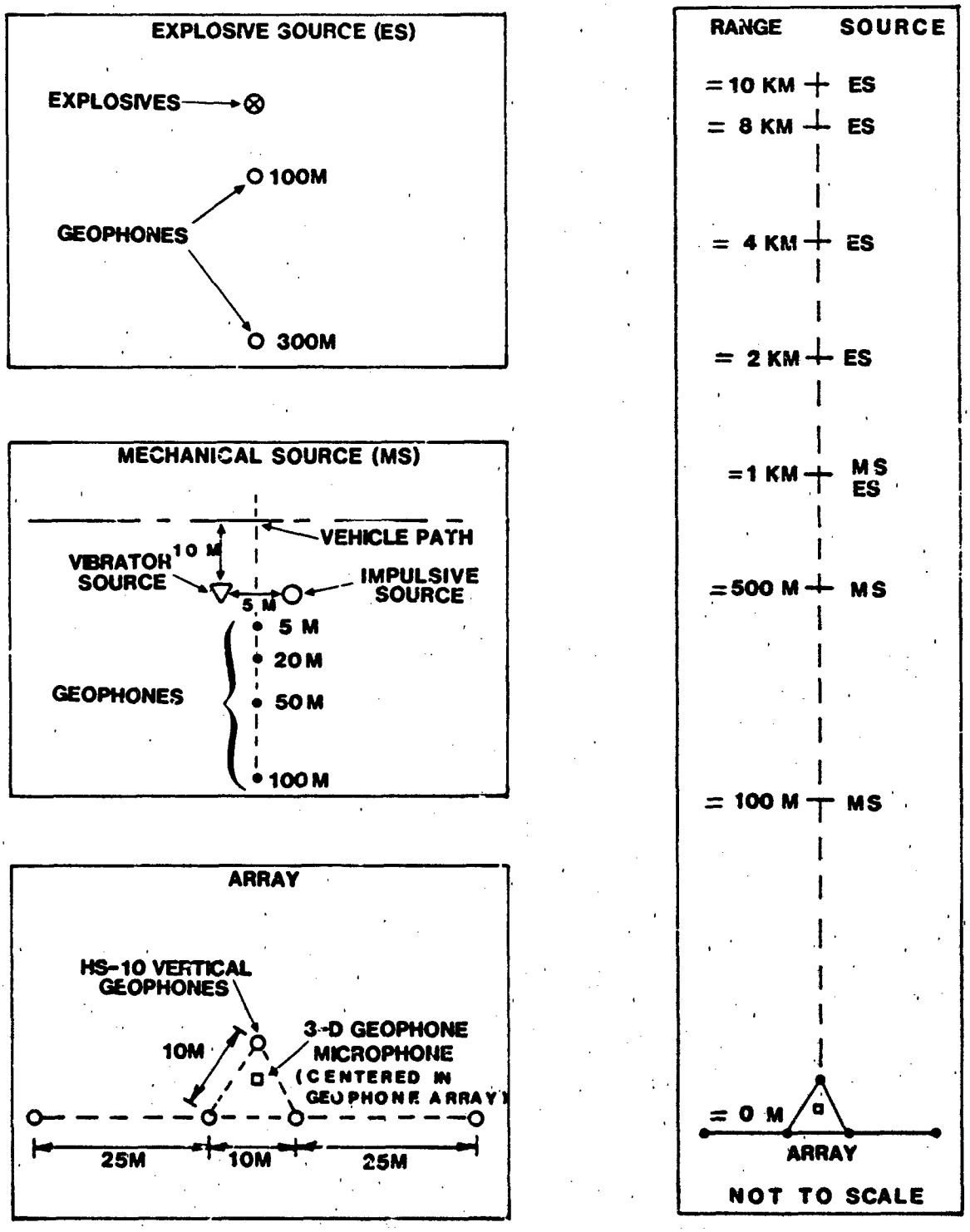

Figure 9. Layout of sources and array

37. Vibration tests. The vibrator was run at discrete frequencies between 1 and 120 Hz, as listed in Table 2, for periods of approximately 60 sec while data were recorded at the source and at the array. The vibrator was also run at a 10-percent offset frequency (i.e., for nominal frequency, f=50 Hz, offset frequency f=55 Hz) for five separate frequencies. In addition, tone bursts were run at each discrete frequency with the vibrator on for 8 to 32 cycles and off for 8 to 128 cycles (to give a reasonable cycle of signal and quiet) and repeated for about 60 sec. The last tests were run with the vibrator set with random noise input for approximately 60 sec and then repeated. All tests conducted with the vibrator are listed in Table 2.

38. Impulse tests. The impactor was placed into position and released five times to seat the plate and establish proper gains for the instrumentation systems. It was then released five times for recording of the seismic signal with a definite break (60 sec) between impacts. The impulse tests conducted are also listed in Table 2.

39. Vehicle tests. The vehicle tests were conducted with an Army 2.5-ton truck, M-35, as the source of seismic and acoustic signals. The M-35 truck provides a complex forcing function composed of both impulsive and multiple frequency components (Engdahl and West 1974). The terrain was so rough that the vehicle could safely be driven to speeds of only 16 km/hr (greater speeds produced excessive driver motion). The vehicle was driven at both 8 km/hr and 16 km/hr perpendicular to the test line for a distance of about 50 m on each side of the line, allowing approximately 5 m for acceleration and deceleration at either end. The vehicle was used unloaded, and since the path was rough, the vehicle motion and vibration at both speeds produced a forcing function for seismic wave excitation. This vehicle response can be used to relate response of both smaller and larger vehicles by relating the forcing function and measured signal with model calculations for the larger or smaller forcing functions.

Explosive-source tests

40. Since the nondestructive attenuation tests did not produce data beyond 1.0 km, explosive sources were used to extend the data to longer ranges. Explosive-source tests were run at ranges of 1, 2, 4, 8, and 10 km (Table 3). The test at 1 km was run to obtain data to relate the explosive-source response with that of the mechanical sources. Preliminary tests were designed to define a specific explosive charge that could propagate a

measurable signal to the array from 10 km. The first explosive shot, which weighed 12.25 kg, produced a good signal at the array (this shot size was selected on the basis of pretest predictions during the planning cycle). Thus, the same size charge was used at each site thereafter, except the last shot (number 136), where excess explosives weighing 63.5 kg were detonated when the program was completed. (This also provided a check of seismic signal for two different strength energy sources at one range.) The explosive used in all the tests was an ANFO mixture buried 3 m for good energy coupling.

41. For the explosive tests, the source geophones were emplaced in a different pattern, since signal levels were expected to be much higher than with the mechanical-source tests. Two vertical geophones were emplaced 300 m from the shot, and one vertical geophone was emplaced 100 m from the shot (except for shot number 130, for which it was emplaced at 200 m). In all but the 8-km shot (number 135), the geophones were emplaced between the shot location and the array. However, in this case the geophones were left in the same emplacement as for the 10-km shots (numbers 134 and 136), leaving the geophones located 1700 m and 1900 m from the 8-km shot.

42. Since the explosive tests were expected to propagate a measurable signal to the array over long distances, an add-on test was designed to measure the signal in an outcrop of the substrate. One triaxial geophone was emplaced in an outcrop lying about 11 km to the east of the 10-km station. This lateral system was used to determine signal characteristics at a high-contrast interface. The geophone was monitored with a battery-powered seismograph that produced oscillograph records of the measured signals.

PART IV: RESULTS

Physical Site Data Obtained

Subsurface properties

43. The test site overburden typically consists of fine material interbedded with occasional layers of coarse sand. The material grades coarser with depth and can be expected to have some patches of caliche and conglomerate. However, the seismic refraction tests showed a reasonable uniformity in subsurface conditions over the 10-km test line. The average seismic P-wave velocities are listed in Table 1. An approximate cross section of subsurface properties is shown in Figure 10. It should be noted that this cross section is a generalized view of the site based on the seismic refraction data and available information, coupled with the experience of the seismologist.

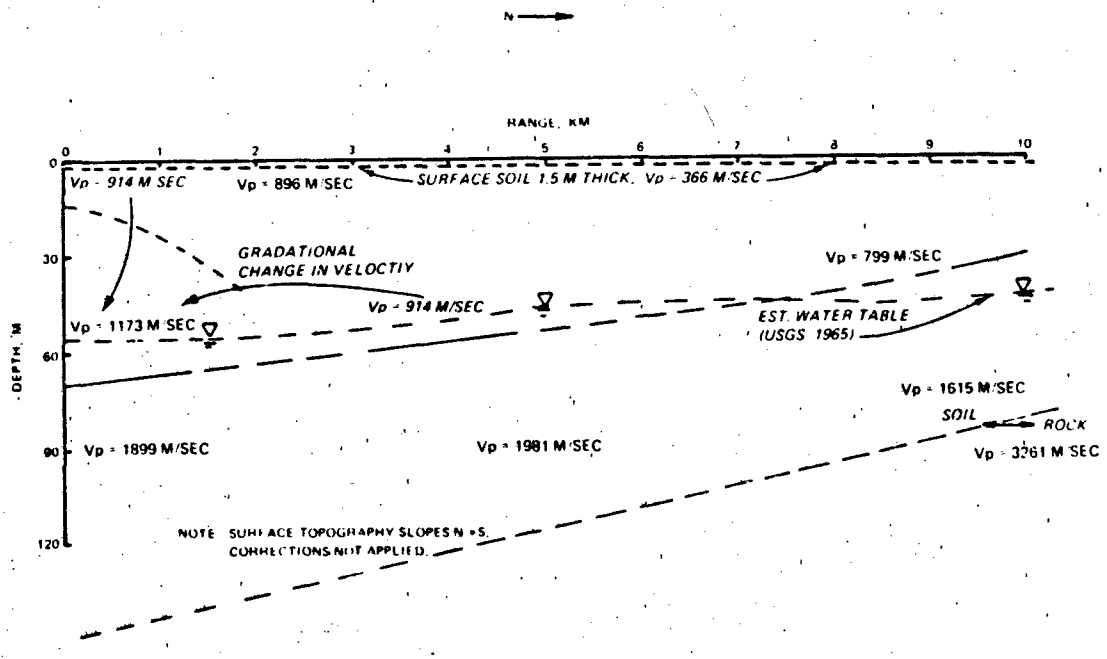

Figure 10. Seismic profile of SAT site

Surface soil properties

44. The surface soil is a silty sand, classified SM by the Unified Soil Classification System (Lambe and Whitman 1969). It had a moisture content of about 6 percent on the surface and about 8.8 percent at a depth of 30 cm. The

soil had a cone index of 100 to 220 on the surface and increased to approximately 300 at a depth of 37.5 cm. All measured properties are listed in Table 1.

Topography

45. The site topography is summarized in Figure 11, which shows a maximum site elevation difference of about 32 m, gradually increasing in elevation

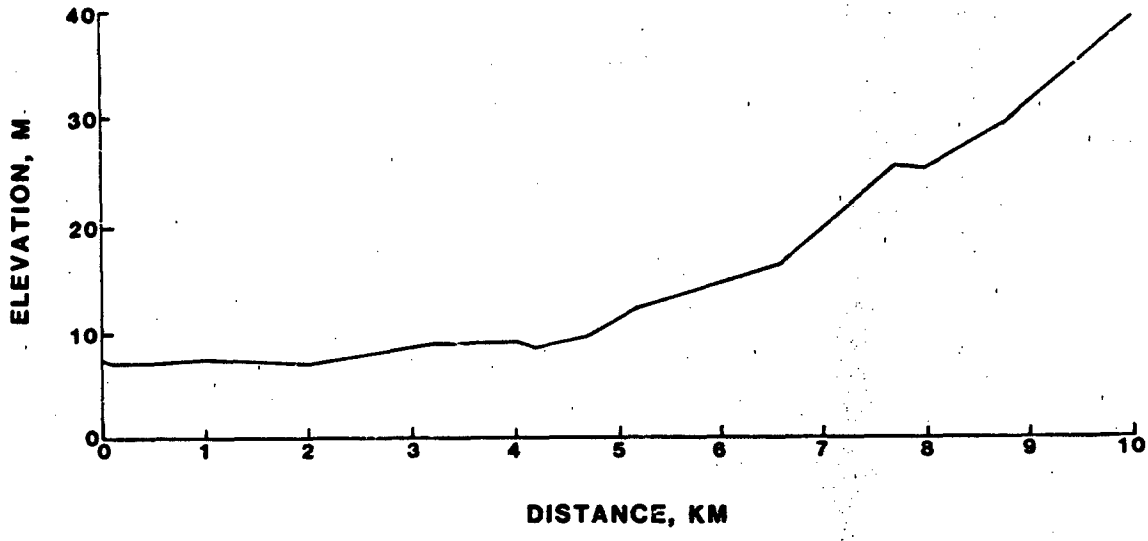

Figure 11. General site profile

from the array to the 10-km station. There were a few localized anomalies, usually in a wash location.

Meteorological conditions

46. Air temperature and wind speed taken at the meteorological station for each test are listed in the last two columns of Tables 4-6. Wind velocities on several days were quite strong. These conditions are contrasted with those on calmer days in Figure 12. Similarly, ground and air temperatures varied considerably over the test period, as shown in Figure 13. Although some light precipitation occurred during the preparation period, no significant precipitation was experienced during the tests. Ground temperatures remained above freezing during the test period. Measured weather data are summarized in Table 7.

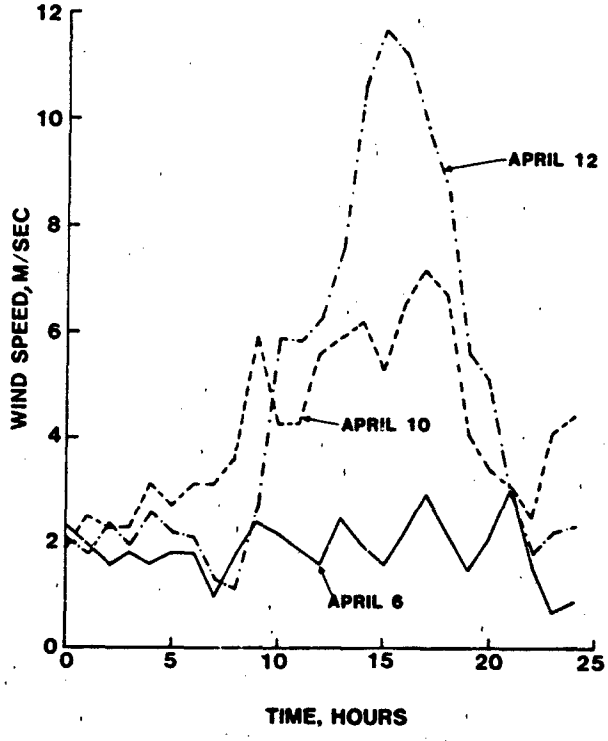

Figure 12. Diurnal wind speed for selected days

Seismic Wave Attenuation Data

Mechanical sources

47. Vibration data. The result of the vibration tests was a great volume of data involving about 1500 channels of analog records. These data are presented in Plates 1-84, as both time and frequency domain plots; peak values are listed in Table 4. The discrete frequency vibration tests are presented in Plates 1-43. Each plate presents the results of one test with the input load shown at the top; next the signal measured at 50 m; and, continuing down the page, the vertical, radial, and transverse signals measured by the triaxial geophone at the main array. Plots of time and frequency domain for each signal are presented side-by-side on the plates for a quick look at the frequency content of the signal.

48. The signals show that measured frequency is within the margin of measurement error of the nominal input frequency. In the 10-percent offset frequency tests, measured frequency is distinguishable from the base frequency, even down to 3.3 Hz and 3.0 Hz. However, because of the digitizing

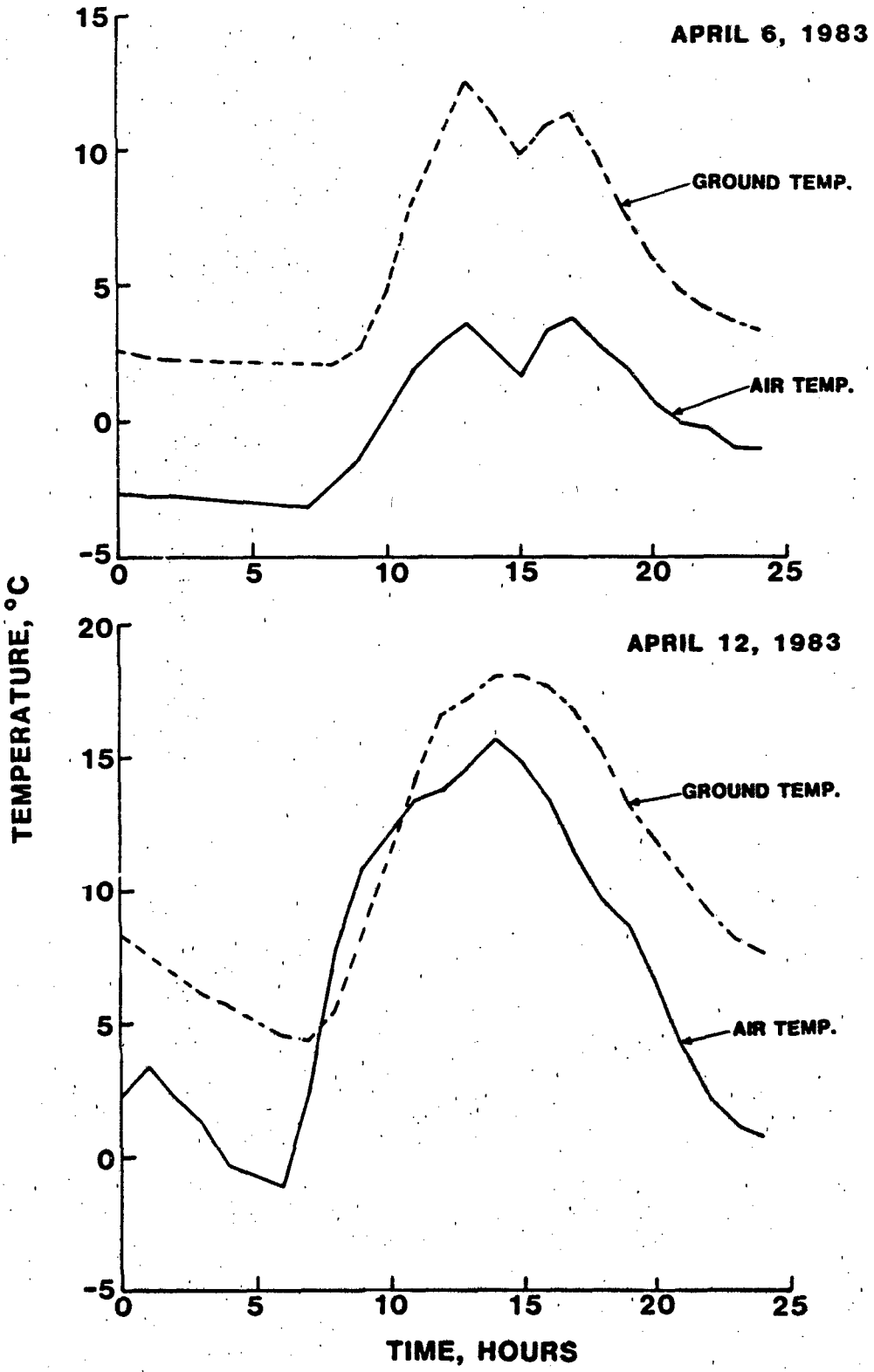

Figure 13. Typical diurnal ground and air temperatures

sampling rate of 1000 points per second and a total 2048 points sampled, there is a minimum frequency resolution of 0.488 Hz in the "fast" Fourier Transform (FFT). In this case the FFT reads 2.928 Hz for the 3.0-Hz signal and 3.416 Hz for the 3.3-Hz signal, which are reasonable values. However, to check frequency differences below 0.25 Hz, a different sampling rate would be required. There appears to be little difference in amplitude between the discrete and offset frequency.

49. The tone burst test data presented in Plates 44-77 are in a form similar to the discrete frequency tests with time and frequency domain plots of input load, 50-m source geophone, and triaxial array geophone records. The tone bursts give an opportunity to describe the accuracy of the measurements at each recording station by comparing amplitude and frequency results with corresponding discrete frequency test results. The measured amplitudes on the tone burst tests compare favorably with the discrete frequency results. There are some differences in the peak velocities as measured in the FFT plots, probably caused by a "rounding" of the input load and by the introduction of harmonics by the vibrator in a tone burst mode. The difference does not necessarily seem to be dependent on frequency or the number of cycles, but rather on whether the sinusoidal input is "clean." There are some other inherent problems in running the vibrator in a tone burst mode. At frequencies below 5 Hz, the vibrator turns on and off with a much larger load than during the "on" cycles of the tone burst. The result is a "framed" tone burst, as seen in Plates 55, 56, and 57. It should be noted that the FFT was selectively run, omitting these peak load sections of the signal.

50. The frequency sweep tests are presented in Plates 78-81. The time domain plot presented in Plate 78 for the 1-km sweep test shows the response of the site at the 5-, 20-, 50-, 100-, and 1000-m ranges to the vibrator frequency sweep. The time domain plot for the 1-km site is presented as representative of the sweep tests since the tests, which took about 4 min to complete, are difficult to display. The FFT plots of Plates 79-81 (for all locations) show amplitude versus frequency. The plot in Figure 14 is a composite of the average peak FFT for each range (taken from Plates 80 and 81), showing the variation of signal with both frequency and range.

51. Results of the random noise tests are presented in Plates 82-84. The data from the source geophones are good. However, the data from the array sensors are affected by the 60-Hz electrical noise, and even with a 40-Hz

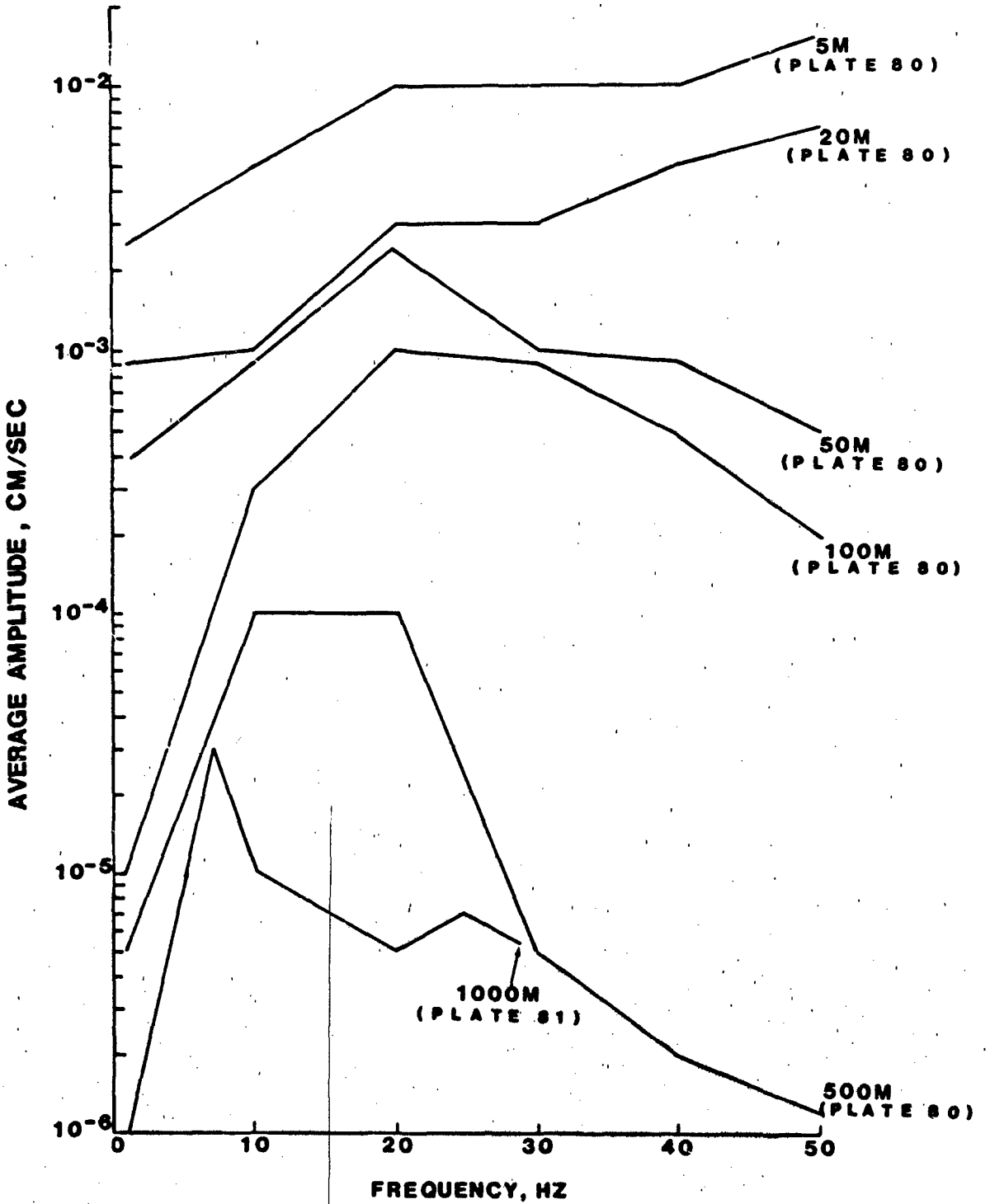

Figure 14. Average amplitude of vertical component versus frequency for various ranges from 50-Hz to 1-Hz frequency sweep tests. Plate number indicates the source of data.

low-pass filter, there is a large 60-Hz component in the signal. The data from the 500-m and 1-km ranges probably are not affected by the 40-Hz filter, but the 100-m data are affected somewhat since some 40- to 120-Hz data are present in the signal at 100 m. Thus, the 100-m source geophone data are substituted for the 100-m vertical data from the array.

52. Impulse data. The impulse test data are presented in Plates 85-87 and peak values are listed in Table 5. Each plate represents one test, with the impulsive acceleration converted to an approximation of load, at the top; the signal measured at 50 m, next; and then the vertical, radial, and transverse signals measured by the triaxial geophone at the main array. Both time and frequency domain plots are shown for each signal. These data show the effect of the site on frequency content of the signal, as the dominant frequency decreases with increasing range.

53. Vehicle data. The vehicle data are presented in Plates 88-93. Each plate represents one test, with the 5-m geophone data at the top; followed by the 50-m geophone data; and then the vertical, radial, and transverse components of the triaxial geophone at the main array. Both slow and fast vehicle speed tests are presented, and both time and frequency domain plots are shown for each signal.

Explosive sources

54. Data from the explosive-source seismic attenuation tests are presented in Plates 94-99 and peak values are listed in Table 6. Each plate represents one test with the close-in data for 100 m at the top; followed by the 300-m data; and then the vertical, radial, and transverse components of data measured by the triaxial geophone at the main array. Time and frequency domain plots of each signal are shown side-by-side. The data are generally good, although there is some wind noise interference at the main array on some of the tests, as can be seen in Plates 97 and 98 (Tests 135 and 134). The 8-km test data, in particular, illustrate how wind noise obscures the signal (signal is the same before and during the active test period), and since frequency contents are similar between the two types of signal, the data cannot be easily filtered to remove the noise.

55. The data for the lateral geophone system are limited to the explosive tests. The system was emplaced in a position about 11 km perpendicular to the test line (see site location map, Figure 7) and was calibrated at the same levels as the array geophones for the 10-km tests. Timing was difficult

because of the limited communication afforded by portable radios with short ranges.

56. The data were limited to those recorded on a strip chart recorder, with less fidelity than data recorded on a tape. However, they address the primary question, whether any unusual seismic signal was loaded into bedrock by the explosive. The triaxial geophone was set into a rock outcrop in this lateral position to give an indication of any unusual seismic signals. Since the geophone was calibrated for the same signal at the array, a large signal would indicate some unusual loading. However, no signal received at the lateral system was as large as the array, and most signals were significantly smaller. As can be seen in Figure 15, the signal produced by Test 132

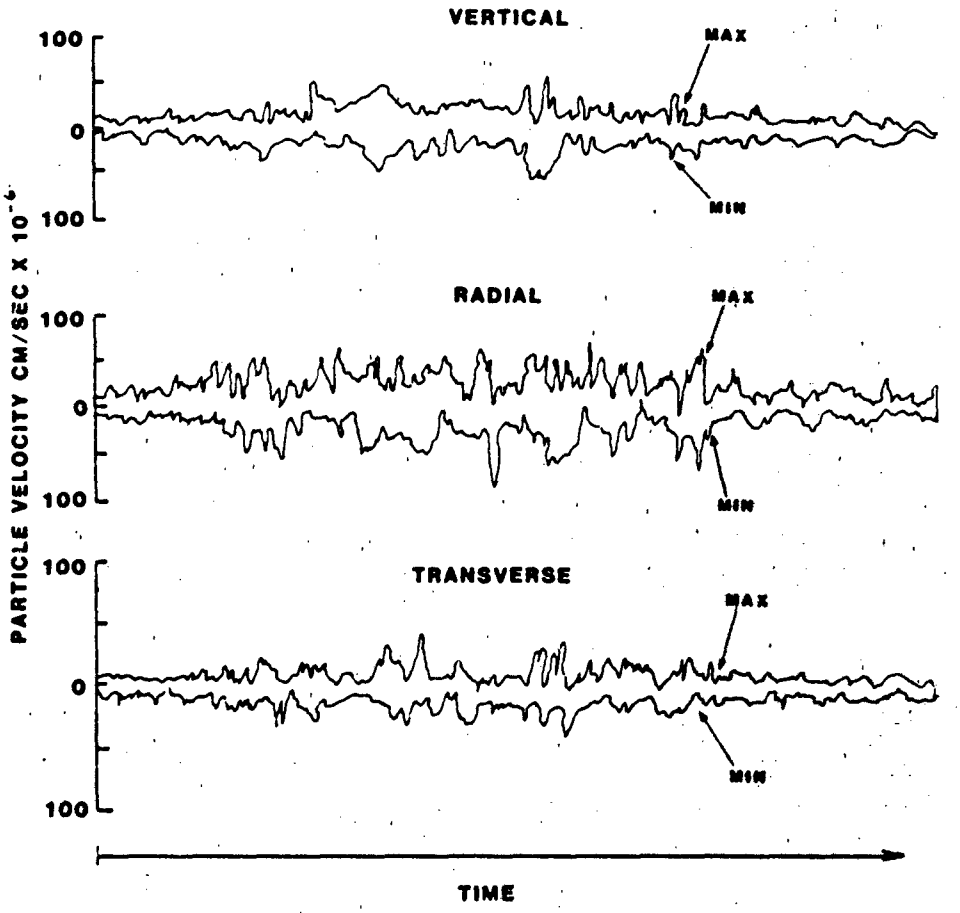

Figure 15. Envelope records from lateral geophone system showing maximum and minimum values for each trace (Test 131)

produced a maximum amplitude of about 75×10^{-6} cm/sec while the signal for the explosive tests received at the array did not fall below 700×10^{-6} cm/sec. Thus, the bedrock was deep enough at the site to be of little significance.

PART V: ANALYSIS AND DISCUSSION

Seismic Waves

57. The generation, propagation, and sensing of seismic energy from targets of military interest consist of a sequence of interrelated physical phenomena (see Figure 16). Anything that moves on the surface of the ground applies a force to the substrate which can be sensed at some distance from that source. If the force is large enough to stress the substrate to a dynamic deformation, the energy is carried from that point by seismic waves. The amplitude and type (to some degree) of seismic wave generated depend on the force history applied by the target. Variations in the target which produce changes in the force history are mainly mass and rate of force application. A large mass will cause greater forces than a small mass and will

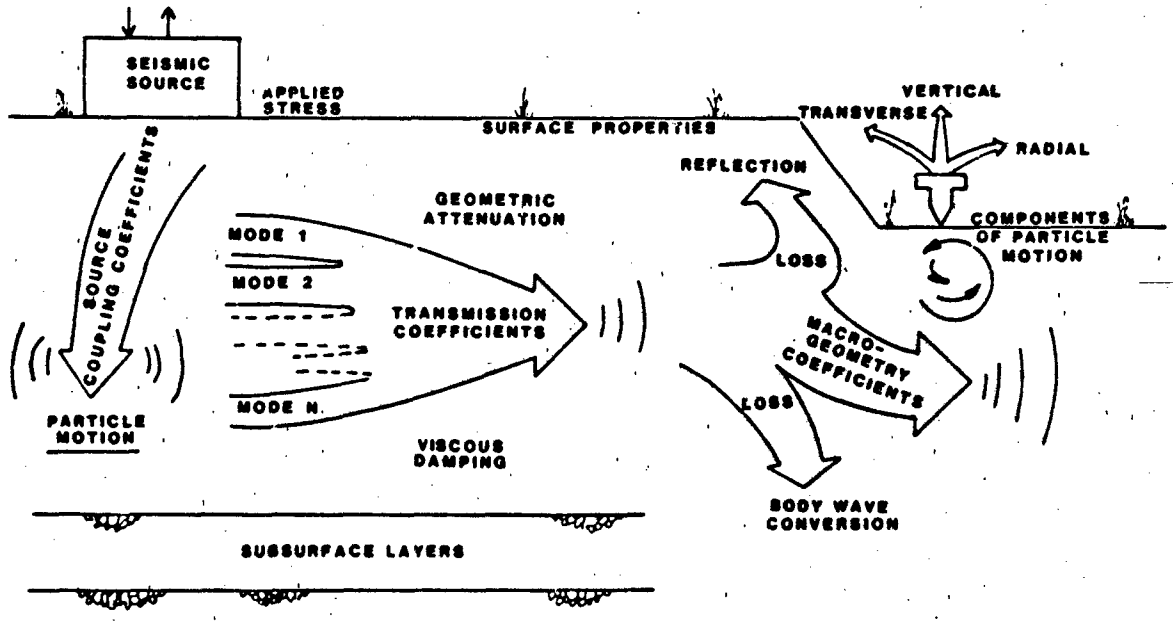

Figure 16. Properties of seismic attenuation

result in a different force history. In addition, a given force applied quickly will produce a different force history than force applied slowly. Variations in the nature of the substrate may also affect the force history, since that history is a record of the relation between force and time as measured at a specific point.

58. There are three major seismic wave modes, all of which move radially outward from a point of substrate deformation (i.e. the point at which stress is applied): (a) compression waves (P-waves), in which the principal particle motion is along a radial; (b) shear waves (S-waves), in which the principal particle motion is at right angles to a radial; and (c) surface waves (Rayleigh waves), in which the principal particle motion is elliptically retrograde in a plane chiefly perpendicular to the surface of the propagating medium. Compression waves move in all directions, so that the advancing wave front is approximately a hemisphere. However, they do not necessarily move at the same velocity as the S-wave, even in the same material. Unlike P-waves and S-waves, Rayleigh waves generally move at shallower depths and parallel to the surface, so that at a point a few metres from the target, the advancing wave front is cylindrical with the vertical axis of the cylinder at the target. For all practical purposes, Rayleigh waves (assuming the very low amplitudes that are of interest in this study) affect a substrate depth equal to about one-third wavelength. Amplitudes of Rayleigh waves are usually at a maximum at the surface and decrease progressively with depth. The propagation velocities are not the same as those of either P-waves or S-waves.

59. Generally, both P-waves and S-waves are diffracted in the direction of greater substrate densities, and since nearly all natural substrates increase in density with depth, these waves tend to diffract downward. The result is that they appear to attenuate very rapidly at the surface. They may, however, reflect from a subsurface discontinuity and reappear at the surface at some distance from the target. Thus, there could be zones in which P-waves and S-waves are difficult to detect at the surface. Conversely, the Rayleigh wave generally propagates along the surface; thus, theoretically, there can be no discontinuities in the area over which the signal can be detected. This knowledge, in addition to the fact that about two-thirds of the energy at the source is carried away in the Rayleigh wave, is the principal reason for choosing the Rayleigh wave as the mode upon which to base this study.

60. The "ideal" or theoretical situation for the propagation of Rayleigh waves would consist of a completely homogeneous elastic half-space. Anything that departs from these ideal conditions serves to attenuate or disperse the wave form more rapidly than would be the case by purely geometric attenuation (i.e., the attenuation resulting from the same amount of energy being applied over a longer wave front as the wave moves outward away from the source). There are several basic types of nonhomogeneities commonly found in nature. The dramatic effects of nonhomogeneities on wave propagation stem primarily from the fact that each type of material tends to act as a specific medium for a specific suite of wave frequencies. That is, a specific type of material tends to propagate certain frequencies more efficiently than others. The result is that substrate materials act as selective filters. For example, most targets generate a seismic wave train (or signal) consisting of a complex of frequencies (or wavelengths) ranging from very low (i.e., very long waves) to very high (i.e., very short waves). Generally, the signal contains a broad spectrum of frequencies as it emerges from the source. However, as the wave train moves radially away from the source, two things happen to it:

a. Since each frequency tends to propagate at a slightly different speed, the wave train tends to separate into sections (disperse), each having a characteristic frequency. This effect is usually not obvious over short distances, since the process rarely has time to produce complete frequency separation.

b. Some frequencies are propagated efficiently over rather long distances, and others die out quickly. The effect of this phenomenon is to filter out some of the original frequencies, leaving a signal characterized only by those frequencies that are efficiently propagated. In practical terms, the implication is that in some terrains and at long detection distances, all targets tend to be characterized by wave trains exhibiting the same frequencies. It is obvious that, in such situations, virtually all targets will look the same insofar as the frequency composition of their signatures is concerned.

61. Variations in substrate characteristics are many, but the most common is stratification. Nearly all areas are stratified to some degree, and many are divided very sharply into distinct layers. Each layer tends to be characterized by somewhat different propagation of seismic waves, with the result that they try to propagate independently through each. The interference caused by the interface absorbs energy and attenuates the wave rapidly. It should be noted that stratification is not a constant with respect to time. The most common cause of a change in stratification is a change in moisture

content that can affect the wave propagation characteristics of the soil. In addition, stratification may also change with respect to small changes in location, affecting wave propagation characteristics, even drastically. Another cause of stratification changes is nonhomogeneous areas. These disparities occur quite often in alluvial deposits where a small section of one material (i.e., caliche) is surrounded by a different matrix material. Other variation comes from faulting (or vertical cracks) and changes in surface geometry which provide more interfaces for complicating Rayleigh wave propagation.

62. As the propagating wave reaches the geophone, it is carried on by the motion of the soil particles if the geophone is properly placed. Three conditions of emplacement affect geophone performance: (a) depth of emplacement, (b) geophone attitude, and (c) coupling of the geophones with the surrounding medium. Depth of emplacement is critical in measuring Rayleigh waves, which usually have maximum signal close to the surface. Geophones operate most efficiently with the axis parallel to the pull of gravity and should thus be leveled for use. Geophones must move with the surrounding particles to measure the motion and thus must be in solid contact with the substrate. If not, the geophone will move less than the surrounding particles, resulting in an erroneous measured signal. The preceding discussion of seismic wave propagation phenomena is based on an analysis by Benn and Smith (1975) and more details are available therein.

Seismic Refraction Data Correlation

63. The seismic refraction tests were conducted to define the substrata of the test site so problem areas similar to those described above are avoided or at least understood. The test site, because of its location in an alluvial valley, was expected to be stratified with similar properties in each layer and some nonhomogeneous areas. The area was relatively homogeneous, with similar properties throughout the 10-km test area, as can be seen in the seismic profile drawing of Figure 10.

Group velocities for seismic waves

64. The S-, P-, and R-wave group velocities calculated from the explosive and impact lists are presented in the time versus distance plots of Figure 17 for comparison with the seismic refraction data. It should be noted

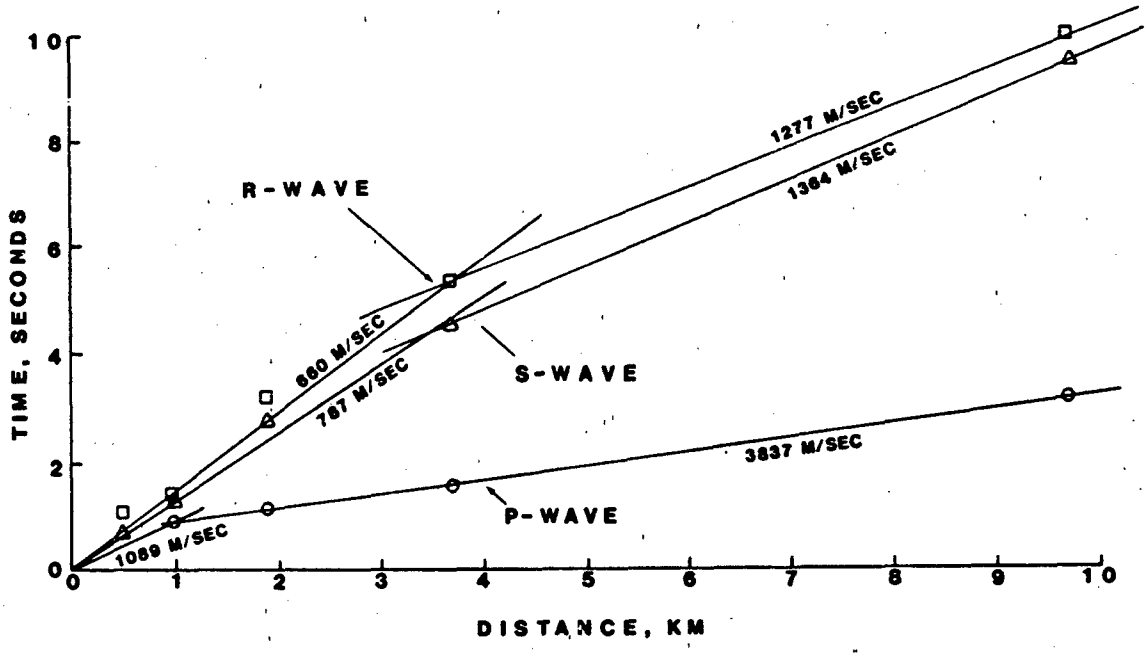

Figure 17. Time versus distance plots for explosive-source tests

that the lower parts of the curves are not refined by extensive seismic refraction data between 0 and 2 km, and thus the lower parts are a biased average of group velocity. The time of arrival of each wave train was calculated from the time domain data of Plates 85-87 and 94-99 and plotted against the distance between the close-in geophone and the array. The P-wave curve is similar to the seismic refraction data of Appendix B, indicating that the P-wave traveled in bedrock at depths over 100 m with a velocity of about 3800 m/sec. The S- and R-wave curves are shown only to document group velocities and their relationship to the P-wave. Velocities from P-, S-, and R-waves are expressed by V_P, V_S and V_R, respectively. These data show that V_S is 1277 m/sec and V_R is 1364 m/sec which gives $V_S/V_P = 0.33$ and $V_R/V_S = 0.94$ for this site. The R-wave has a dominant frequency of 3 Hz in the 10-km test, indicating a wavelength of about 455 m, which means that R-wave would be spread over the upper ±150 m. (This is estimated by the following: $d_R = V_R/2f$.) Thus, the long-range attenuation data confirm and support the seismic refraction data.

Seismic attenuation

65. The explosive-source test data were also used to generate the attenuation curve shown in Figure 18. This curve is a plot of peak particle velocity amplitude (R-wave) versus range. Since it uses data from the 1-km through 10-km ranges, it is also called a site attenuation curve. The curve shape is another indicator that no major anomalies exist in the substrate.

66. Selected discrete frequency vibration data were used to prepare the attenuation curve presented in Figure 19. This curve shows particle velocity amplitude versus range for several different frequencies. The variation of frequency with range can be seen in the curves as they flatten out as frequency decreases. The higher frequency components attenuate faster than the lower frequency components, which extend over long ranges. The data were taken at ranges ranging from 5 m to 1 km and relate quite well, showing that site attenuation is relatively consistent. This curve also shows that the data are relatively consistent over the range of frequencies, another example of the quality of this data set.

Signal Characteristics

Mechanical-source tests

67. Vibration. The vibration tests have signal amplitudes that correlate well over the 100-m, 500-m, and 1000-m test ranges. The only differences occur at the 100-m range where the amplitudes vary between geophones in the array. This is probably because of the significant difference between the cylindrical wave front and a plane wave front at 100 m or because, for continuous wave signals, the P-, S-, and R-waves will add or subtract, causing signal variations over short distances. Another difference occurs in the tone burst data, caused by variations in the vibrator output as frequency changes. The data described below are summarized in Table 8.

68. The random noise tests have signal characteristics similar to the discrete frequency vibration tests. The vertical array data from the 100-m test have a center frequency of 25 Hz and a bandwidth of 10 Hz. Bandwidth is defined as the width of the band described by the points 6 db down from the peak amplitude (one-half the peak amplitude). The 500-m random noise test has a center frequency of 15 Hz and a bandwidth of 15 Hz. The 1-km random noise

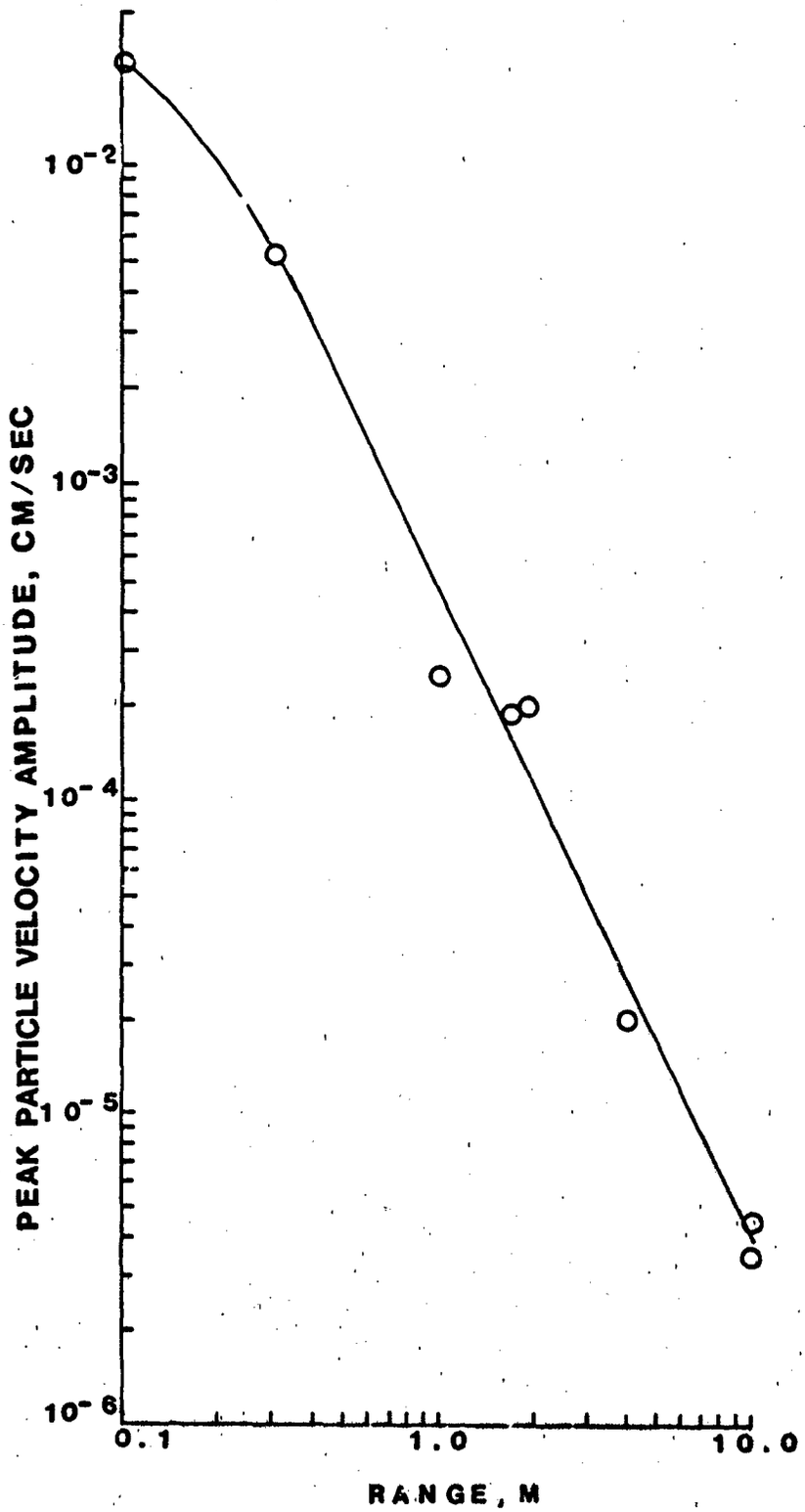

Figure 18. Attenuation curve generated from explosive-source test data

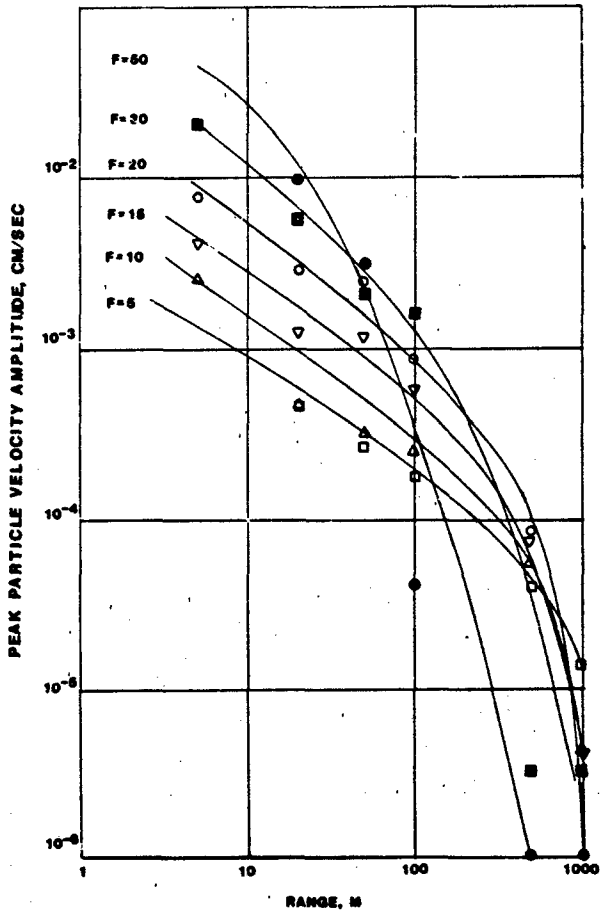

Figure 19. Attenuation curves for discrete frequency vibration tests

test has a center frequency of 4.6 Hz and a bandwidth of 1.5 Hz. The signal appears to be dispersed to a lower frequency at the 1-km range.

69. The vertical array signal on the 100-m-frequency sweep test has a center frequency of 23.2 Hz and a bandwidth of 7 Hz. The signal on the 500-m-frequency sweep test has a center frequency of 16.7 Hz and a bandwidth of 1.7 Hz. The signal on the 1-km-frequency sweep test has a center frequency of 8 Hz and a bandwidth of 6 Hz. This set of tests shows the signal frequency decrease as the range is increased, even though the higher frequency signals are input by the source.

70. Impulse. The vertical array signal for the 100-m impulse test has a center frequency of 24 Hz and a bandwidth of 12 Hz. The 500-m impulse test has a center frequency of 13 Hz and a bandwidth of 15 Hz. The 1-km impulse test produced a center frequency of 8 Hz and a bandwidth of 4 Hz. These data are listed in Table 8.

71. Vehicle. The vehicle tests produced signals of similar shape and frequency content at both speeds. The amplitudes varied somewhat. Only one set of numbers is presented for this discussion. The vertical array signals for the 100-m vehicle tests have a center frequency of 12 Hz and a bandwidth of 7.2 Hz. The 500-m vehicle tests have a center frequency of 2.9 Hz and a bandwidth of 2.4 Hz. The 1-km vehicle tests have a center frequency of 2.9 Hz and a bandwidth of 3.4 Hz. Vehicle test data are also listed in Table 8.

Explosive-source tests

72. Beginning at the 1-km location, the explosive-source test produced a center frequency of 7.2 Hz and a bandwidth of 3.7 Hz. This compares favorably with the impulse test at 1 km. The 2-km explosive-source test produced a center frequency of 3.9 Hz and a bandwidth of 1.5 Hz (although it is a relatively noisy record). The 4-km test produced a center frequency of 3.6 Hz and a bandwidth of 1.0 Hz. The 10-km test (number 134) produced a center frequency of 3.3 Hz and a bandwidth of 1.0 Hz, while Test 136 (also 10 km, but more explosive) had a center frequency of 3.2 Hz and a bandwidth of 0.6 Hz. The 8-km test signal had much wind noise and was not included. It could feasibly be used by employing some frequency search filtering techniques, but this was not done. These signal characteristics are also presented in Table 8 for comparison with other test data.

Background Noise Effects

73. As noted earlier, background noise was high on certain days of testing. Overall, however, the background noise, both seismic and acoustic, was relatively low except for windy days. Plates 100-102 illustrate background noise for the three nondestructive test locations, which encompass three different test days. The data in Plate 100 for Test 14 represent a moderate noise day with engines off. The data in Plate 101 for Test 89 represent a moderate noise day with engines running. The data in Plate 101 for Test 132 represent a high background noise day. It is interesting to note the average wind speed for the three tests: 5.6 m/sec, 5.3 m/sec, and 10.6 m/sec, respectively. It appears that above a wind level of about 8 m/sec, data acquisition beyond 2 km is definitely impaired because the signal-to-noise ratio may be as low as 0.1. Even with a spectrum analyzer, it would be difficult to pinpoint the signal of interest within an extremely noisy database,

since the wind causes low-frequency noise which looks like actual data. However, this problem could be helped by deeper geophone burial and averaging of multiple sensor array data.

74. Electrical noise is a problem in some tests. The 60-Hz noise introduced into the array system produces problems when tests are run above 50 Hz. The signals can be and were filtered; however, the filter does not provide the capability to separate real 60-Hz data and the 60-Hz noise. The electrical power also introduces harmonics of the 60-Hz noise in the signal (especially 120 Hz and 180 Hz).

75. The background noise from the generator, vibrator, and impactor engines is relatively insignificant seismically because of the favorable signal-to-noise ratio condition. The vibratory or impulse data signal is high in relation to the background noise caused by these gasoline engines. For example, the seismic background noise measured 5 m from the engines after Test 89 was about 5×10^{-4} cm/sec, while a typical vibratory signal was on the order of 5×10^{-3} cm/sec. The background noise measured at the array after Test 89 was about 1.2×10^{-6} cm/sec, while a typical vibratory signal at the 500-m range was on the order of 5×10^{-5} cm/sec. Thus, the signal appears to be at least an order of magnitude greater than the noise caused by the engines. The acoustic signal measured on the same test at a range of 50 m from the engines was about 10 dynes/cm^2, while the array microphone at a range of 500 m measured about 1.3×10^{-1} dynes/cm^2.

Evaluation of Model Analysis

76. Model predictions were made after preliminary site characterization was completed but prior to the initiation of testing. The model predictions, summarized in Figures 20-23, are discussed individually below. First, the Rayleigh wave phase velocity is plotted versus frequency for the preliminary site characteristics (Figure 20). Actual group velocities were about 660 m/sec in the mid-frequency range, compared to the 400 m/sec phase velocity prediction. The low-frequency (3-Hz) signal that arrived at the 10-km range traveled at a rate of about 1364 m/sec, compared to 820 m/sec predicted by the model since the deep high-velocity layer was not included in the model input. Most seismic input by vehicles or other similar activity would not have such low-frequency components. However, should frequency input below 3 Hz become

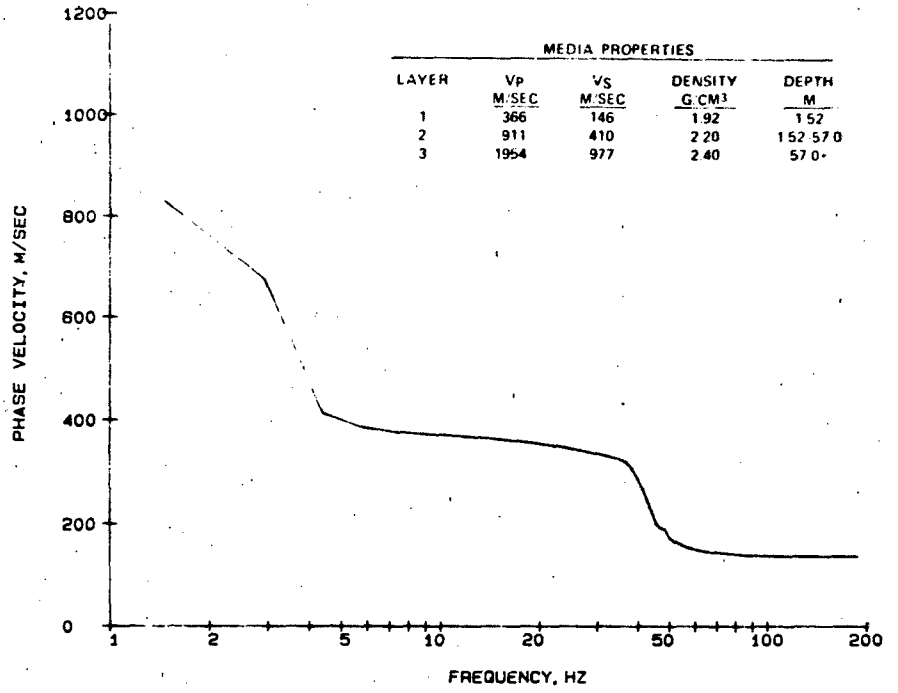

Figure 20. Rayleigh wave phase velocity calculated for SAT site by WES seismic model

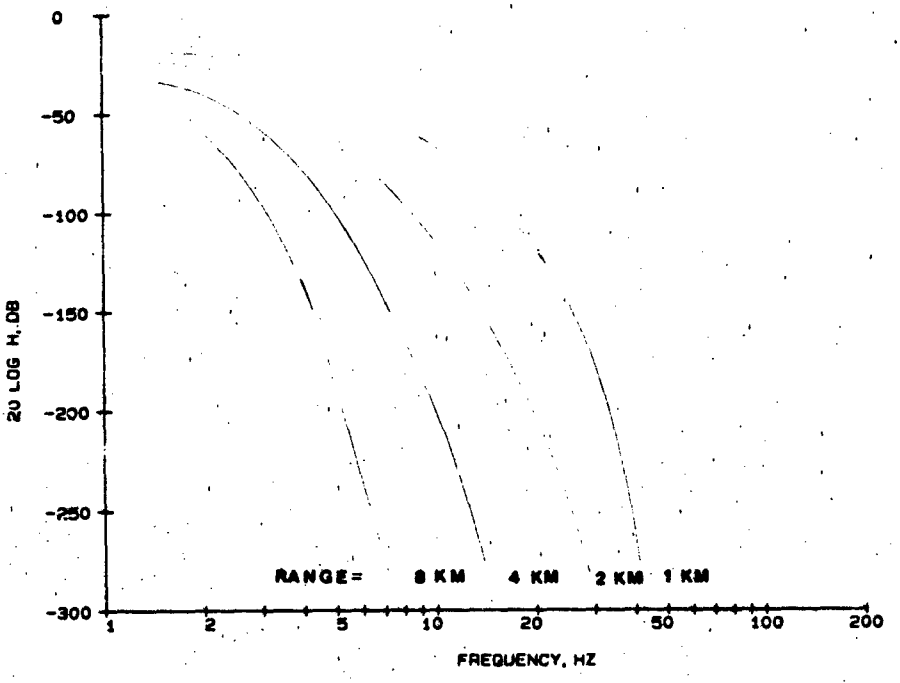

Figure 21. Transmission coefficient H versus frequency predicted by model

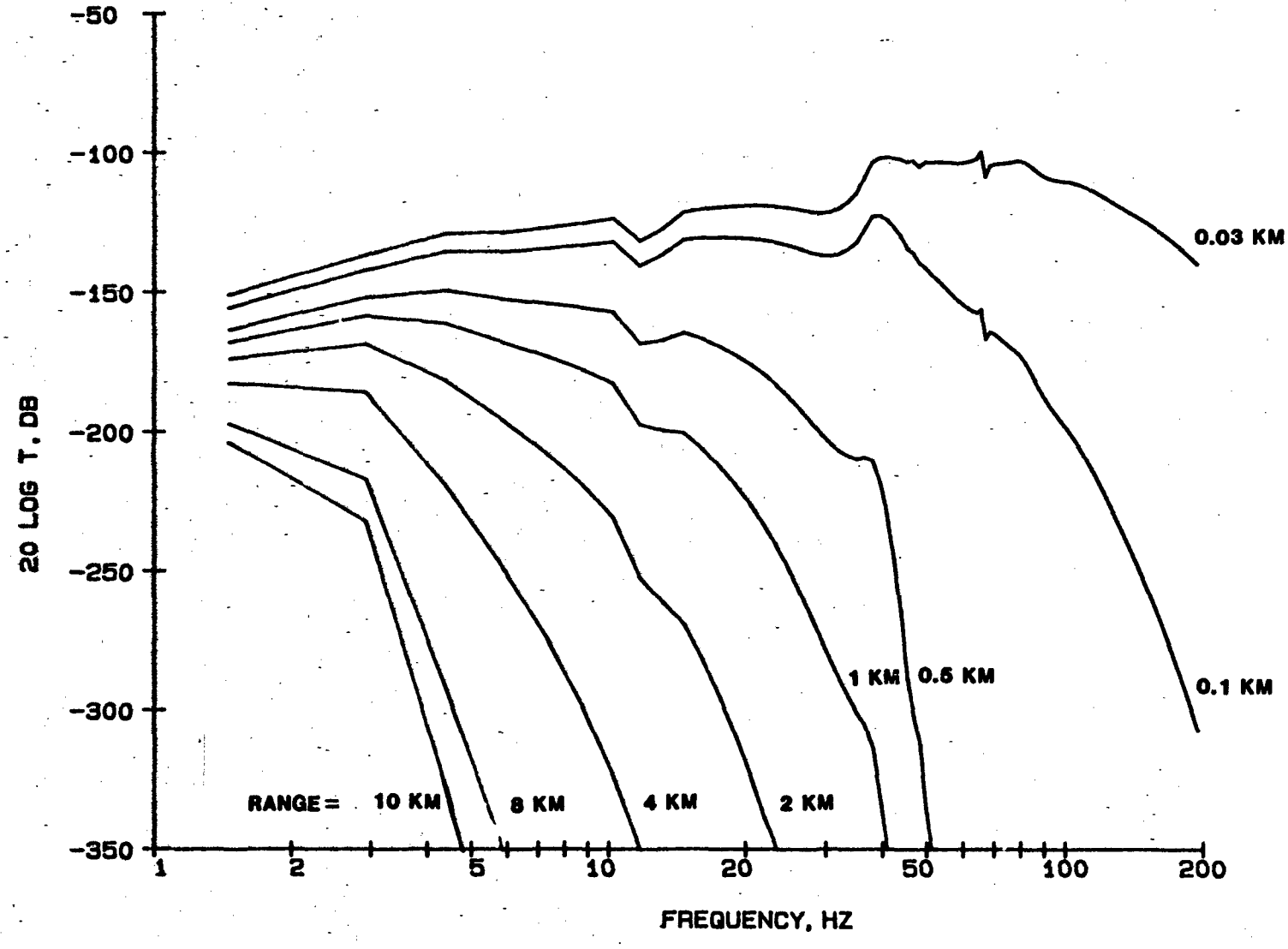

Figure 22. Transfer function T versus frequency predicted by model

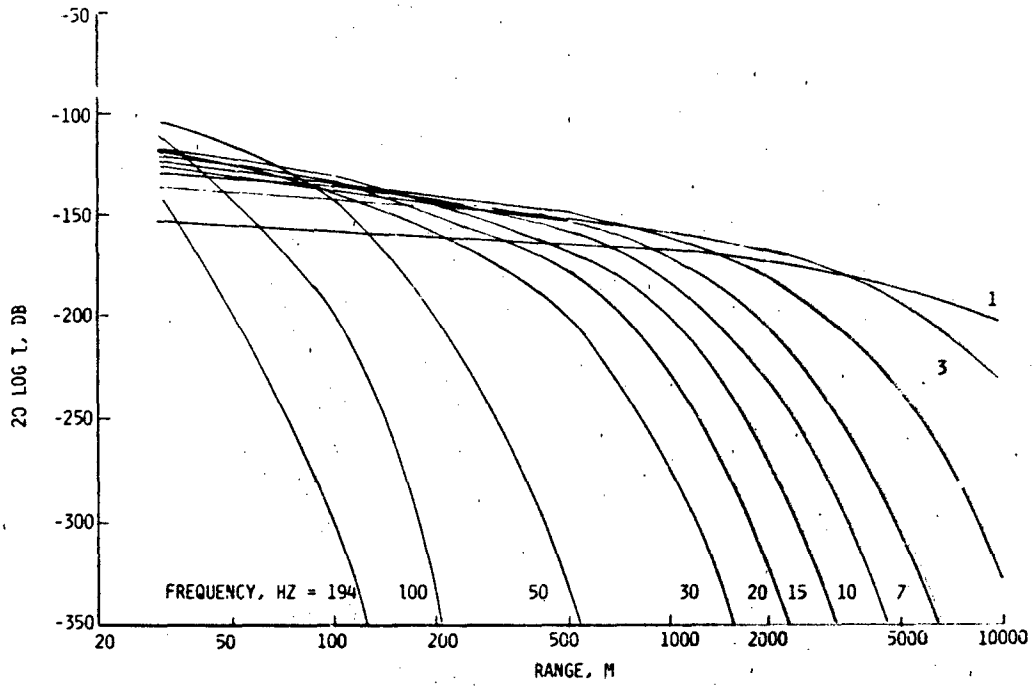

Figure 23. Transfer function T versus range predicted by model

of interest, more extensive site characteristics would have to be obtained for the model.

77. The transmission coefficient or R-wave attenuation was predicted by the computer model for the test site, as seen in Figure 21, as plots of transmission coefficient versus frequency for various ranges. This same transmission coefficient (or attenuation) was calculated from signals of the explosive tests and is illustrated in Figures 24, 25, and 26 for P-waves, S-waves, and R-waves. The R-wave values compare favorably with predictions but also provide a refinement of the model predictions in the high-frequency range.

78. The site attenuation ratio is the relationship of the propagating wave amplitude with respect to frequency f_k and spatial separation of two points (Williams 1981), given by

$$M_k = Y_k/X_k$$

where

Y_k = amplitude associated with frequency f_k at point Y, cm/sec

X_k = amplitude associated with frequency f_k at point X, cm/sec

Attenuation ratio M is shown in Figures 27-30, as calculated from the

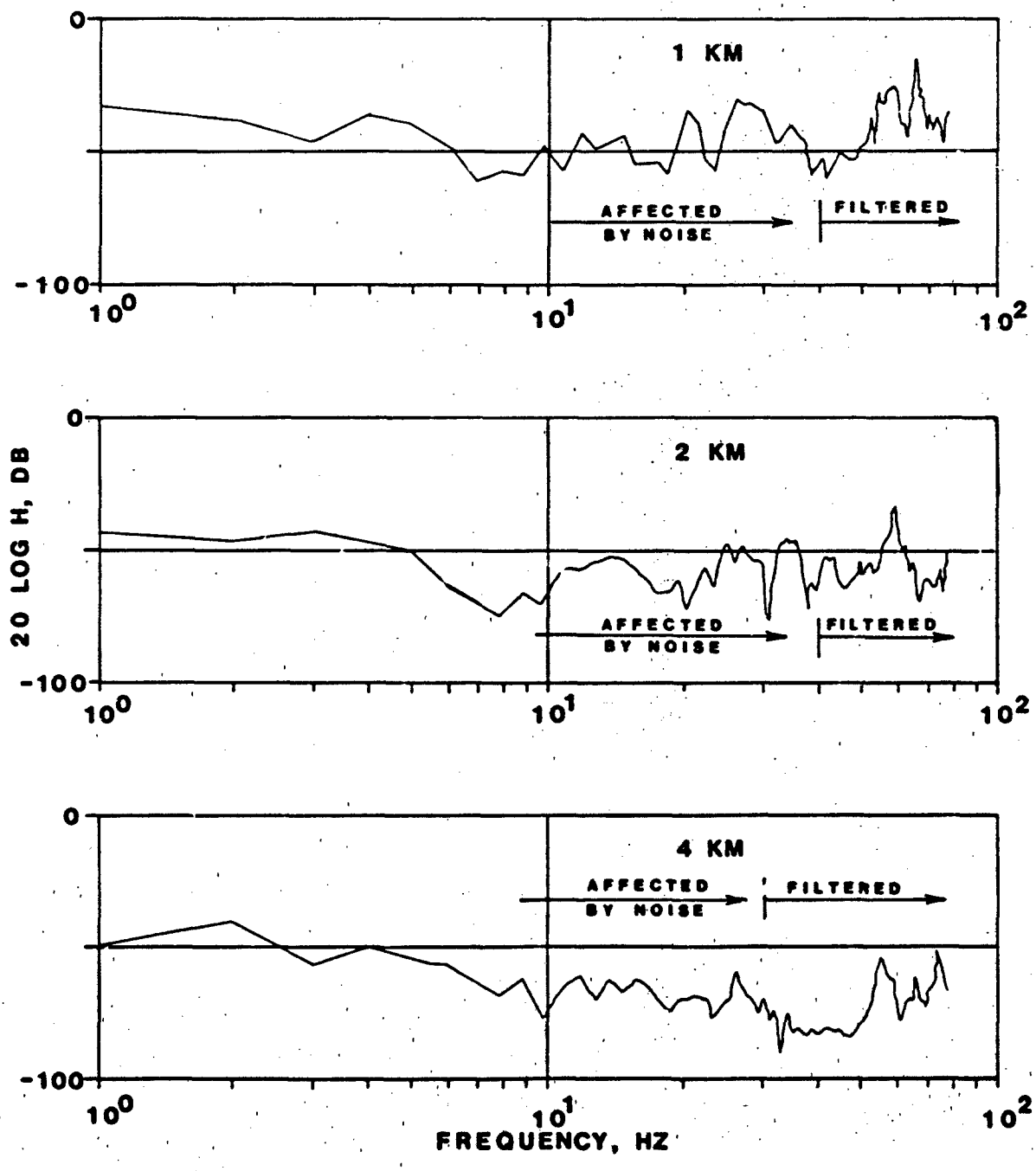

Figure 24. P-wave transmission coefficient H versus frequency calculated from explosive-source tests. Areas above about 10 Hz are noise and/or filter contaminated.

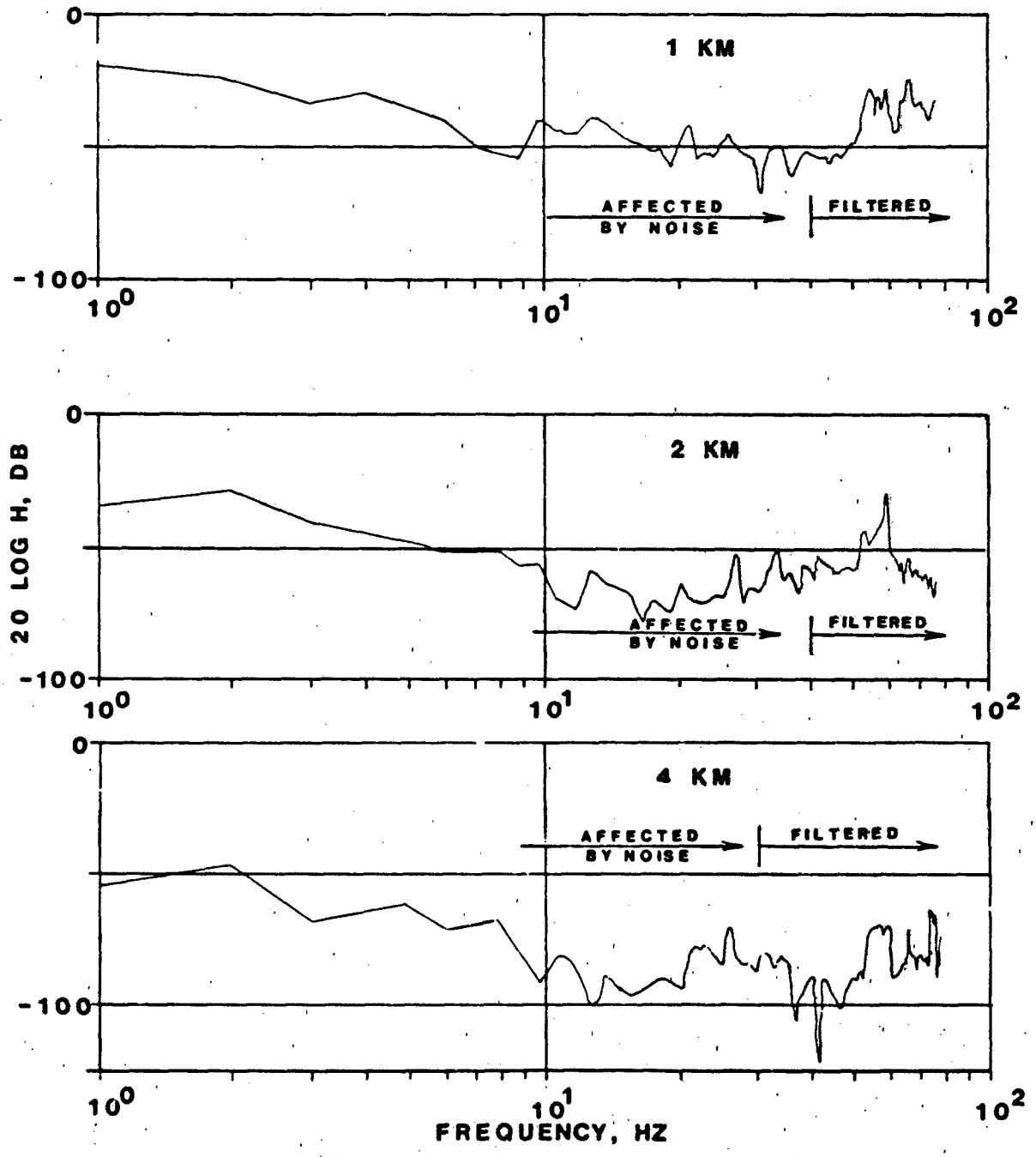

Figure 25. S-wave transmission coefficient H versus frequency calculated from explosive-source test data. Areas above about 10 Hz are noise and/or filter contaminated.

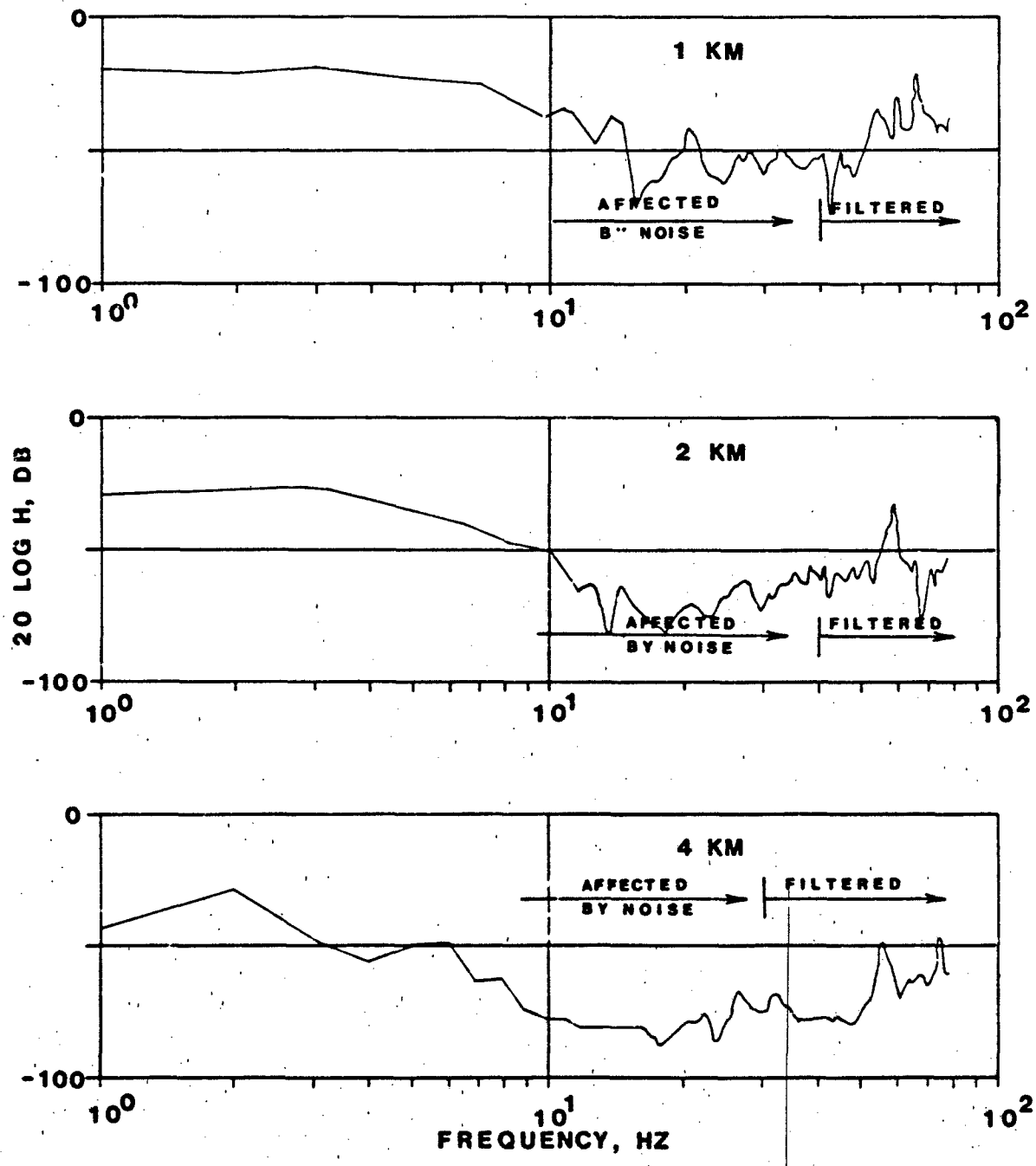

Figure 26. R-wave transmission coefficient H versus frequency calculated from explosive-source test data. Areas above 10 Hz are noise and/or filter contaminated.

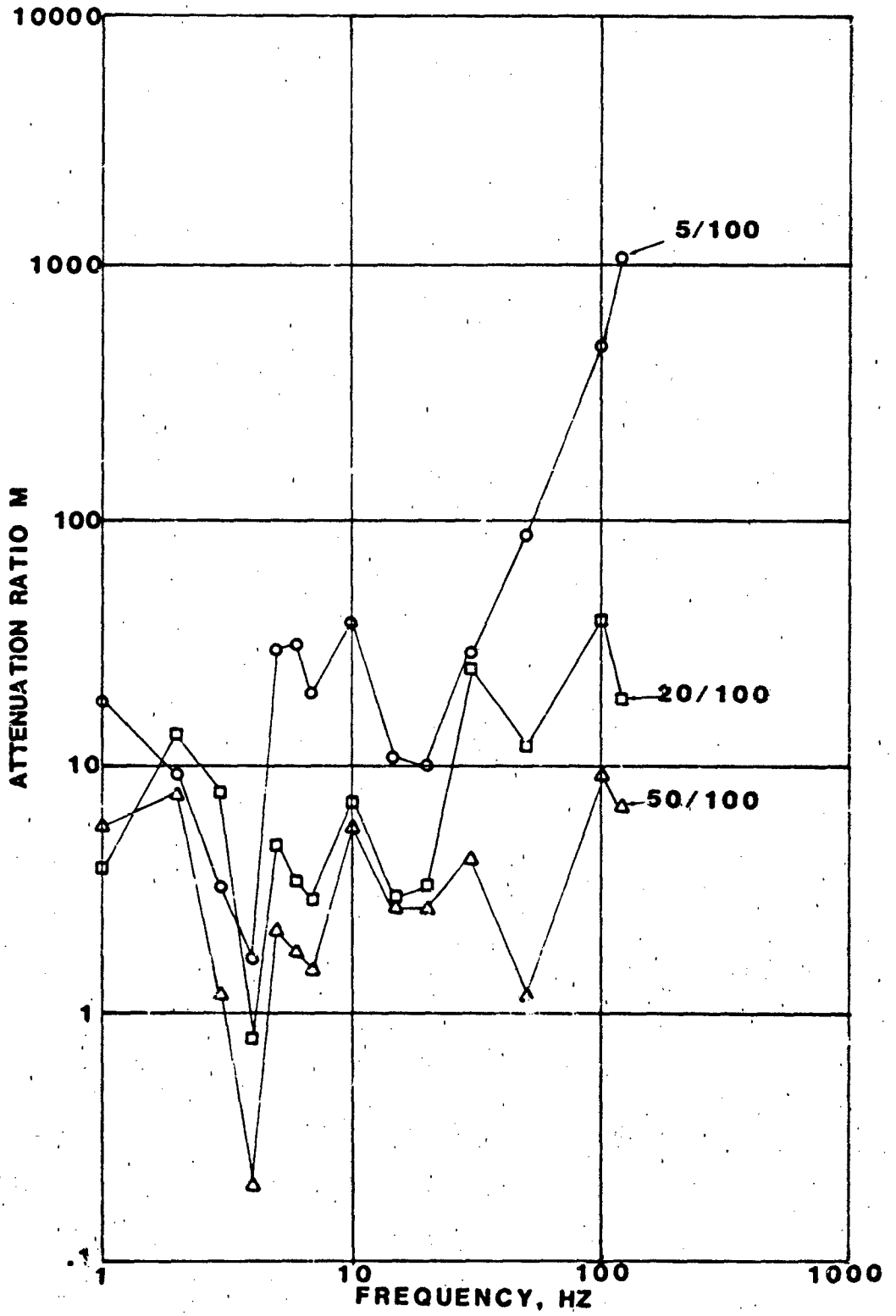

Figure 27. Attenuation ratio M versus frequency for 100-m discrete frequency vibration tests. Numbers indicate location of compared data.

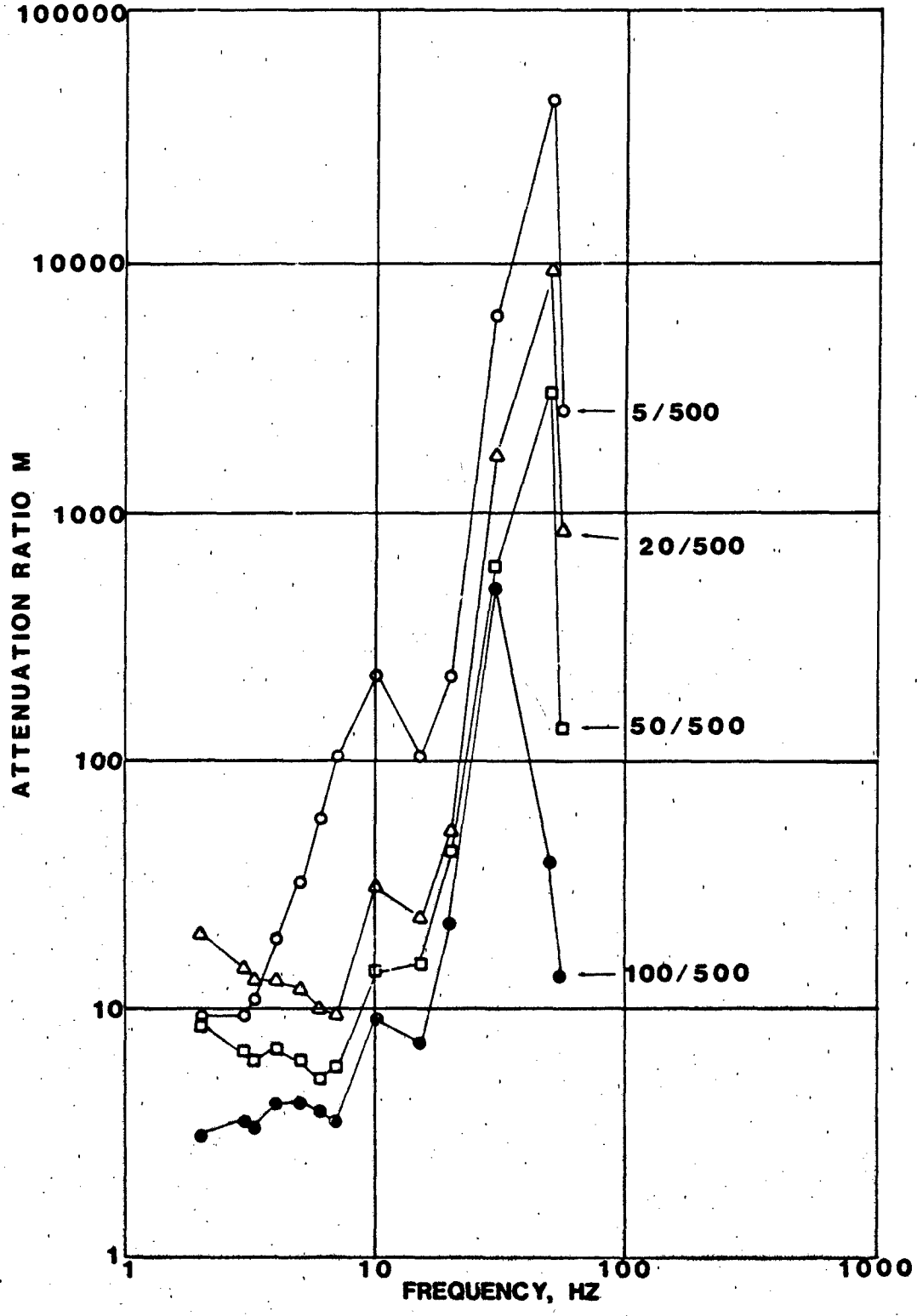

Figure 28. Attenuation ratio M versus frequency for 500-m discrete frequency vibration tests. Numbers indicate locations of compared data.

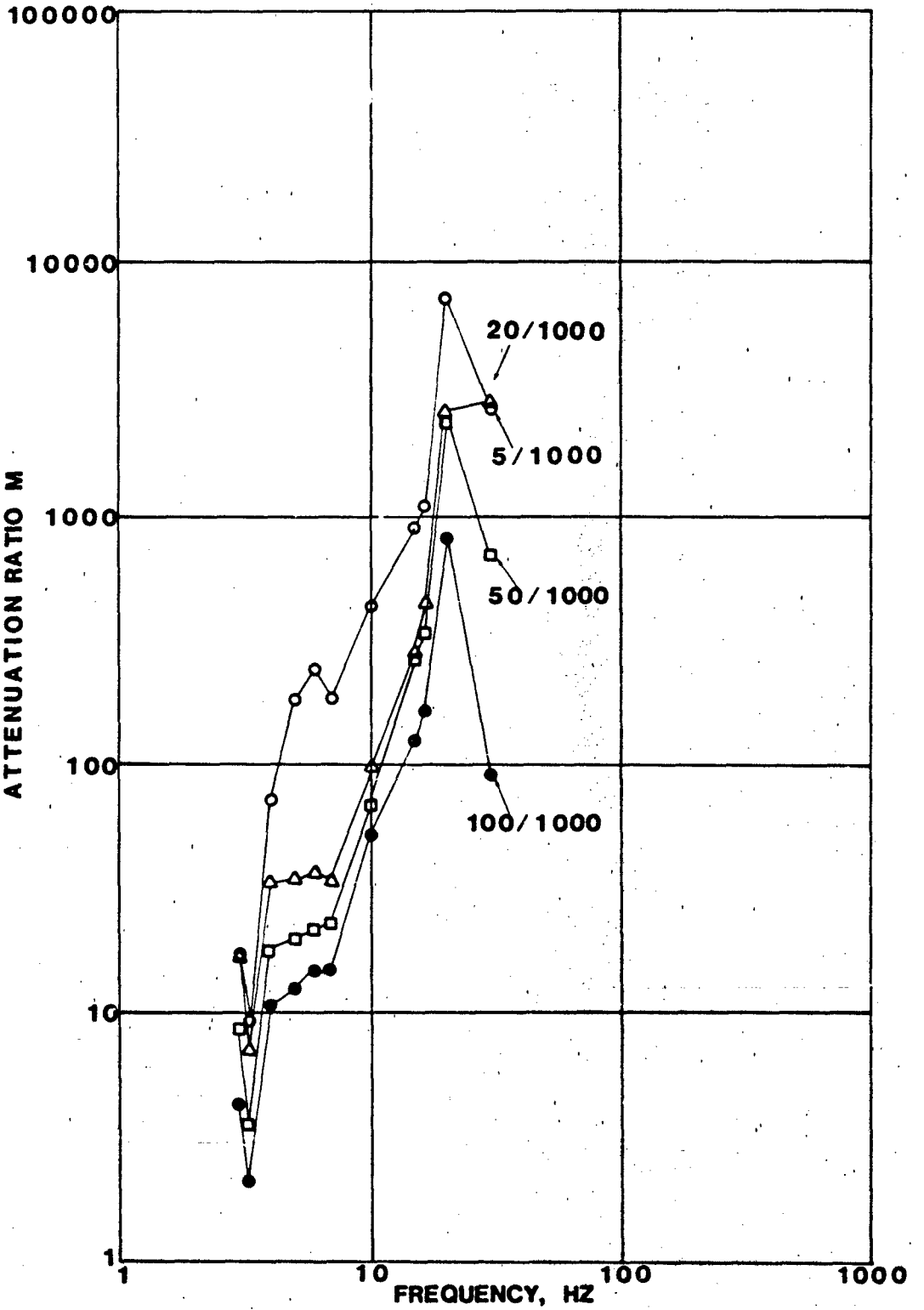

Figure 29. Attenuation ratio M versus frequency for 1-km discrete frequency vibration tests. Numbers indicate locations of compared data.

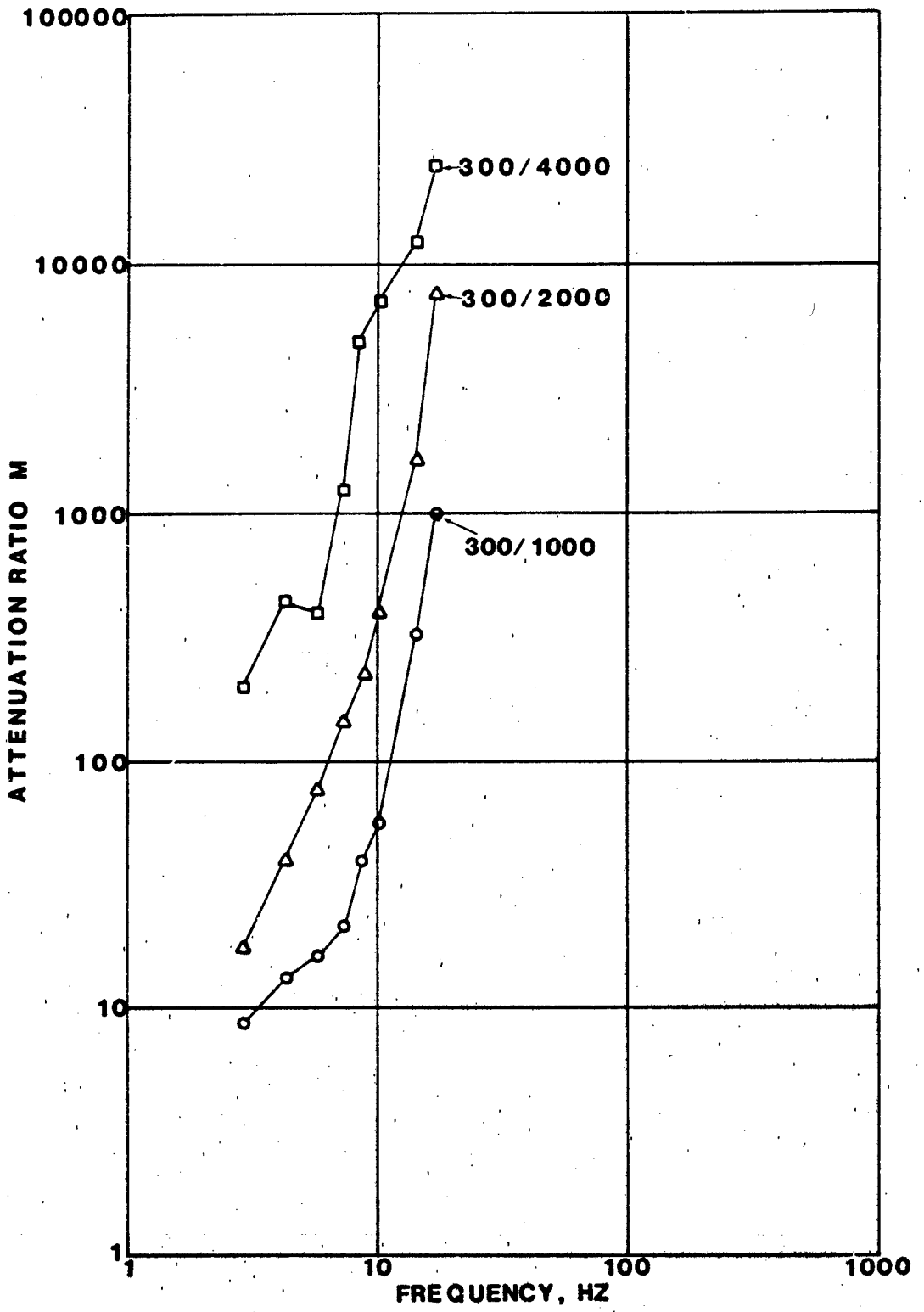

Figure 30. Attenuation M versus frequency for 1-km, 2-km, and 4-km explosive-source test data. Numbers indicate locations of compared data.

vibration tests and the explosive tests using the above equation. The attenuation ratio M can be calculated by the model for an internal damping factor of 0.03 by taking the ratio of transfer function T for two ranges (from Figure 22). The values of M from the field tests were used to calculate new internal damping factors in the model by changing the internal damping factor for each frequency until the proper value of M was achieved. The results are shown in Figures 31-34 plotted against frequency, revealing several observations that can be made from the data. The original estimated internal

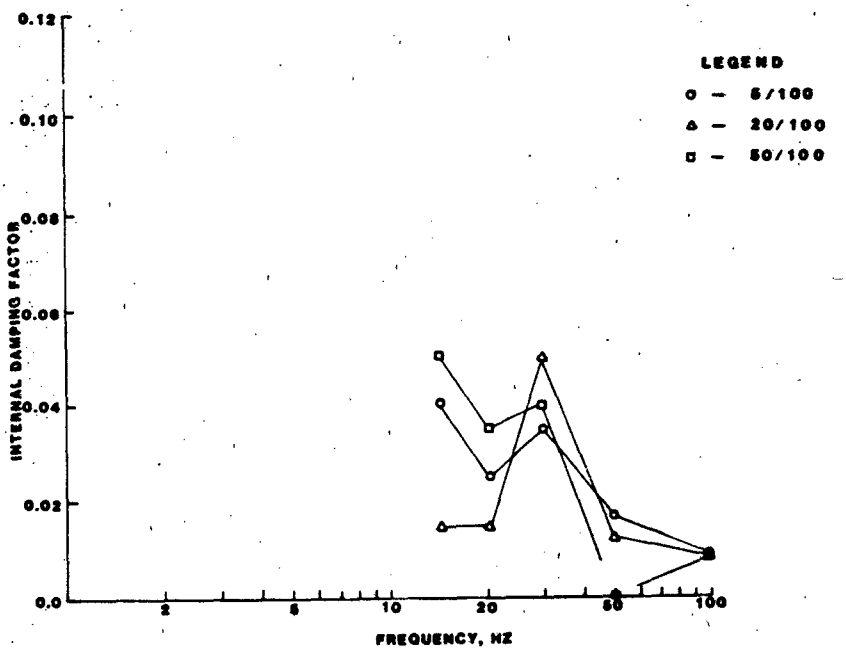

Figure 31. Internal damping versus frequency calculated from attenuation ratio for 100-m discrete frequency vibration data. Numbers indicate location of compared data.

damping factor of 0.03 compares favorably with an average of 0.02 from the field data out to 1.0 km. It should be noted that at short ranges, a large change in internal damping factor produces a small change in M , which means that 0.03 produces M values not unlike those from 0.02. Thus, future calculations for this type of site should include an internal damping factor of 0.02 for ranges up to 1 km. Both M and the internal damping factor become more scattered as the range is decreased; for example, the 100-m and 500-m data curves are more scattered than the 1-km, 2-km, and 4-km data curves.

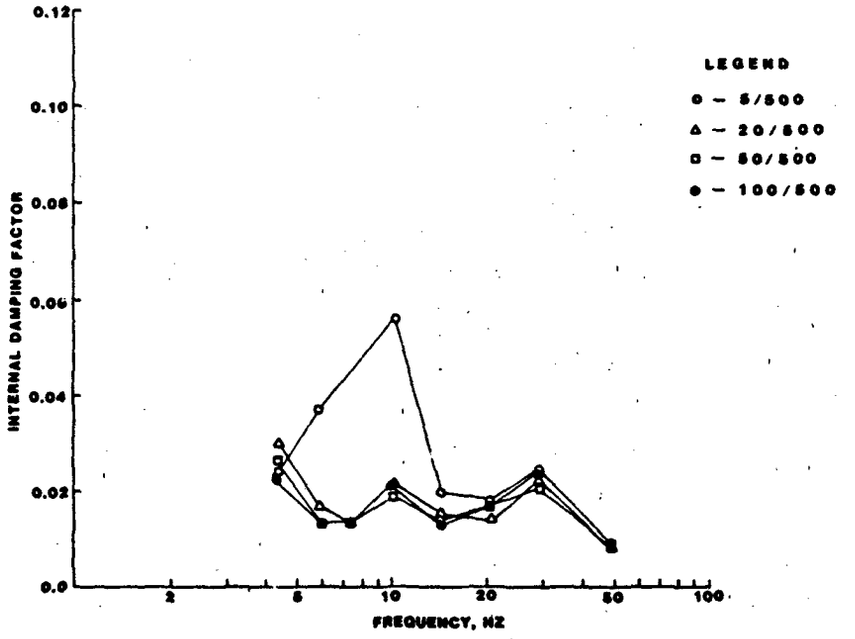

Figure 32. Internal damping factor versus frequency calculated from attenuation ratio for 500-km discrete frequency vibration test data. Numbers indicate locations of compared data.

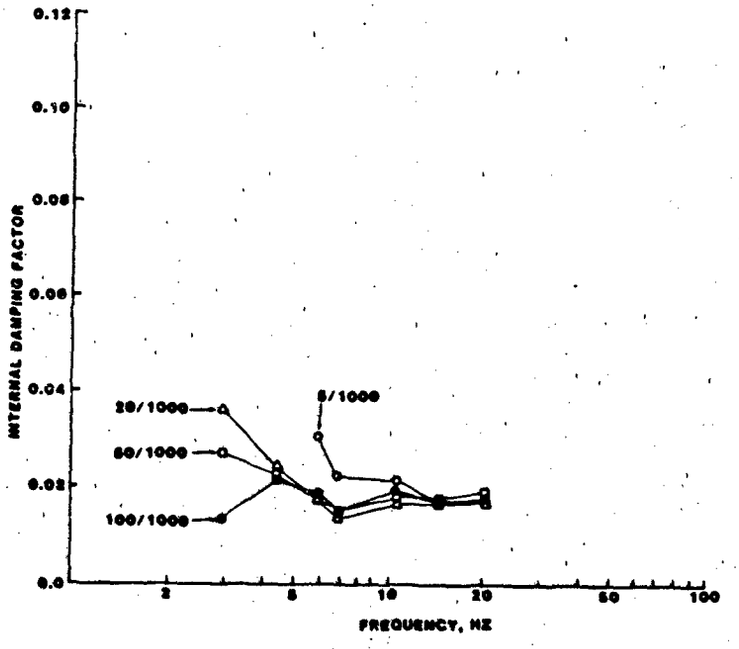

Figure 33. Internal damping factor versus frequency calculated from attenuation ratio for 1-km discrete frequency test data. Numbers indicate locations of compared data.

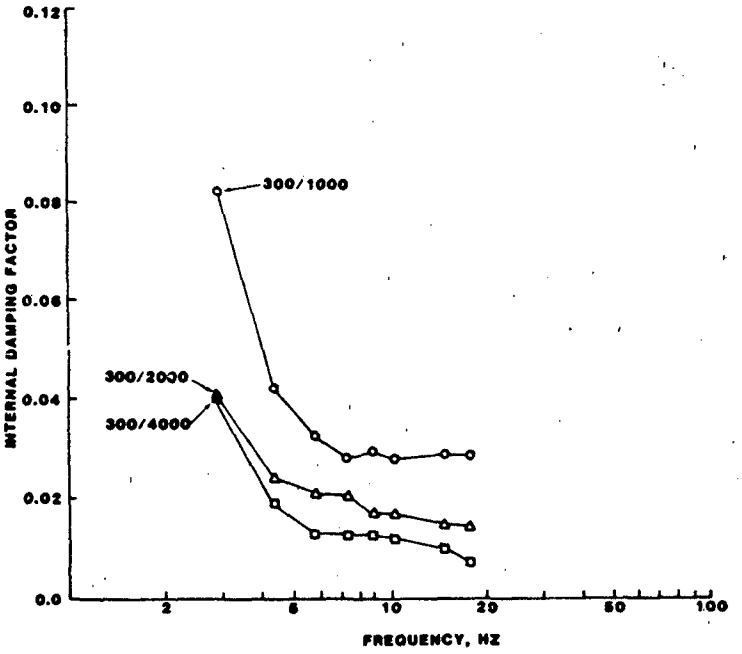

Figure 34. Internal damping factor versus frequency calculated from attenuation ratio for explosive-source test data. Numbers indicate locations of compared data.

This is because at short ranges, small measurement errors in R-wave amplitudes (or noisy signals) cause large changes in M and larger changes in the resultant internal damping factor. The 2-km and 4-km data indicate that the internal damping factor may decrease even below 0.02.

79. To weigh properly the effect of frequency and range on the computed values of internal damping factors, it is appropriate to refer to the procedure used in the WES microseismic wave propagation model to normalize the variables for the transmission coefficient H. In the model, the transmission coefficient for the surface wave varies as a function of kR and the internal damping factor where kR is defined as follows:

$$kR = \frac{2 \pi f R}{V_R}$$

where

f = frequency, Hz

R = range, m

V_R = Raleigh wave velocity, m/sec
k = wave number = $\frac{2\pi}{\lambda}$, m^{-1}

The losses due to the effects of internal damping are in excess of geometric losses due to wave spreading as the waves propagate away from the source. When computations are made to convert field measurements to values of the internal damping factor, it is appropriate to limit these calculations to those data where background noise and measurement errors are less troublesome. Thus, two limits must be defined: (a) the frequencies must be less than those defined as upper limits in the data collection system (i.e., data must have good signal-to-noise ratios) and (b) the frequencies must be greater than those defined by a lower limit where the internal damping factor is significant. If a value for kR is assumed as 30 to define this lower limit, a frequency-range table can be assembled as follows.

Frequency, Hz	Range, m, that must be exceeded for useful internal damping factor calculation results
50	15
20	83
10	172
5	401
2	1815

This table was used to define the lower frequency limits for the results presented in Figures 31-34.

80. The site transfer function is calculated by relating measured peak velocity amplitude at a particular range with the load input by the energy source (Williams 1981).

$$T_k = \frac{L_k}{X_k}$$

where

T_k = transfer function for frequency f_k
L_k = complex amplitude of measured load for frequency f_k

Transfer function T predicted by the model is shown in Figure 22 plotted versus frequency for different ranges and in Figure 23 plotted versus range for different frequencies. The plots of T versus frequency for the impact tests are shown in Figure 35 and for discrete frequency vibrations and explosive tests in Figure 36. Figure 35 shows that the consistency for the field test data is within about 5 db for the 100-m geophone data from each impact test station. The curves compare favorably with the predictions, although the values predicted by the model fall slightly below the field data. It should be noted that the site characteristics input into the model did not account for the depth of bedrock, thus affecting the relative values. The change in internal damping factor would also have a significant effect. Background and electrical noise (60-Hz) affected the explosive test data above to 10 Hz, and no calculation was made for explosive source transfer function above 10 Hz.

81. Overall, the model did well in making predictions. The basic assumptions used in the model were proved out, and the only area in which difference occurred was in the low-frequency realm. The change in site characteristics would adjust this area. The slight adjustment in the internal damping factor would make predictions better at most frequencies and ranges. Site properties are quite important in making model predictions and must be accurate for good predictions (Lundien and Nikodem 1973).

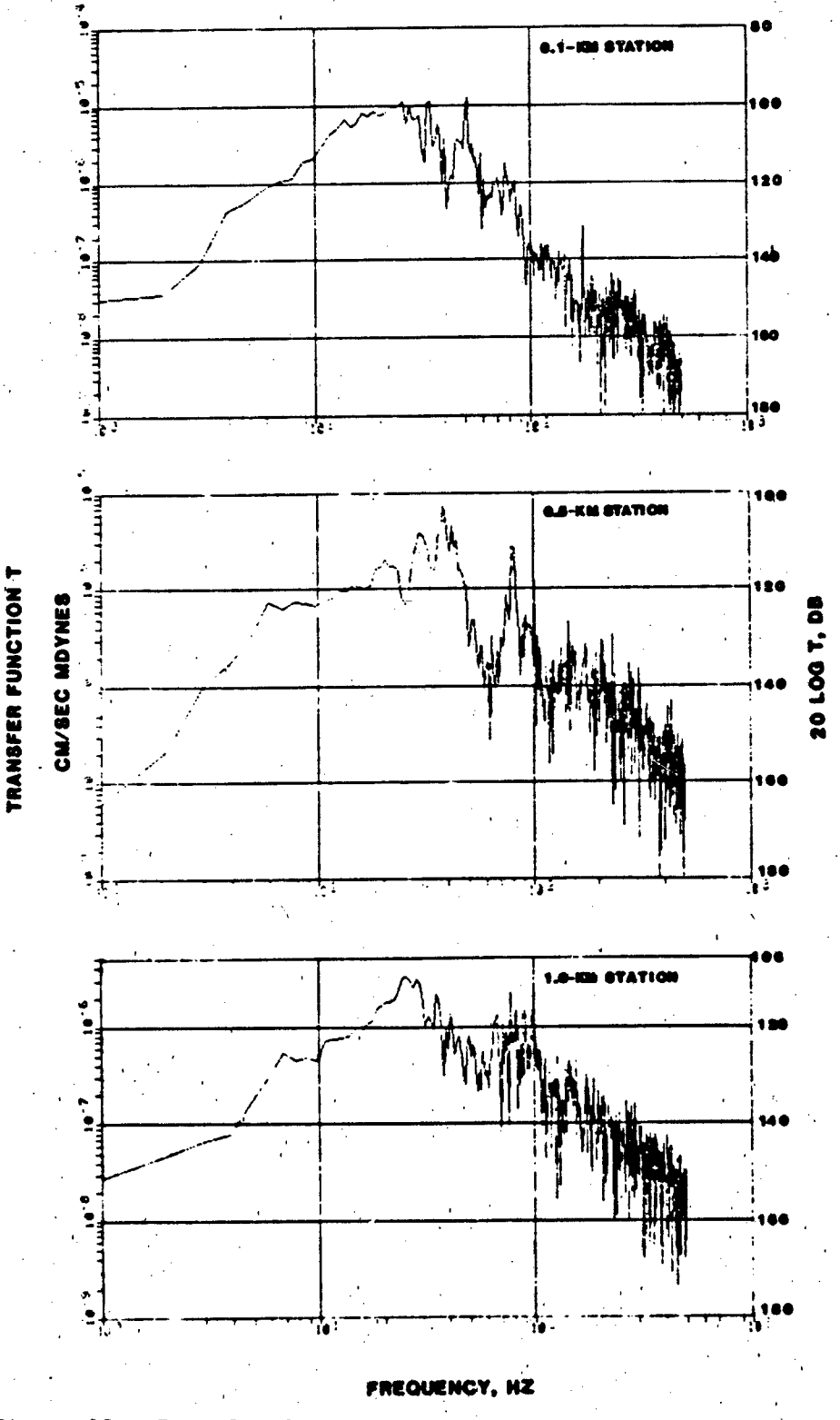

Figure 35. Transfer function calculated for 100-m location of each impact test station to show data consistency

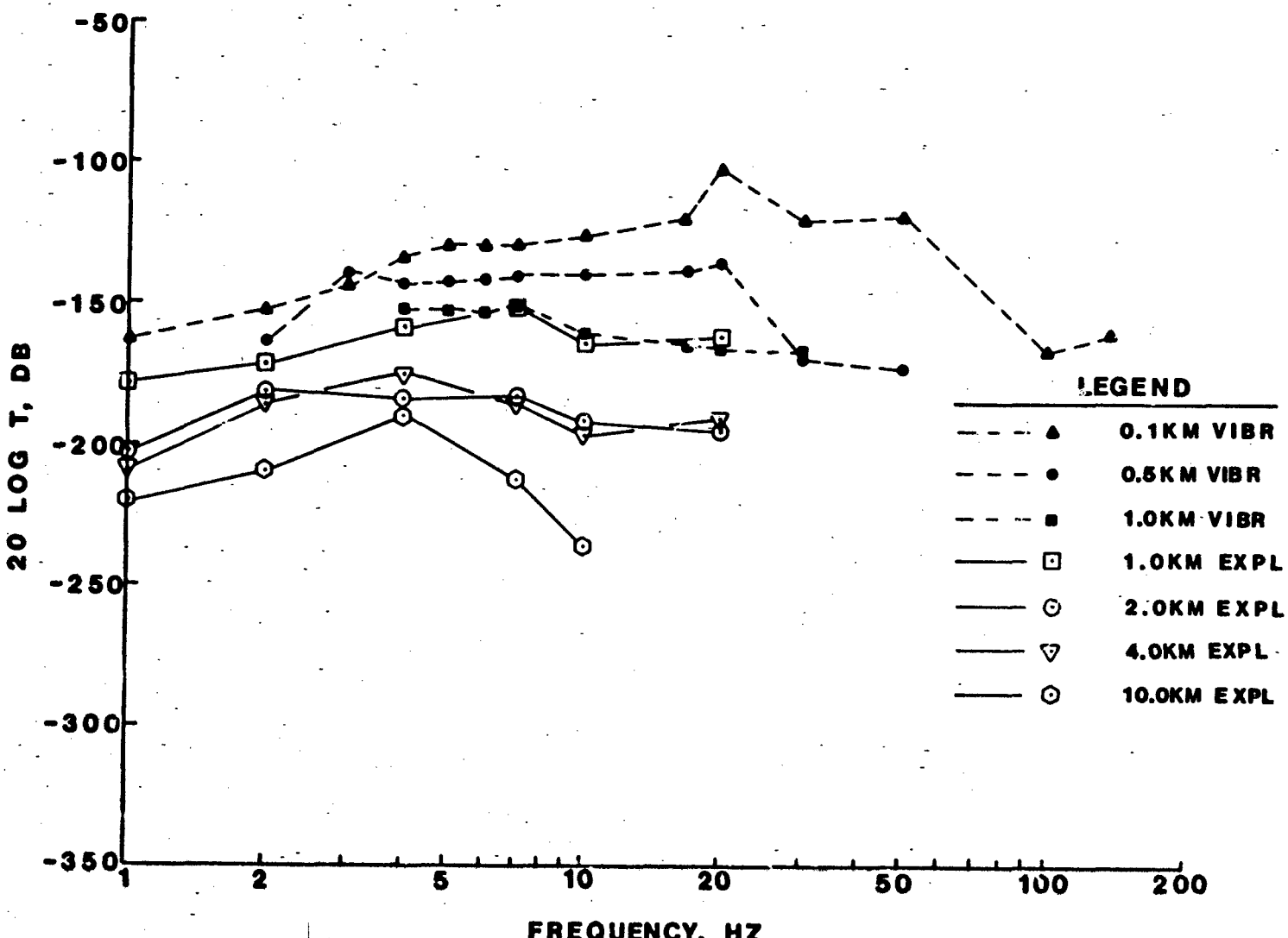

Figure 36. Transfer function T versus frequency calculated for discrete frequency vibration tests (top three curves) and for explosive-source tests

PART VI: CONCLUSIONS AND RECOMMENDATIONS

Conclusions

82. The set of data obtained in this study is relatively complete, encompassing not only close-in measurements using vibratory, impulsive, and vehicular sources, but also far-field impulsive-source measurements covering signal variation in both frequency and range. Although this analysis is limited, several conclusions are evident by observing the data set.

83. Signal amplitude at high frequency falls off rapidly with increasing range (paragraphs 48, 50, 64, 66-67, 70, 72, and 76, and Figures 19 and 26). This is also illustrated by the fact that little or no frequency above 50 Hz was found beyond 100 m, and the frequency sweep tests produced larger amplitudes at smaller frequencies (see Figure 14). Also, only frequencies of about 3 Hz were received at a range of 10 km, and in all the explosive tests, only frequencies below 10 Hz were dominant in the measured signal (Plates 94-98) even though the explosions produced multispectral loading.

84. Measured signal frequencies are accurate within the built-in error of the FFT (about 0.5 Hz in this case) in comparison to the input loading frequencies (paragraph 48). The frequency resolution depends on the length of the record and the stability of the source. Tone bursts produce signals similar to the discrete frequency vibrations except for vibrator-induced anomalies such as "rounding" of the signal, the introduction of harmonics, and the introduction of a large load at the beginning and end of the tone burst. In cases where the vibrator-induced anomalies were insignificant, frequency and amplitude correlate well with the corresponding discrete frequency test results (paragraph 49).

85. Wind noise can be a problem in making seismic measurements. It appears from these tests that for ranges greater than 2 km, wind speeds above 8 m/sec cause a major problem in signal measurement. In fact, when dealing with one sensor, it is difficult even with a spectrum analyzer to determine where the signal is when winds are high and constant and no precise method of timing is furnished (paragraph 73). The use of multiple sensors, triaxial sensors, and a digital system can help to provide signals which can be filtered, cross-sensor correlated, velocity filtered, or otherwise manipulated

to better define the source. Such methods are described by Aki (1981), Allen (1982), Mykkeltveit et al. (1983), and Ringdal and Huseby (1982). However, this type of system would currently be bulky to handle and complicated to operate (Benn and Smith 1975).

86. Electrical noise can also be a problem if a power source introduces 60-Hz noise into the signal. The 60-Hz noise can be filtered out, but the filtering affects the signal characteristics if the test is run above the 60-Hz level. Second and third harmonics of the 60-Hz noise also affect the signal (paragraph 74).

87. The vibration tests conducted at a 10-percent offset frequency to the 3-, 15-, 30-, and 50-Hz discrete frequency tests produced signal results similar to the base frequency tests. The frequency difference is distinguishable to the 3- to 3.3-Hz tests, and the limitation on resolution appears to be in the FFT calculation, although at some point the two frequencies would be difficult to distinguish (paragraph 48).

88. The vehicle produced signals with a low center frequency, and the speed at which it traveled made little difference in signal amplitude. The vehicle did not produce a measurable signal beyond 1 km (paragraph 71).

89. The WES mathematical computer model can make relatively accurate predictions. These tests have verified that the concepts upon which the model is based are correct and that the model's predictions are not only qualitative but also quantitative in most instances. The field tests verified the model calculations of transfer functions, transmission coefficients, and phase velocities. In most cases, the model predicted these values within 20 percent for frequency and range (paragraphs 76-78). Since the test site was relatively homogeneous, the model predictions are quite good and sufficiently accurate for prediction and analysis purposes (paragraphs 76-81). It should be noted that quality predictions come from quality site characteristics. The prediction is only as good as the data on which it is based. The model internal damping factor should be refined somewhat to 0.02 or below, and the site characteristics have been refined through the complete testing (paragraphs 78 and 80).

90. The seismic waves (P, S, and R) measured in these tests confirm the data measured in the seismic refraction tests, and as the range increased, so did the depth of travel and the velocity. This homogeneous, deep overburden

layer helps to disperse the R-wave into bedrock to a low-frequency wave (paragraph 64).

91. It appears from the lateral geophone system data that the high-contrast interface of bedrock was so deep that no enhancement of signal propagation occurred (paragraph 56).

Recommendations

92. The following recommendations are made as a result of the conduct of this study:

a. This data set should be used for further analysis of seismic data. The analysis available to date is by no means complete and should be extended to include pointing angle consistency and correlation with local geology, time of arrival for mode analysis, cross-correlation and coherence between wave types, and extrapolation of results to other sites with known properties.

b. The WES seismic model should be used for predictions in any seismic study of surface wave propagation. This study affirms the basis of the WES model and its predictions, but also confirms that empirical data are valuable in verifying the model. The internal damping factor should be refined to 0.02 or below for the White Sands Missile Range site, and the site input should include a fourth layer to simulate high-velocity bedrock layers where appropriate. The long-range data should be further evaluated with model calculations to determine whether the internal damping factor of below 0.02 will refine predictions for 2- to 10-km ranges. Caution should be exercised in assuming that a particular site can be predicted without preliminary data.

c. When further long-range testing is done, a lateral geophone system should be emplaced with complete instrumentation to accommodate signal analysis.

d. Future tests should incorporate variation in both frequency and range and should include data for as great a range as is practicable.

e. This data set is presented as a generic study so that the results can be applied to a number of related studies. In particular, these results can be applied to site security analyses and activity detection studies.

REFERENCES

Aki, K. 1981. "Attenuation and Scattering of Short-Period Seismic Waves in the Lithosphere," Identification of Seismic Sources - Earthquakes or Underground Explosions, D. Reidel Publishing Company, Dordecht, Holland.

Allen, R. 1982. "Automatic Phase Pickers: Their Present Uses and Future Prospects," Bulletin of the Seismological Society of America, Vol 72.

Benn, B. O., and Smith, P. A. 1975. "A Guide for Collecting Seismic, Acoustic, and Magnetic Data for Multiple Uses," Miscellaneous Paper M-75-2, US Army Engineer Waterways Experiment Station, Vicksburg, Miss.

Carnes, B. L. 1974. An Analysis of Permanent Displacements Resulting from Surface or Near Surface Explosions, Master's Thesis, Mississippi State University, Mississippi State, Miss.

Engdahl, T. L., and West, H. W. 1974. "Effects of Environment on Microseismic Wave Propagation Characteristics in Support of SID Testing at Fort Bragg, North Carolina; Report 2: Comparison of Summer- and Winter-Season Conditions," Technical Report M-73-2, US Army Engineer Waterways Experiment Station, Vicksburg, Miss.

Headquarters, Department of the Army. 1968. "Transportation Reference Data," Field Manual 55-15, Washington, DC.

Headquarters, Department of the Army. 1979. "Geophysical Exploration Engineering and Design," Engineer Manual 1110-1-1802, Washington, DC.

Herland, C. A. 1963. Geophysical Exploration, Hafner, New York.

Lambe, T. W., and Whitman, R. V. 1969. Soil Mechanics, John Wiley & Sons, New York.

Lundien, J. R., and Nikodem, H. 1973. "A Mathematical Model for Predicting Microseismic Signals in Terrain Materials," Technical Report M-73-4, US Army Engineer Waterways Experiment Station, Vicksburg, Miss.

Mykkeltveit, S., et al. 1983. "Seismic Array Configuration Optimization," Bulletin of the Seismological Society of America, Vol 73.

Ringdal, F., and Huseby, E. S. 1982. "Application of Arrays in the Detection, Location, and Identification of Seismic Events," Bulletin of the Seismological Society of America, Vol 72.

Rooke, A. D., Jr., Carnes, B. L., and Davis, L. K. 1974. "Cratering by Explosion: A Compendium and An Analysis," Technical Report N-74-1, US Army Engineer Waterways Experiment Station, Vicksburg, Miss.

US Department of the Interior. 1965. "Geology and Availability of Ground Water in the Northern Part of the White Sands Missile Range and Vicinity, New Mexico," Geological Survey Water-Supply Paper 1801, US Government Printing Office, Washington, DC.

Williams, O. 1981. "Raleigh Wave Velocity Measurements Using Broad Band Frequency Sources," Miscellaneous Paper EL-81-3, US Army Engineer Waterways Experiment Station, Vicksburg, Miss.

Table 1

Summary of Site Characteristics

Station	Cone Penetrometer Tests: Depth cm	Cone Index	Relative Density of Soil (Sand) g/cc
Array	7.5	100	1.5 - 1.6
	15.0	125	1.5 - 1.6
	12.5	142	1.5 - 1.6
	30.0	250	1.6 - 1.7
	37.5	317	1.6 - 1.7
0.1 km	7.5	100	1.5 - 1.6
	15.0	167	1.5 - 1.6
	22.5	133	1.5 - 1.6
	30.0	142	1.5 - 1.6
	37.5	233	1.6 - 1.7
4.0 km	7.5	160	1.5 - 1.6
	15.0	165	1.5 - 1.6
	22.5	160	1.5 - 1.6
	30.0	345	1.6 - 1.7
	37.5	310	1.6 - 1.7
10.0 km	7.5	220	1.6 - 1.7
	15.0	330	1.6 - 1.7
	22.5	600	1.7 - 1.8
	30.0	750+	1.7 - 1.8
	37.5	750+	1.7 - 1.8

Topography
Flat to rolling

Vegetation	Coverage %
Sparse/desert	5
Grass/creosote	10
Yucca/cactus	2

Weather	Date
Snow/calm	5-8 April
Dry/calm	9-10 April
Dry/windy	11-13 April

Station	Moisture Content: Depth, cm	Value, %
0.1 km	0-5	5.4
	15-30	9.9
1.0 km	0-15	6.4
	15-30	7.6

Average Seismic Properties: Depth, m	P-wave Velocity, m/sec
0-6	365-853
6-42.7	853-1525
42.7-91.5	914-2012
91.5+	1890-3292

Table 2

Summary of Mechanical-Source Tests Conducted

Test No.	Frequency Hz	Type*	Date	Time	Test No.	Frequency Hz	Type*	Date	Time
	100-m Station					100-m Station (Cont.)			
1	120	Discrete	4/8/83	1752	37	2	TB 8/8	4/9/83	1134
2	100	↓	↓	1757	38	1	TB 8/8	↓	1138
3	50			1803	39	--	Random noise		1154
4	30			1807	40	--	Random noise		1157
5	20			1810	41	--	Random noise		1159
6	15			1813	42	--	Impactor		1400
7	10			1817	43	--	↓		1405
8	7			1820	44	--			1410
9	6			1825	45	--			1415
10	5			1827	46	--			1420
11	4			1831	47	--	Vehicle slow		1514
12	3			1840	48	--	Vehicle slow		1518
13	2			1851	49	--	Vehicle fast		1522
14	1	↓		1853	50	--	Vehicle fast	↓	1524
15	120+1	Sweep	↓	1911					
16	110	Offset	4/9/83	0958		500-m Station			
17	100	Discrete		1000					
18	55	Offset		1003	52	50+1	Sweep	4/10/83	1126
19	50	Discrete		1006	53	50+1	Sweep	↓	1138
20	16.5	Discrete		1010	54	50	Discrete		1150
21	15	Discrete		1012	55	50	TB 16/128*		1152
22	3.3	Offset		1017	56	55	Offset		1155
23	3.0	Discrete		1019	57	30	Discrete		1200
24	120	TB 32/128		1034	58	30	TB 16/128		1202
25	100	TB 32/128		1039	59	20	Discrete		1206
26	50	TB 16/128		1045	60	20	TB 16/128		1208
27	30	TB 16/128		1048	61	16.5	Offset		1213
28	20	TB 16/128		1052	62	15	Discrete		1215
29	15	TB 16/64		1057	63	15	TB 16/64		1217
30	10	TB 16/32		1104	64	10	Discrete		1220
31	7	TB 16/32		1108	65	10	TB 16/32		1222
32	6	TB 16/32		1111	66	7	Discrete		1228
33	6	TB 8/32		1114	67	7	TB 16/32		1229
34	5	TB 8/16		1119	68	6	Discrete		1233
35	4	TB 8/16		1124	69	6	TB 16/32		1237
36	3	TB 8/16	↓	1129	70	5	Discrete	↓	1242

(Continued)

NOTE: On all vibration, impact, and vehicle tests (except 124-129), data were recorded at both the source and the array.

* Test types are: Discrete - discrete frequency; Sweep - frequency sweep; Offset - offset frequency (selected discrete frequency + 10%); TB - tone bursts (cycles on/cycles off).

Table 2 (Concluded)

Test No.	Frequency Hz	Type*	Date	Time
	500-m Station (Cont.)			
71	5	TB 8/16	4/10/83	1243
72	4	Discrete		1248
73	4	TB 8/16		1249
74	3.3	Offset		1252
75	3	Discrete		1256
76	3	TB 8/8		1258
77	2	Discrete		1301
78	2	TB 8/8		1303
79	--	Random Noise		1358
80	--	Random Noise		1401
81	--	Vehicle Slow		1419
82	--	Vehicle Slow		1422
83	--	Vehicle Fast		1423
84	--	Vehicle Fast		1425
85	--	Impactor		1501
86	--	↓		1502
87	--			1503
88	--			1504
89	--			1505
	1-km Station			
90	30+1	Sweep	4/11/83	0940
91	30+1	Sweep		0950
92	30	Discrete		1002
93	30	TB 16/128		1004
94	20	Discrete		1008
95	20	TB 16/128		1011
96	16.5	Offset		1020
97	15	Discrete		1023
98	15	TB 16/64		1024
99	10	Discrete		1027
100	10	TB 16/32	4/11/83	1028
101	7	Discrete		1033
102	7	Discrete		1035
103	7	TB 16/32		1036
104	6	Discrete		1038
105	6	TB 16/32		1039
106	5	Discrete		1043
107	5	TB 8/16		1046
108	4	Discrete		1050
109	4	TB 8/16		1052
110	3.3	Offset		1055
111	3	Discrete		1057
112	--	Random Noise		1103
113	--	Random Noise		1107
114	--	Impulse		1132
115	--	↓		1134
116	--			1135
117	--			1136
118	--			1137
119	--	Vehicle Fast		1153
120	--	Vehicle Fast		1154
121	--	Vehicle Slow		1155
122	--	Vehicle Slow		1156
	2-km Station			
123	6	Discrete		1354
124	6	TB		1356
125	5	Discrete		1358
126	5	TB		1359
127	20+1	Sweep		1402
128	--	Vehicle Fast		1418
129	--	Vehicle Fast		1420

* Test types are: Discrete - discrete frequency; Sweep - frequency sweep; Offset - offset frequency (selected discrete frequency ± 10%); TB - tone bursts (cycles on/cycles off).

Table 3

Summary of Explosive-Source Tests Conducted

2-km Station

Test No.	Explosive weight, kg	Explosive Charge Location, km	Date	Time
51	12.25	10	4/9/83	1730
130	12.25	10	4/11/83	1642
131	12.25	4	4/11/83	1824
132	12.25	2	4/12/83	1432
133	12.25	1	4/12/83	1602
134	12.25	10	4/13/83	0859
135	12.25	8	4/13/83	1122
136	63.50	10	4/13/83	1421

NOTE: On all test shots (except 51), data were recorded at the source, array, and lateral systems.

Table 4

Peak Amplitudes for Selected Vibration Tests

No.	Frequency Hz	Load at Vibrator mdynes	Source System, cm/sec				Array Geophone Position, cm/sec			Filters* Hz	Air Temp C°	Wind Speed m/sec
			5-m	20-m	50-m	100-m	Vertical	Radial	Transverse			
						100-m Range						
1	120	4.51×10^{2}	2.77×10^{-3}	5×10^{-5}	1.8×10^{-5}	4×10^{-6}	3.30×10^{-6}	1.95×10^{-6}	1.24×10^{-6}	140	4.8	2.2
2	100	6.09×10^{2}	1.68×10^{-3}	1.4×10^{-4}	3.2×10^{-5}	2.6×10^{-6}	2.20×10^{-6}	3.14×10^{-6}	2.11×10^{-6}	120		
3	50	6.93×10^{2}	1.96×10^{-2}	2.6×10^{-3}	2.7×10^{-4}	8.3×10^{-4}	4.23×10^{-4}	1.32×10^{-3}	3.12×10^{-4}	60		
4	30	9.10×10^{2}	8.6×10^{-3}	7.4×10^{-3}	2.3×10^{-3}	8.9×10^{-4}	1.29×10^{-3}	4.53×10^{-3}	8.69×10^{-4}	40		
5	20	7.66×10^{2}	2.0×10^{-2}	6.6×10^{-3}	5.4×10^{-3}	2.5×10^{-3}	2.78×10^{-3}	3.78×10^{-3}	8.73×10^{-4}	40		
6	15	6.95×10^{2}	7.9×10^{-3}	2.2×10^{-3}	2.0×10^{-3}	8.8×10^{-4}	9.00×10^{-4}	7.97×10^{-4}	1.70×10^{-4}	30		
7	10	8.80×10^{2}	5.5×10^{-3}	1×10^{-3}	7.8×10^{-4}	5.6×10^{-4}	1.79×10^{-4}	1.26×10^{-4}	7.55×10^{-6}	30		
8	7	9.55×10^{2}	6.2×10^{-3}	8.9×10^{-4}	4.6×10^{-4}	4×10^{-4}	3.47×10^{-4}	2.03×10^{-4}	7.47×10^{-5}	20		
9	6	8.88×10^{2}	7.8×10^{-3}	8.4×10^{-4}	4.2×10^{-4}	3.3×10^{-4}	2.52×10^{-4}	1.83×10^{-4}	2.69×10^{-5}	20		
10	5	4.85×10^{2}	3.6×10^{-3}	5.7×10^{-4}	2.6×10^{-4}	1.8×10^{-4}	1.33×10^{-4}	9.16×10^{-5}	1.77×10^{-5}	20		
11	4	2.22×10^{2}	6.7×10^{-4}	3.1×10^{-4}	9.5×10^{-5}	6.3×10^{-5}	4.04×10^{-5}	3.25×10^{-5}	1.42×10^{-6}	20	2.0	5.6
12	3	2.35×10	1.1×10^{-4}	2.6×10^{-4}	3.8×10^{-5}	1.9×10^{-5}	3.23×10^{-5}	2.15×10^{-5}	1.85×10^{-6}	10		
13	2	1.04×10^{2}	1.1×10^{-5}	1.6×10^{-5}	9.3×10^{-6}	3×10^{-6}	1.18×10^{-6}	6.93×10^{-7}	3.32×10^{-7}	10		
14	1	1.58×10^{2}	9×10^{-6}	1.8×10^{-6}	2.7×10^{-6}	1.4×10^{-6}	5.76×10^{-7}	2.11×10^{-7}	5.79×10^{-7}	10		
						500-m Range						
54	50	8.7×10^{2}	4.4×10^{-2}	9.8×10^{-3}	3.2×10^{-3}	4.1×10^{-5}	1.90×10^{-6}	3.14×10^{-6}	2.20×10^{-6}	70	16.9	4.2
56	55	9.27×10^{2}	3.3×10^{-2}	1.1×10^{-2}	1.7×10^{-3}	1.7×10^{-4}	2.77×10^{-5}	2.59×10^{-5}	2.74×10^{-5}	70		
57	30	8.76×10^{2}	2.1×10^{-2}	5.8×10^{-3}	2.1×10^{-3}	1.7×10^{-3}	3.17×10^{-6}	2.18×10^{-5}	1.45×10^{-5}	40		
59	20	8.21×10^{2}	1.9×10^{2}	4.4×10^{-3}	3.7×10^{-3}	1.9×10^{-3}	1.41×10^{-4}	1.15×10^{-4}	4.59×10^{-5}	40		
62	15	6.99×10^{2}	7.8×10^{-3}	1.7×10^{-3}	1.1×10^{-3}	5.4×10^{-4}	8.52×10^{-5}	4.10×10^{-5}	1.32×10^{-5}	30		
64	10	5.40×10^{2}	1.2×10^{-2}	1.7×10^{-3}	7.4×10^{-4}	4.9×10^{-4}	5.98×10^{-5}	6.19×10^{-5}	1.29×10^{-5}	30		
66	7	1.02×10^{3}	1.1×10^{-2}	9.9×10^{-4}	6×10^{-4}	3.6×10^{-4}	1.08×10^{-4}	8.84×10^{-5}	1.03×10^{-5}	20		
68	6	8.68×10^{2}	4.1×10^{-3}	7.2×10^{-4}	3.7×10^{-4}	2.7×10^{-4}	6.97×10^{-5}	6.66×10^{-5}	4.82×10^{-6}	20	18.1	5.6
70	5	5.49×10^{2}	1.3×10^{-3}	4.7×10^{-4}	2.5×10^{-4}	1.7×10^{-4}	4.10×10^{-5}	3.56×10^{-5}	2.34×10^{-6}	20		
72	4	2.12×10^{2}	3×10^{-4}	2.1×10^{-4}	1.1×10^{-4}	6.5×10^{-5}	1.55×10^{-5}	1.35×10^{-5}	9.25×10^{-7}	20		
74	3.3	6.09 x 10	9×10^{5}	1.1×10^{-4}	5.1×10^{-5}	2.8×10^{-5}	7.86×10^{-6}	7.39×10^{-6}	7.38×10^{-7}	10		
75	3	4.17 x 10	5.3×10^{-5}	8.3×10^{-5}	3.8×10^{-5}	2.0×10^{-5}	5.25×10^{-6}	4.11×10^{-6}	8.22×10^{-7}	10		
77	2	1.04×10^{2}	9.3×10^{-6}	2×10^{-5}	8.8×10^{-6}	3.1×10^{-6}	8.39×10^{-7}	5.36×10^{-7}	5.95×10^{-7}	10		

*. All filtering was done with a low-pass filter.

Table 4 (Concluded)

No.	Frequency Hz	Load at Vibrator mdynes	Source System, cm/sec 5-m	20-m	50-m	100-m	Array Geophone Position, cm/sec Vertical	Radial	Transverse	Filters* Hz	Air Temp C°	Wind Speed m/sec
						1-km Range						
92	30	9.02×10^{2}	9.7×10^{-3}	9.9×10^{-3}	2.5×10^{-3}	3.2×10^{-4}	4.42×10^{-6}	5.14×10^{-6}	5.45×10^{-6}	40	14.7	9.5
94	20	8.13×10^{2}	7.8×10^{-3}	2.9×10^{-3}	2.6×10^{-3}	9×10^{-4}	3.34×10^{-6}	3.22×10^{-6}	2.02×10^{-6}	40	↓	↓
96	16.5	8.04×10^{2}	5.2×10^{-3}	2.0×10^{-3}	1.6×10^{-3}	7.7×10^{-4}	5.25×10^{-6}	5.27×10^{-6}	2.28×10^{-6}	30		
97	15	7.58×10^{2}	4.1×10^{-3}	1.3×10^{-3}	1.2×10^{-3}	5.8×10^{-4}	4.73×10^{-6}	1.43×10^{-6}	2.14×10^{-6}	30		
99	10	6.05×10^{2}	2.1×10^{-3}	4.8×10^{-4}	3.4×10^{-4}	2.6×10^{-4}	5.17×10^{-6}	1.02×10^{-5}	3.76×10^{-6}	30		
102	7	9.76×10^{2}	4.6×10^{-3}	8.4×10^{-4}	5.7×10^{-4}	3.8×10^{-4}	2.67×10^{-5}	1.45×10^{-5}	3.95×10^{-6}	20	16.1	7.4
104	6	9.07×10^{2}	5.2×10^{-3}	7.8×10^{-4}	4.6×10^{-4}	3.1×10^{-4}	2.21×10^{-5}	2.49×10^{-5}	7.47×10^{-6}	20	↓	↓
106	5	5.62×10^{2}	2.6×10^{-3}	4.9×10^{-4}	2.8×10^{-4}	1.8×10^{-4}	1.55×10^{-5}	1.22×10^{-5}	3.32×10^{-6}	20		
108	4	2.10×10^{2}	4.8×10^{-4}	2.2×10^{-4}	1.2×10^{-4}	7×10^{-5}	5.90×10^{-6}	3.71×10^{-6}	5.10×10^{-6}	20		
110	3.3	5.88×10	1.3×10^{-4}	1×10^{-4}	5×10^{-5}	3×10^{-5}	1.30×10^{-5}	6.65×10^{-6}	3.46×10^{-5}	10		
111	3	1.94×10	8.1×10^{-5}	8×10^{-5}	4×10^{-5}	2×10^{-5}	4.40×10^{-6}	4.87×10^{-6}	2.09×10^{-6}	10	↓	↓

Table 5

Peak Amplitudes for Selected Impulse Tests

Test No.	Range, m	Peak Amplitude: Source: Input mydnes	Peak Amplitude: Source: 50-m cm/sec	Peak Amplitude: Array: Vertical cm/sec	Peak Amplitude: Array: Radial cm/sec	Peak Amplitude: Array: Transverse cm/sec	Filters* Hz	Air Temp °C	Wind Speed m/sec
45	100	1.3×10^{-2}	1.6×10^{-4}	1.1×10^{-4}	1.5×10^{-4}	5.5×10^{-5}	140	17.4	4.4
87	500	2.5×10^{-2}	2.2×10^{-4}	5.1×10^{-6}	5.1×10^{-6}	2.2×10^{-6}	40	21.7	5.3
116	1000	1.5×10^{-3}	1.4×10^{-4}	1.7×10^{-6}	1.7×10^{-6}	1.1×10^{-6}	20	22.2	7.9

* All filtering was done with a low-pass filter.

Table 6

Peak Amplitudes for Selected Explosive Tests

Test No.	Range, m	Peak Amplitude: Source: 100-m cm/sec	Peak Amplitude: Source: 300-m cm/sec	Peak Amplitude: Array: Vertical cm/sec	Peak Amplitude: Array: Radial cm/sec	Peak Amplitude: Array: Transverse cm/sec	Filters* Hz	Air Temp °C	Wind Speed m/sec
131	4 km	1.4×10^{-2}	9.0×10^{-3}	2.0×10^{-5}	1.5×10^{-5}	1.4×10^{-5}	30	18.0	10.6
132	2 km	1.7×10^{-2}	6.0×10^{-3}	1.5×10^{-5}	1.8×10^{-5}	6.8×10^{-6}	40	20.3	10.6
133	1 km	1.7×10^{-2}	5.1×10^{-3}	2.6×10^{-4}	2.3×10^{-4}	8.1×10^{-5}	40	19.2	11.2
134	10 km	2×10^{-2}	4.8×10^{-3}	4.2×10^{-6}	3.4×10^{-6}	1.9×10^{-6}	40	9.1	2.0
135	8 km	1.7×10^{-4}	2×10^{-4}**	7.2×10^{-6}	6.5×10^{-6}	7.1×10^{-6}	30	16.3	4.3
136†	10 km	7.2×10^{-2}	2.2×10^{-3}	5.3×10^{-6}	3.5×10^{-6}	6.0×10^{-6}	30	19.4	3.7

* All filtering was done with a low-pass filter.

** Actual range is 1900 m on the 8-km shot.

† 10-km shot using 63.5 kg of explosive. To scale amplitudes to an equivalent 12.25-kg charge, multiply value by 0.578.

Table 7

Meteorological Data

DATE JULIAN	DATE CALENDAR	LOCAL TIME HOUR	GROUND TEMP		AIR TEMP ABOVE SOIL SURFACE 30 CM	120 CM	RELATIVE HUMIDITY PERCENT	PYRANOMETER ABOVE SOIL SURF 200 CM	WIND SPEED M/SEC	WIND DIRECTION DEG	RAIN GAGE MM
95	5 APR 83	1700	7.236	6.916	-0.683	-1.320	91.70	66.030	3.16	219.50	0
95	5 APR 83	1800	6.267	5.948	-1.480	-1.890	94.40	26.440	2.48	266.40	0
95	5 APR 83	1900	5.218	4.746	-1.990	-2.350	96.40	1.823	2.80	248.50	0
95	5 APR 83	2000	4.311	3.855	-2.320	-2.640	96.60	-0.783	1.90	273.10	0
95	5 APR 83	2100	3.765	3.367	-2.340	-2.650	97.20	-0.824	2.47	264.10	0
95	5 APR 83	2200	3.374	3.039	-2.190	-2.500	97.20	-0.756	3.26	249.90	0
95	5 APR 83	2300	3.040	2.752	-2.280	-2.570	96.60	-0.702	2.85	245.60	0
95	5 APR 83	2400	2.837	2.574	-2.350	-2.630	97.20	-0.783	2.32	259.00	0
96	6 APR 83	100	2.522	2.423	-2.460	-2.690	97.40	-0.783	2.04	262.70	0
96	6 APR 83	200	2.401	2.335	-2.470	-2.700	97.50	-0.783	1.64	269.60	0
96	6 APR 83	300	2.337	2.246	-2.580	-2.790	97.60	-0.783	1.78	222.40	0
96	6 APR 83	400	2.306	2.209	-2.700	-2.870	97.50	-0.607	1.64	255.20	0
96	6 APR 83	500	2.235	2.141	-2.760	-2.950	97.60	-0.796	1.79	226.60	0
96	6 APR 83	600	2.196	2.071	-2.930	-3.100	97.00	-0.243	1.81	237.60	0
96	6 APR 83	700	2.095	2.016	-2.890	-3.150	95.60	19.030	1.05	252.70	0
96	6 APR 83	800	2.575	2.156	-1.650	-2.420	93.70	79.900	1.75	222.10	0
96	6 APR 83	900	3.922	2.644	0.078	-1.470	90.90	244.100	2.40	252.30	2.0
96	6 APR 83	1000	7.007	4.930	2.368	0.190	82.30	450.900	2.18	241.60	0
96	6 APR 83	1100	9.980	8.080	4.007	1.870	70.94	526.300	1.86	227.80	0
96	6 APR 83	1200	11.440	10.240	4.747	2.770	64.43	586.600	1.55	199.30	0
96	6 APR 83	1300	13.040	12.540	5.708	3.500	57.42	527.600	2.47	312.40	0
96	6 APR 83	1400	11.690	11.340	3.609	2.630	59.73	217.400	1.96	135.80	0
96	6 APR 83	1500	10.400	9.870	2.699	1.950	74.29	229.200	1.57	234.10	0
96	6 APR 83	1600	10.620	10.970	6.123	3.810	64.20	510.700	2.19	347.10	0
96	6 APR 83	1700	10.300	11.390	5.257	3.730	54.72	296.200	2.85	296.80	0
96	6 APR 83	1800	9.320	9.620	2.942	2.730	53.08	44.630	2.17	189.70	0
96	6 APR 83	1900	7.802	7.666	1.047	1.910	56.93	8.370	1.49	125.40	0
96	6 APR 83	2000	6.383	6.090	0.156	0.600	71.89	-0.553	2.15	116.00	0
96	6 APR 83	2100	5.222	4.851	-0.456	-0.050	71.52	-0.634	3.07	132.60	0
96	6 APR 83	2200	4.546	4.107	-0.772	-0.350	72.18	-0.621	1.63	136.80	0
96	6 APR 83	2300	4.065	3.587	-1.670	-1.020	76.22	-0.796	0.66	281.80	0
96	6 APR 83	2400	3.759	3.261	-1.420	-1.200	77.54	-0.783	0.89	183.10	0
97	7 APR 83	100	3.597	3.106	-0.725	-0.840	77.64	-0.729	1.73	150.80	0
97	7 APR 83	200	3.420	2.947	-0.805	-0.810	75.39	-0.783	1.52	182.30	0
97	7 APR 83	300	3.337	2.848	-0.974	-0.950	79.14	-0.742	0.82	299.90	0
97	7 APR 83	400	3.216	2.730	-1.240	-1.260	85.20	-0.729	1.44	276.70	0
97	7 APR 83	500	2.977	2.495	-1.550	-1.630	86.60	-0.810	1.67	300.30	0
97	7 APR 83	600	2.833	2.402	-1.370	-1.500	84.90	-0.040	0.74	47.70	0
97	7 APR 83	700	2.768	2.370	-1.470	-1.630	86.30	38.970	1.07	288.60	0
97	7 APR 83	800	3.389	2.729	-0.220	-1.050	89.00	152.300	2.46	222.60	0
97	7 APR 83	900	4.433	3.667	1.208	0	82.10	204.500	2.87	185.40	0
97	7 APR 83	1000	6.265	5.191	3.036	1.370	70.00	311.900	2.72	196.70	0
97	7 APR 83	1100	7.453	6.454	2.359	0.910	80.50	299.400	2.86	202.00	0
97	7 APR 83	1200	8.490	7.397	3.030	1.470	83.70	348.900	1.69	227.40	0
97	7 APR 83	1300	9.660	8.830	4.735	2.820	76.15	451.700	1.67	236.70	0

(Continued)

Table 7 (Continued)

DATE JULIAN	DATE CALENDAR	LOCAL TIME HOUR	GROUND TEMP		AIR TEMP ABOVE SOIL SURFACE 30 CM	120 CM	RELATIVE HUMIDITY PERCENT	PYRANOMETER ABOVE SOIL SURF 200 CM	WIND SPEED M/SEC	WIND DIRECTION DEG	RAIN GAGE MM
97	7 APR 83	1400	10 060	9 430	3 212	2 020	81 40	255 400	2 51	180 40	0
97	7 APR 83	1500	9 580	8 800	2 797	1 900	87 60	259 100	1 84	211 10	0
97	7 APR 83	1600	9 780	8 930	3 024	1 840	82 10	217 300	1 89	201 20	0
97	7 APR 83	1700	9 220	8 480	2 894	2 090	77 87	153 300	2 21	145 20	0
97	7 APR 83	1800	8 270	7 698	1 791	1 350	84 50	88 400	3 49	142 10	0
97	7 APR 83	1900	6 749	6 159	0 009	0 220	86 80	7 456	2 81	160 40	0
97	7 APR 83	2000	5 299	4 574	-1 760	-1 020	93 00	-0 648	1 64	187 50	0
97	7 APR 83	2100	4 167	3 502	-2 490	-1 830	94 10	-0 648	1 38	86 80	0
97	7 APR 83	2200	3 455	3 040	-2 380	-2 040	93 50	-0 661	1 67	37 14	0
97	7 APR 83	2300	3 013	2 712	-3 060	-2 560	94 20	-0 702	1 36	73 19	0
97	7 APR 83	2400	2 640	2 319	-2 840	-2 460	92 10	-0 769	2 40	123 90	0
98	8 APR 83	100	2 440	2 077	-1 680	-1 710	87 20	-0 810	3 01	127 50	0
98	8 APR 83	200	2 324	1 900	-1 650	-1 690	87 30	-0 864	3 34	131 90	0
98	8 APR 83	300	2 292	1 879	-1 560	-1 670	88 00	-0 810	2 68	117 40	0
98	8 APR 83	400	2 168	1 803	-1 580	-1 720	87 70	-0 769	3 55	137 00	0
98	8 APR 83	500	2 023	1 732	-1 620	-1 770	90 00	-0 742	3 36	130 60	0
98	8 APR 83	600	1 950	1 664	-1 540	-1 700	92 30	0 472	3 22	131 50	0
98	8 APR 83	700	1 949	1 632	-1 120	-1 450	94 50	27 710	3 57	132 30	0
98	8 APR 83	800	2 170	1 629	-0 151	-0 950	93 60	136 300	3 60	130 00	0
98	8 APR 83	900	3 668	3 002	2 432	0 910	86 70	307 600	2 67	132 30	0
98	8 APR 83	1000	5 945	5 527	3 535	2 210	76 76	273 600	2 09	153 70	0
98	8 APR 83	1100	8 100	7 341	5 991	3 970	69 10	442 900	2 46	150 20	0
98	8 APR 83	1200	10 180	9 570	8 250	5 990	58 73	758 600	2 78	153 60	0
98	8 APR 83	1300	13 020	12 670	8 810	7 220	49 09	542 000	3 06	147 30	0
98	8 APR 83	1400	10 310	10 470	2 101	2 100	80 60	128 900	3 49	304 90	0
98	8 APR 83	1500	9 440	9 750	5 164	3 050	93 10	523 700	2 88	161 70	1 0
98	8 APR 83	1600	10 570	11 340	5 652	4 450	83 20	307 600	2 19	147 90	0
98	8 APR 83	1700	10 060	10 840	5 472	4 800	74 56	212 800	2 22	153 30	0
98	8 APR 83	1800	8 850	9 440	4 304	3 920	83 00	102 000	4 73	134 20	0
98	8 APR 83	1900	7 014	7 223	1 644	2 040	90 70	13 980	5 56	125 80	0
98	8 APR 83	2000	5 417	5 402	0 467	0 950	94 30	-0 540	5 95	126 00	0
98	8 APR 83	2100	4 373	4 297	0 093	0 510	95 70	-0 648	4 86	116 80	0
98	8 APR 83	2200	3 639	3 531	0 041	0 490	95 50	-0 648	4 88	122 50	0
98	8 APR 83	2300	3 103	2 973	-0 086	0 390	95 30	-0 688	4 33	116 40	0
98	8 APR 83	2400	29 000	2 588	0 119	0 680	94 00	-0 783	5 15	122 40	0
99	9 APR 83	100	2 563	2 492	-0 077	0 460	93 80	-0 661	4 39	120 80	0
99	9 APR 83	200	2 307	2 315	-0 625	-0 030	93 80	-0 810	3 40	107 90	0
99	9 APR 83	300	2 137	2 064	-1 140	-0 570	94 30	-0 634	3 11	102 80	0
99	9 APR 83	400	1 961	1 813	-1 670	-1 110	94 50	-0 607	3 09	103 50	0
99	9 APR 83	500	1 799	1 598	-1 820	-1 310	94 80	-0 742	3 13	102 60	0
99	9 APR 83	600	1 681	1 414	-2 020	-1 530	95 20	3 498	3 16	102 80	0
99	9 APR 83	700	1 495	1 208	0 065	0 540	91 60	107 700	2 50	98 40	0
99	9 APR 83	800	2 375	1 329	4 593	2 970	82 40	326 100	3 10	120 20	0
99	9 APR 83	900	6 077	3 331	8 450	6 460	62 24	539 700	3 82	126 20	0
99	9 APR 83	1000	10 040	7 436	11 120	8 980	53 40	674 400	3 78	130 50	0

(Continued)

Table 7 (Continued)

DATE JULIAN	DATE CALENDAR	LOCAL TIME HOUR	GROUND TEMP		AIR TEMP ABOVE SOIL SURFACE 30 CM	AIR TEMP ABOVE SOIL SURFACE 120 CM	RELATIVE HUMIDITY PERCENT	PYRANOMETER ABOVE SOIL SURF 200 CM	WIND SPEED M/SEC	WIND DIRECTION DEG	RAIN GAGE MM
99	9 APR 83	1100	13 500	11 450	13 330	11 520	41 20	807 000	2 46	112 00	0
99	9 APR 83	1300	15 060	15 040	15 530	13 780	26 05	921 000	2 14	94 80	0
99	9 APR 83	1200	17 290	13 770	17 360	15 940	19 62	881 000	3 20	208 10	0
99	9 APR 83	1400	17 260	18 270	15 660	14 560	26 90	447 000	4 36	125 90	0
99	9 APR 83	1500	16 630	17 220	14 170	15 070	24 09	423 200	4 11	141 20	0
99	9 APR 83	1600	15 760	17 510	19 080	17 230	20 30	578 800	3 19	142 50	0
99	9 APR 83	1700	15 570	18 780	18 970	17 590	15 92	375 500	3 17	222 30	0
99	9 APR 83	1800	14 420	16 340	16 760	16 440	16 26	163 900	2 79	202 20	0
99	9 APR 83	1900	12 770	13 910	11 740	13 280	26 18	17 460	2 83	104 00	0
99	9 APR 83	2000	10 940	11 760	9 430	10 290	38 30	-0 337	3 72	93 10	0
99	9 APR 83	2100	9 660	10 240	9 000	9 830	37 13	-0 432	3 83	96 10	0
99	9 APR 83	2200	8 760	9 200	7 781	8 750	40 24	-0 364	3 39	96 50	0
99	9 APR 83	2300	7 892	8 170	5 240	6 350	46 75	-0 459	2 66	98 60	0
99	9 APR 83	2400	7 018	7 130	3 000	4 470	53 01	-0 445	1 97	93 00	0
100	10 APR 83	100	6 250	6 336	3 832	4 580	54 29	-0 688	2 53	97 50	0
100	10 APR 83	200	5 695	5 709	2 534	3 910	57 04	-0 621	2 31	84 10	0
100	10 APR 83	300	5 108	5 060	0 683	1 780	69 98	-0 580	2 31	84 90	0
100	10 APR 83	400	4 580	4 514	1 562	2 180	74 96	-0 688	3 11	78 83	0
100	10 APR 83	500	4 228	4 140	1 525	2 530	69 26	-0 661	2 76	91 10	0
100	10 APR 83	600	3 832	3 734	1 512	1 970	72 99	4 363	3 07	92 20	0
100	10 APR 83	700	3 990	3 672	5 357	4 970	61 17	114 400	3 13	101 00	0
100	10 APR 83	800	6 321	4 833	11 650	10 290	43 72	337 900	3 64	124 30	0
100	10 APR 83	900	9 650	7 527	14 310	12 310	35 78	554 100	3 90	133 60	0
100	10 APR 83	1000	13 150	11 010	17 060	14 950	26 78	725 600	4 25	143 10	0
100	10 APR 83	1100	16 670	14 840	18 920	16 890	21 06	860 000	4 24	132 10	0
100	10 APR 83	1200	19 160	17 860	20 000	18 090	19 18	934 000	5 56	129 20	0
100	10 APR 83	1300	20 900	20 180	20 870	19 350	16 48	911 000	5 85	125 20	0
100	10 APR 83	1400	21 490	21 170	22 430	20 610	14 25	859 000	6 20	176 40	0
100	10 APR 83	1500	21 790	22 020	23 350	21 370	13 70	750 600	5 29	170 70	0
100	10 APR 83	1600	20 590	21 660	22 330	20 910	13 93	540 700	6 46	164 10	0
100	10 APR 83	1700	19 080	20 690	21 670	20 450	14 06	393 100	7 16	138 40	0
100	10 APR 83	1800	17 500	18 920	19 400	19 190	14 48	169 100	5 67	151 40	0
100	10 APR 83	1900	15 720	16 470	14 030	15 380	16 48	15 830	4 05	129 20	0
100	10 APR 83	2000	13 880	14 310	12 270	13 090	18 08	-0 405	3 45	109 60	0
100	10 APR 83	2100	12 550	12 840	10 630	12 030	19 58	-0 445	3 08	110 10	0
100	10 APR 83	2200	11 390	11 350	8 470	9 860	23 34	-0 513	2 50	96 50	0
100	10 APR 83	2300	10 470	10 560	10 170	10 980	23 33	-0 459	4 13	116 70	0
100	10 APR 83	2400	9 950	10 120	10 790	11 550	21 78	-0 769	4 36	106 90	0
101	11 APR 83	100	9 560	9 710	10 070	11 600	21 28	-0 648	5 00	110 00	0
101	11 APR 83	200	9 220	9 410	10 810	12 010	20 75	-0 378	5 34	141 30	0
101	11 APR 83	300	8 830	9 020	10 620	11 790	20 48	-0 567	4 86	162 10	0
101	11 APR 83	400	8 400	8 680	10 070	11 180	20 32	-0 688	4 63	171 00	0
101	11 APR 83	500	8 100	8 400	9 670	11 070	21 30	-0 648	4 14	174 50	0
101	11 APR 83	600	7 691	7 980	8 190	9 300	24 24	5 308	3 90	172 30	0
101	11 APR 83	700	7 703	7 766	11 410	11 280	21 92	121 600	5 72	170 00	0

(Continued)

Table 7 (Continued)

DATE JULIAN	DATE CALENDAR	LOCAL TIME HOUR	GROUND TEMP		AIR TEMP ABOVE SOIL SURFACE 30 CM	120 CM	RELATIVE HUMIDITY PERCENT	PYRANOMETER ABOVE SOIL SURF 200 CM	WIND SPEED M/SEC	WIND DIRECTION DEG	RAIN GAGE MM
101	11 APR 83	800	9 830	8 830	14 770	13 580	19 88	346 400	9 22	183 90	0.
101	11 APR 83	900	12 840	10 810	16 570	14 650	18 20	567 400	9 45	188 60	0.
101	11 APR 83	1000	16 060	13 380	18 480	16 080	16 39	733 600	7 36	186 20	0
101	11 APR 83	1100	19 230	15 960	19 800	17 270	15 28	866 000	7 02	203 60	0.
101	11 APR 83	1200	21 660	18 320	21 180	18 460	14 66	965 000	7 38	202 80	0.
101	11 APR 83	1300	22 230	19 460	20 240	18 430	14 57	674 700	7 86	206 40	0
101	11 APR 83	1400	22 800	20 150	21 320	19 420	14 23	760 000	9 00	213 20	0
101	11 APR 83	1500	22 290	20 190	21 220	19 490	14 20	763 400	10 64	222 70	0
101	11 APR 83	1600	21 380	20 150	19 970	18 500	14 56	592 500	11 14	227 50	0
101	11 APR 83	1700	19 680	19 150	18 220	17 070	15 12	392 300	10 63	227 60	0
101	11 APR 83	1800	17 880	17 500	15 440	14 970	15 96	168 000	9 76	231 90	0
101	11 APR 83	1900	15 880	15 [illegible]	11 920	12 510	16 98	16 870	7 30	237 20	0
101	11 APR 83	2000	14 060	13 740	9 350	10 250	18 81	-0 405	4 97	250 90	0
101	11 APR 83	2100	12 550	12 230	5 791	7 420	22 32	-0 432	2 49	196 80	0
101	11 APR 83	2200	11 170	10 860	4 209	5 620	23 52	-0 580	2 57	220 20	0
101	11 APR 83	2300	9 940	9 660	1 846	3 410	30 04	-0 540	2 01	45 74	0
101	11 APR 83	2400	8 780	8 480	1 091	2 170	38 33	-0 621	2 09	92 30	0
102	12 APR 83	100	7 880	7 574	1 812	3 410	33 69	-0 594	1 80	138 40	0
102	12 APR 83	200	7 103	6 844	0 721	2 280	36 13	-0 661	2 43	121 50	0
102	12 APR 83	300	6 452	6 210	0 123	1 310	40 89	-0 783	1 99	100 70	0
102	12 APR 83	400	5 821	5 596	-1 220	-0 300	50 97	-0 594	2 62	76 98	0.
102	12 APR 83	500	5 247	5 040	-1 730	-0 740	56 14	-0 715	2 17	76 72	0.
102	12 APR 83	600	4 740	4 518	-2 130	-1 190	64 41	5 943	2 06	69 49	0
102	12 APR 83	700	4 089	4 380	2 917	2 550	59 03	103 000	1 33	37 19	0
102	12 APR 83	800	7 162	5 541	9 720	7 950	39 58	333 800	1 14	223 50	0.
102	12 APR 83	900	11 120	8 290	13 290	10 820	27 62	547 000	2 65	213 00	0.
102	12 APR 83	1000	15 010	11 490	15 140	12 200	21 41	718 400	5 89	206 30	0
102	12 APR 83	1100	18 190	14 330	16 610	13 490	18 82	878 000	5 84	196 00	0.
102	12 APR 83	1200	20 080	16 640	16 530	13 890	18 45	762 400	6 29	194 90	0.
102	12 APR 83	1300	20 330	17 380	16 910	14 510	17 30	707 500	7 60	187 90	0.
102	12 APR 83	1400	20 700	18 100	17 590	15 570	15 96	764 100	10 64	201 00	0.
102	12 APR 83	1500	20 260	18 080	16 720	14 810	16 42	638 600	11 66	204 80	0
102	12 APR 83	1600	19 210	17 650	15 110	13 450	18 11	530 400	11 21	210 40	0.
102	12 APR 83	1700	17 790	16 750	12 670	11 340	20 60	356 700	9 82	229 70	0.
102	12 APR 83	1800	15 960	15 280	10 130	9 620	21 22	139 200	8 65	234 80	0
102	12 APR 83	1900	14 080	13 360	7 369	7 660	23 43	16 180	5 60	238 60	0.
102	12 APR 83	2000	12 630	11 930	6 179	6 560	22 06	-0 445	5 12	209 20	0.
102	12 APR 83	2100	11 170	10 610	2 662	4 010	26 19	-0 486	2 89	210 30	0
102	12 APR 83	2200	9 790	9 250	0 534	2 160	32 97	-0 540	1 77	202 10	0.
102	12 APR 83	2300	8 630	8 110	0 410	1 110	39 40	-0 607	2 24	181 50	0
102	12 APR 83	2400	8 040	7 590	-0 122	0 760	42 76	-0 594	2 34	200 30	0.
103	13 APR 83	100	7 115	6 748	-1 700	-0 640	49 31	-0 675	2 23	197 00	0.
103	13 APR 83	200	6 464	6 051	-1 090	-0 590	52 16	-0 702	2 62	195 50	0.
103	13 APR 83	300	5 769	5 552	-0 965	-0 150	48 79	-0 702	3 41	227 40	0
103	13 APR 83	0	5 013	4 878	-2 310	-1 210	50 35	-0 688	2 27	166 60	0

(Continued)

Table 7 (Concluded)

DATE JULIAN	DATE CALENDAR	LOCAL TIME HOUR	GROUND TEMP		AIR TEMP ABOVE SOIL SURFACE 30 CM	120 CM	RELATIVE HUMIDITY PERCENT	PYRANOMETER ABOVE SOIL SURF 200 CM	WIND SPEED M/SEC	WIND DIRECTION DEG	RAIN GAGE MM
103	13 APR 83	500	4 295	4 110	-3 800	-1 850	52 23	-0 742	1 36	142 00	0
103	13 APR 83	600	3 630	3 402	-4 270	-3 240	59 78	6 078	1 86	108 10	0
103	13 APR 83	700	3 516	3 162	-1 800	-2 140	61 10	71 450	1 50	109 30	0
103	13 APR 83	800	5 208	4 117	4 438	2 640	42 50	315 400	1 93	221 70	0
103	13 APR 83	900	9 100	6 570	7 867	5 220	32 07	563 400	1 94	326 10	0
103	13 APR 83	1000	13 040	10 070	10 160	7 180	25 46	723 400	2 26	355 20	0
103	13 APR 83	1100	16 340	13 290	11 120	7 880	22 91	834 000	4 31	233 20	0
103	13 APR 83	1200	18 430	15 260	11 380	8 710	21 66	803 000	4 74	269 00	0
103	13 APR 83	1300	19 530	16 830	12 130	9 300	20 90	783 500	4 43	267 70	0
103	13 APR 83	1400	19 050	17 340	9 830	8 490	21 72	303 200	3 77	271 90	0
103	13 APR 83	1500	16 910	15 450	8 300	6 660	38 94	439 200	2 98	189 80	0
103	13 APR 83	1600	16 170	15 290	8 290	7 750	26 63	140 900	2 61	111 10	0
103	13 APR 83	1700	14 670	13 380	5 878	5 710	41 40	87 100	4 29	53 49	0
103	13 APR 83	1800	12 630	12 070	6 469	6 460	41 03	72 060	2 13	78 55	0
103	13 APR 83	1900	11 030	10 870	3 991	4 840	46 24	14 730	2 67	87 90	0
103	13 APR 83	2000	9 840	9 420	2 610	3 190	54 61	-0 661	3 37	107 10	0
103	13 APR 83	2100	8 600	8 240	1 229	2 010	61 10	-0 567	2 88	128 70	0
103	13 APR 83	2200	7 608	7 256	0 276	1 200	60 87	-0 688	2 29	104 60	0
103	13 APR 83	2300	6 866	6 522	-0 569	-0 190	73 57	-0 648	2 04	78 89	0
103	13 APR 83	2400	6 484	6 109	-0 260	-0 770	71 31	-0 783	1 83	92 90	0
104	14 APR 83	100	5 712	5 381	-3 210	-2 170	60 20	-0 648	1 85	70 95	0
104	14 APR 83	200	4 894	4 604	-2 300	-2 430	86 50	-0 702	1 94	93 10	0
104	14 APR 83	300	4 746	4 420	-0 414	-0 660	84 20	-0 769	1 67	78 63	0
104	14 APR 83	400	4 854	4 685	0 020	0 510	80 10	-0 783	1 72	60 61	0
104	14 APR 83	500	4 970	4 334	-1 520	-1 020	84 10	-0 702	1 81	64 32	0
104	14 APR 83	600	4 241	4 009	-2 540	-1 370	85 70	6 240	1 16	43 69	0
104	14 APR 83	700	4 216	3 979	1 882	0 940	82 90	133 000	1 17	86 60	0
104	14 APR 83	800	6 557	4 761	6 665	5 040	54 53	309 900	2 18	239 90	0

(Concluded)

Table 8

Signal Characteristics

Type of Test	Range m	Peak FFT Amplitude cm/sec	Center Frequency Hz	Bandwidth* Hz
Random noise	100	2×10^{-4}	25.0	10.0
	500	1×10^{-6}	15.0	15.0
	1000	6×10^{-6}	4.6	1.5
Frequency sweep	100	4×10^{-3}	23.2	7.0
	500	2.2×10^{-4}	16.7	1.7
	1000	3×10^{-5}	8.0	6.0
Vehicle (16 km/hr)	100	5.6×10^{-5}	12.0	7.2
	500	1.8×10^{-5}	2.9	2.4
	1000	1.4×10^{-5}	2.9	3.4
Impulse	100	1.1×10^{-4}	24.0	12.0
	500	5.1×10^{-6}	13.0	1.5
	1000	1.7×10^{-6}	8.0	4.0
Explosive (12.25 kg)	1000	2.6×10^{-4}	7.2	3.7
(12.25 kg)	2000	2×10^{-5}	3.9	1.5
(12.25 kg)	4000	1.5×10^{-5}	3.6	1.0
(12.25 kg)	10000	4.2×10^{-6}	3.3	1.0
(63.5 kg)	10000	4.0×10^{-6}	3.2	0.6
Background noise (seismic)	0/500**	1.2×10^{-6}	72.0	37.0
	95/100	$.8 \times 10^{-4}$	61.0	1.5
	495/500**	5×10^{-4}	48.0	2.5
	900/1000	1.2×10^{-4}	10.0	20.0
	800/1000	1×10^{-4}	5.0	15.0
Background noise (acoustic)	0/500**	1.3×10^{-1} †	8.0	14.0
	50/100	7×10^{-1} †	5.0	11.0
	450/500**	10	5.0	9.0
	0/1000	3.8×10^{3}	4.0	6.0

NOTE: Background noise test shows location measured/location of test. 0 = measured at array; others measured 5 m or 50 m from source.

* Width of band described by points 6 db down from the peak amplitude (at one-half the peak amplitude).

** Engines running (vibrator, impactor, and generator).

† Units are dynes/cm^2.

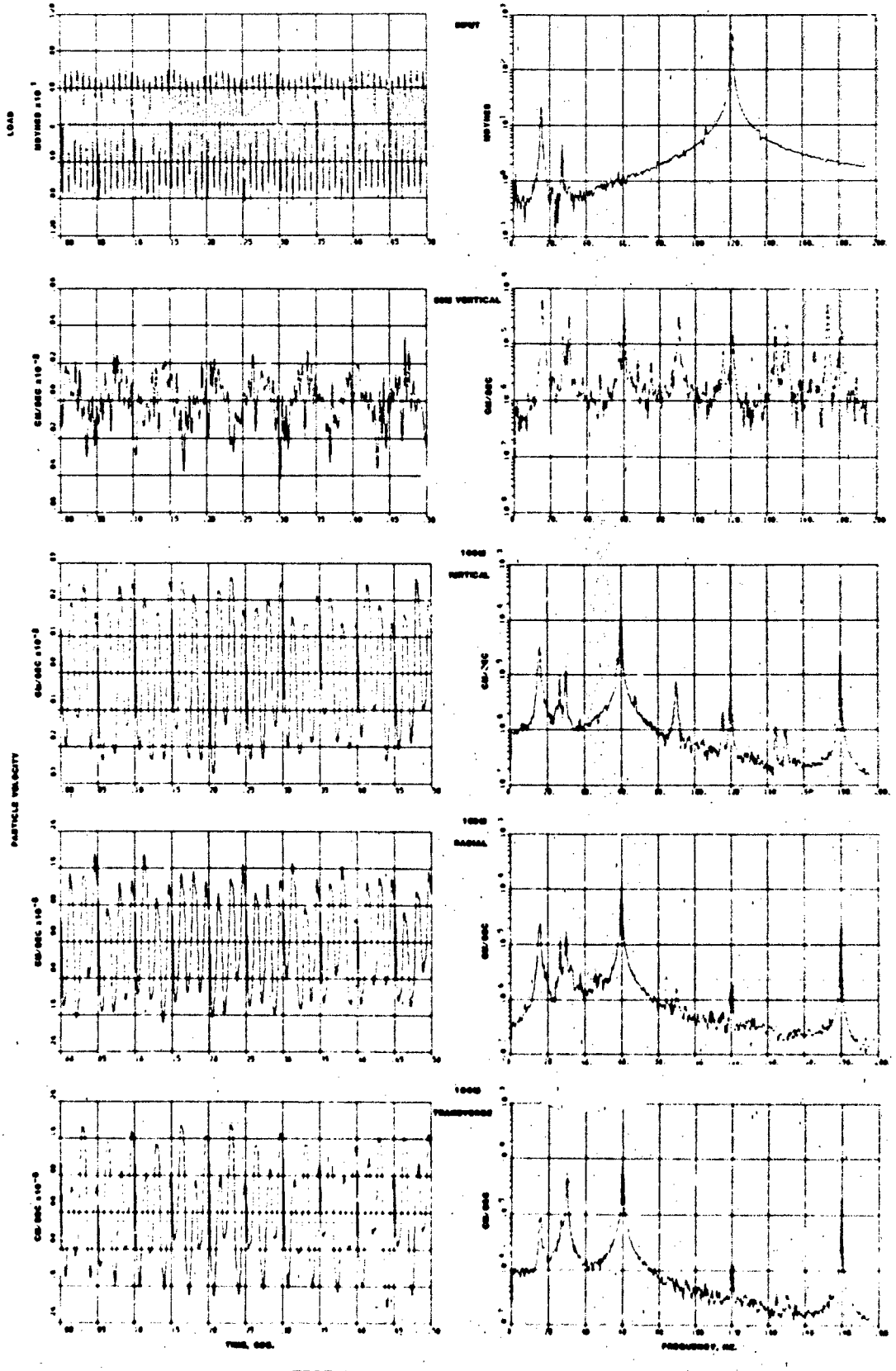

TEST 1 120HZ DISCRETE FREQUENCY SINE WAVE

PLATE 1

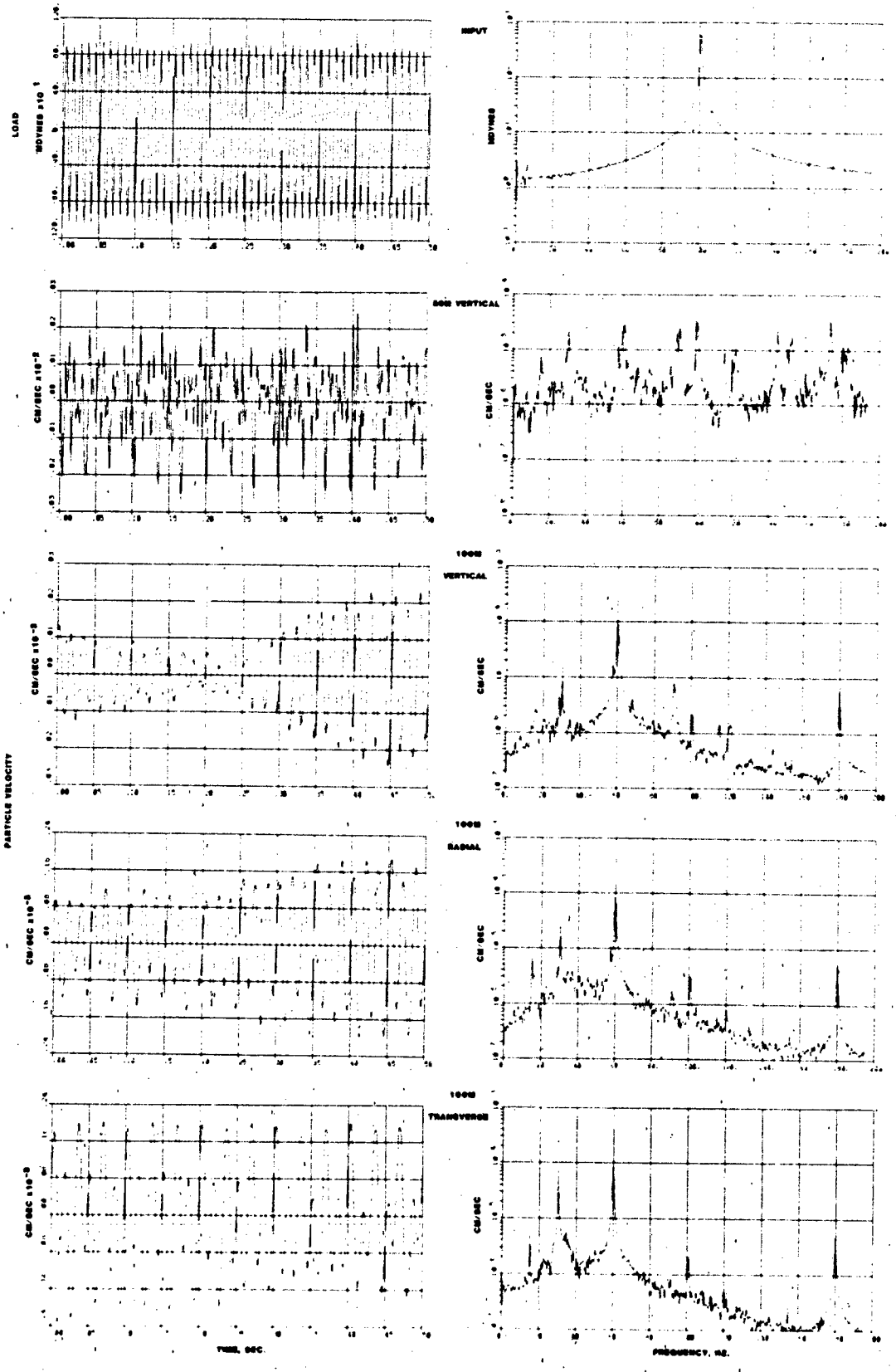

PLATE 2

TEST 2 100HZ DISCRETE FREQUENCY SINE WAVE

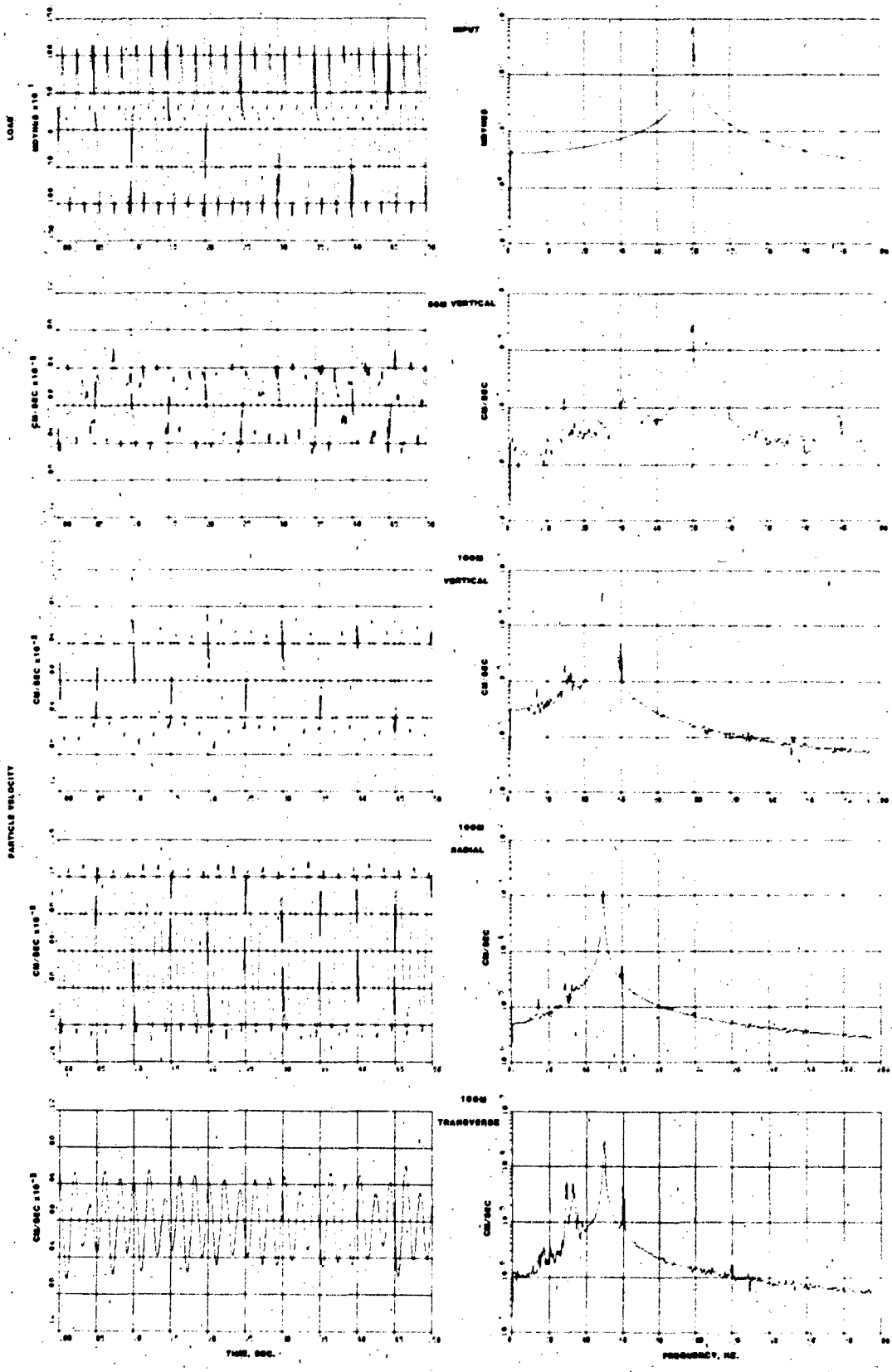

TEST 3 50HZ DISCRETE FREQUENCY SINE WAVE

PLATE 3

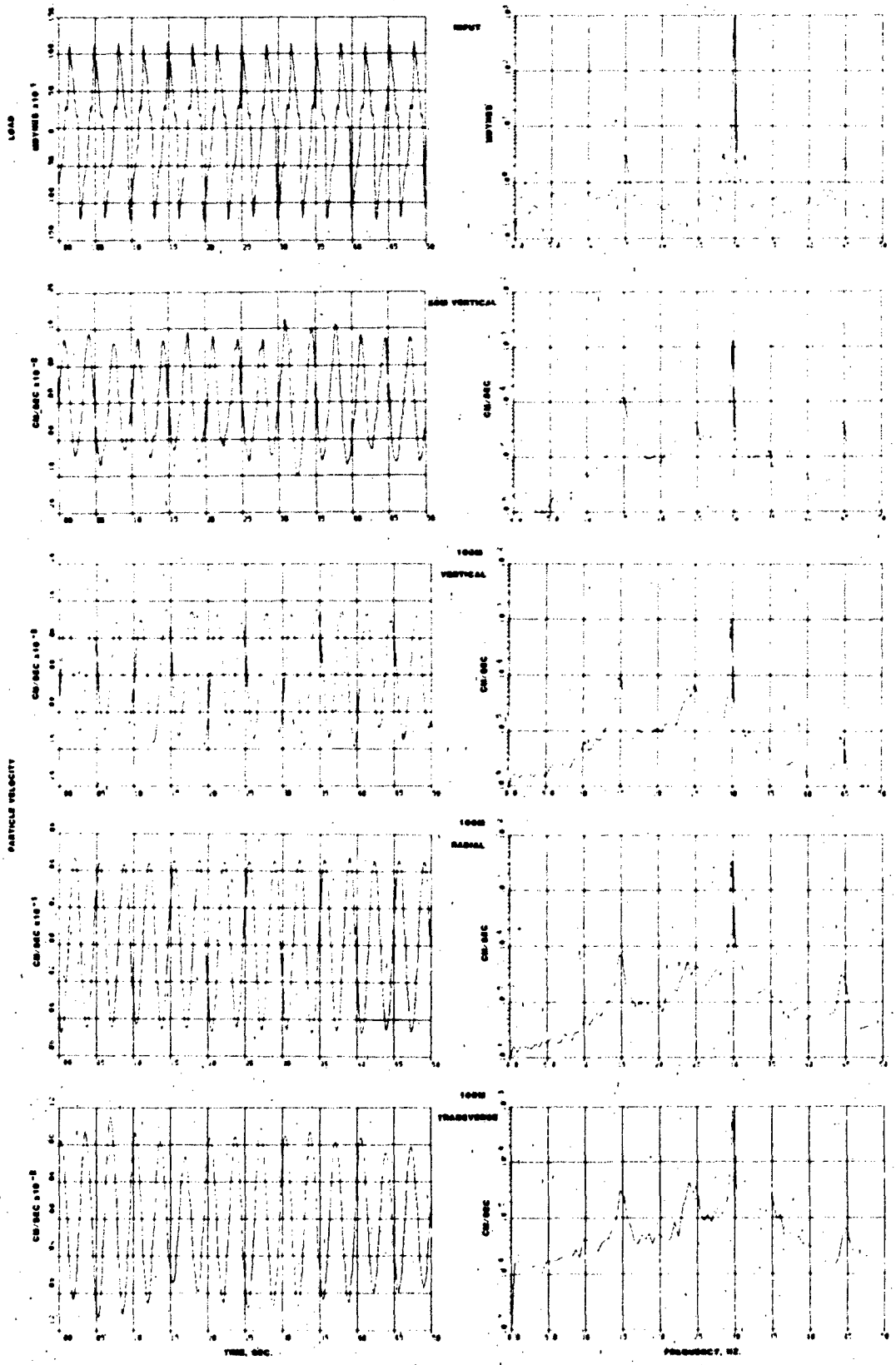

TEST 4 30HZ DISCRETE FREQUENCY SINE WAVE

PLATE 4

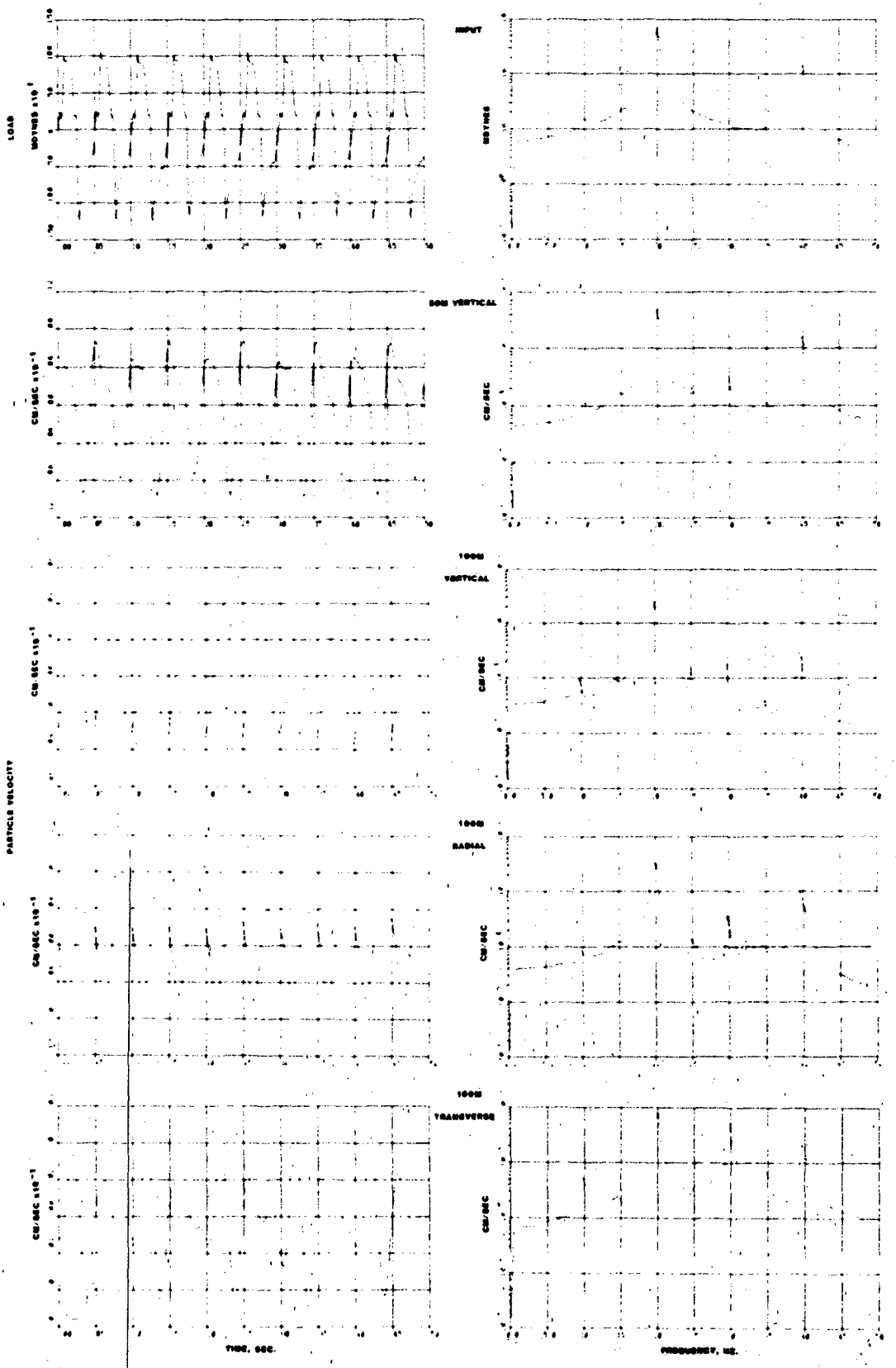

TEST 5 20HZ DISCRETE FREQUENCY SINE WAVE

PLATE 5

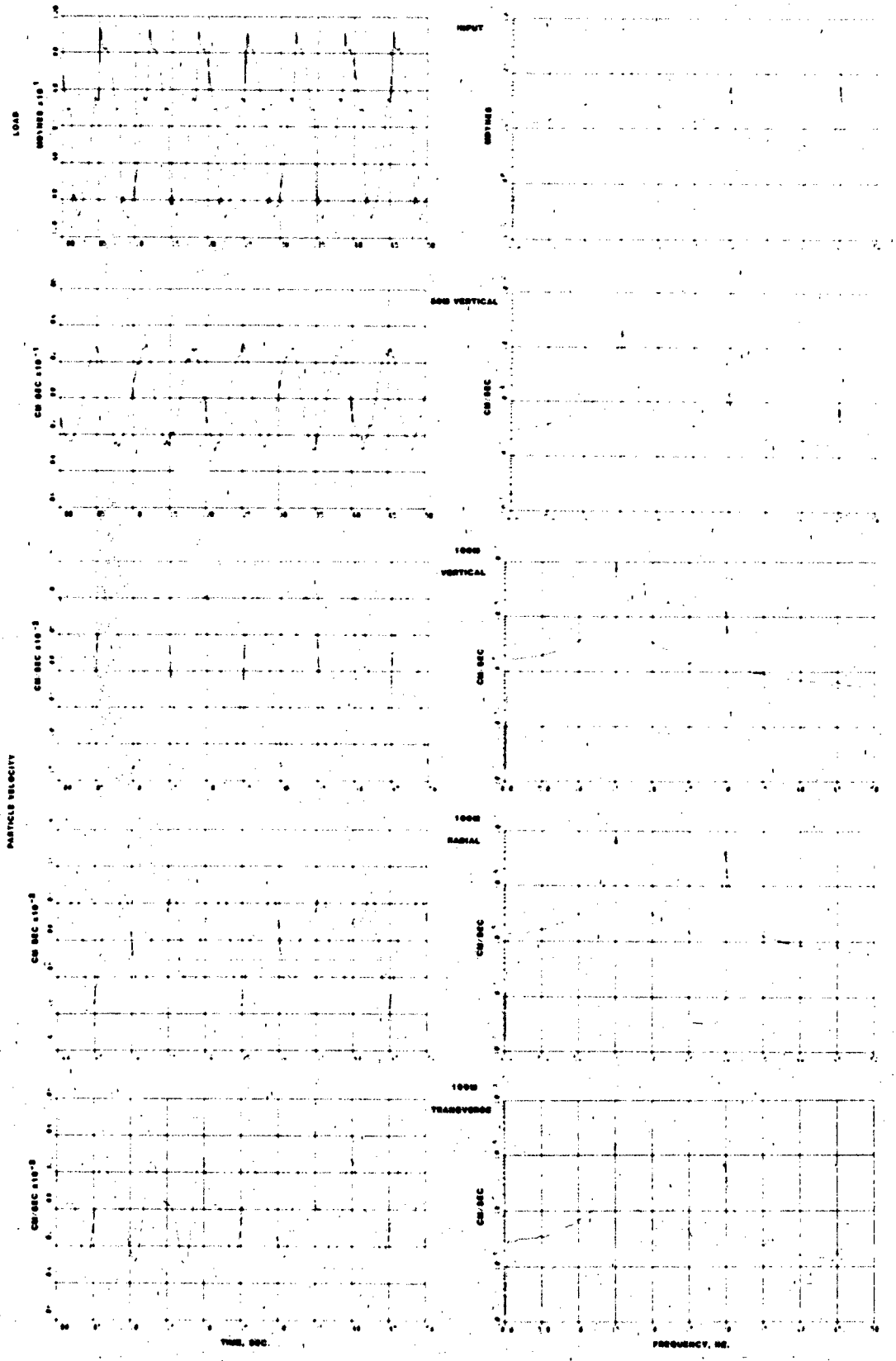

TEST 6 15HZ DISCRETE FREQUENCY SINE WAVE

PLATE 6

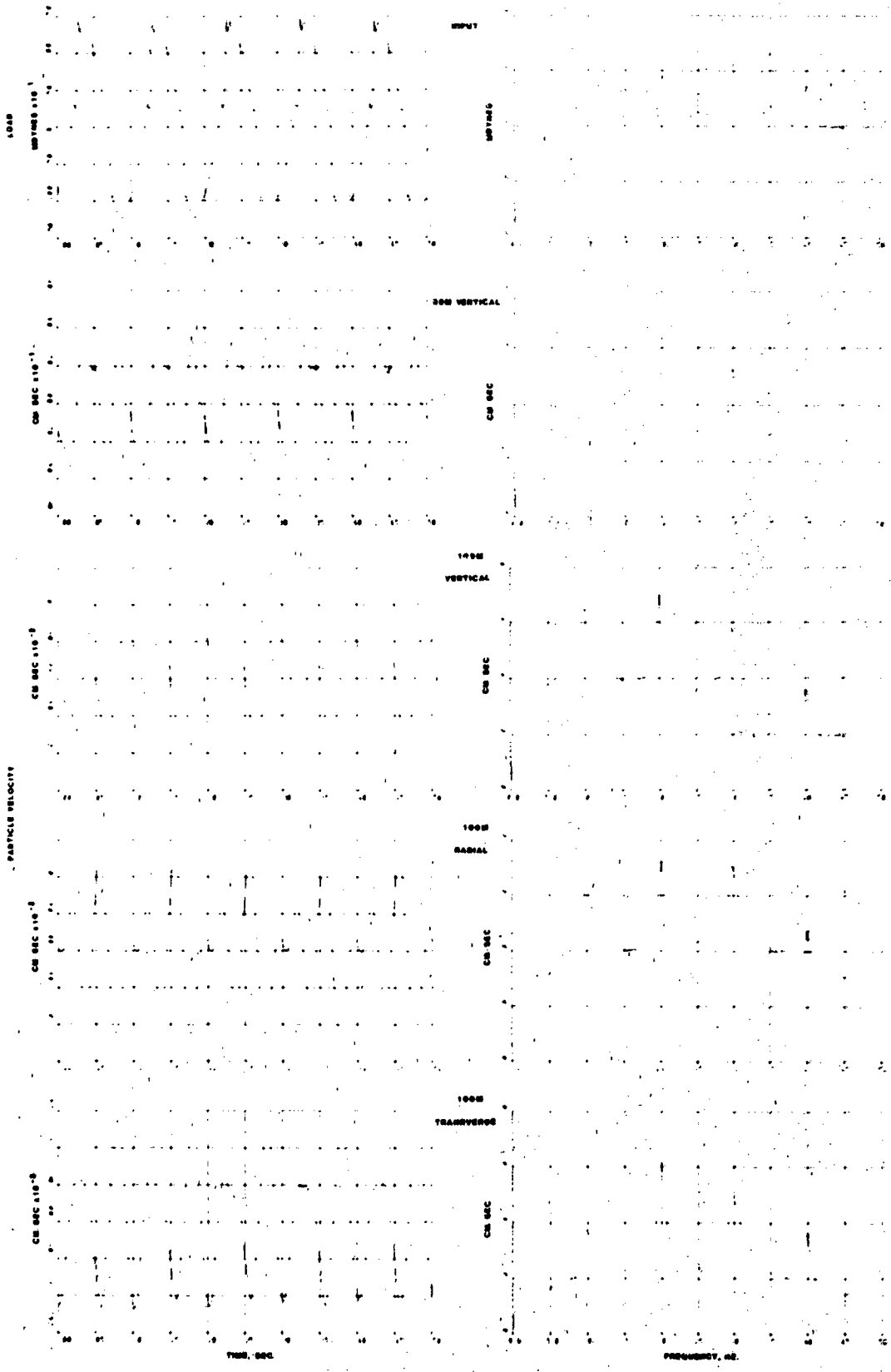

TEST 7 10HZ DISCRETE FREQUENCY SINE WAVE

PLATE 7

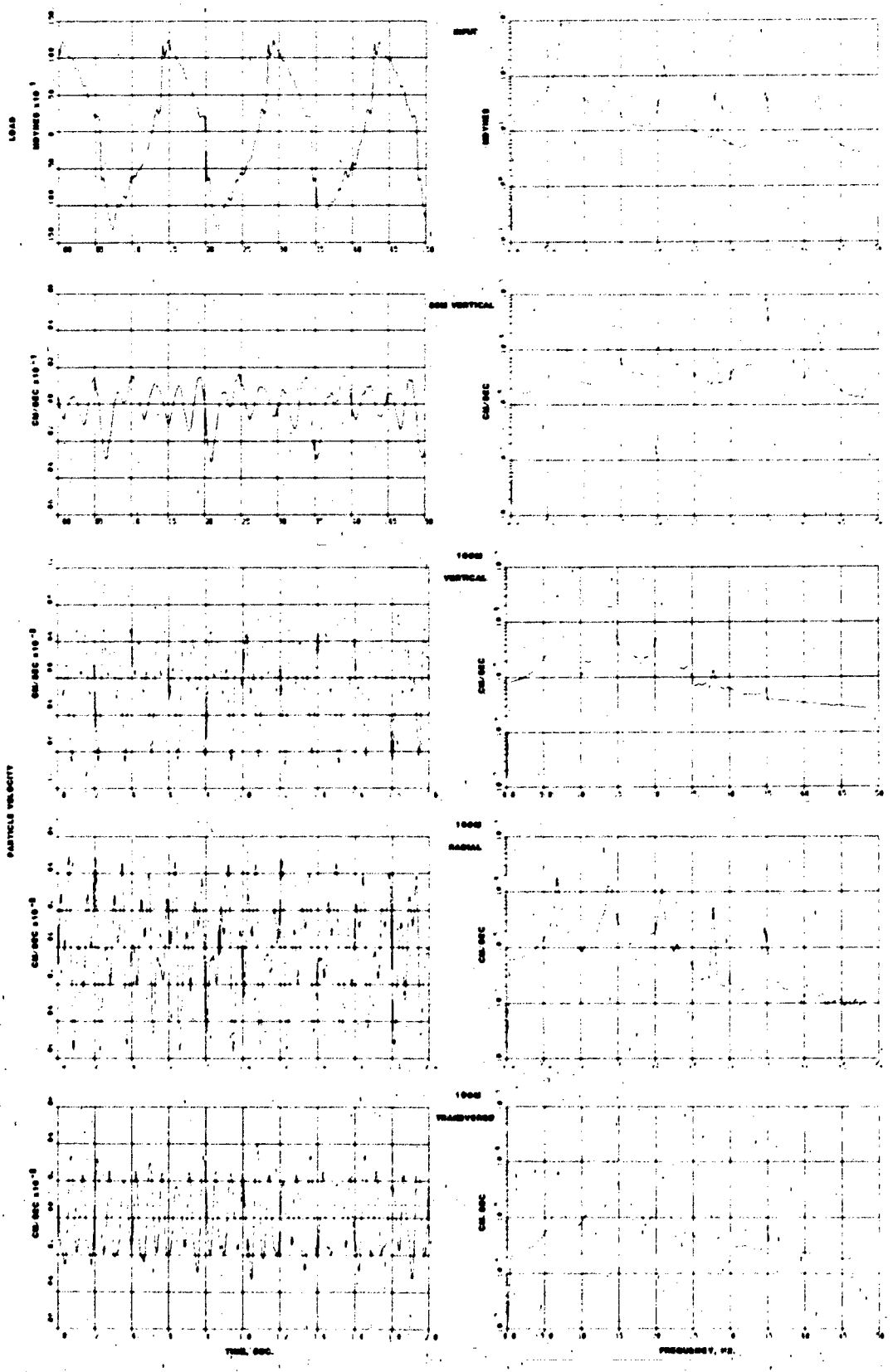

PLATE 8

TEST 8 7HZ DISCRETE FREQUENCY SINE WAVE

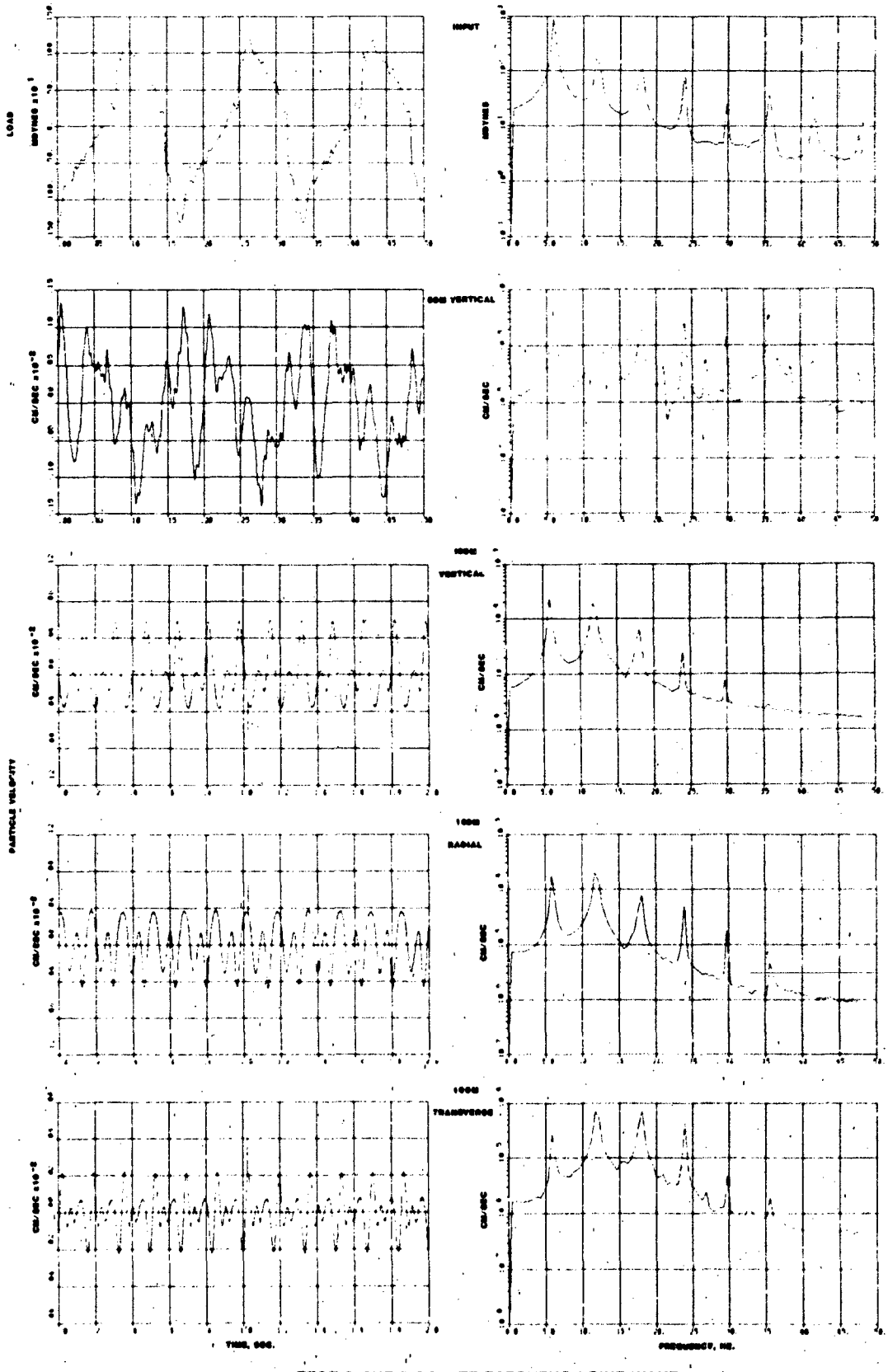

TEST 9 6HZ DISCRETE FREQUENCY SINE WAVE

PLATE 9

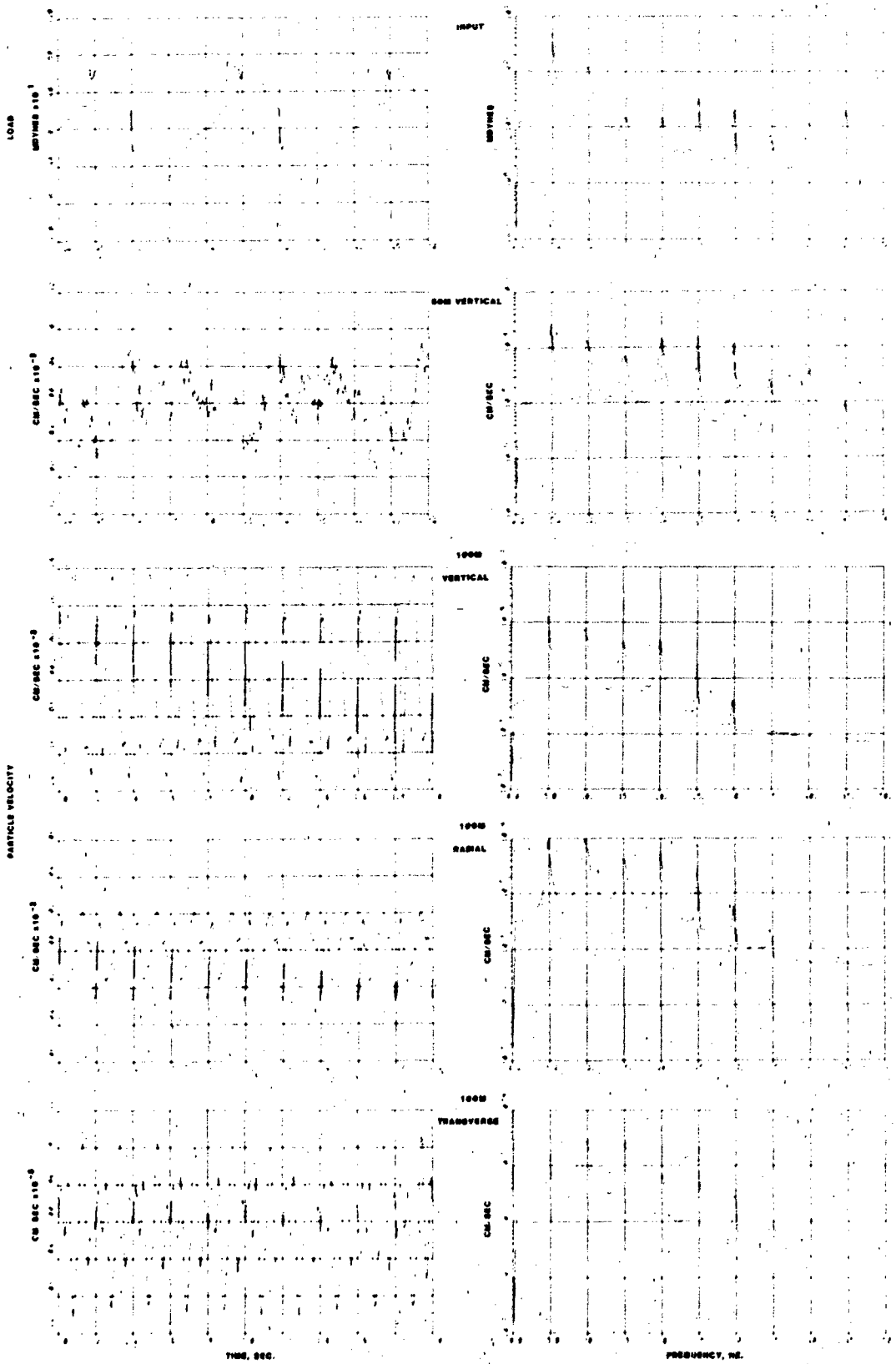

TEST 10 5HZ DISCRETE FREQUENCY SINE WAVE

PLATE 10

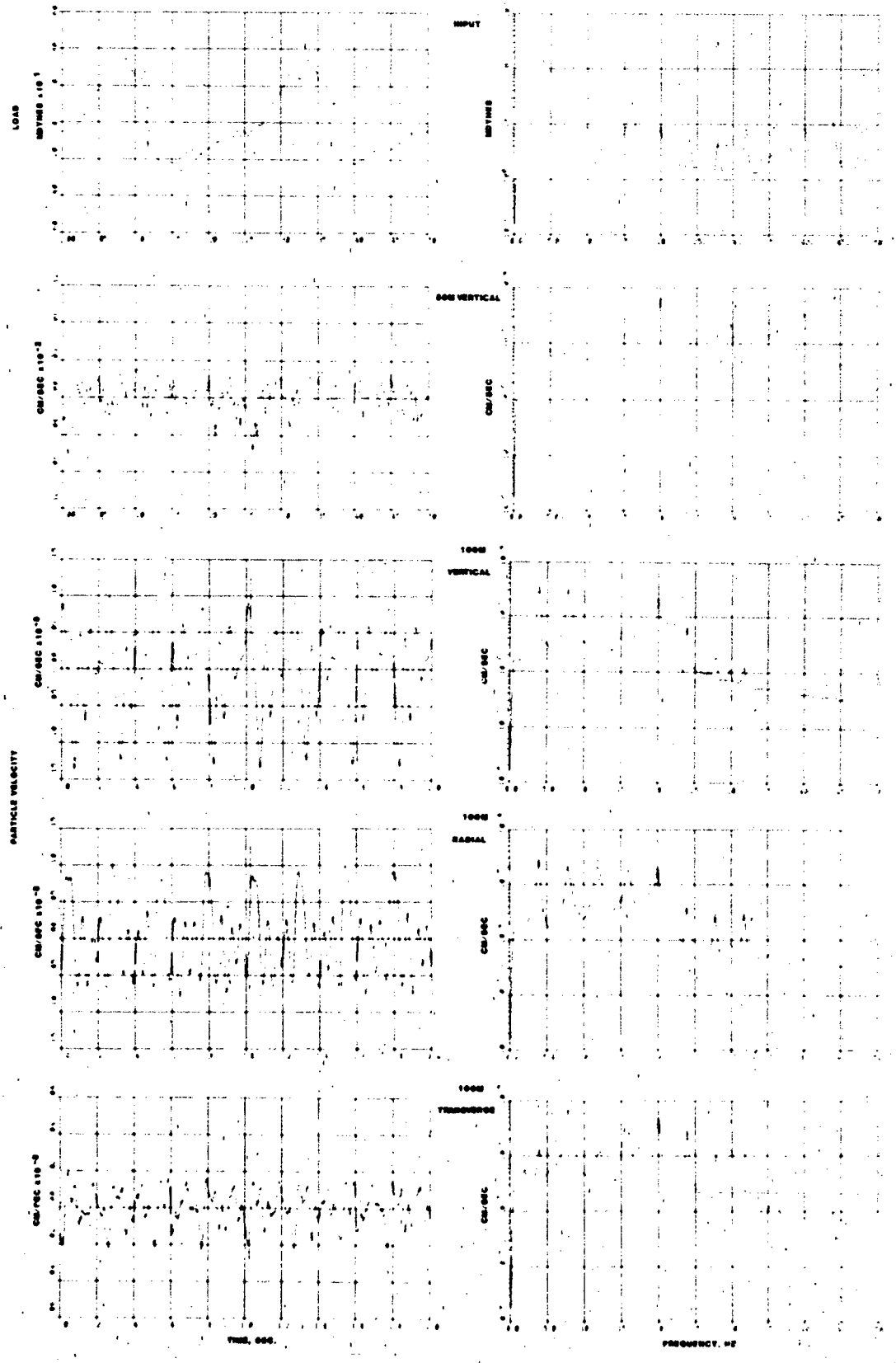

TEST 11 4HZ DISCRETE FREQUENCY SINE WAVE

PLATE 11

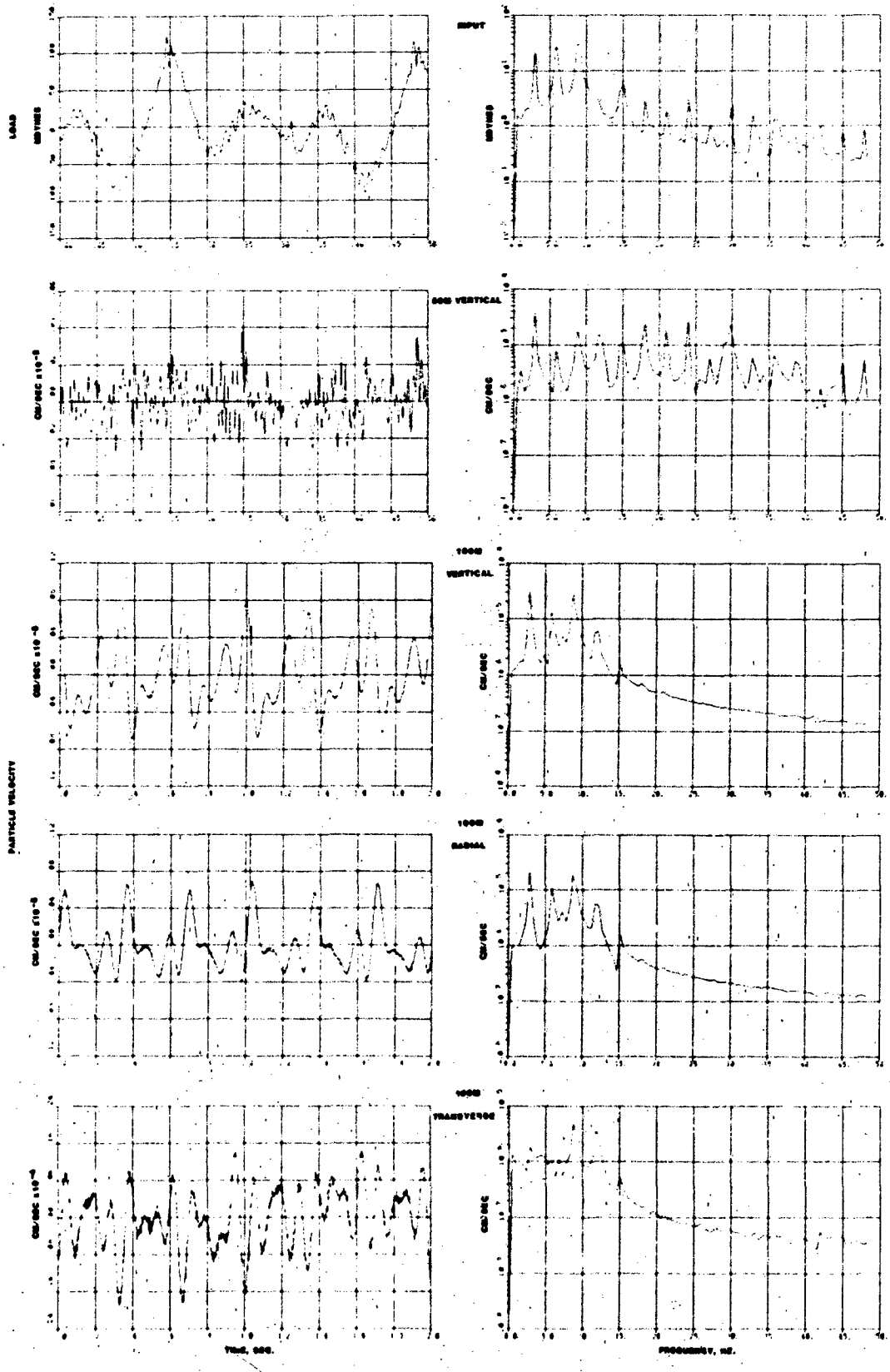

TEST 12 3-HZ DISCRETE FREQUENCY SINE WAVE

PLATE 12

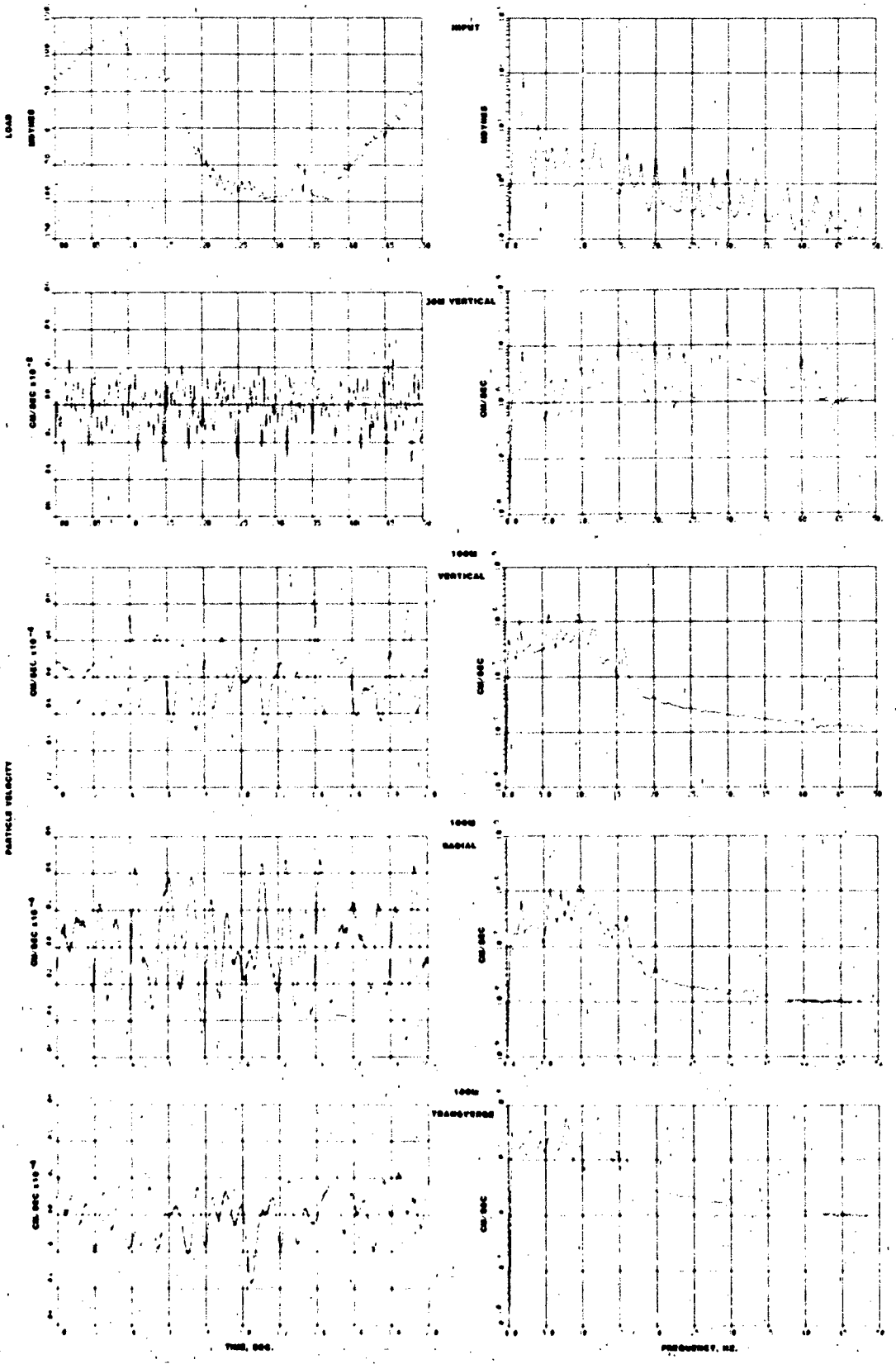

TEST 13 2HZ DISCRETE FREQUENCY SINE WAVE

PLATE 13

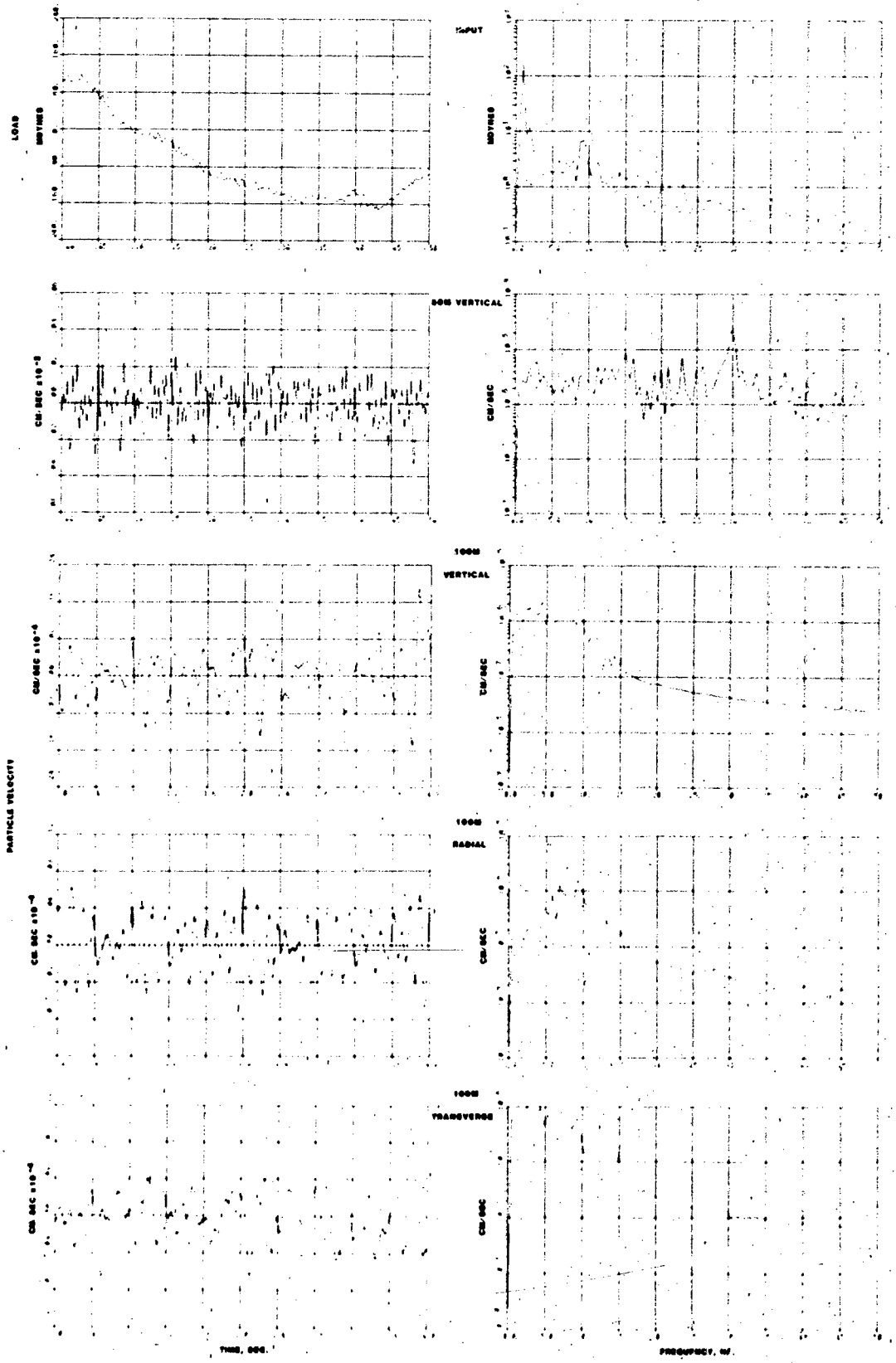

PLATE 14

TEST 14 1HZ DISCRETE FREQUENCY SINE WAVE

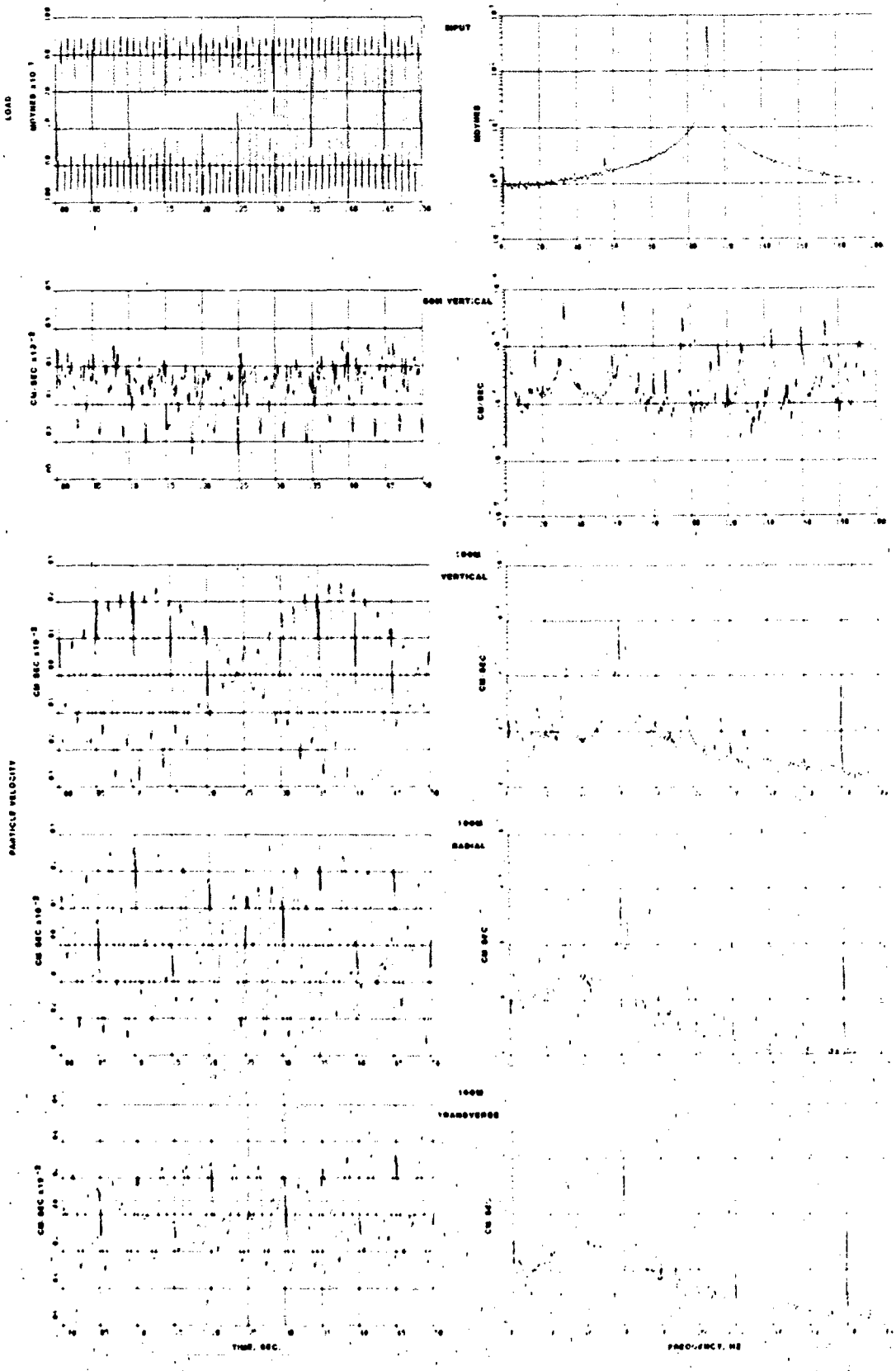

TEST 16 110HZ DISCRETE FREQUENCY SINE WAVE

PLATE 15

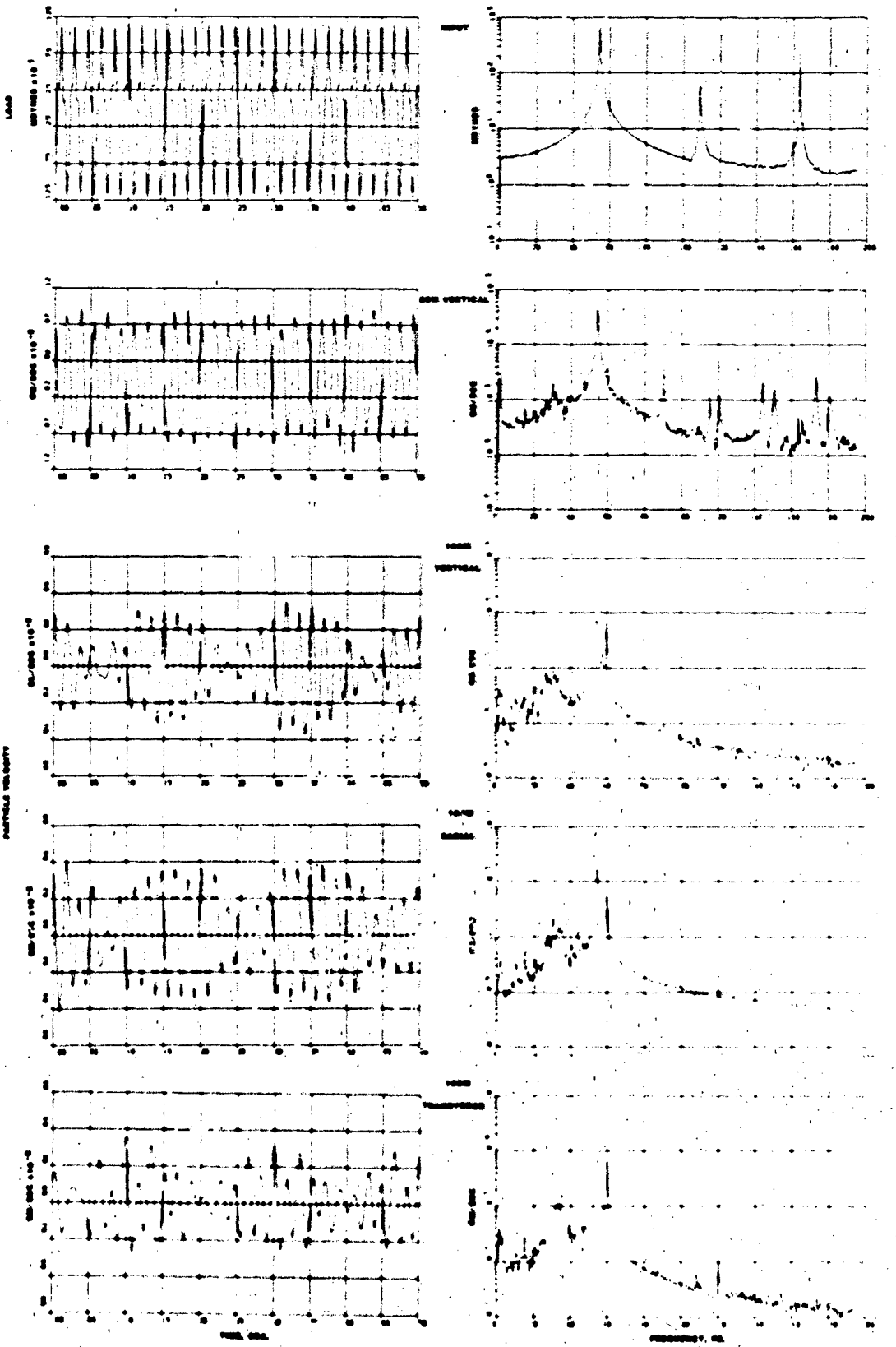

PLATE 16

TEST 18 55HZ DISCRETE FREQUENCY SINE WAVE

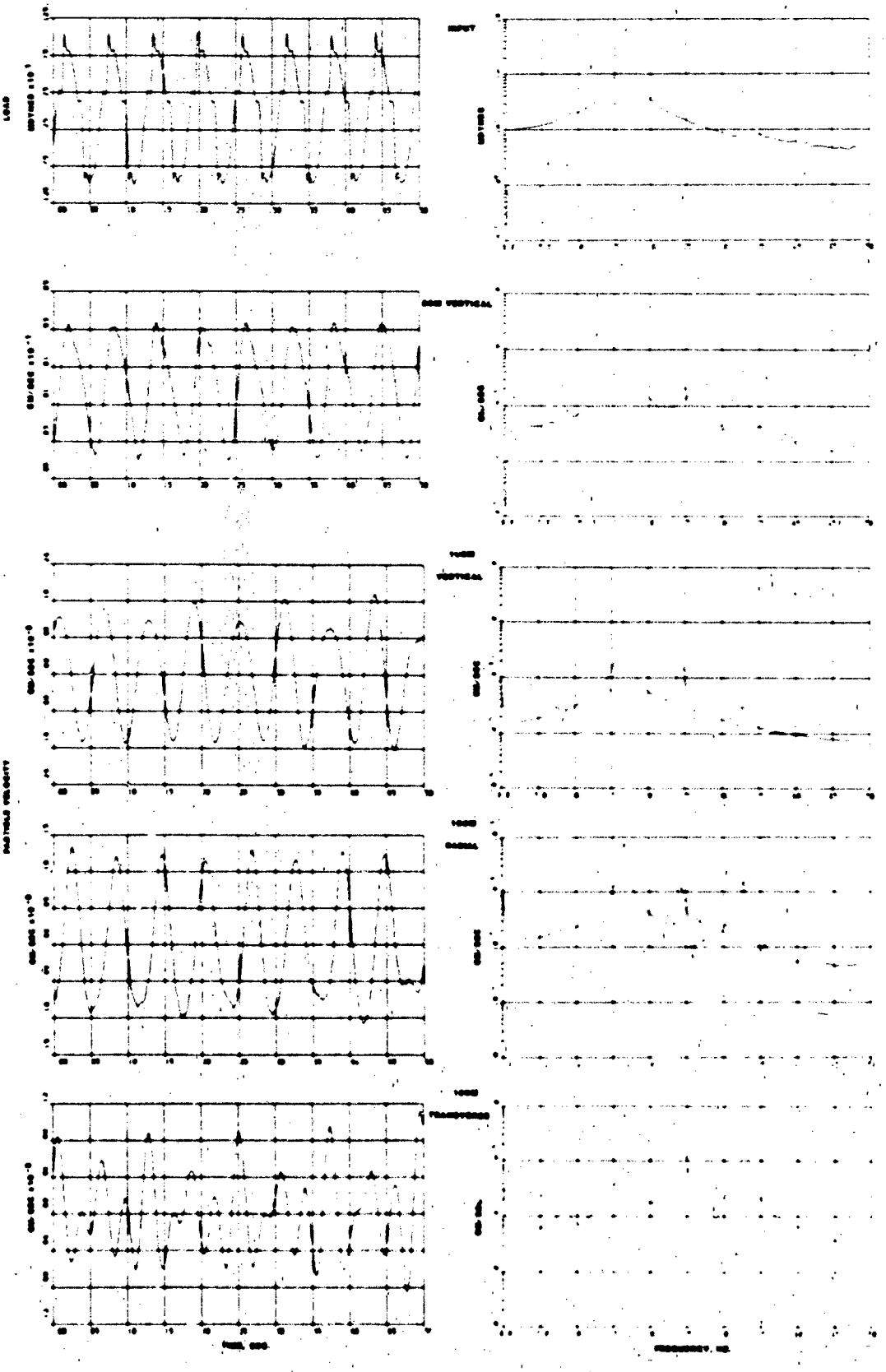

TEST 20 16.6HZ DISCRETE FREQUENCY SINE WAVE

PLATE 17

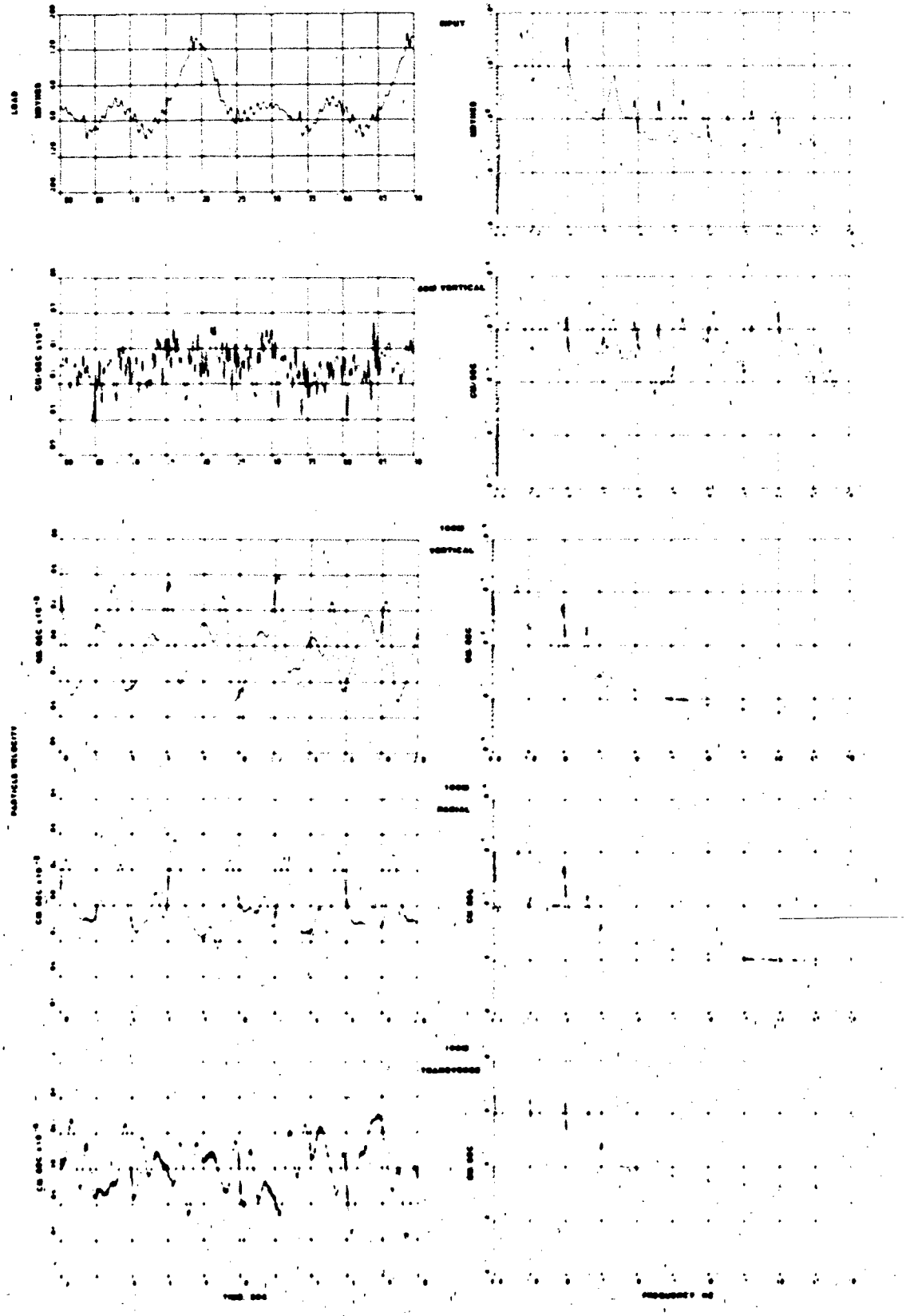

TEST 22 3.3HZ DISCRETE FREQUENCY SINE WAVE

PLATE 18

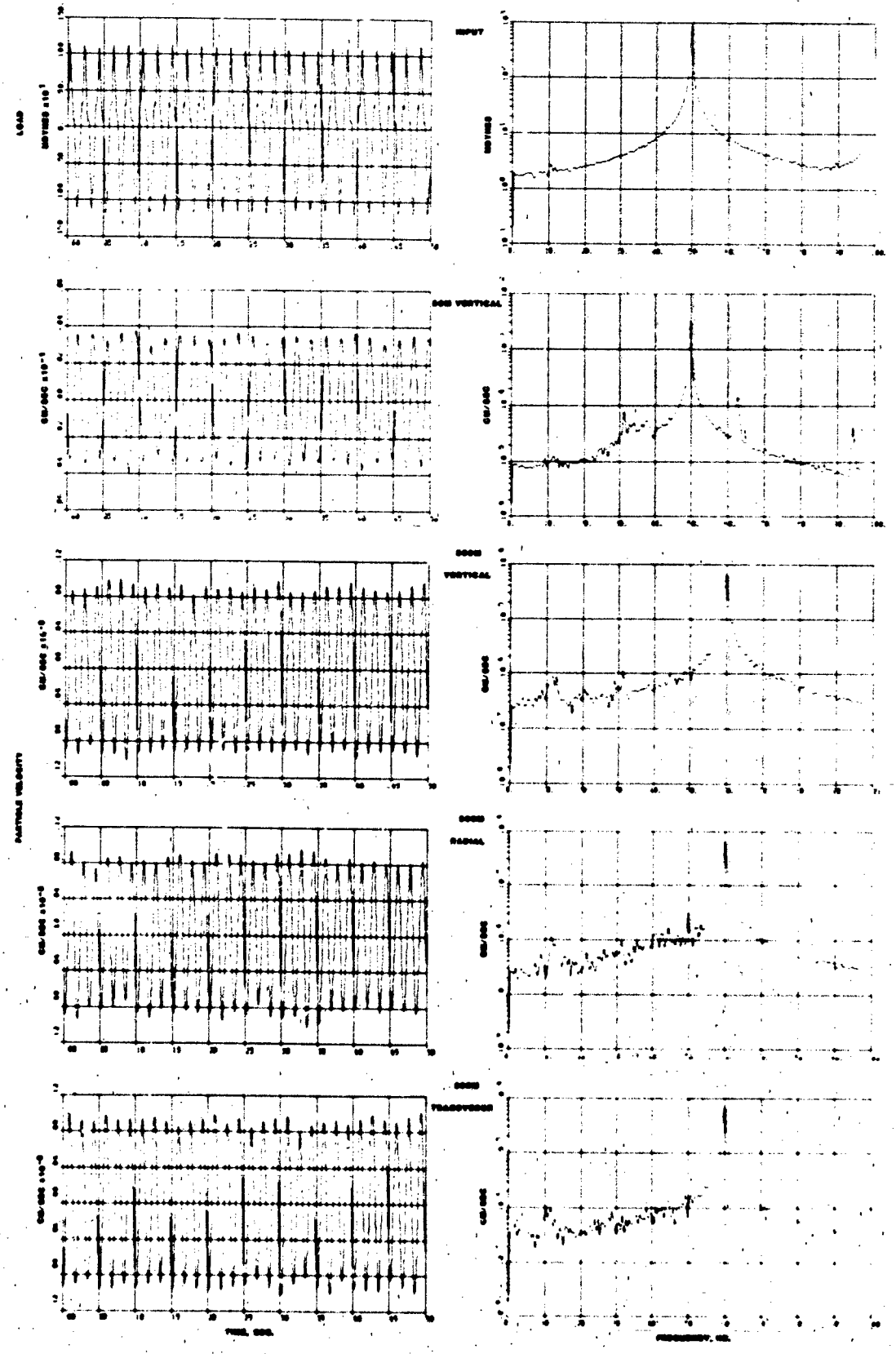

TEST 54 50HZ DISCRETE FREQUENCY SINE WAVE

PLATE 19

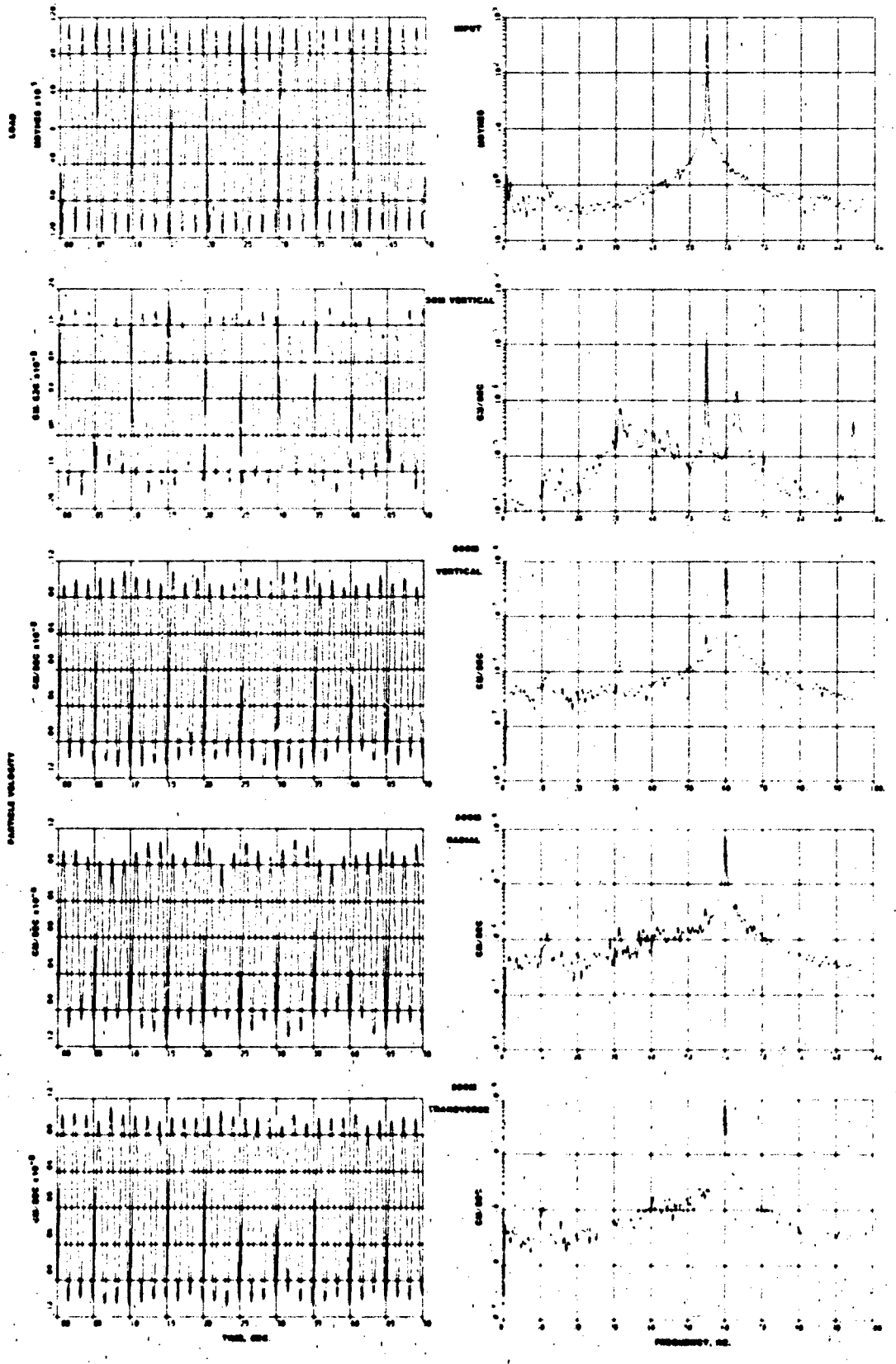

TEST 56 55HZ DISCRETE FREQUENCY SINE WAVE

PLATE 20

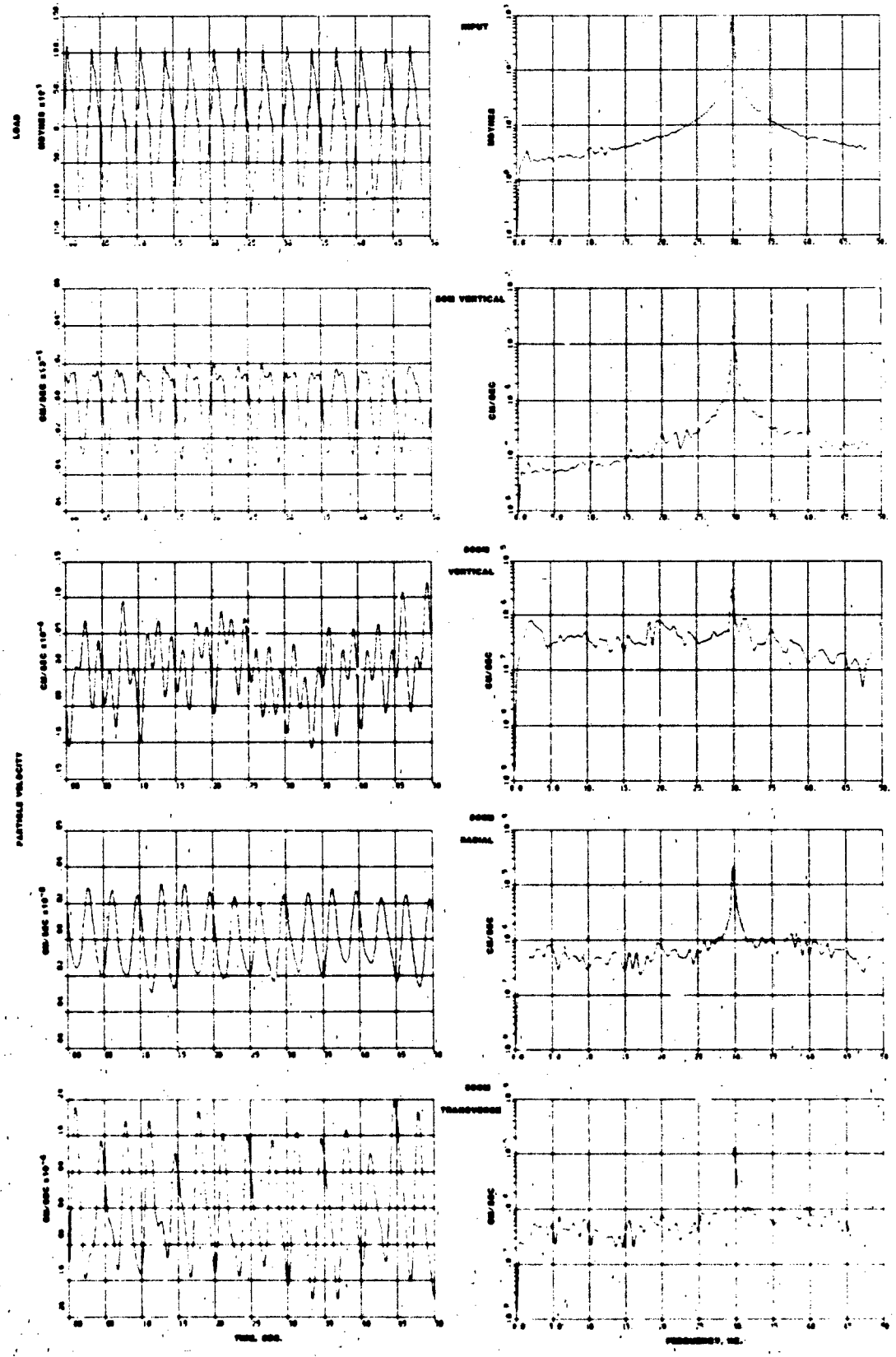

TEST 57 30HZ DISCRETE FREQUENCY SINE WAVE

PLATE 21

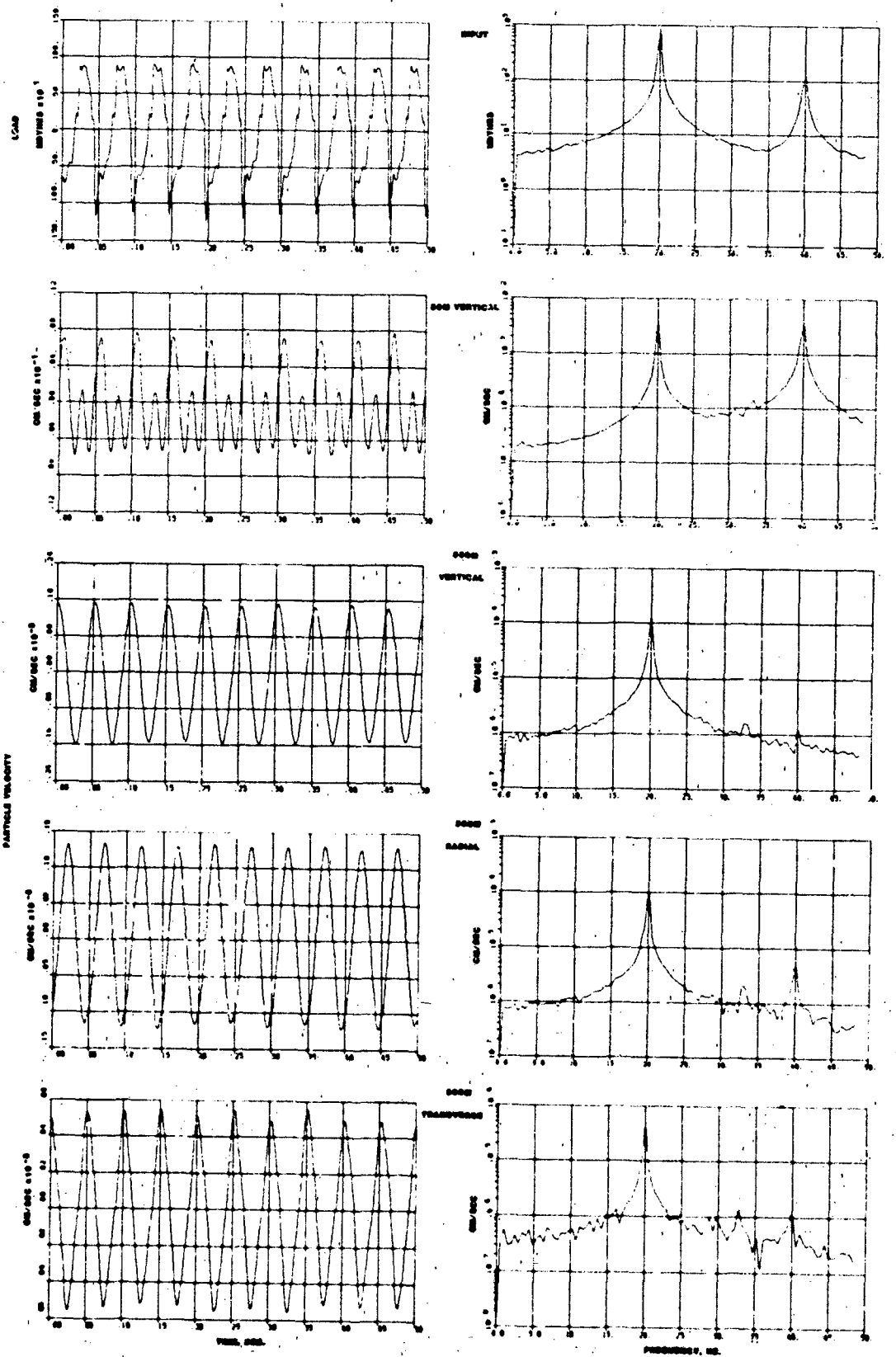

PLATE 22

TEST 59 20HZ DISCRETE FREQUENCY SINE WAVE

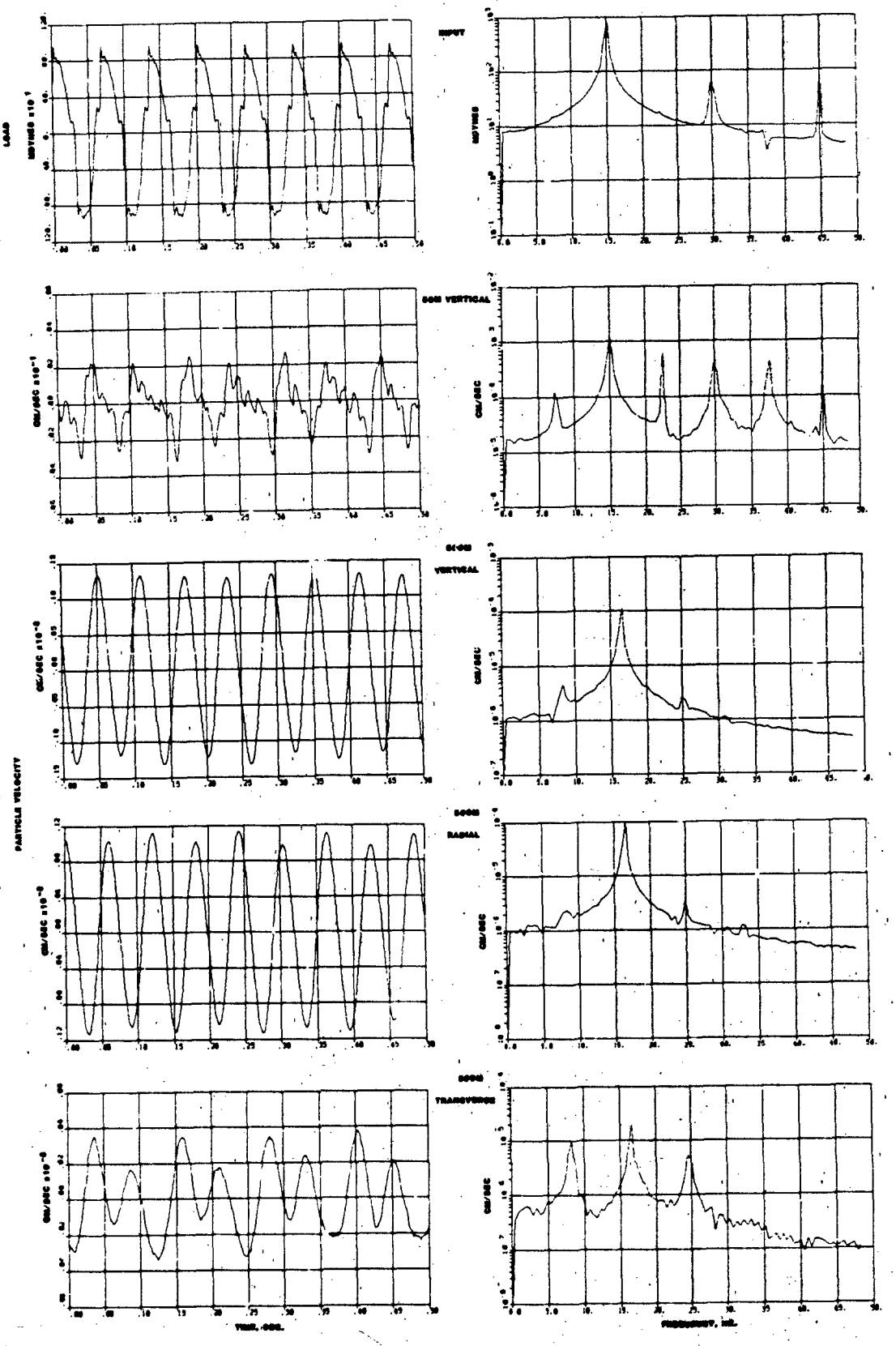

TEST 31 16.5HZ DISCRETE FREQUENCY SINE WAVE

PLATE 23

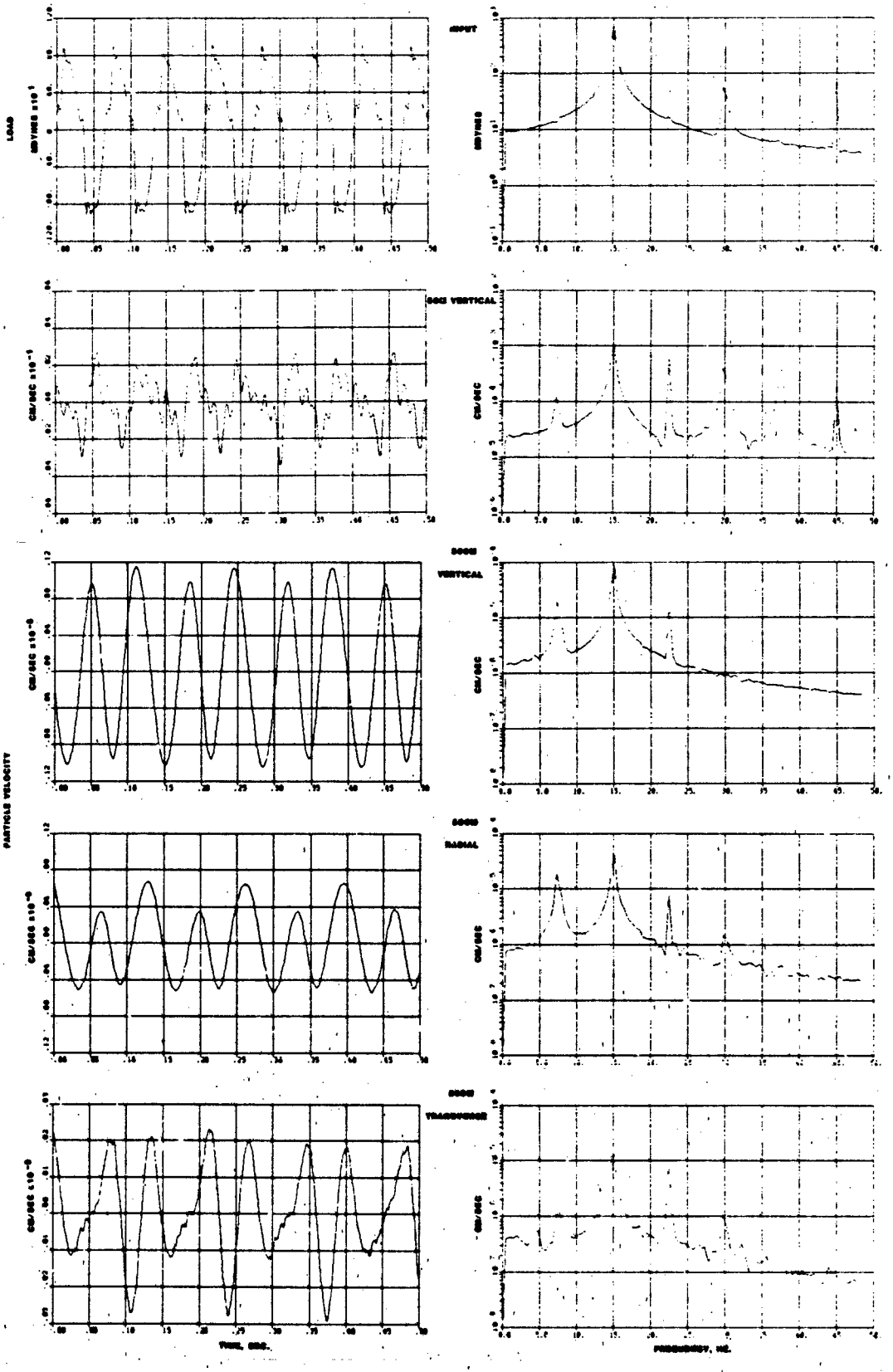

TEST 62 15HZ DISCRETE FREQUENCY SINE WAVE

PLATE 24

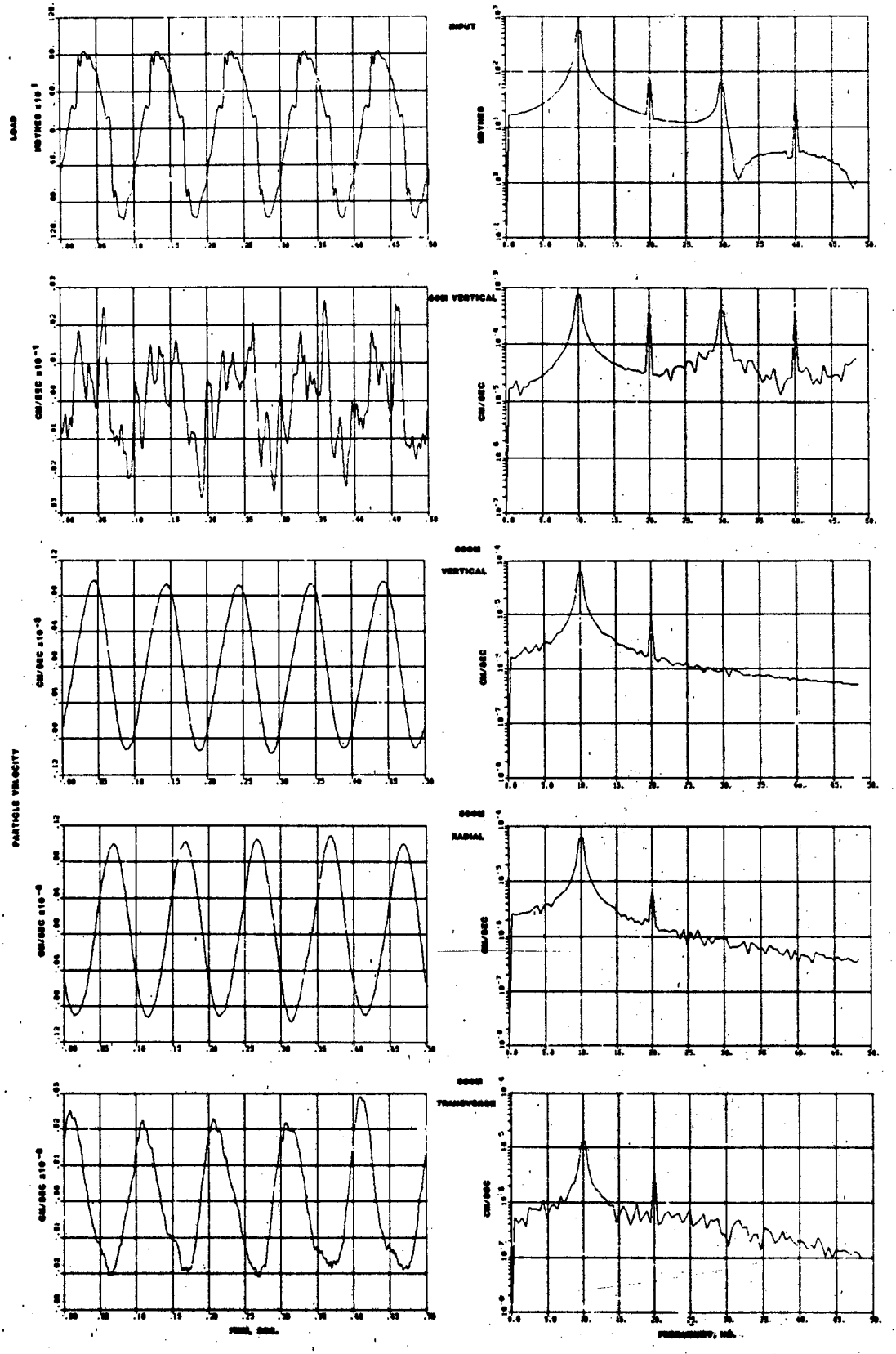

TEST 84 10HZ DISCRETE FREQUENCY SINE WAVE

PLATE 25

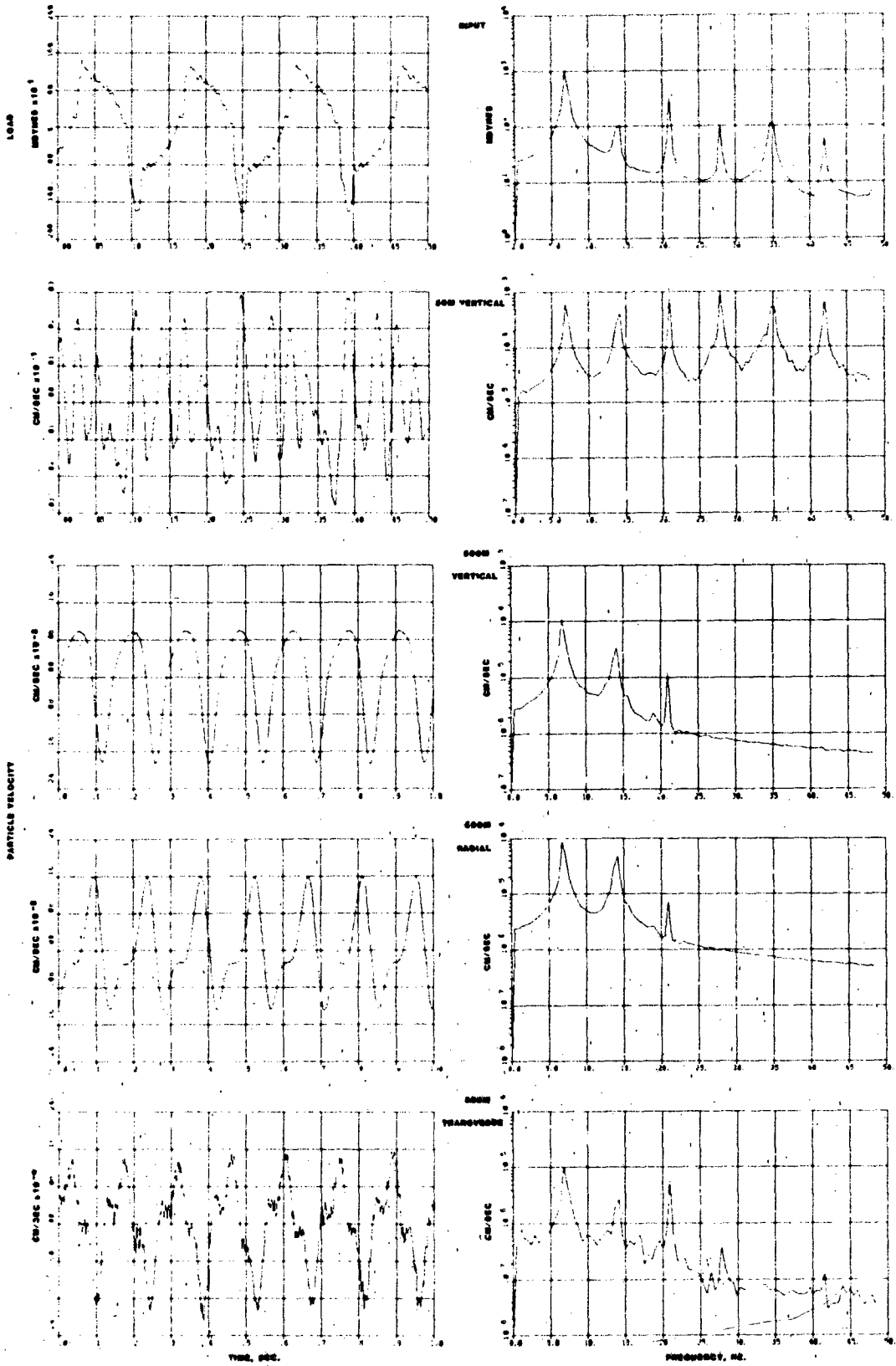

TEST 66 7HZ DISCRETE FREQUENCY SINE WAVE

PLATE 26

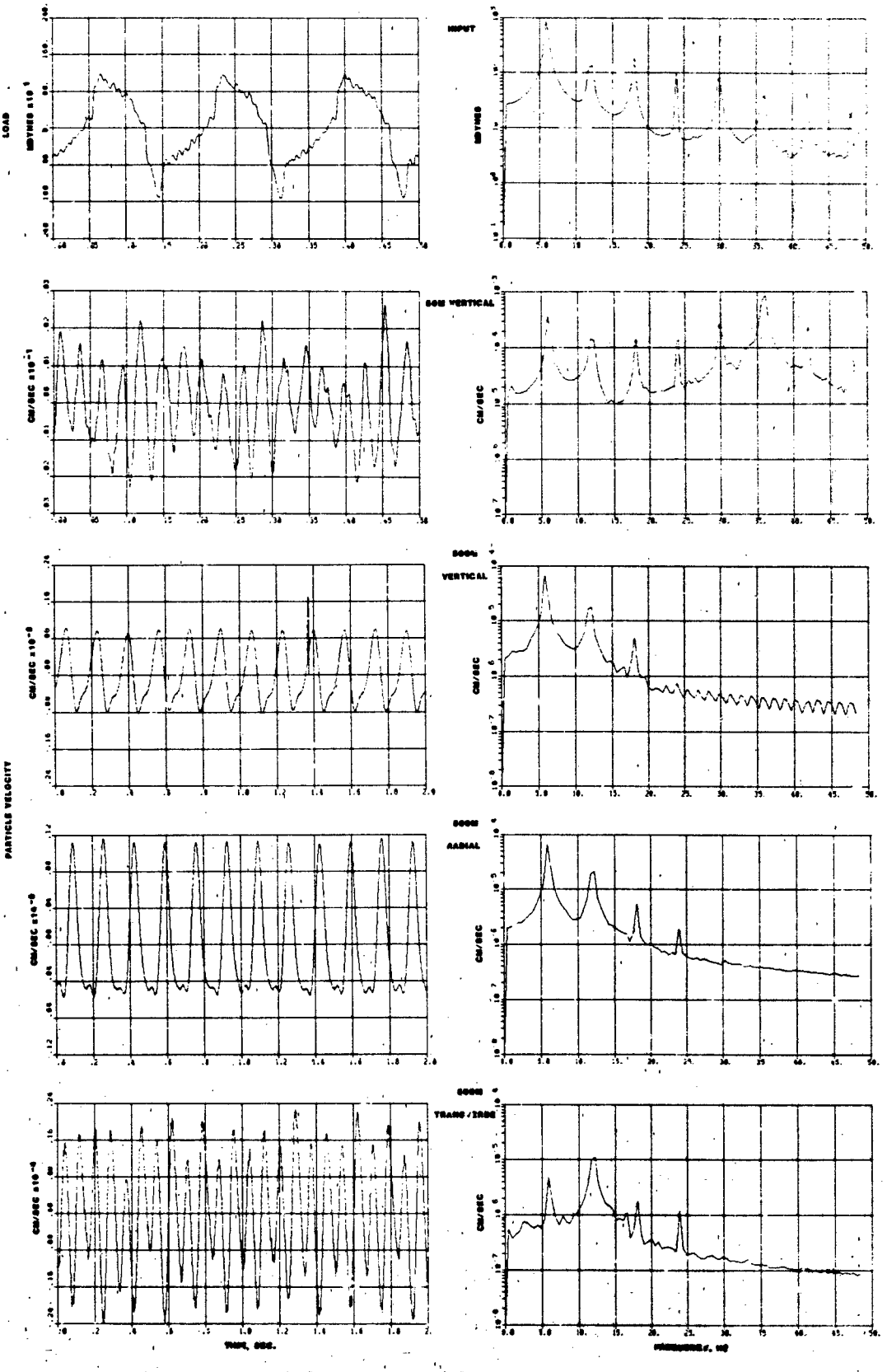

TEST 68 6HZ DISCRETE FREQUENCY SINE WAVE

PLATE 27

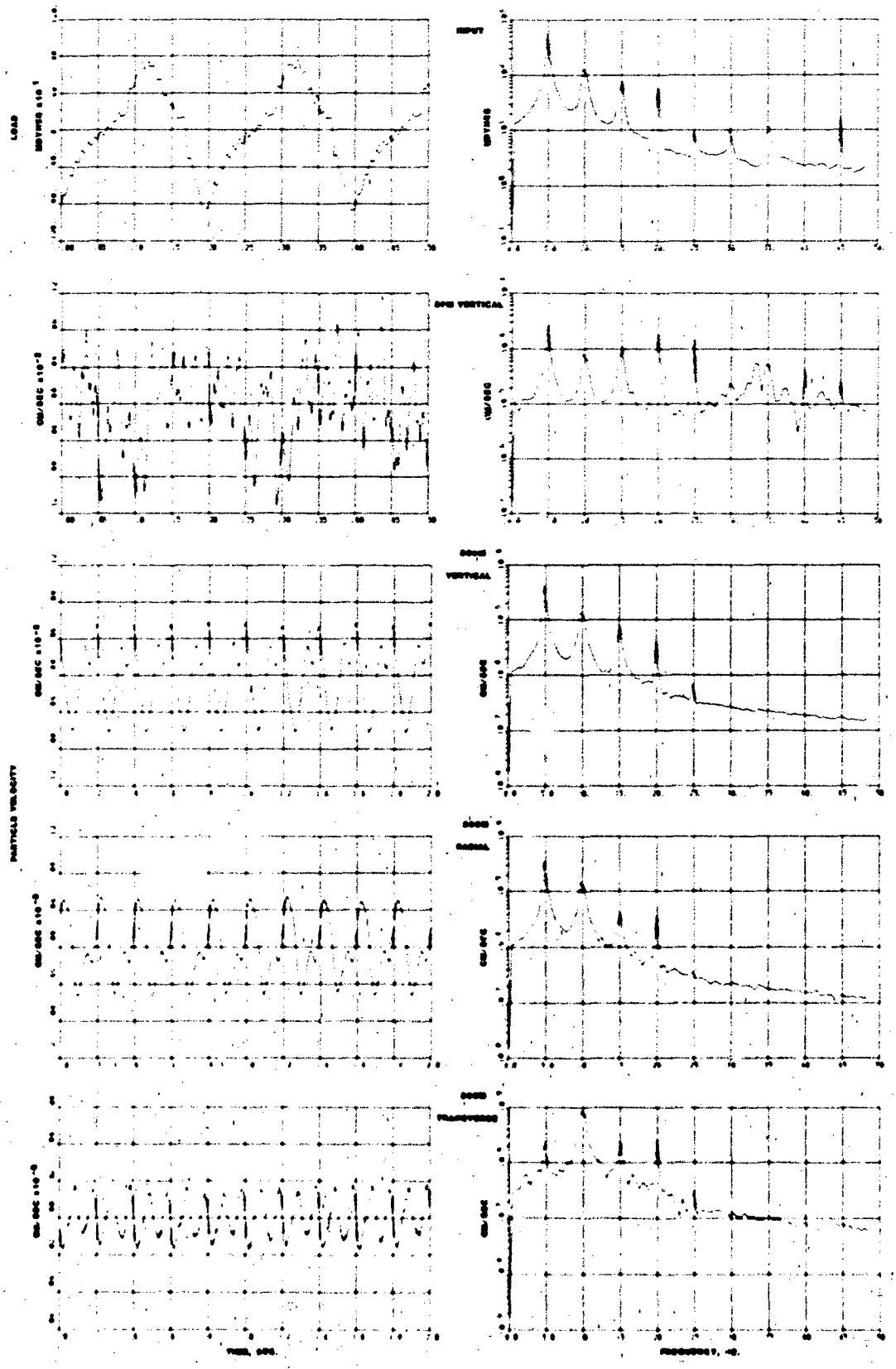

TEST 70 SHZ DISCRETE FREQUENCY SINE WAVE

PLATE 28

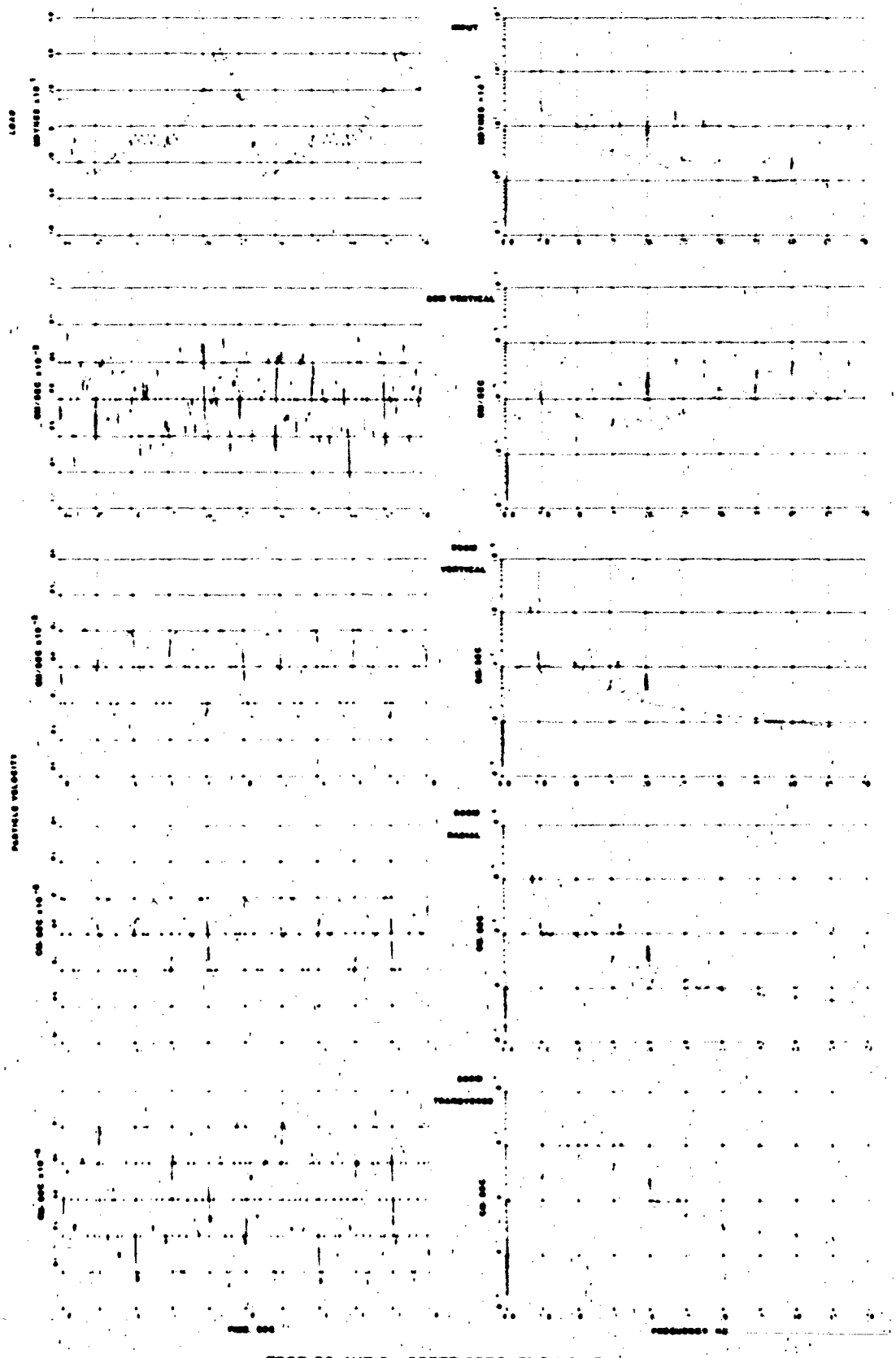

TEST 72 4HZ DISCRETE FREQUENCY SINE WAVE

PLATE 29

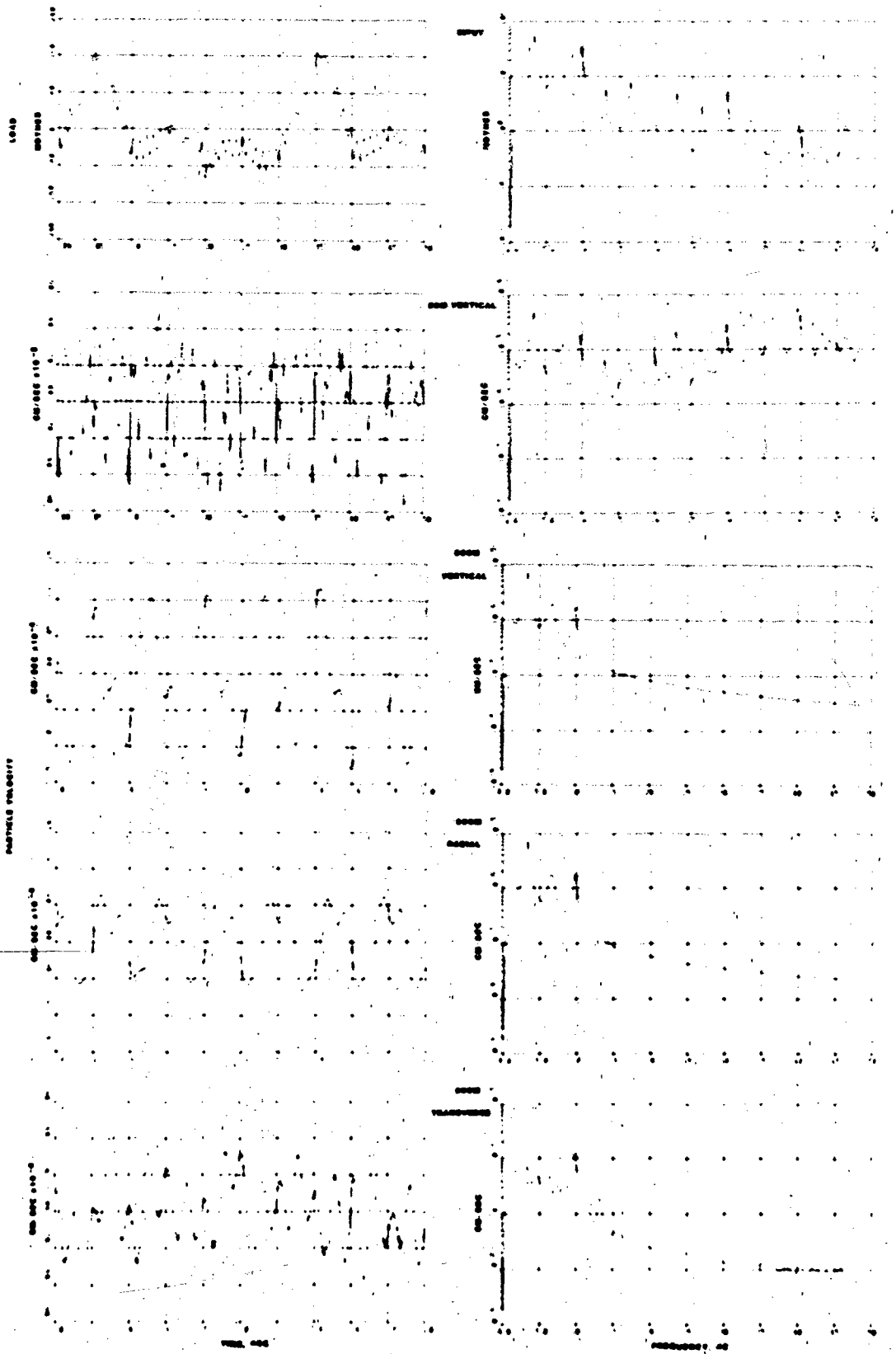

TEST 74 3.3HZ DISCRETE FREQUENCY SINE WAVE

PLATE 30

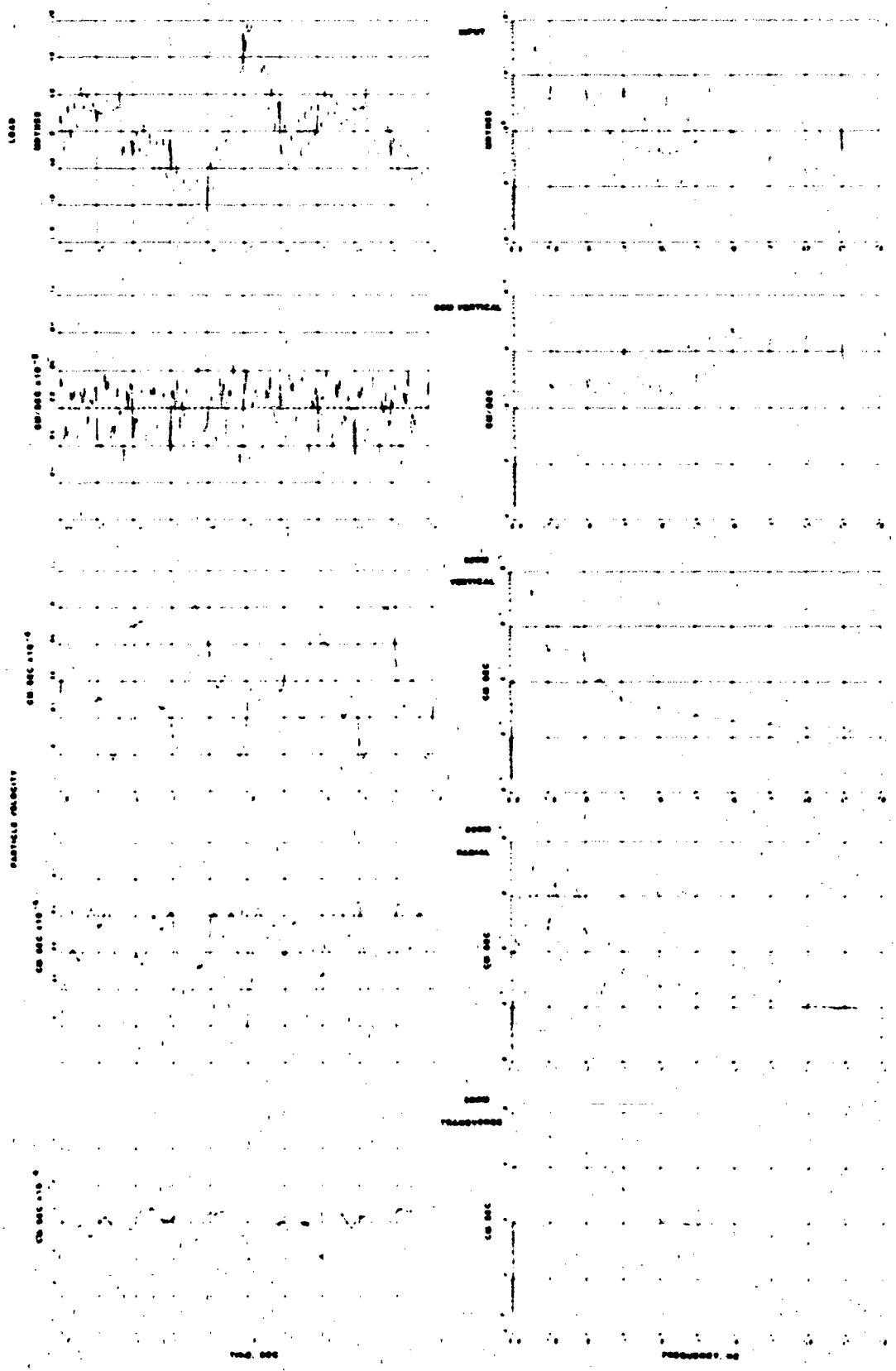

TEST 75 3HZ DISCRETE FREQUENCY SINE WAVE

PLATE 31

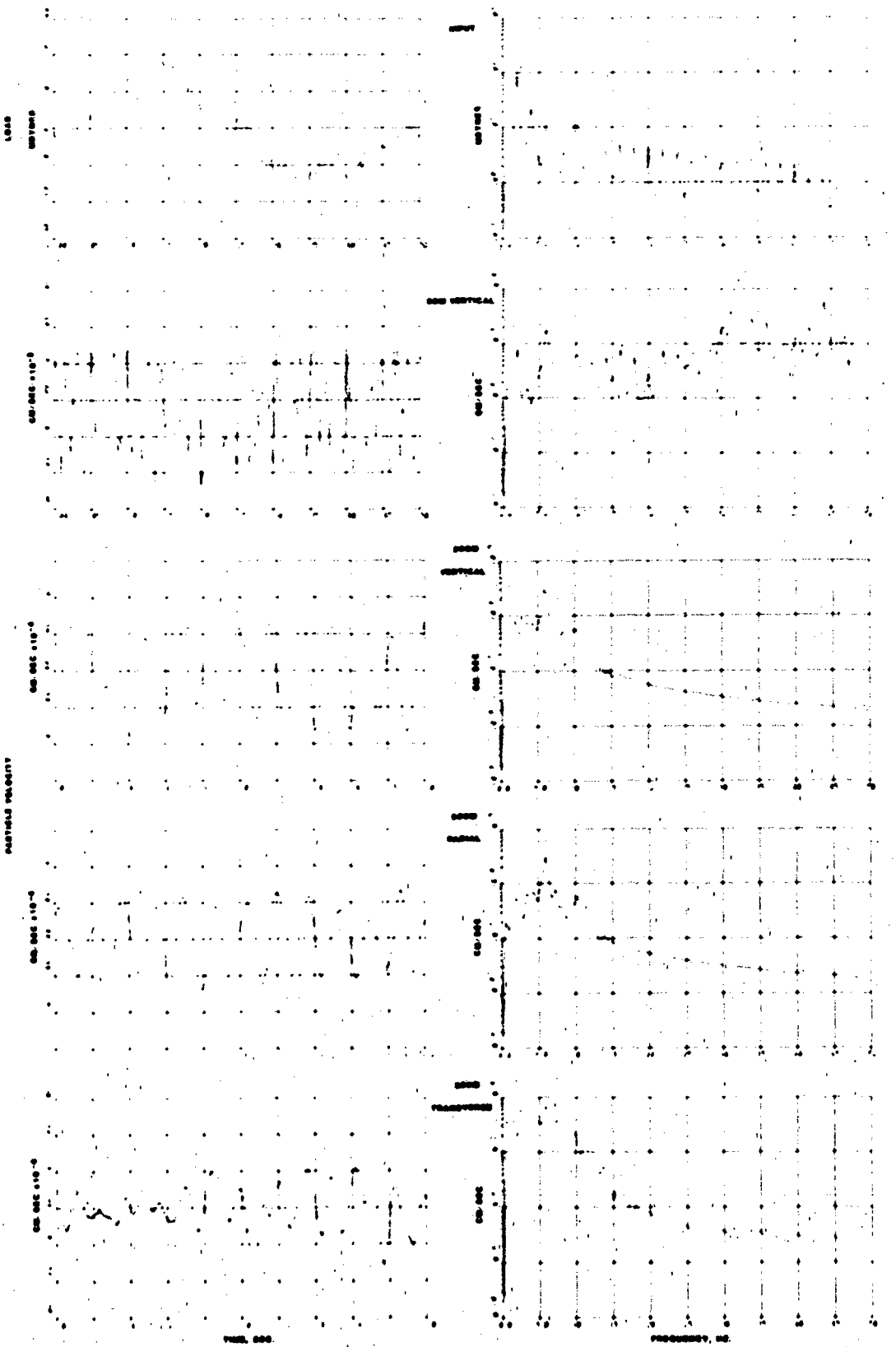

TEST 77 2HZ DISCRETE FREQUENCY SINE WAVE

PLATE 32

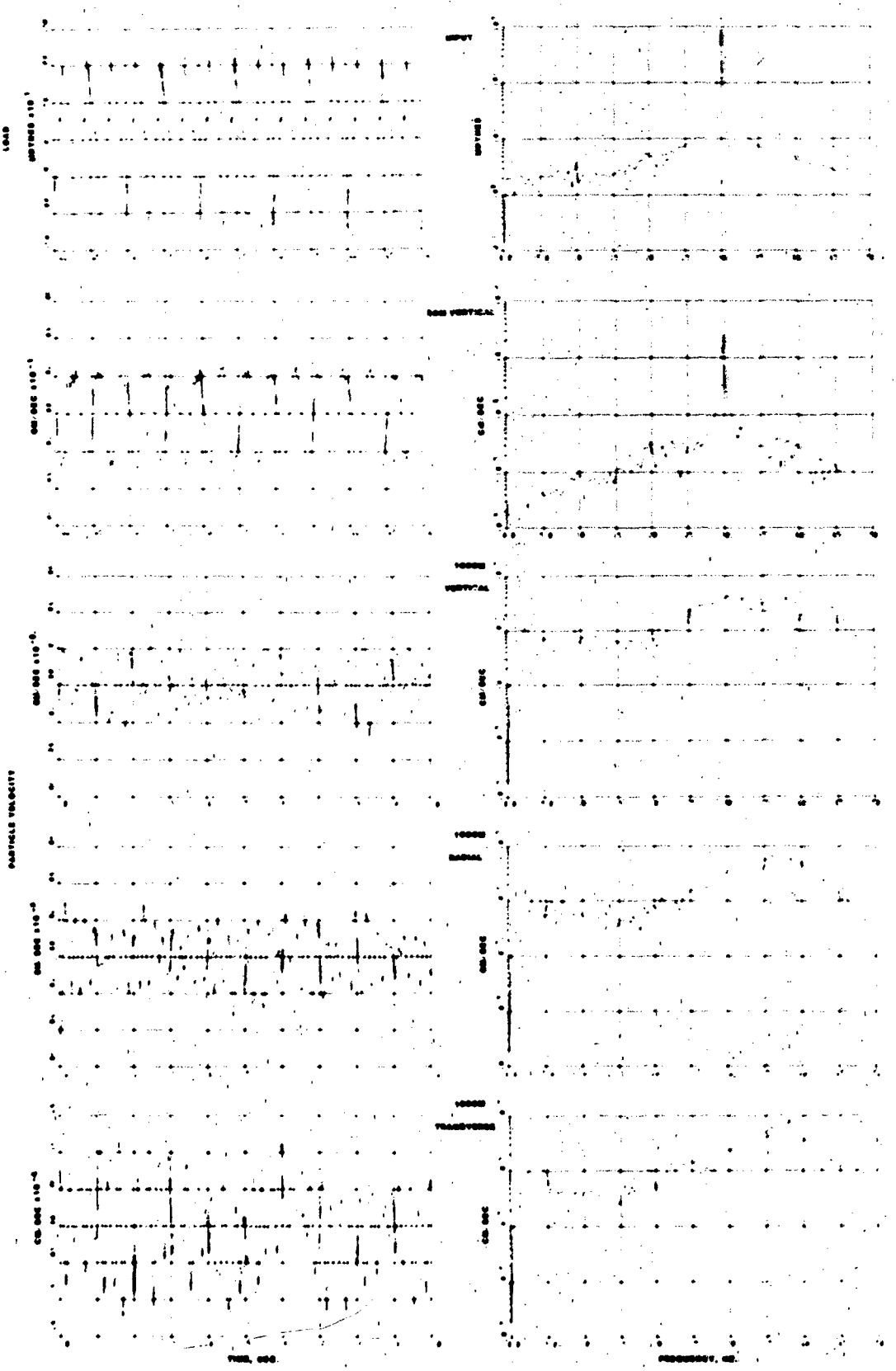

TEST 92 30HZ DISCRETE FREQUENCY SINE WAVE

PLATE 33

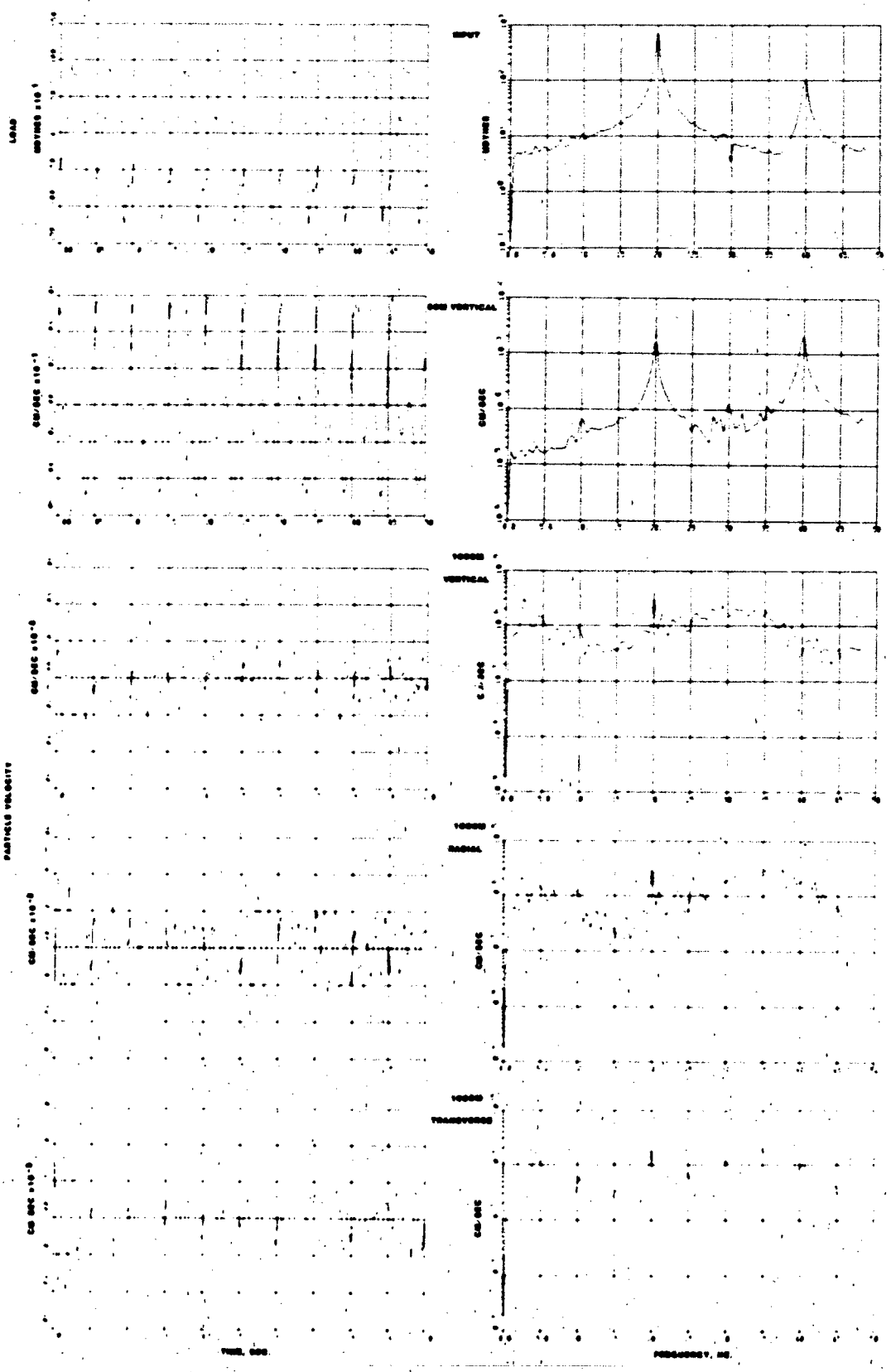

PLATE 34

TEST 94 20HZ DISCRETE FREQUENCY SINE WAVE

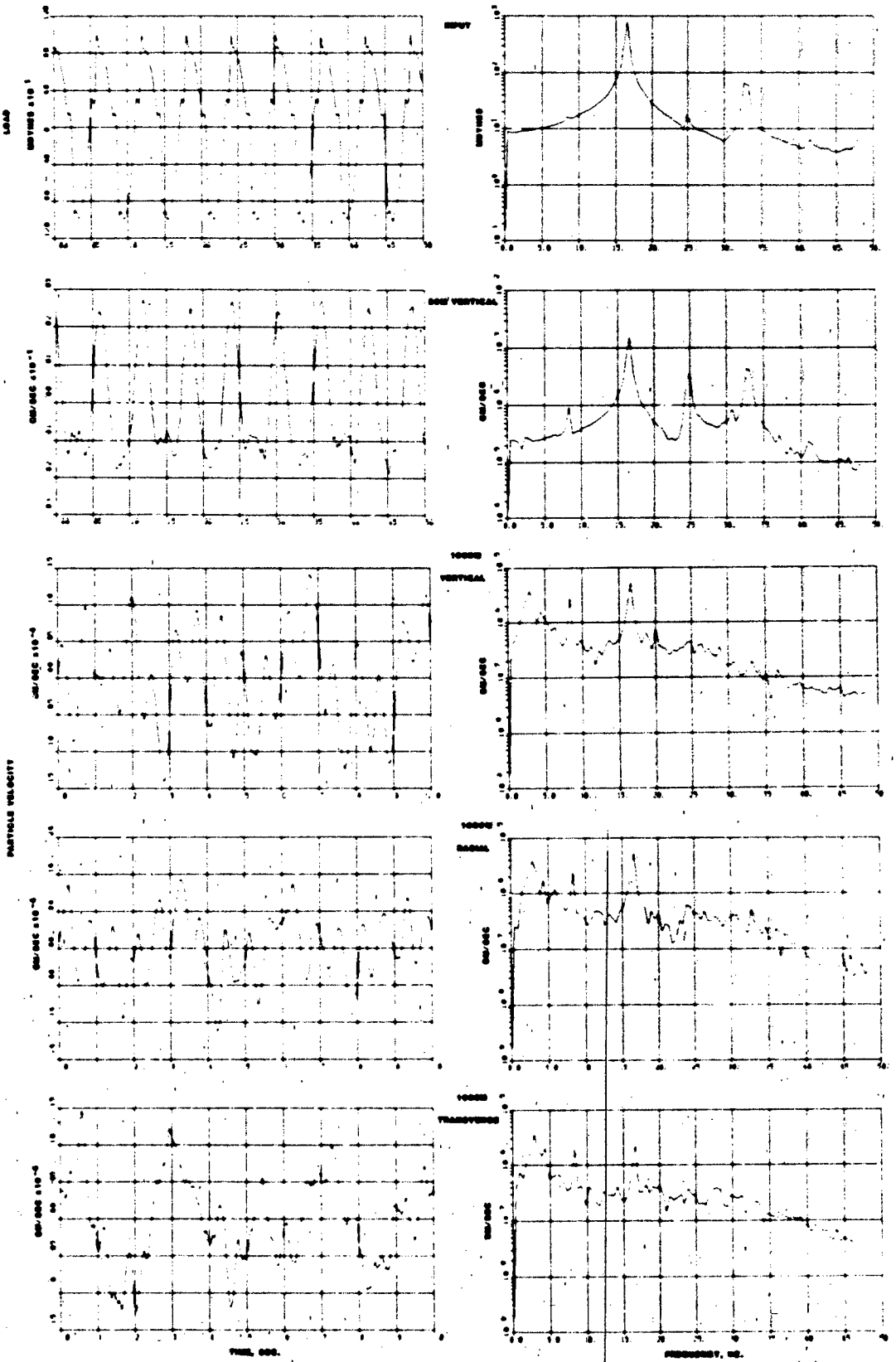

TEST 96 16.5HZ DISCRETE FREQUENCY SINE WAVE

PLATE 35

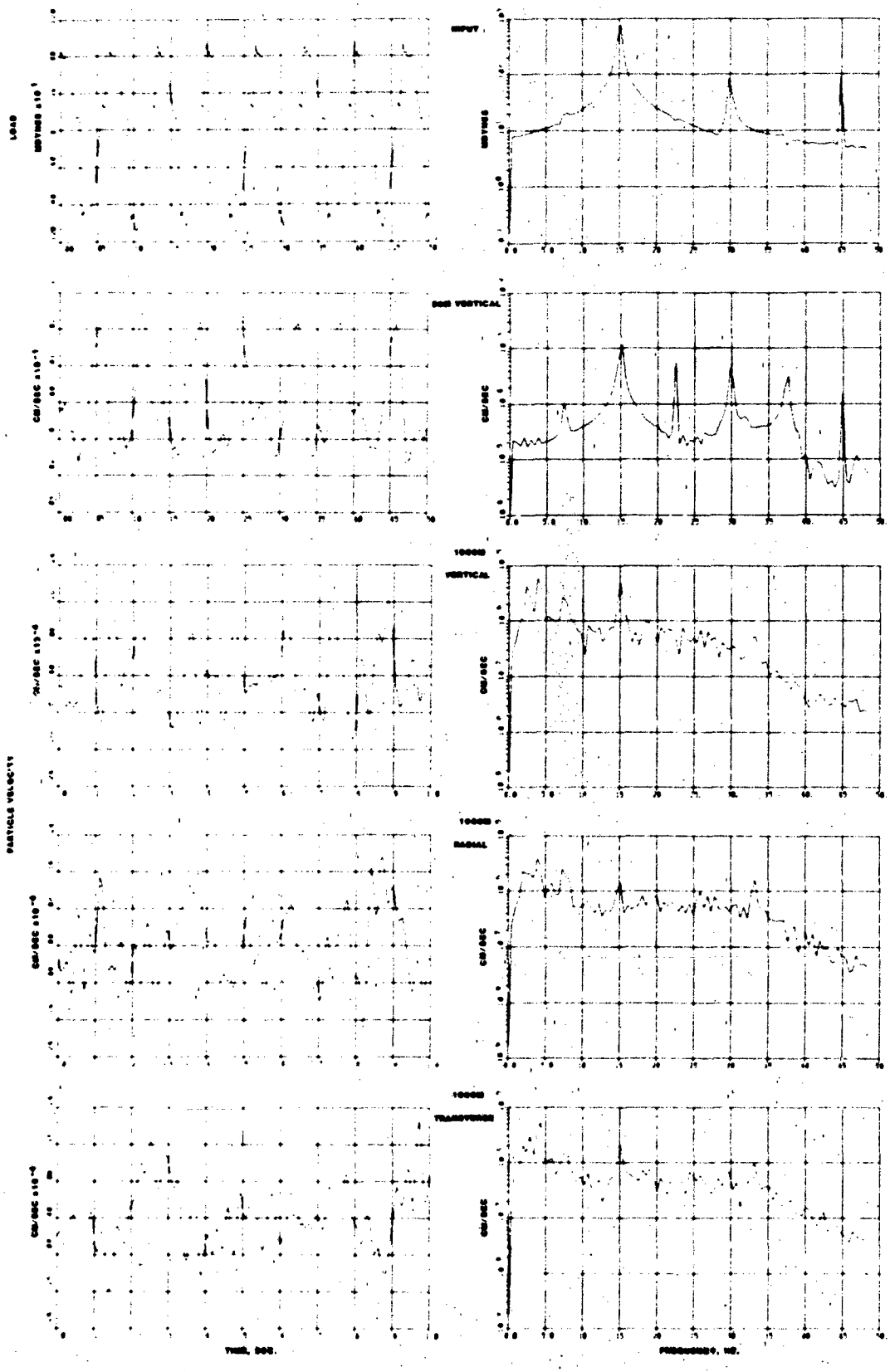

TEST 97 15HZ DISCRETE FREQUENCY SINE WAVE

PLATE 36

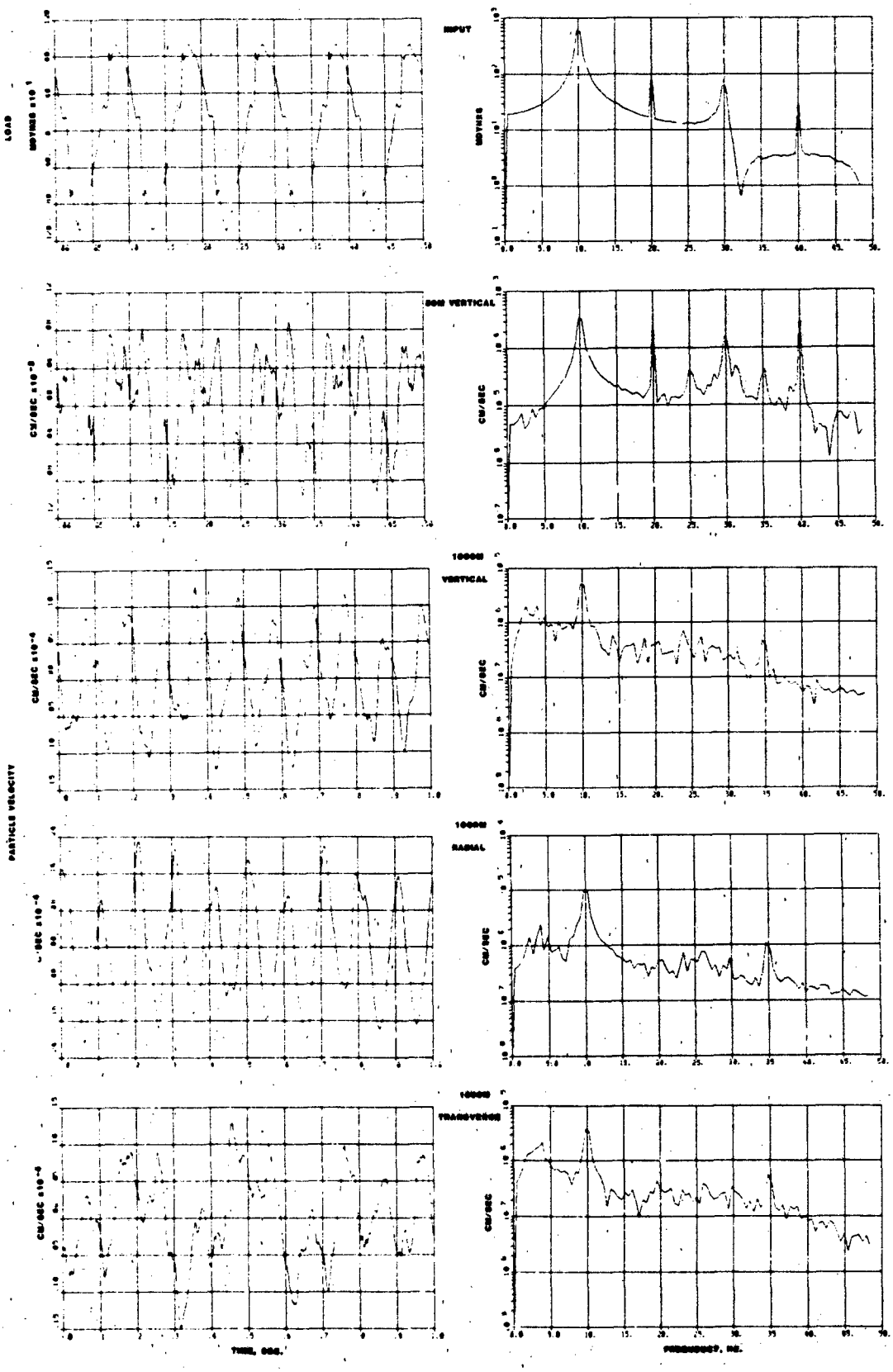

TEST 99 10HZ DISCRETE FREQUENCY SINE WAVE

PLATE 37

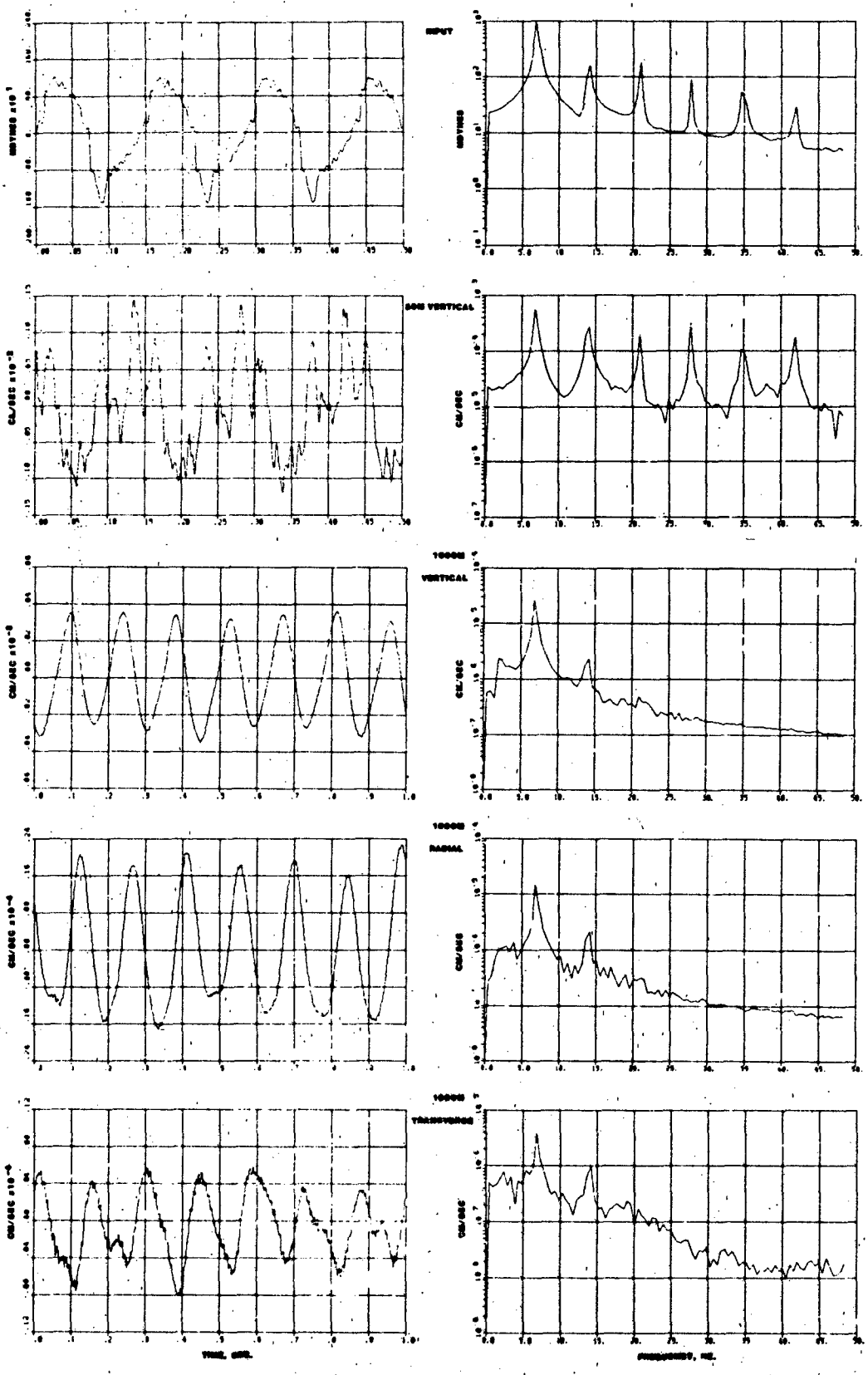

TEST 102 7HZ DISCRETE FREQUENCY SINE WAVE

PLATE 38

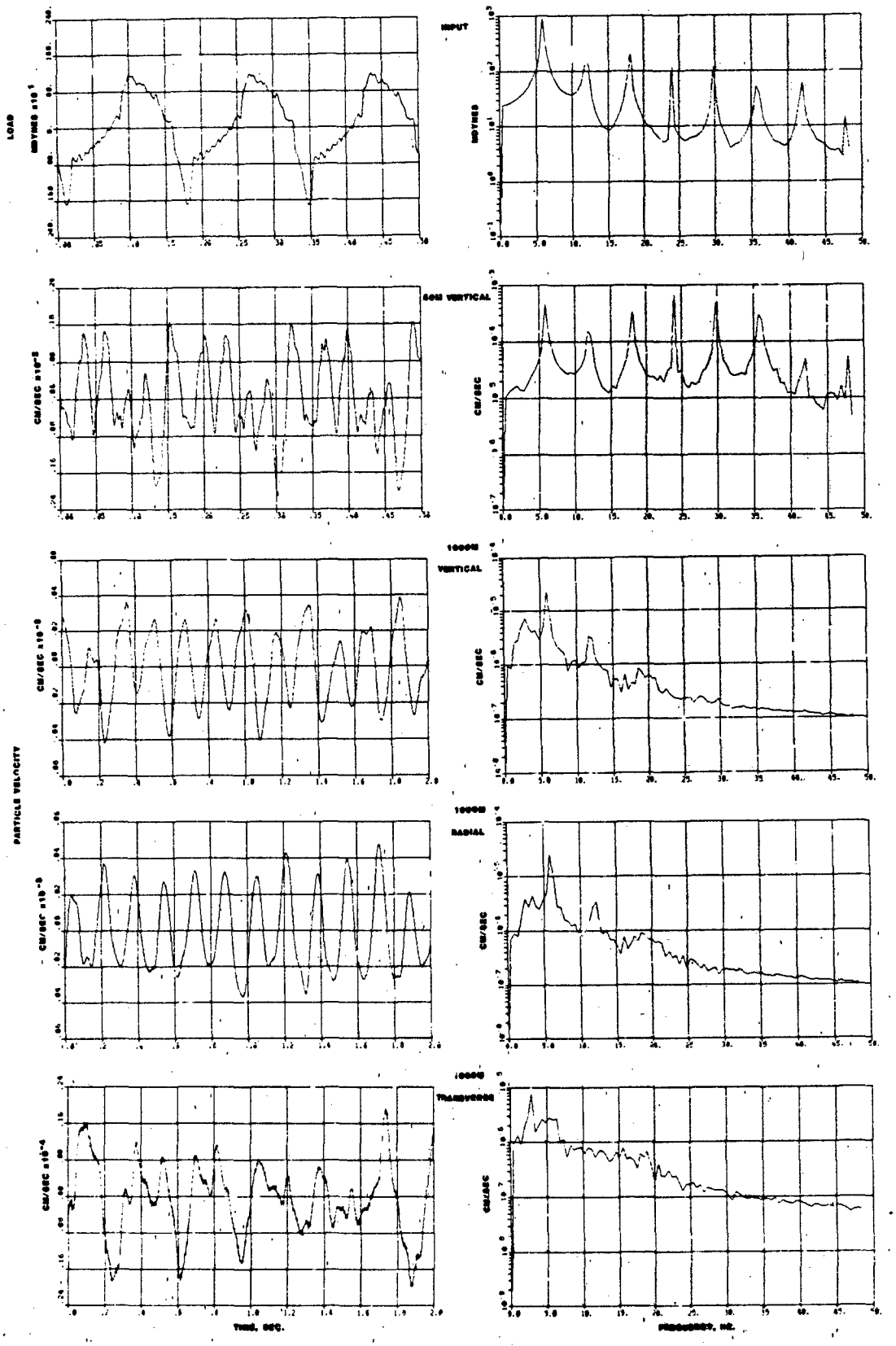

TEST 104 6HZ DISCRETE FREQUENCY SINE WAVE

PLATE 39

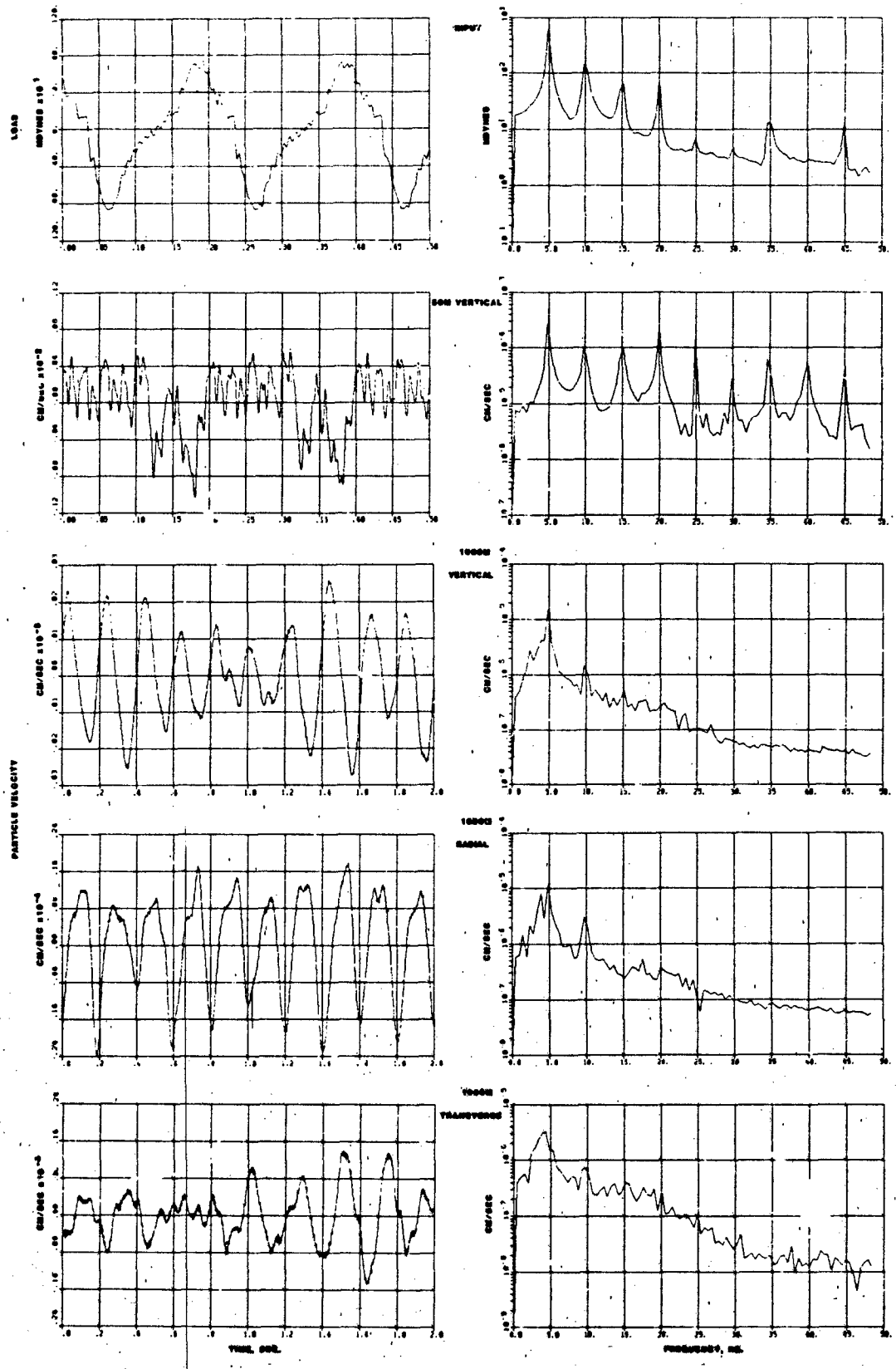

TEST 106 5HZ DISCRETE FREQUENCY SINE WAVE

PLATE 40

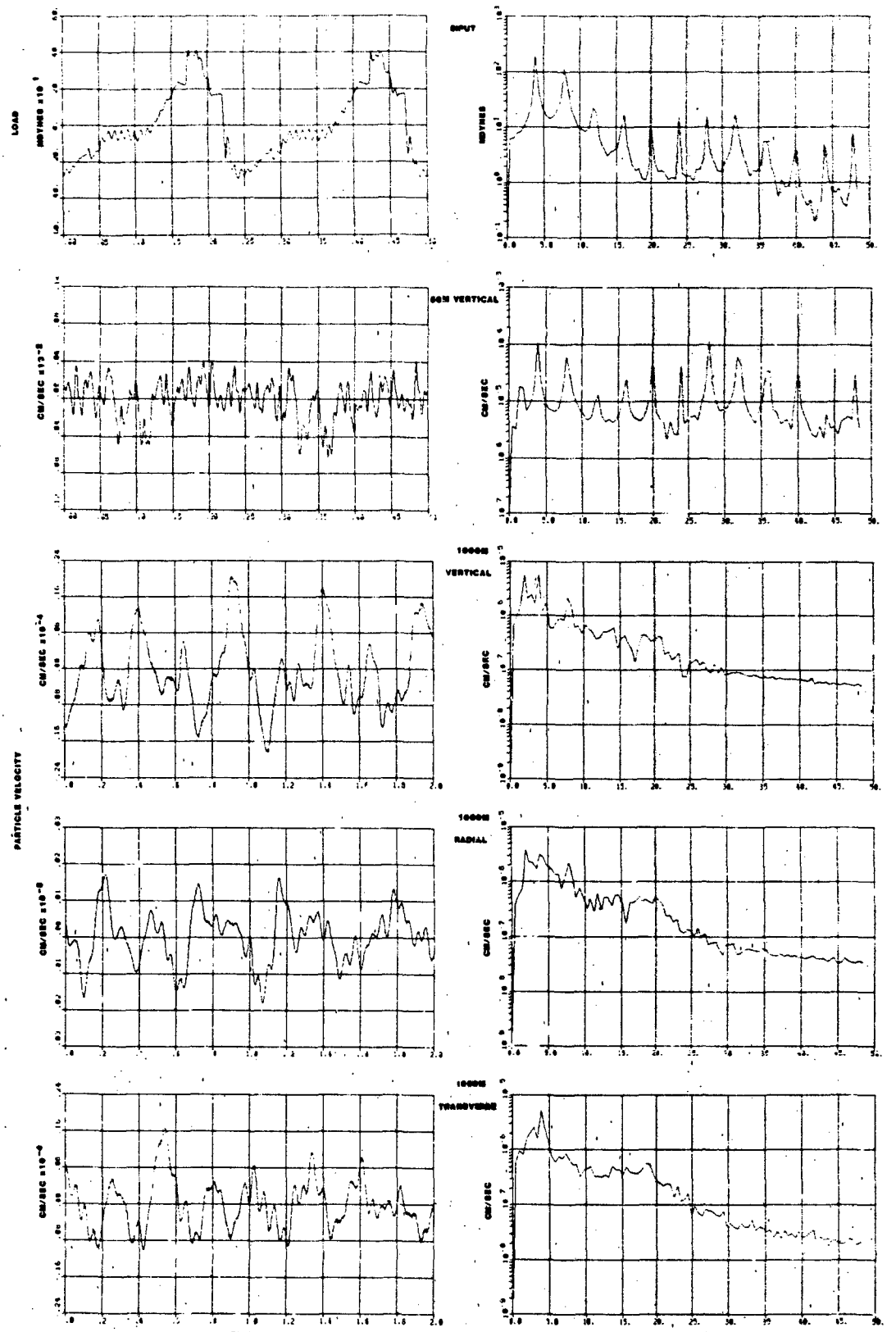

TEST 108 4HZ DISCRETE FREQUENCY SINE WAVE

PLATE 41

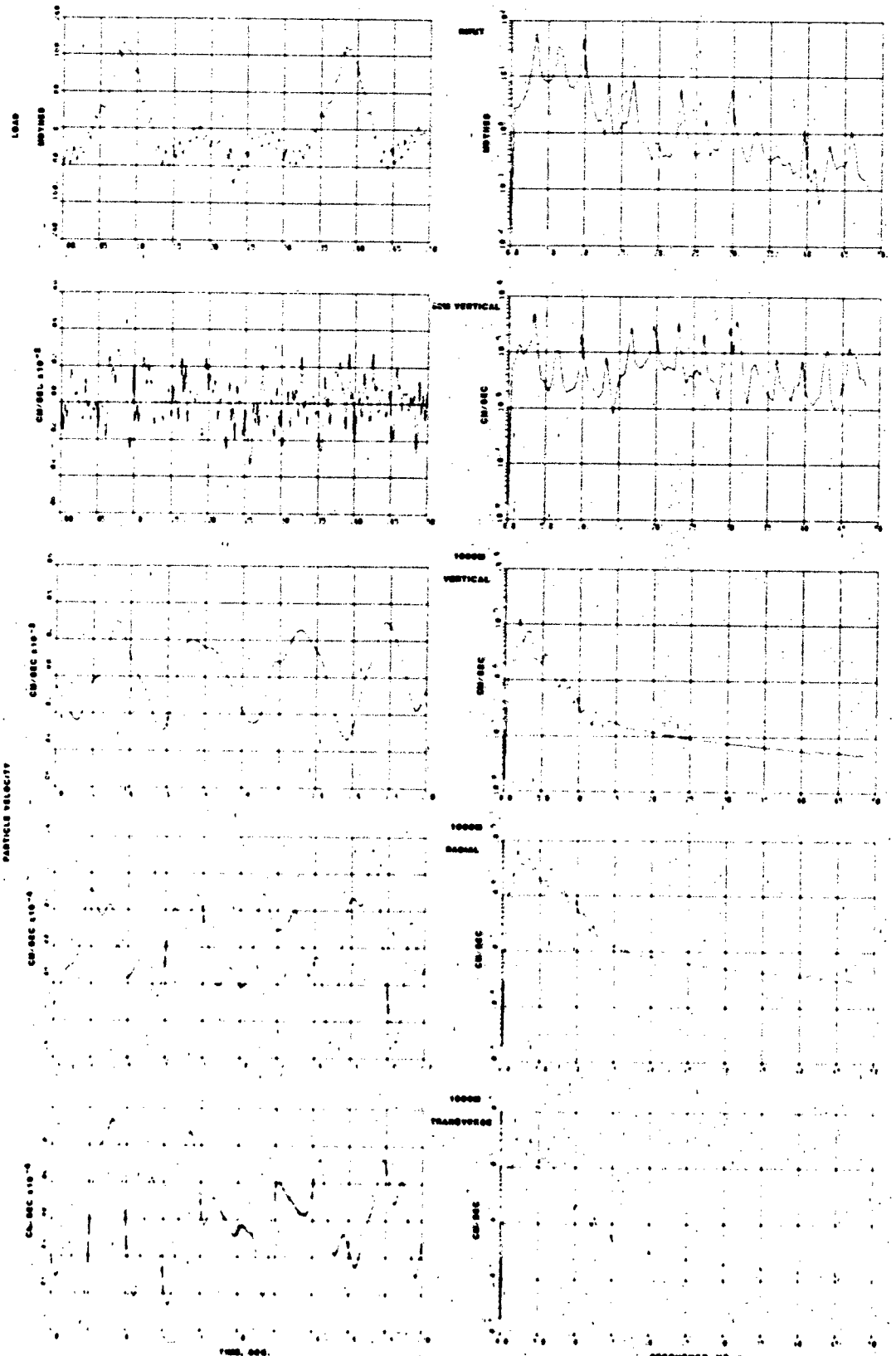

PLATE 42

TEST 110 3.3HZ DISCRETE FREQUENCY SINE WAVE

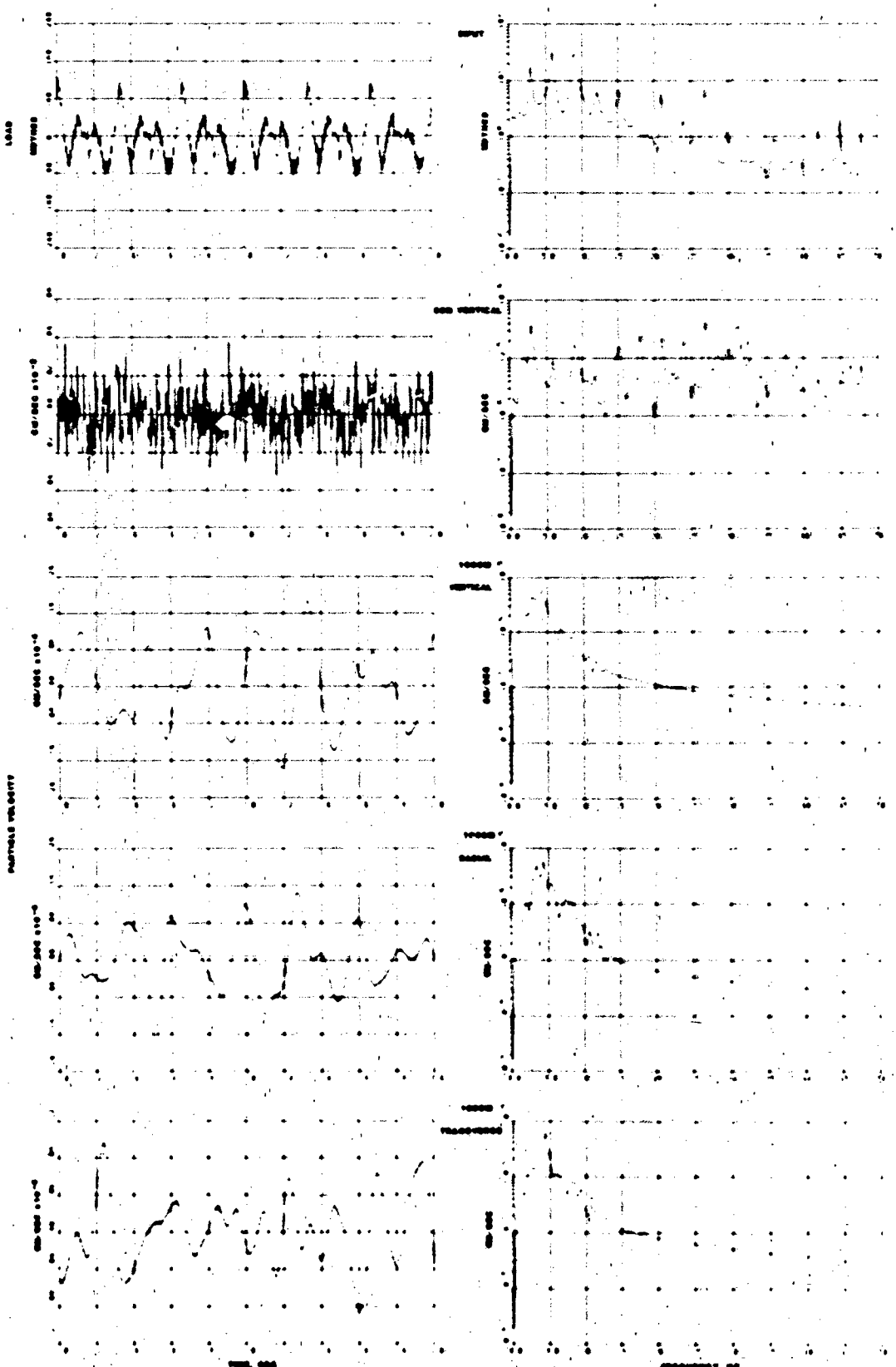

TEST 111 3HZ DISCRETE FREQUENCY SINE WAVE

PLATE 43

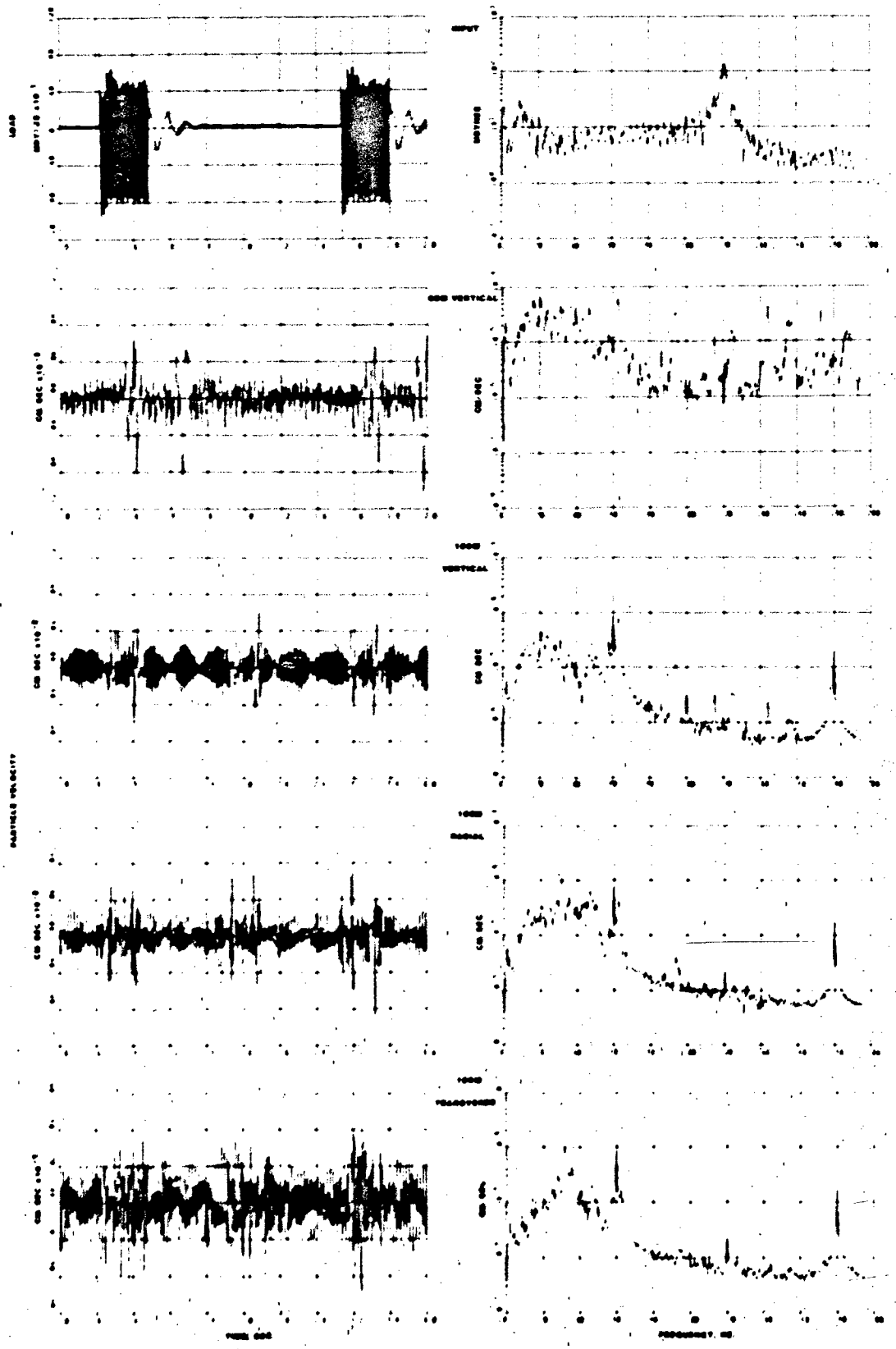

TEST 24 120HZ SINE WAVE TONE BURST

PLATE 44

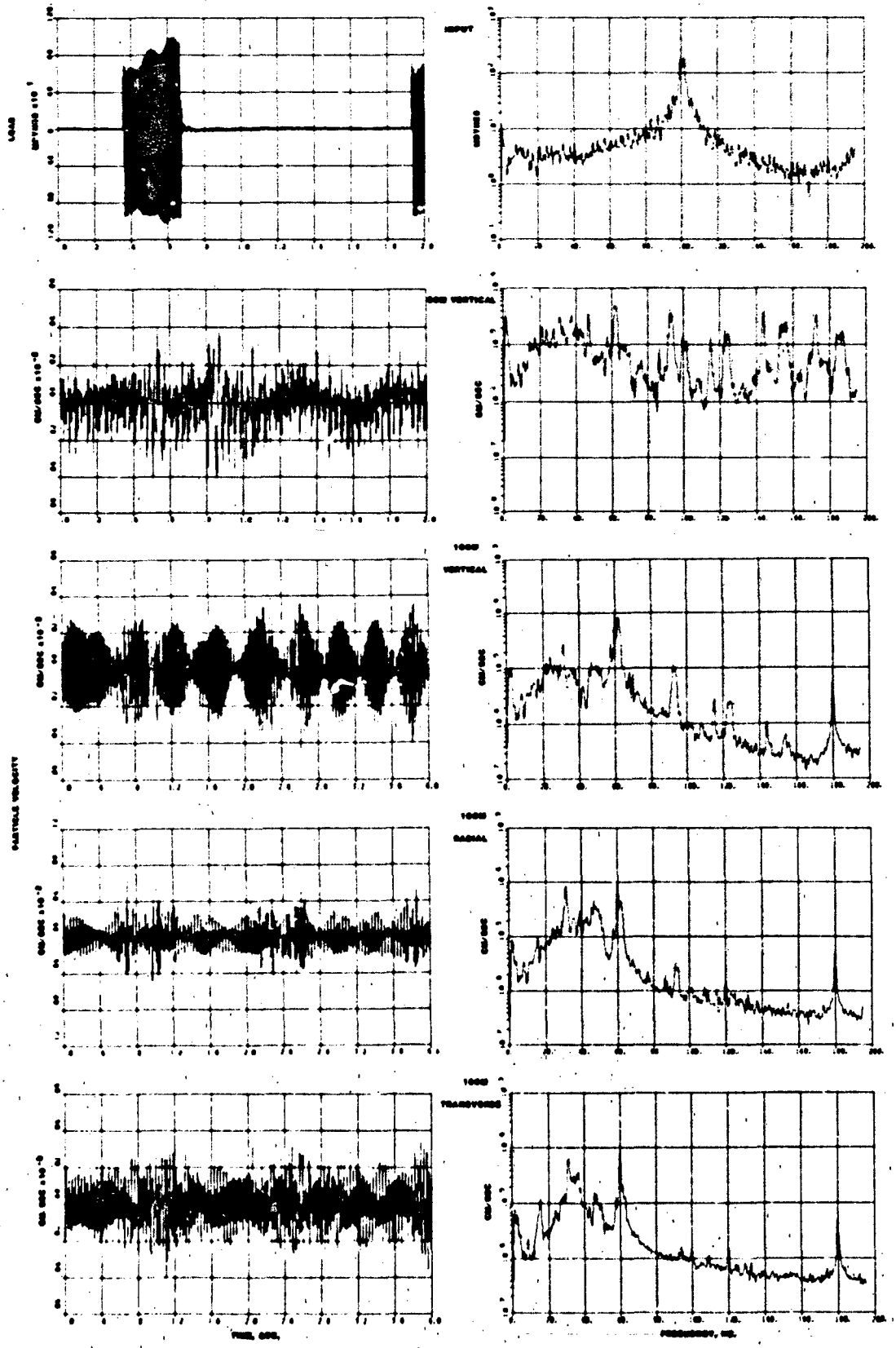

TEST 25 100HZ SINE WAVE TONE FIRST

PLATE 45

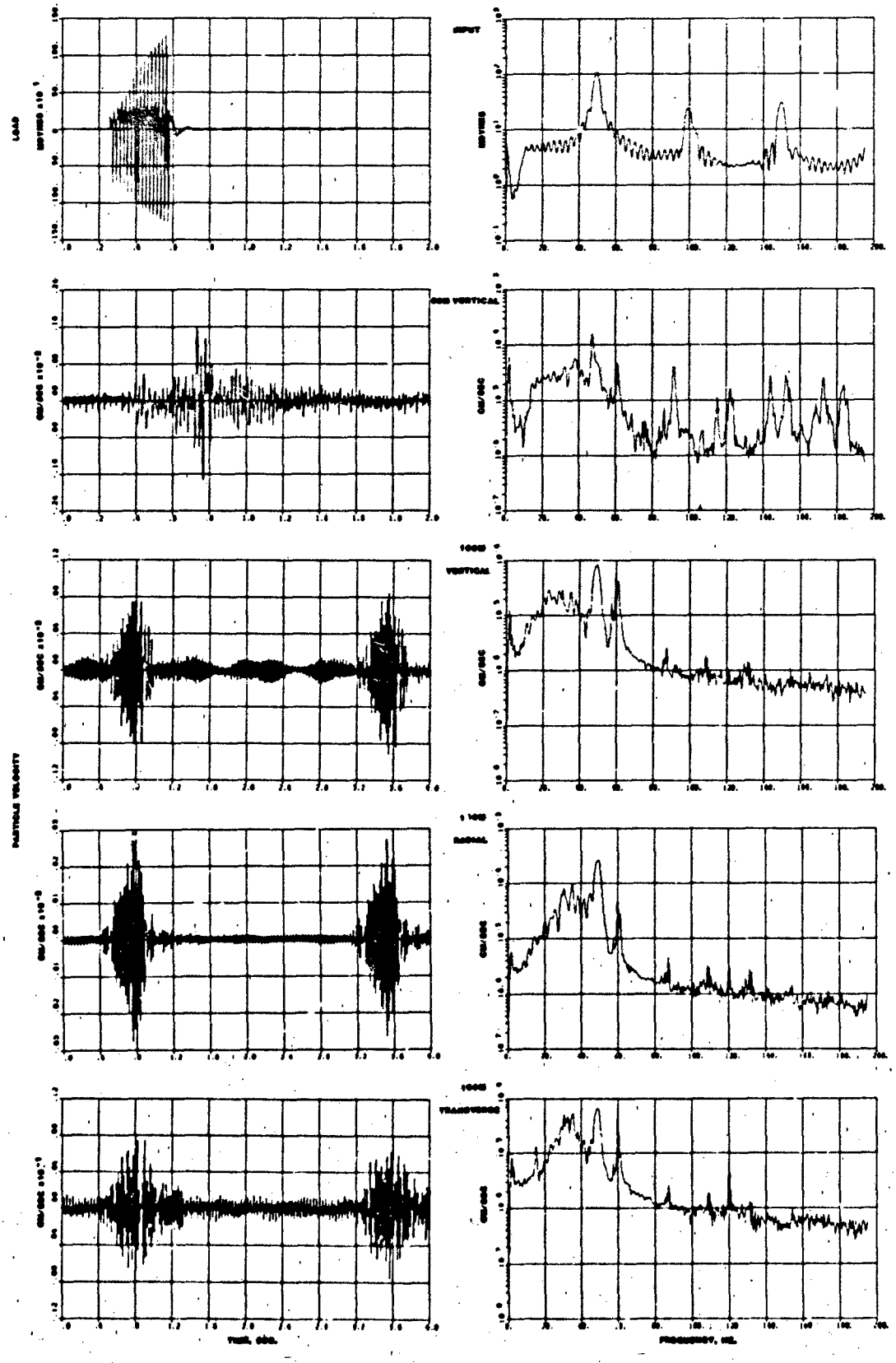

PLATE 46

TEST 26 50HZ SINE WAVE TONE BURST

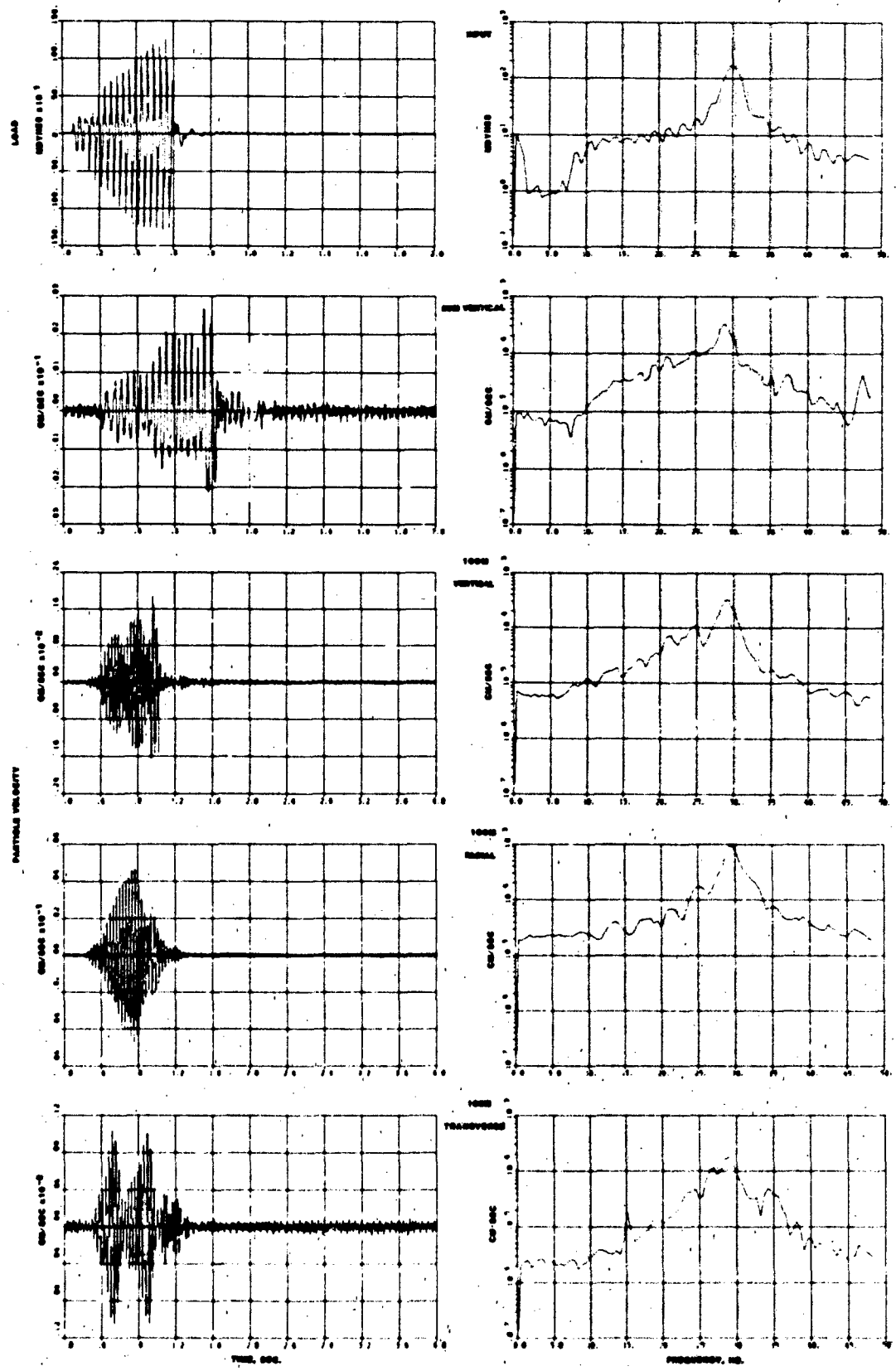

TEST 27 30HZ SINE WAVE TONE BURST

PLATE 47

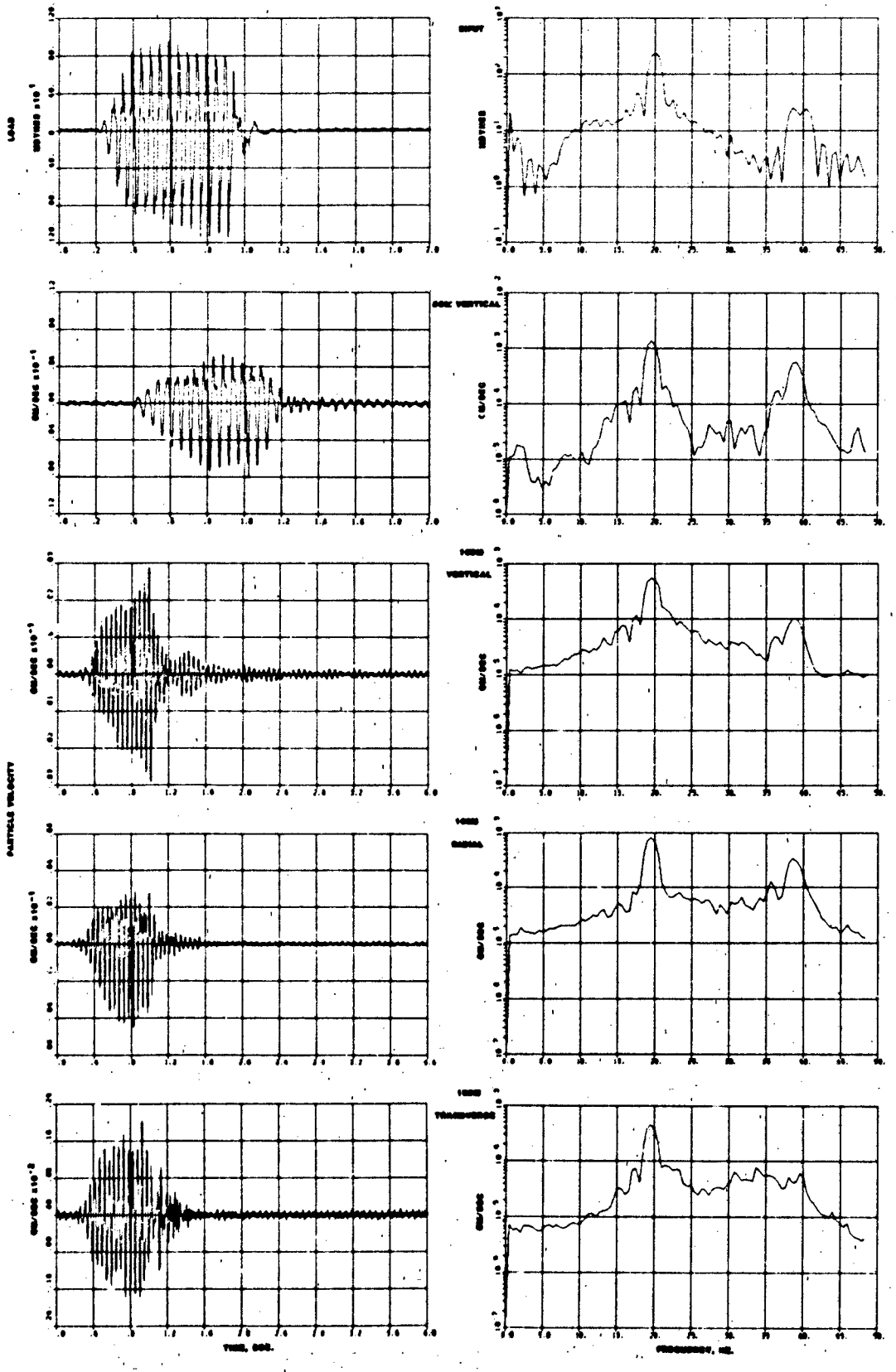

PLATE 48

TEST 28 20HZ SINE WAVE TONE BURST

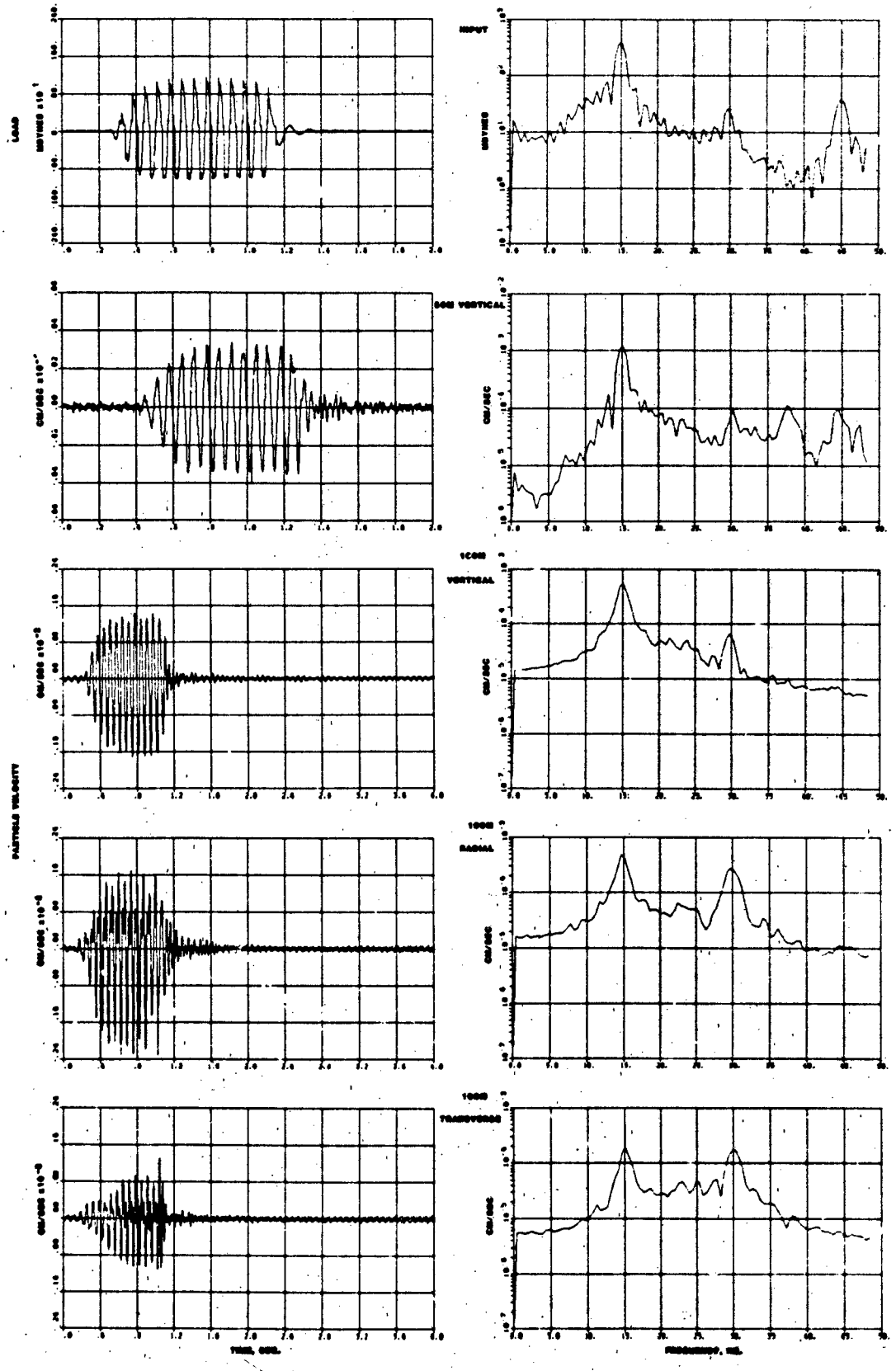

TEST 29 15HZ SINE WAVE TONE BURST

PLATE 49

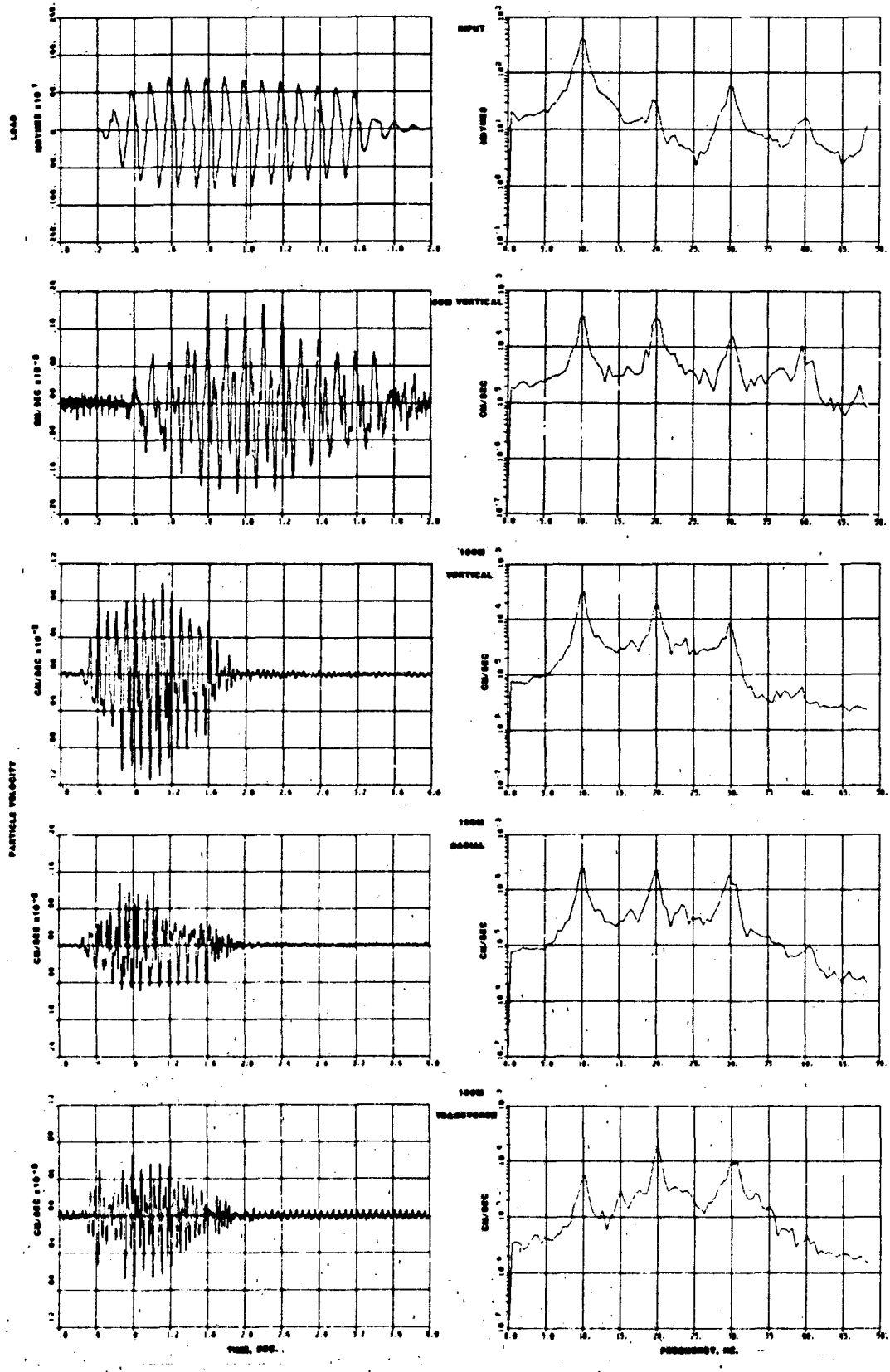

TEST 30 10HZ SINE WAVE TONE BURST

PLATE 50

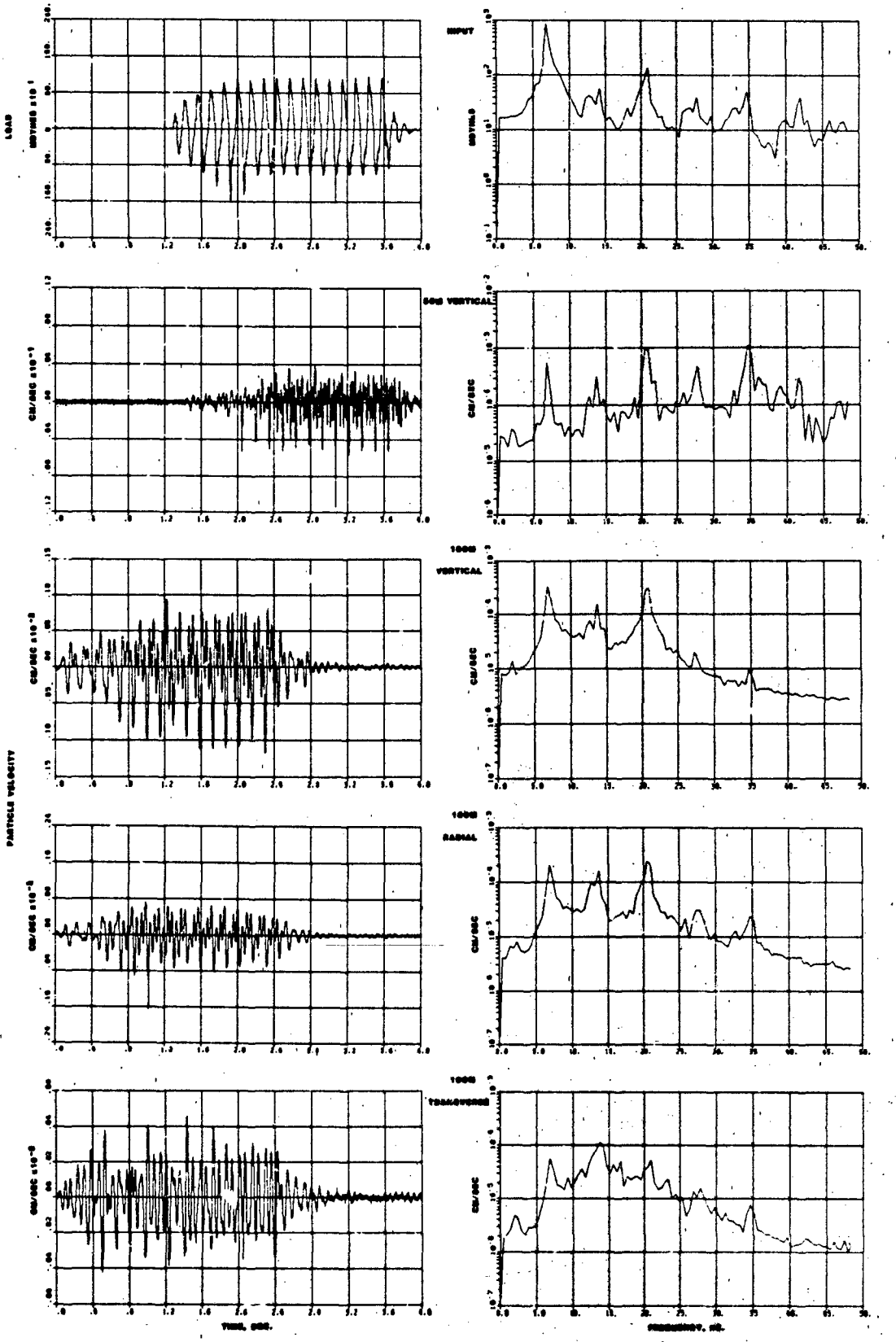

TEST 31 7HZ SINE WAVE TONE BURST

PLATE 51

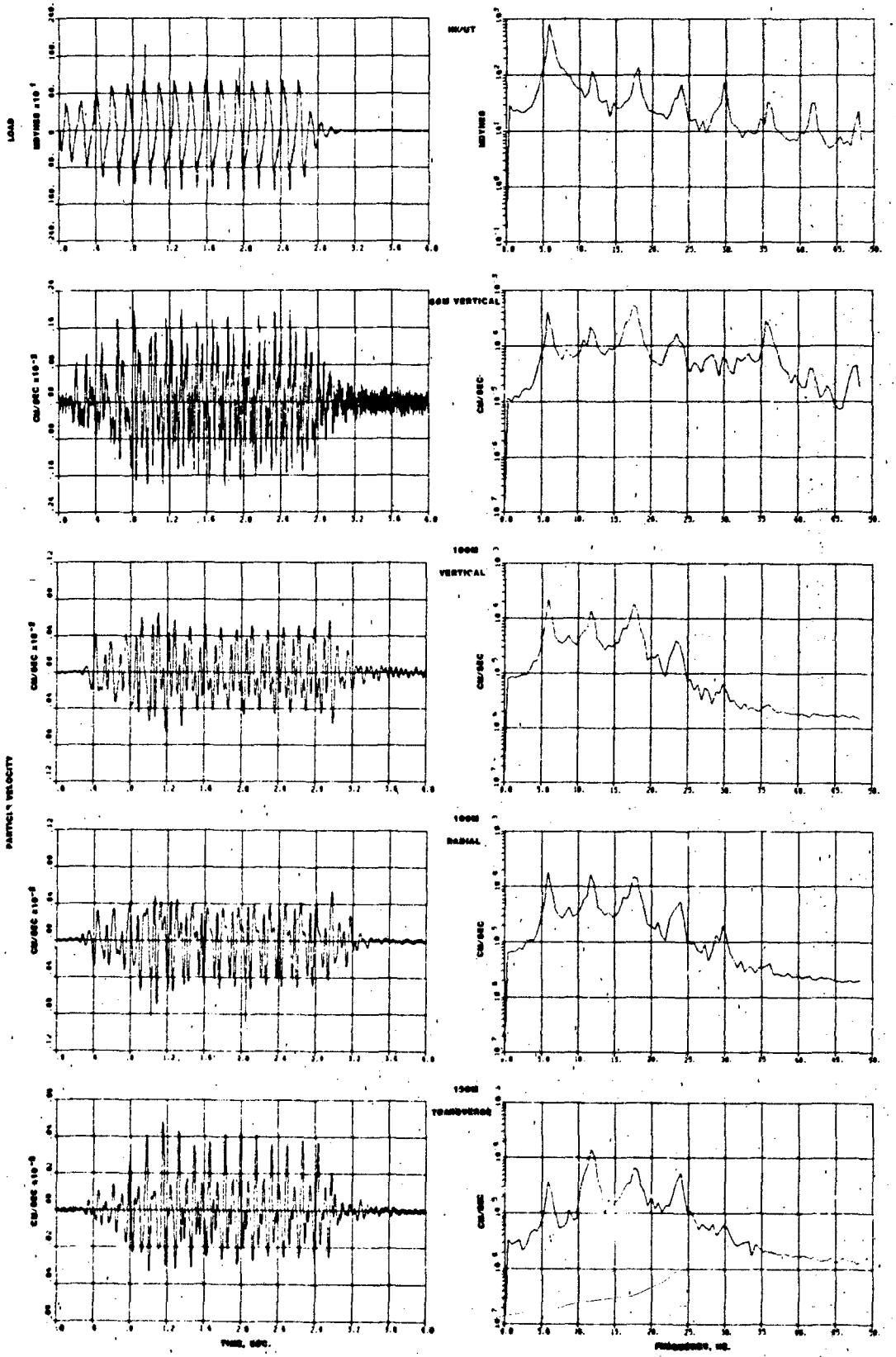

PLATE 52

TEST 32 6HZ SINE WAVE TONE BURST

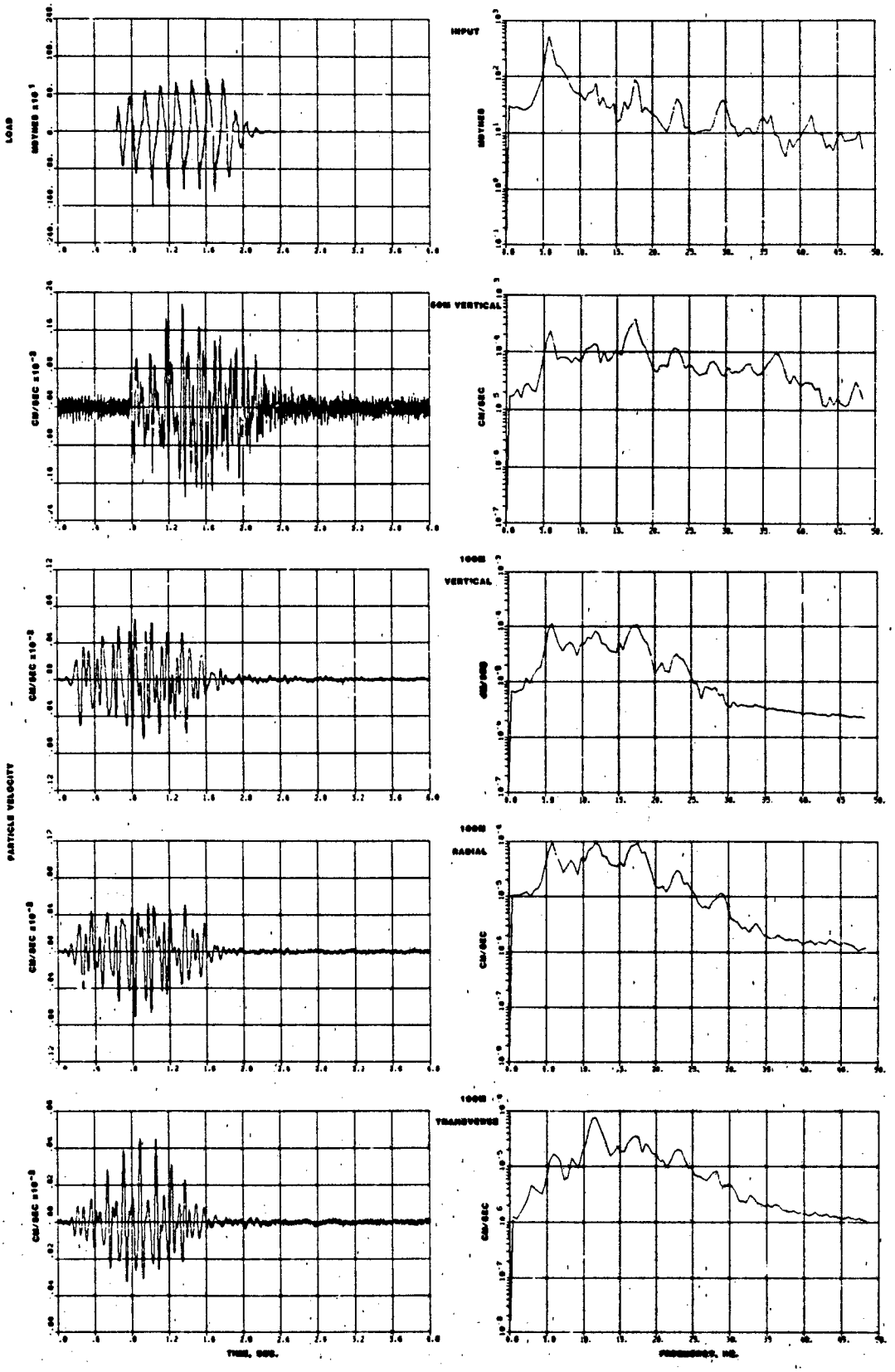

TEST 33 6HZ SINE WAVE TONE BURST

PLATE 53

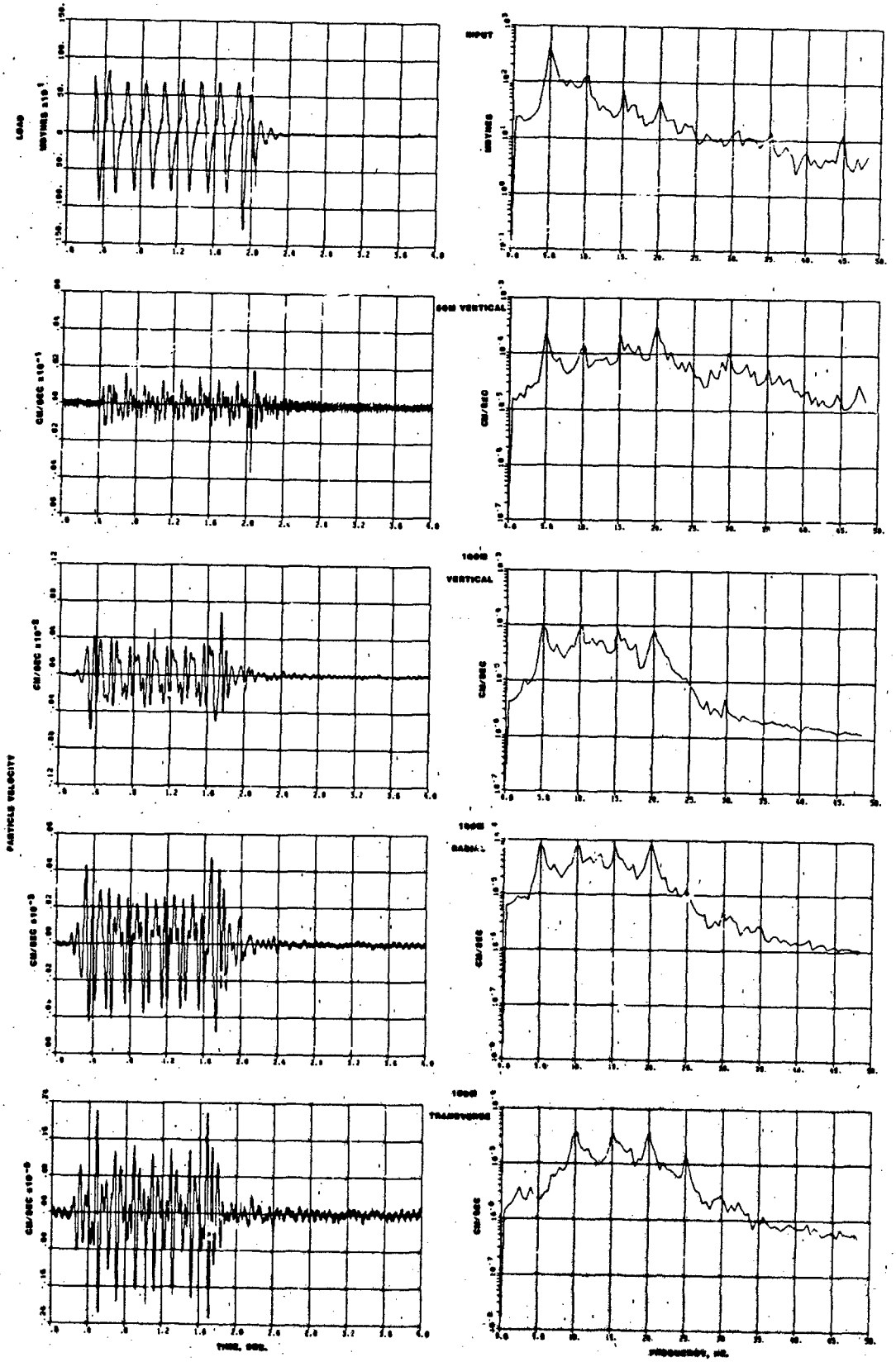

PLATE 54

TEST 34 5HZ SINE WAVE TONE BURST

Frames 1
Signal Y

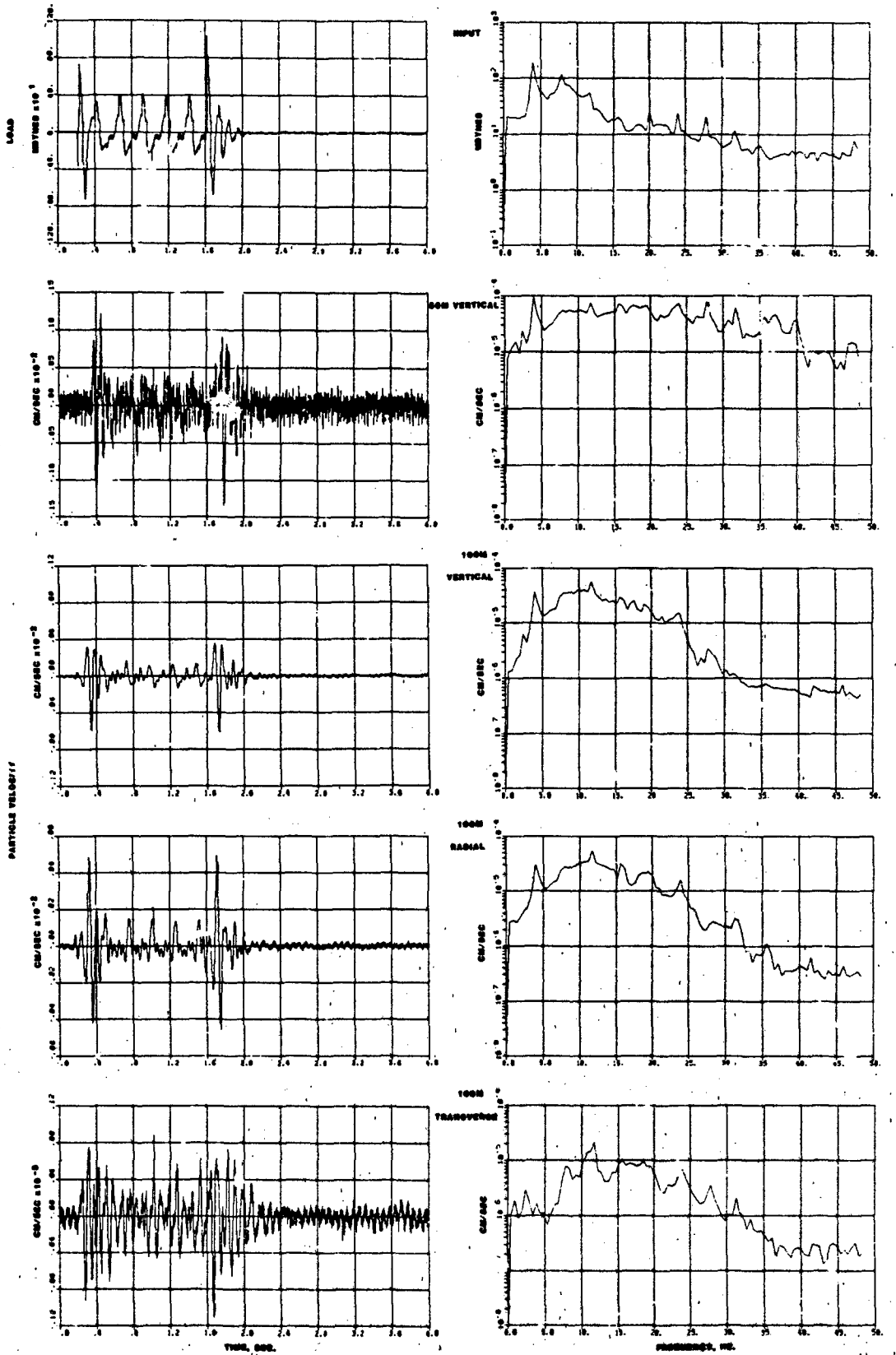

TEST 35 4HZ SINE WAVE TONE BURST

PLATE 55

Firmes Signal

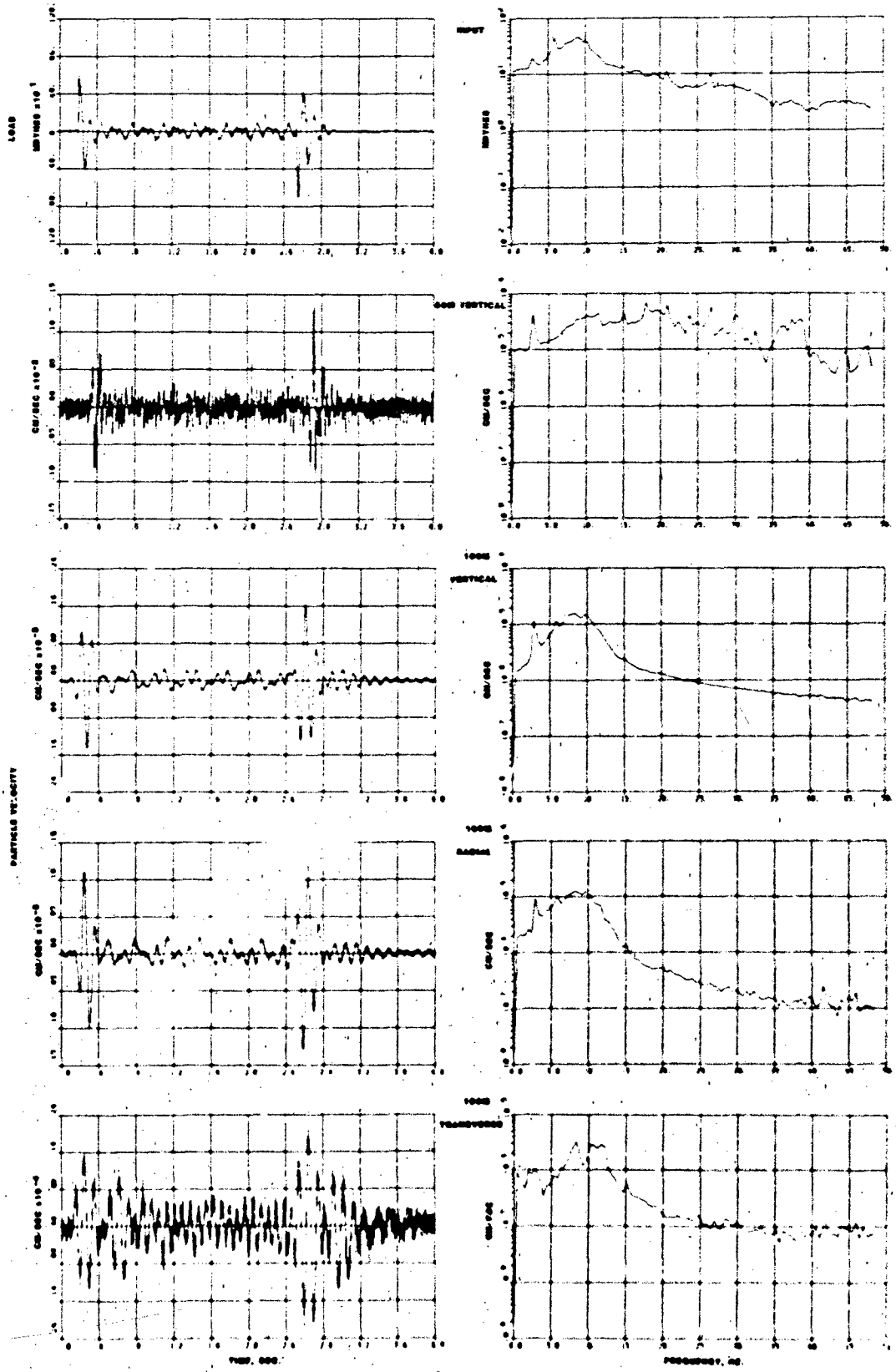

PLATE 56

TEST 39 3HZ SINE WAVE TONE BURST

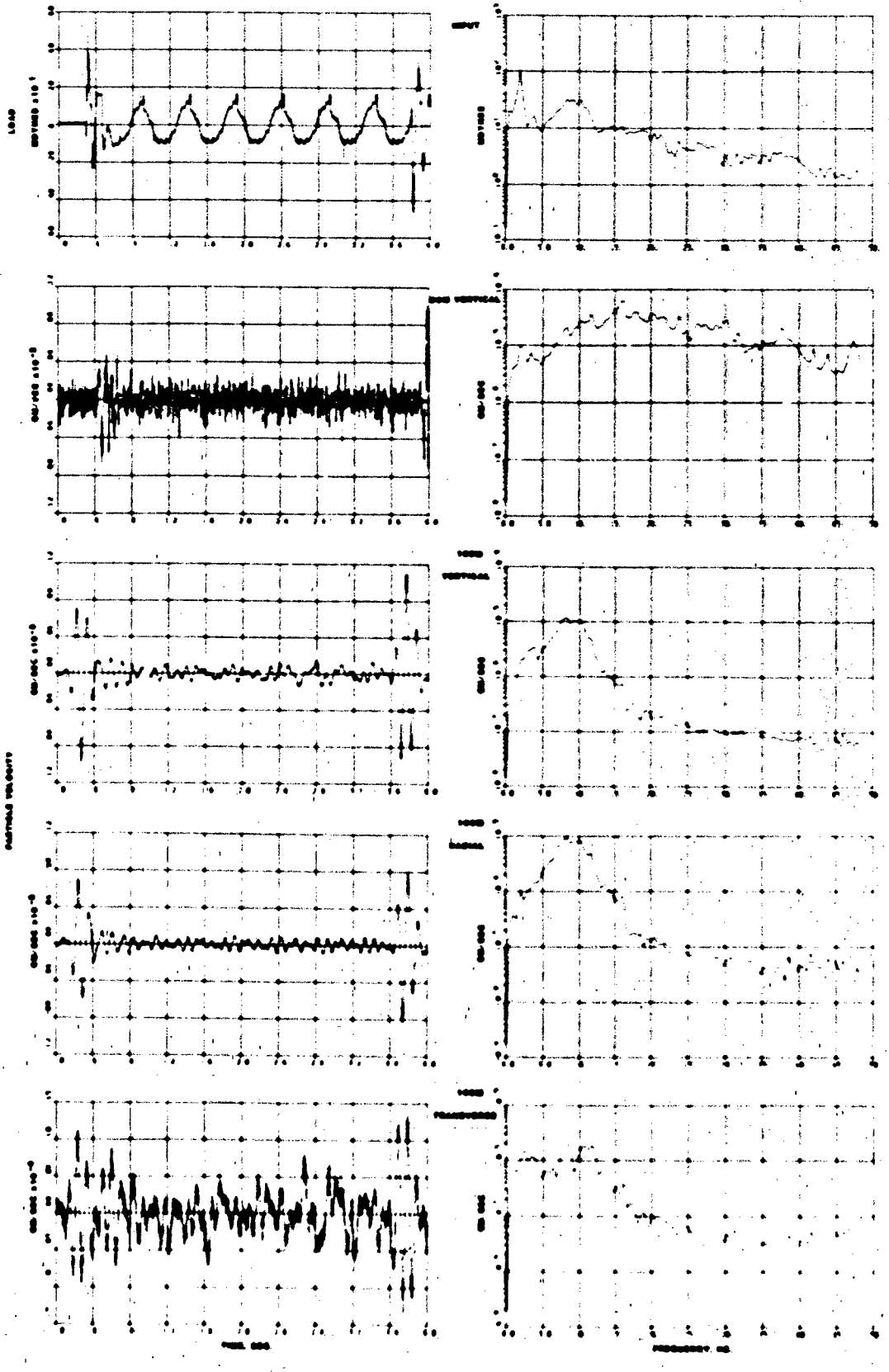

TEST 37 2HZ SINE WAVE TONE BURST

PLATE 57

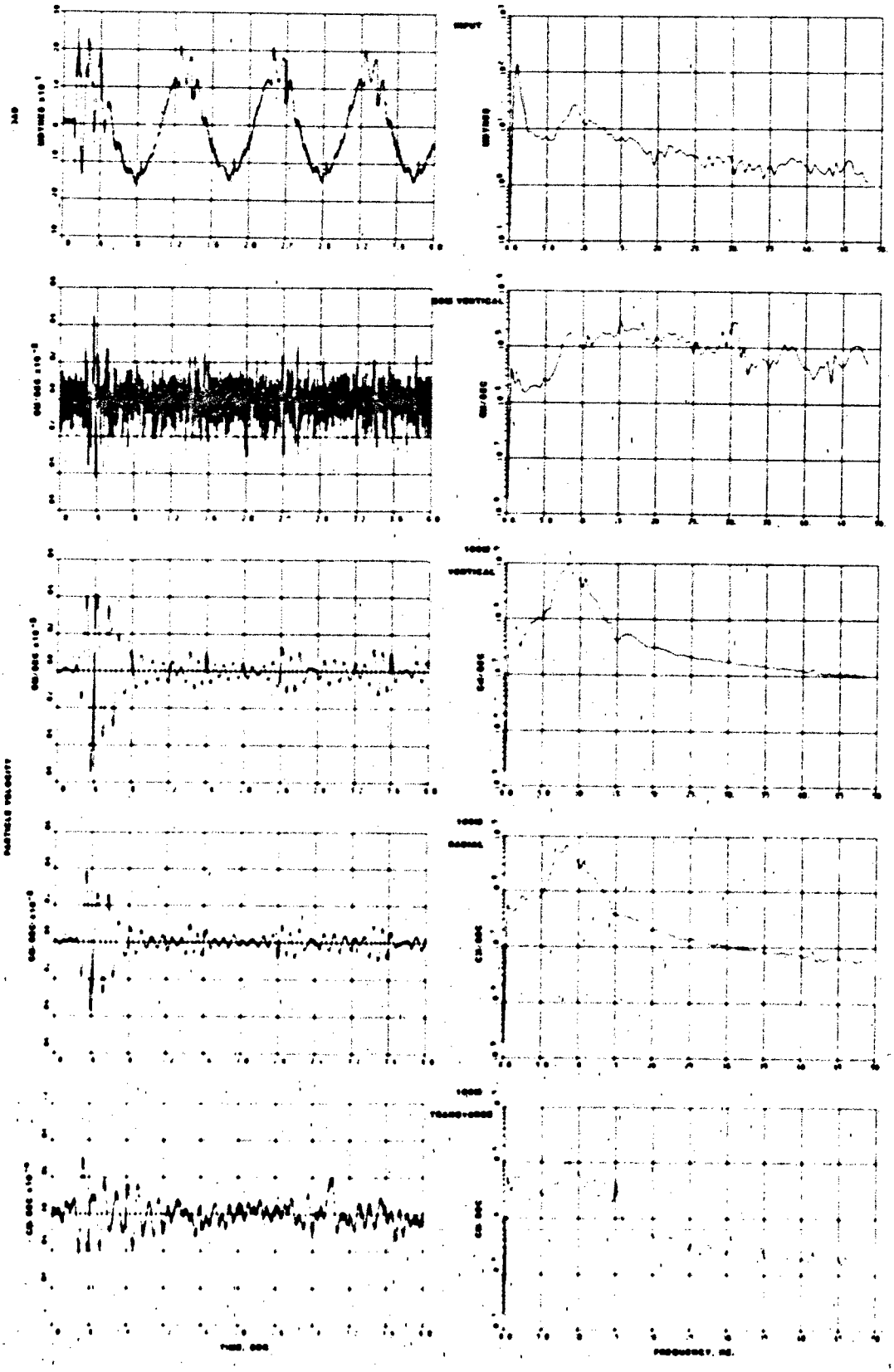

PLATE 58

TEST 38 1HZ SINE WAVE TONE BURST

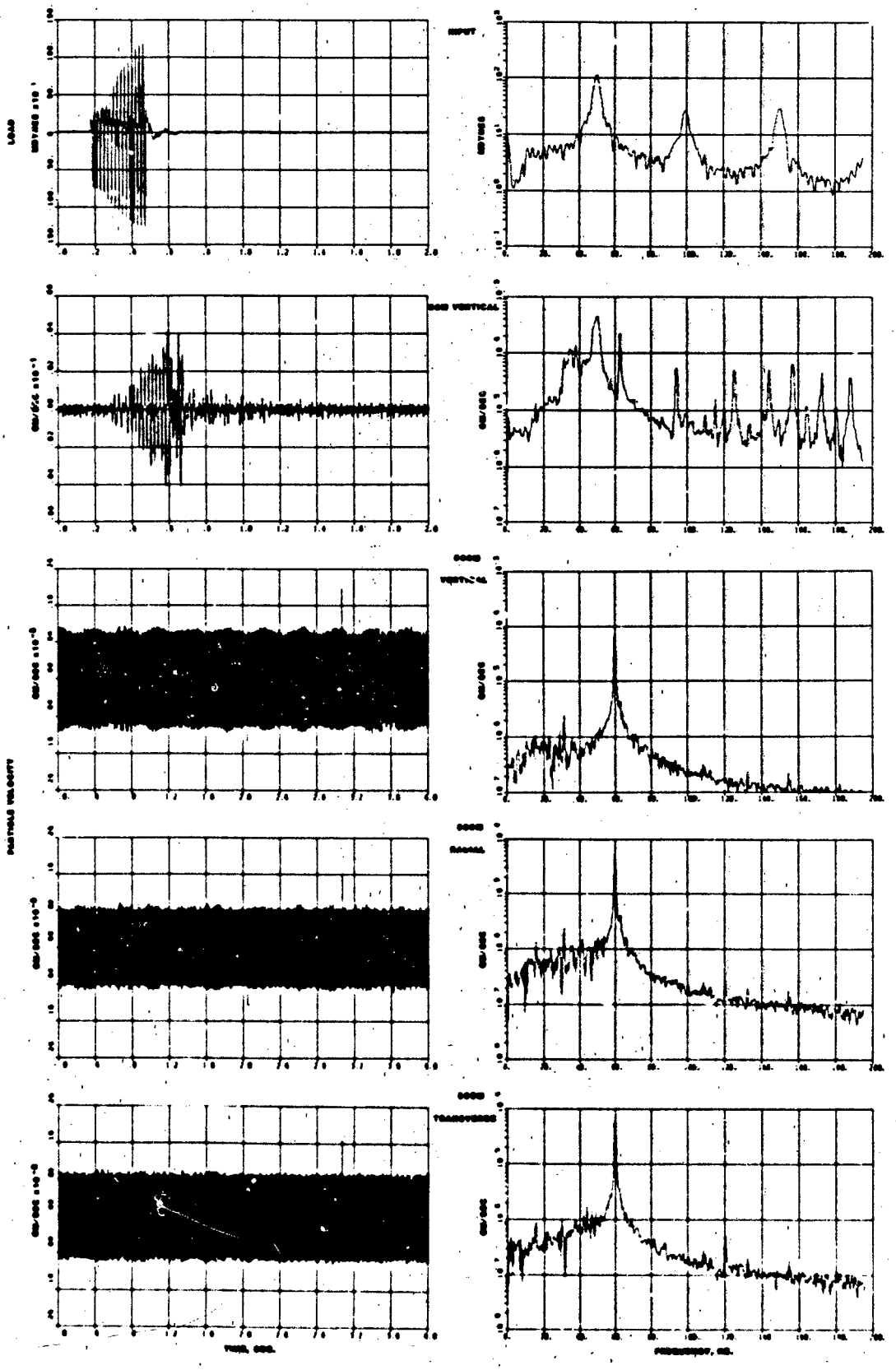

TEST 56 50HZ SINE WAVE TONE BURST

PLATE 59

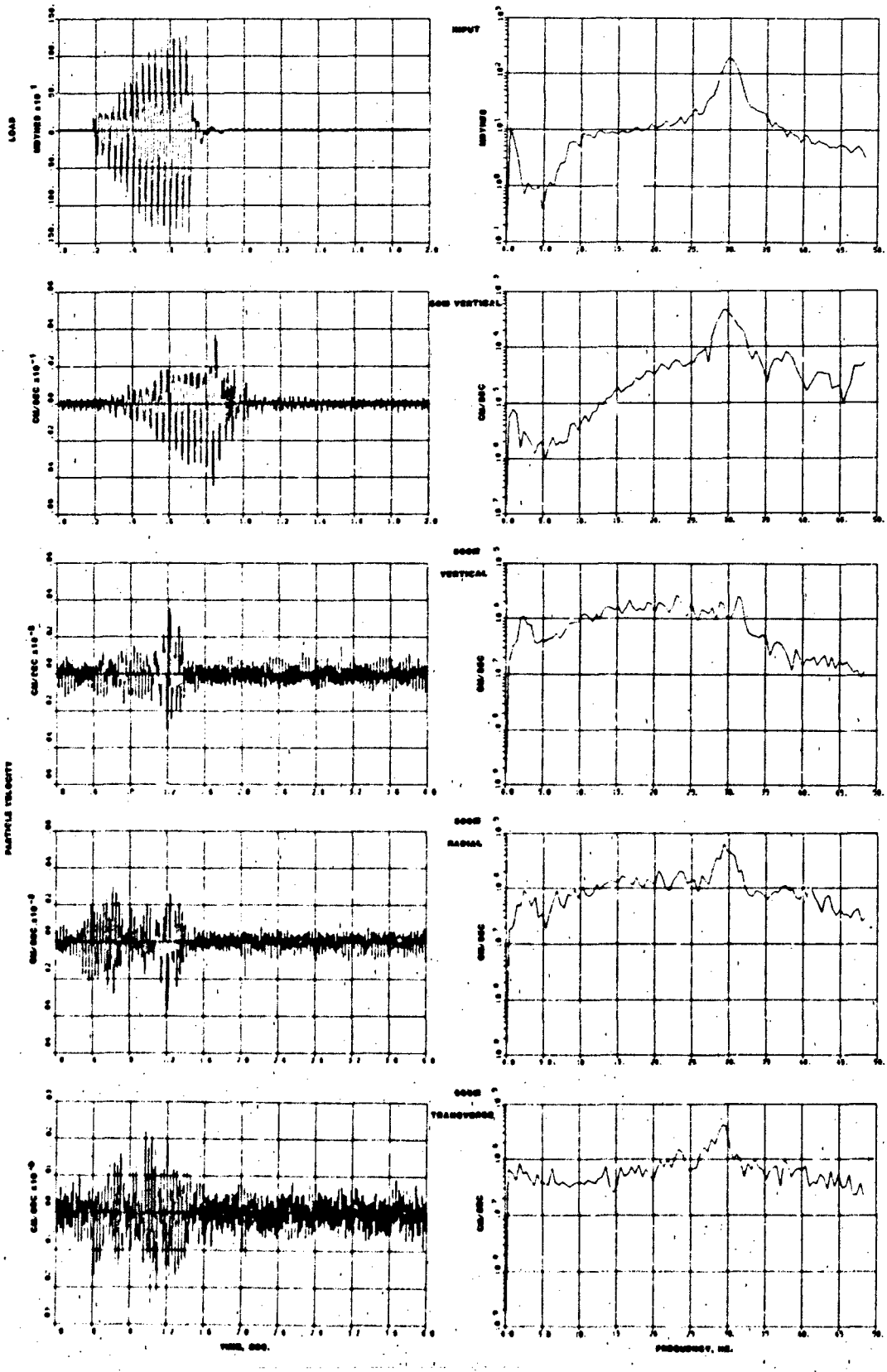

PLATE 60

TEST 58 30HZ SINE WAVE TONE BURST

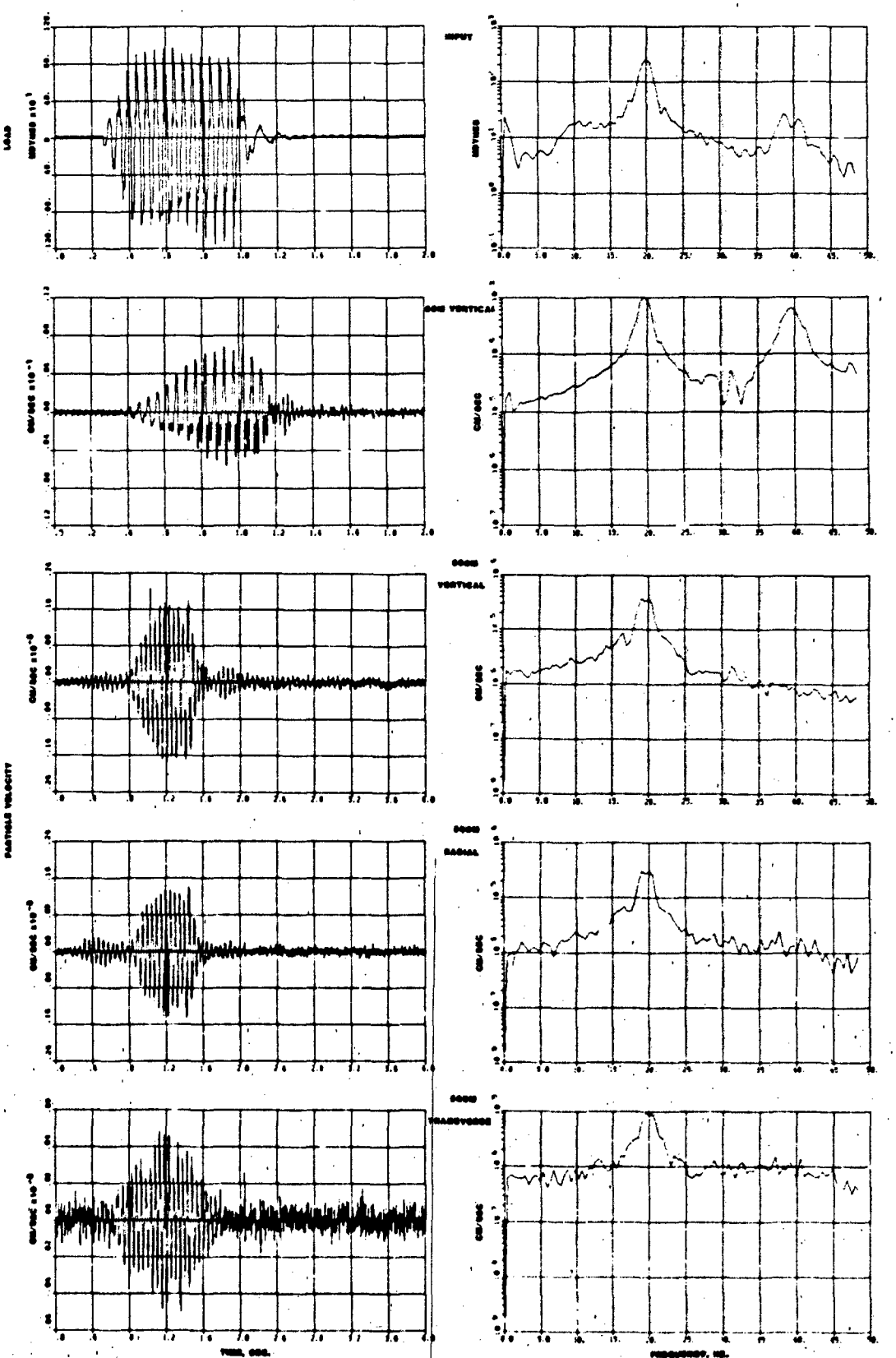

TEST 60 20HZ SINE WAVE TONE BURST

PLATE 61

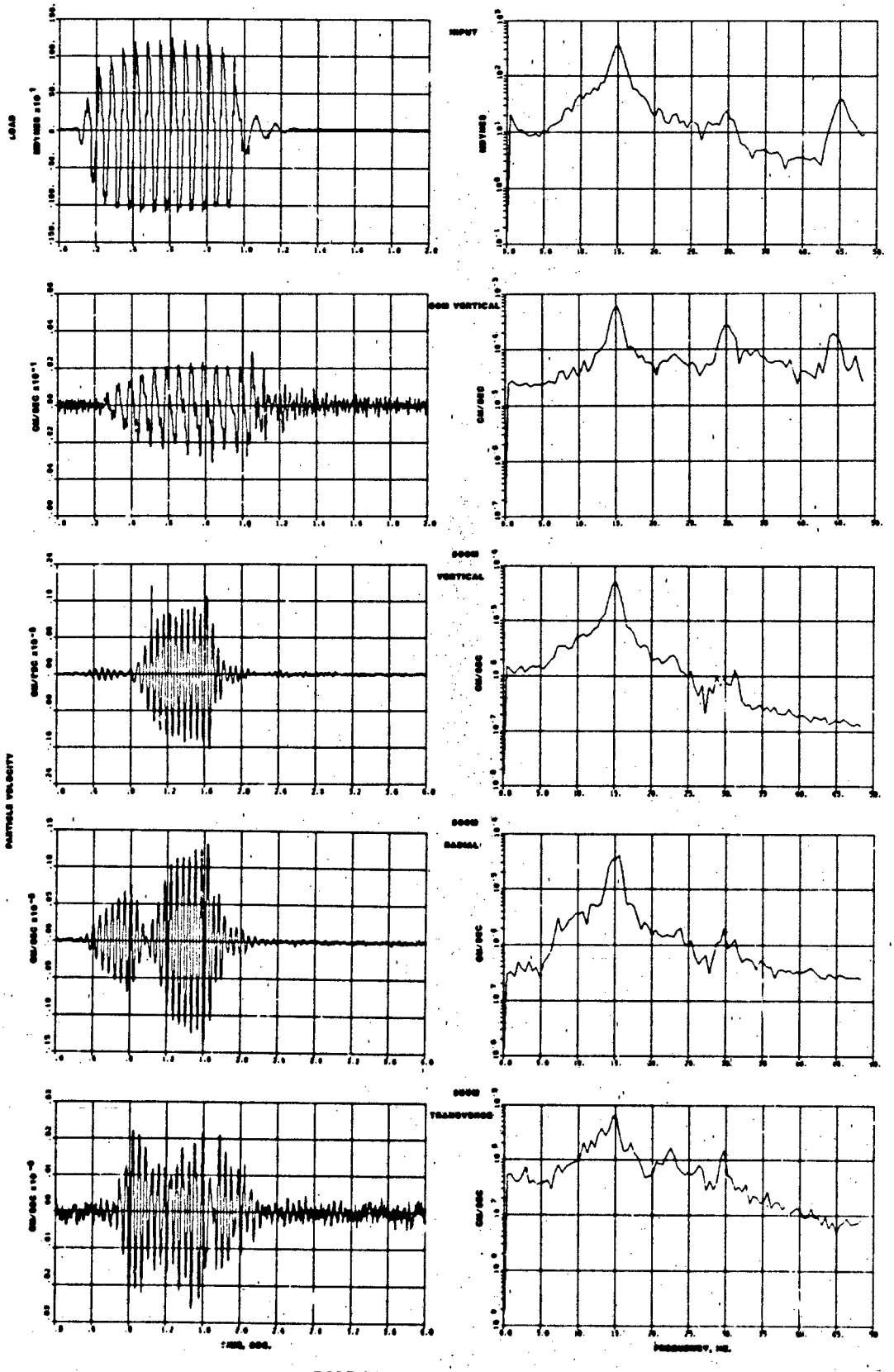

PLATE 62

TEST 63 15HZ SINE WAVE TONE BURST

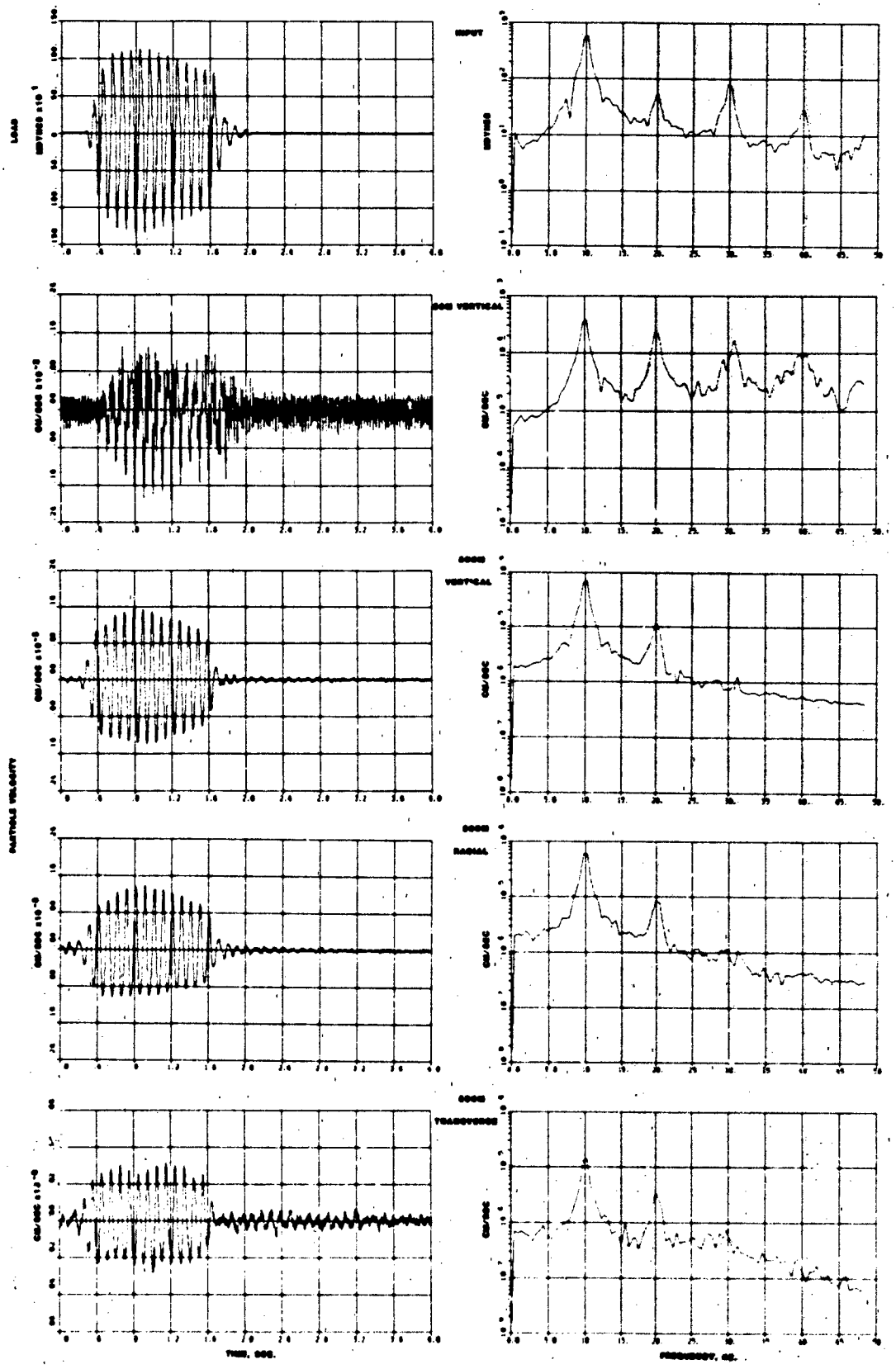

TEST 65 10HZ SINE WAVE TONE BURST

PLATE 63

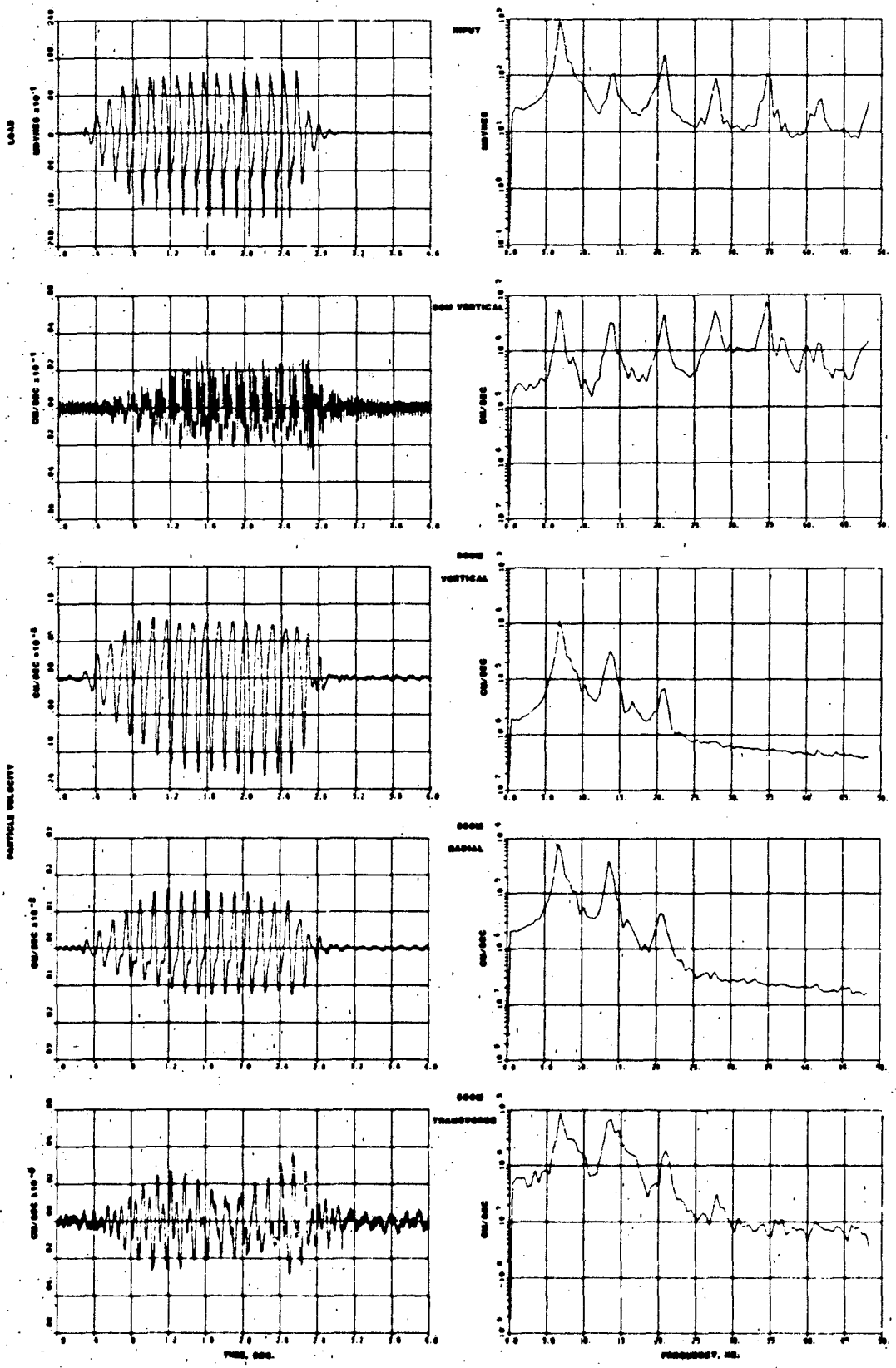

TEST 67 7HZ SINE WAVE TONE BURST

PLATE 64

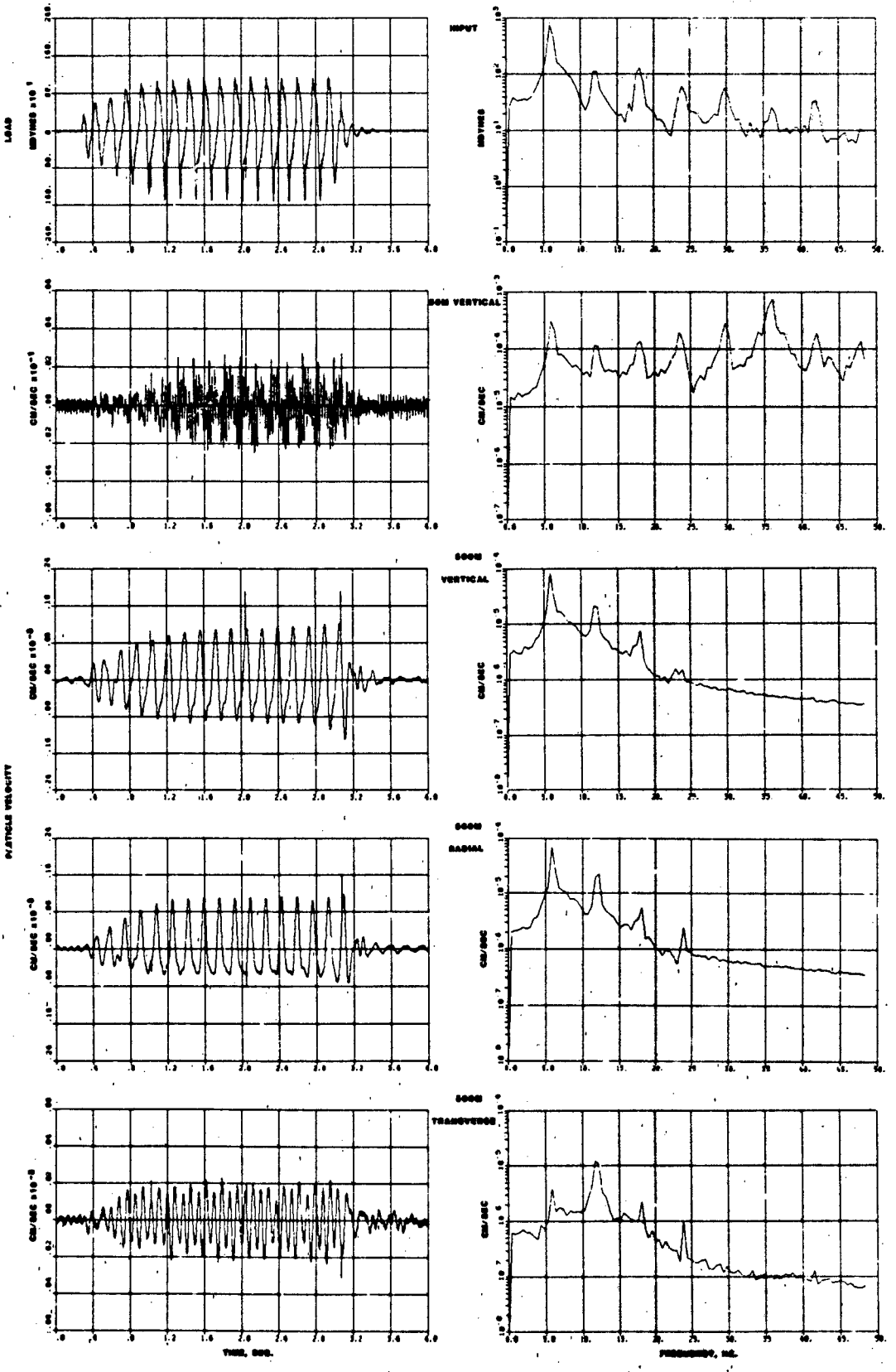

TEST 69 GHZ SINE WAVE TONE BURST

PLATE 65

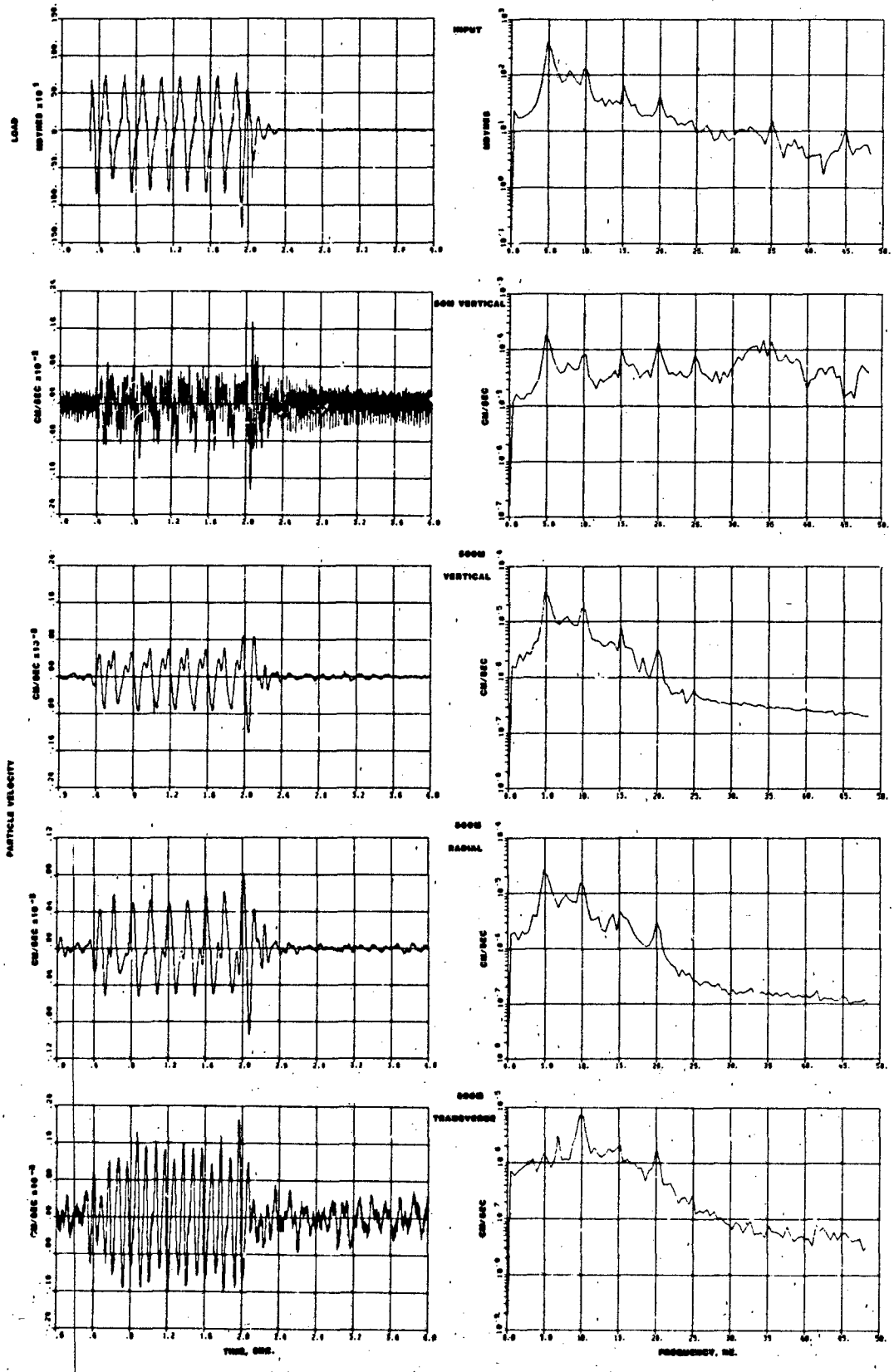

TEST 71 5HZ SINE WAVE TONE BURST

PLATE 66

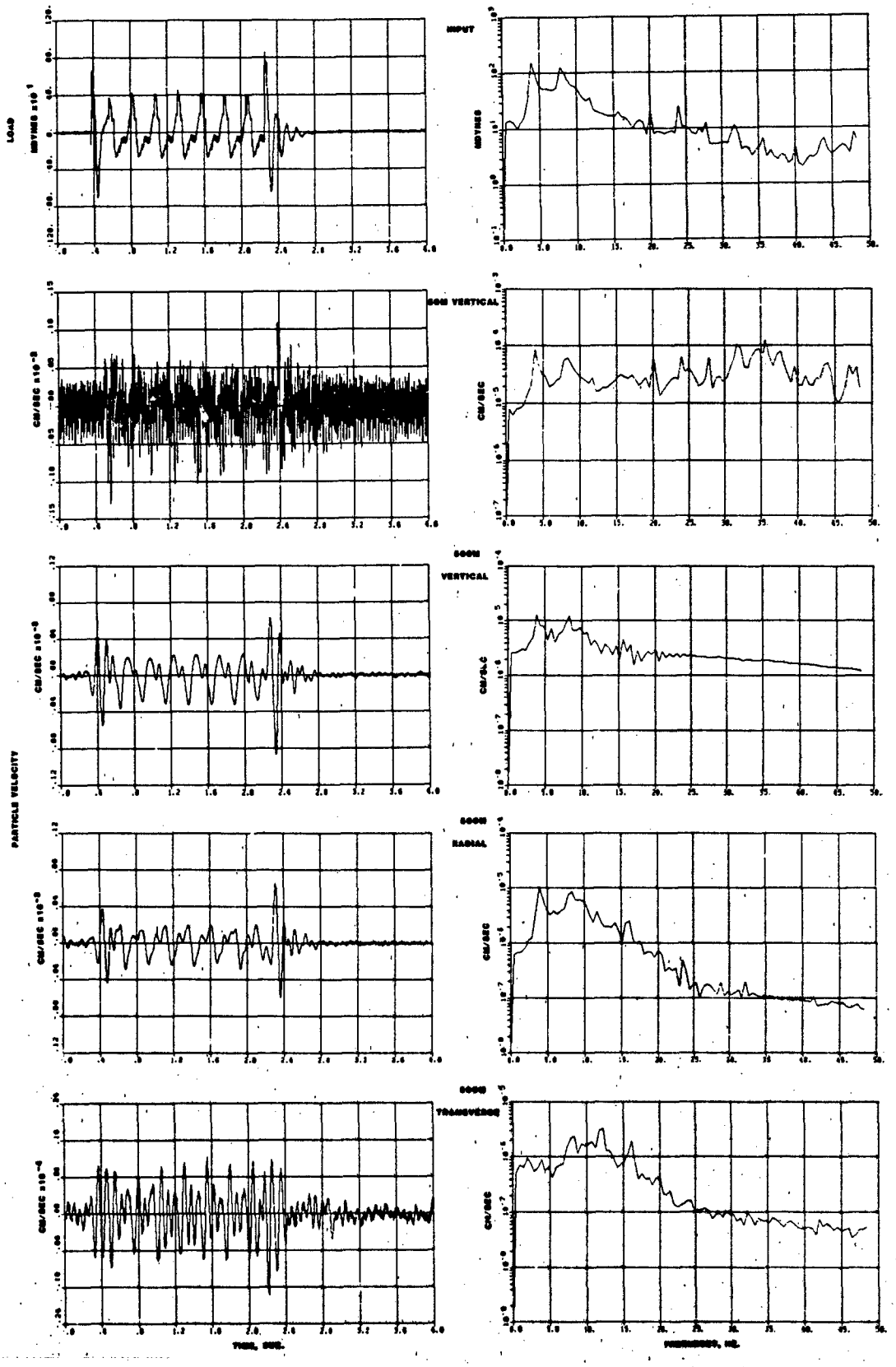

TEST 73 4HZ SINE WAVE TONE BURST

PLATE 67

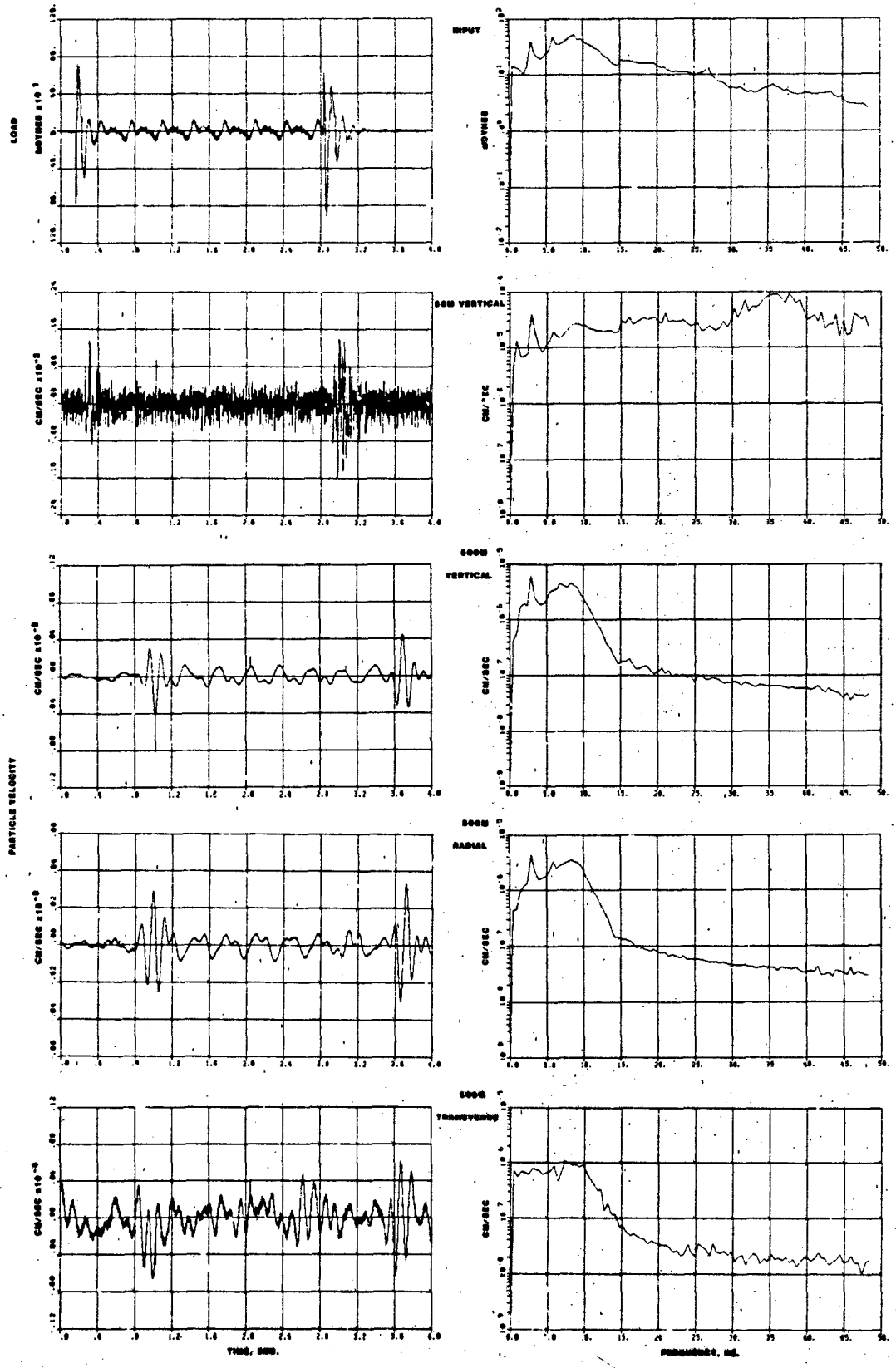

TEST 78 3HZ SINE WAVE TONE BURST

PLATE 68

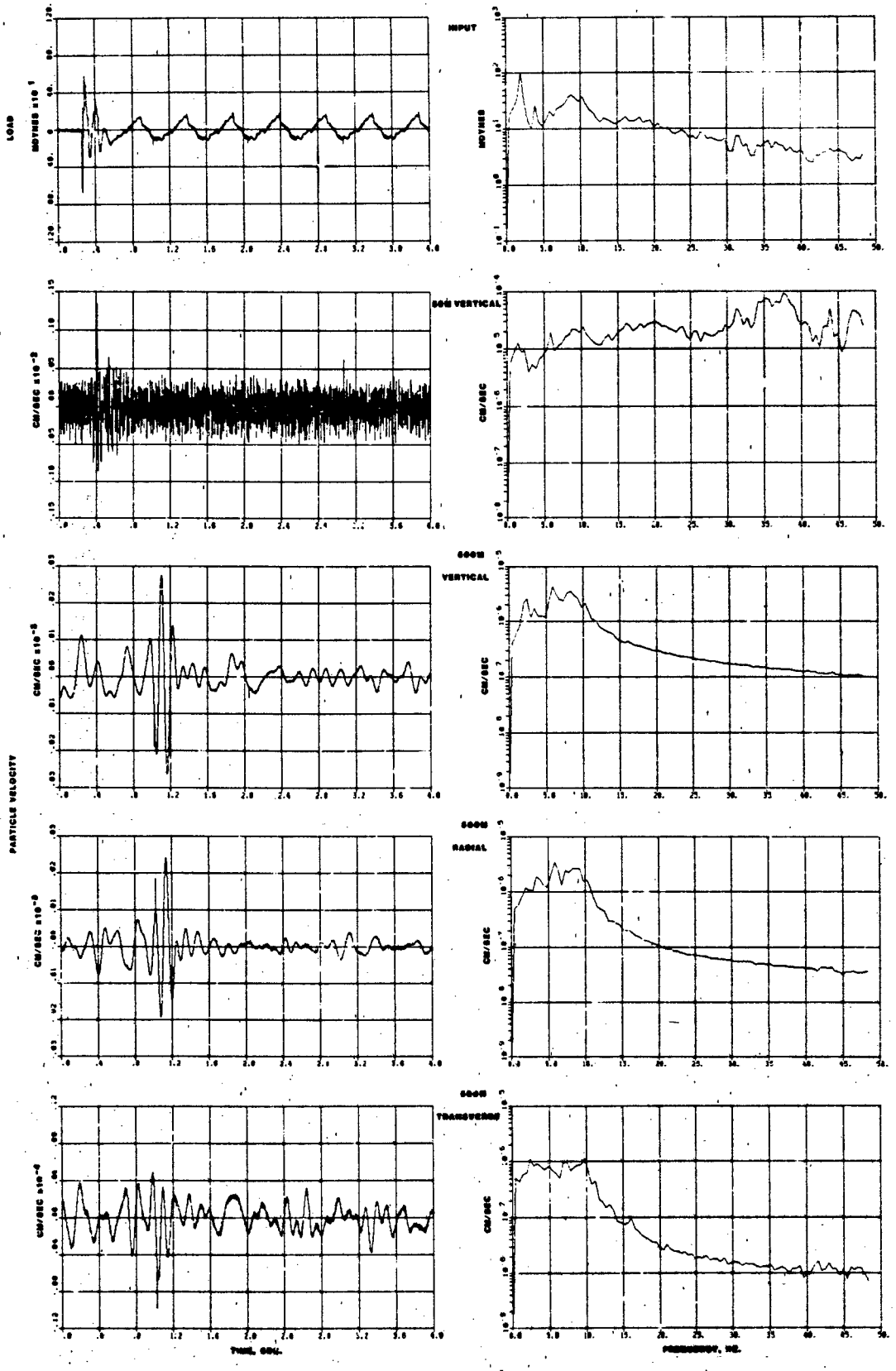

TEST 78 2HZ SINE WAVE TONE BURST

PLATE 69

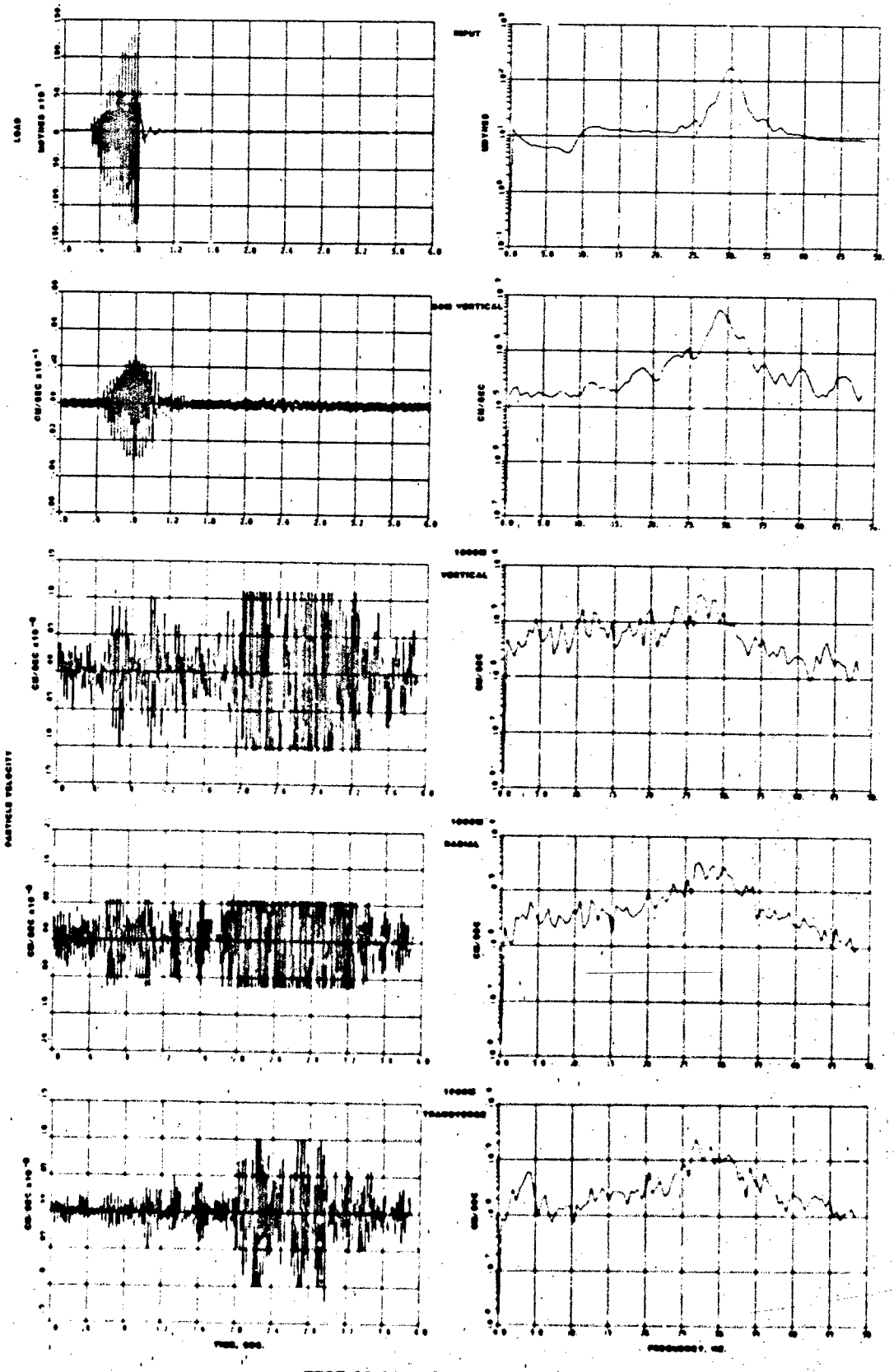

PLATE 70

TEST 93 30HZ SINE WAVE TONE BURST

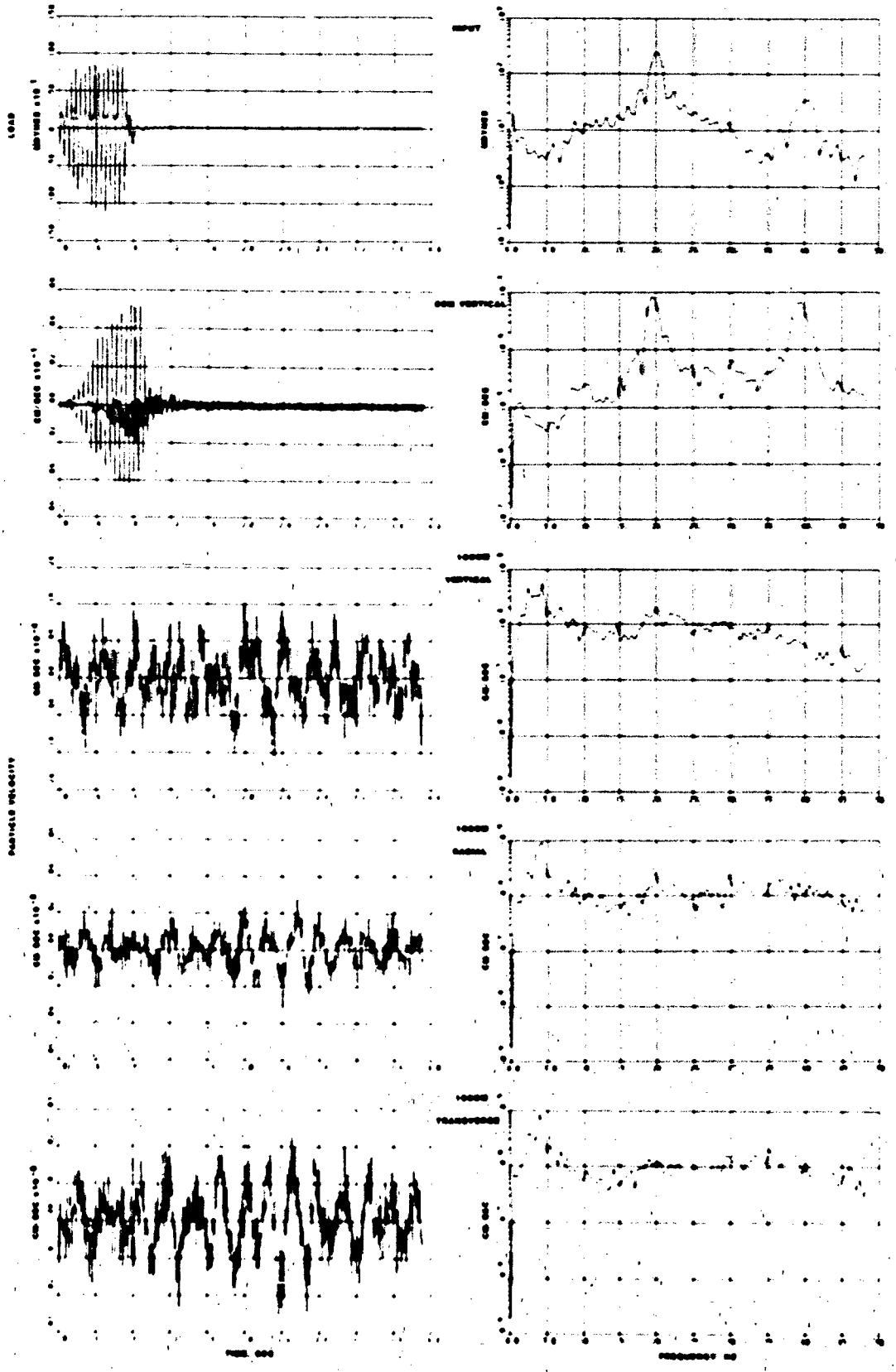

TEST 95 20HZ SINE WAVE TONE BURST

PLATE 71

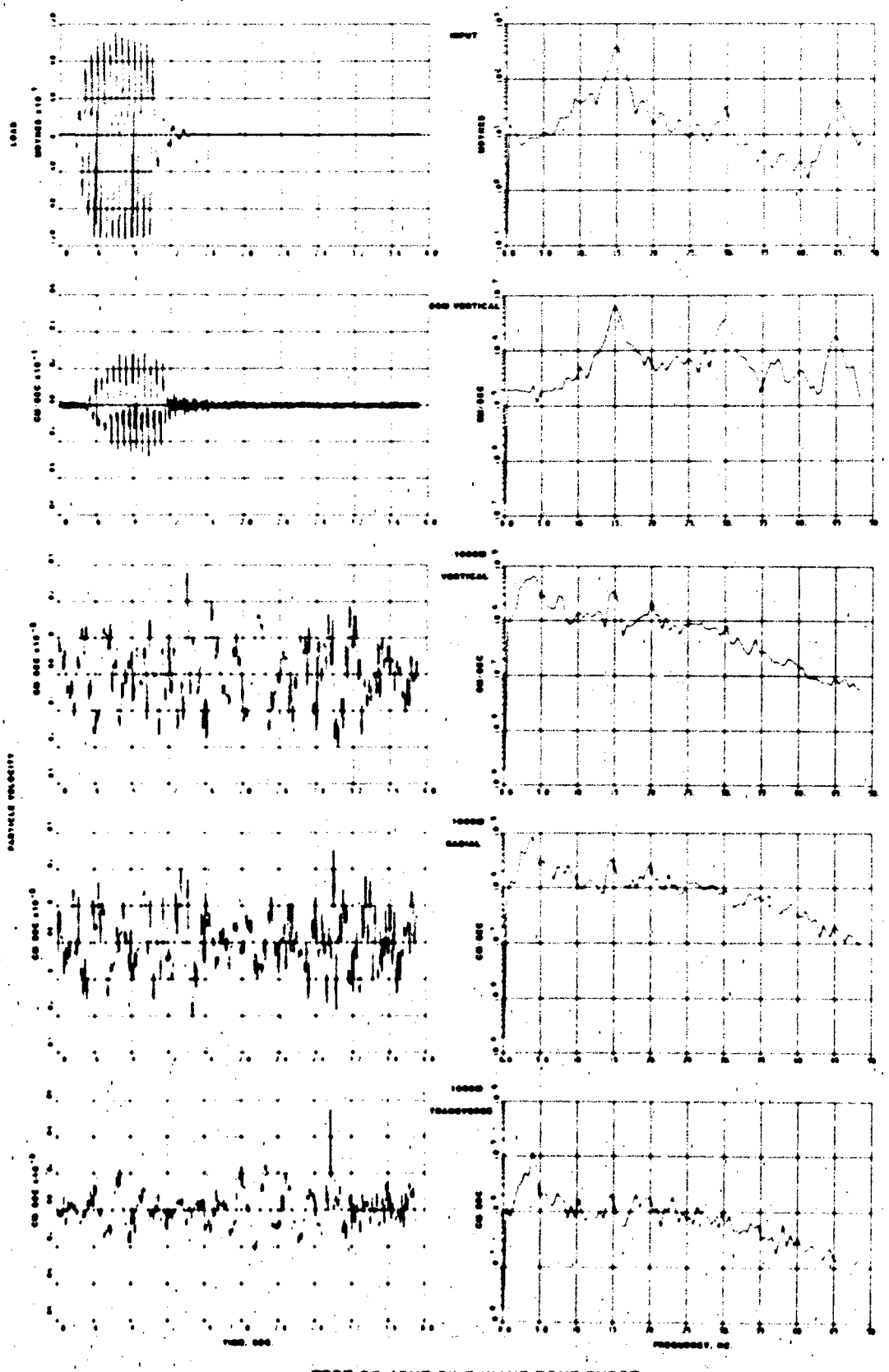

PLATE 72

TEST 98 15HZ SINE WAVE TONE BURST

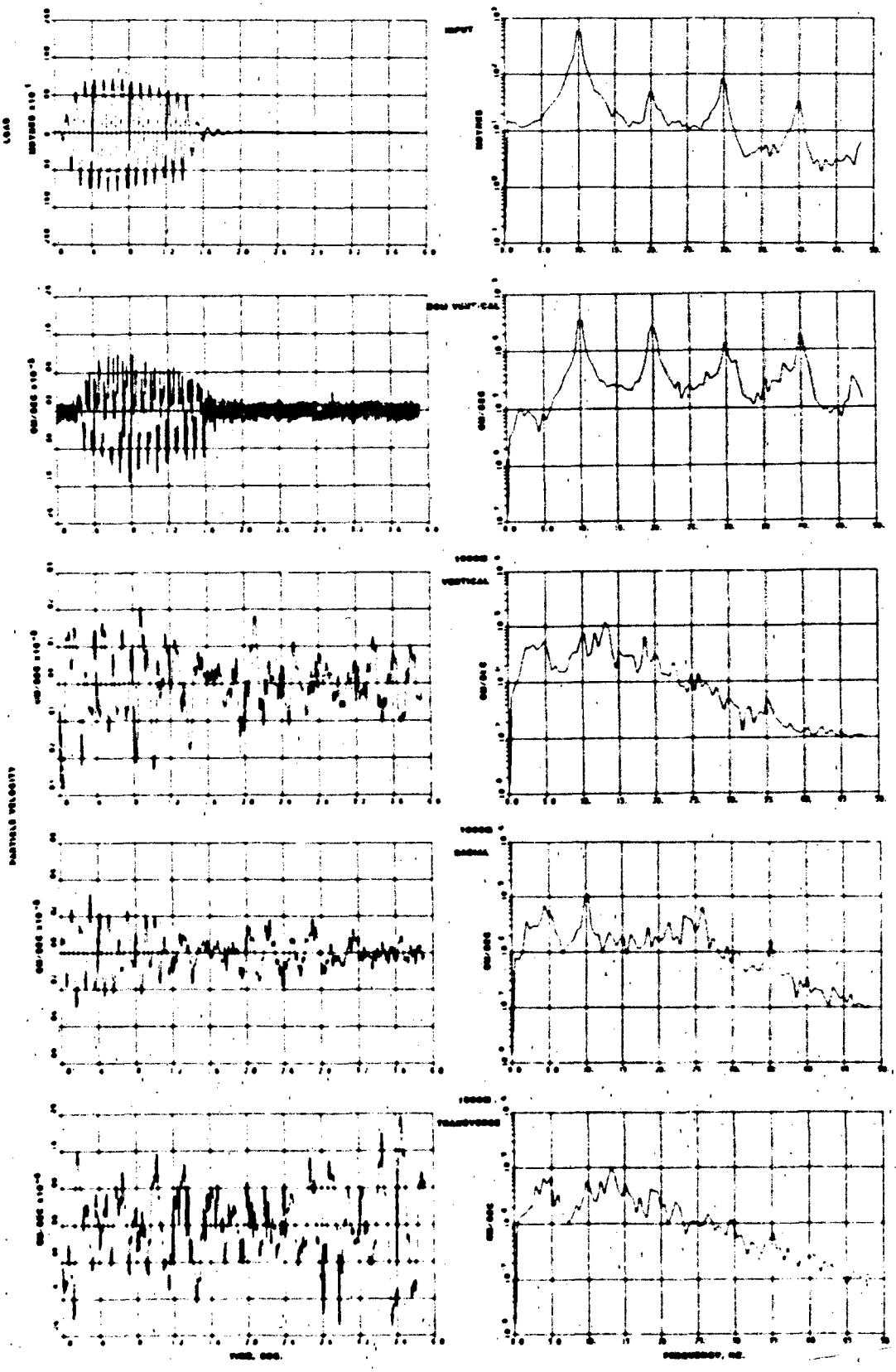

TEST 100 10HZ SINE WAVE TONE BURST

PLATE 73

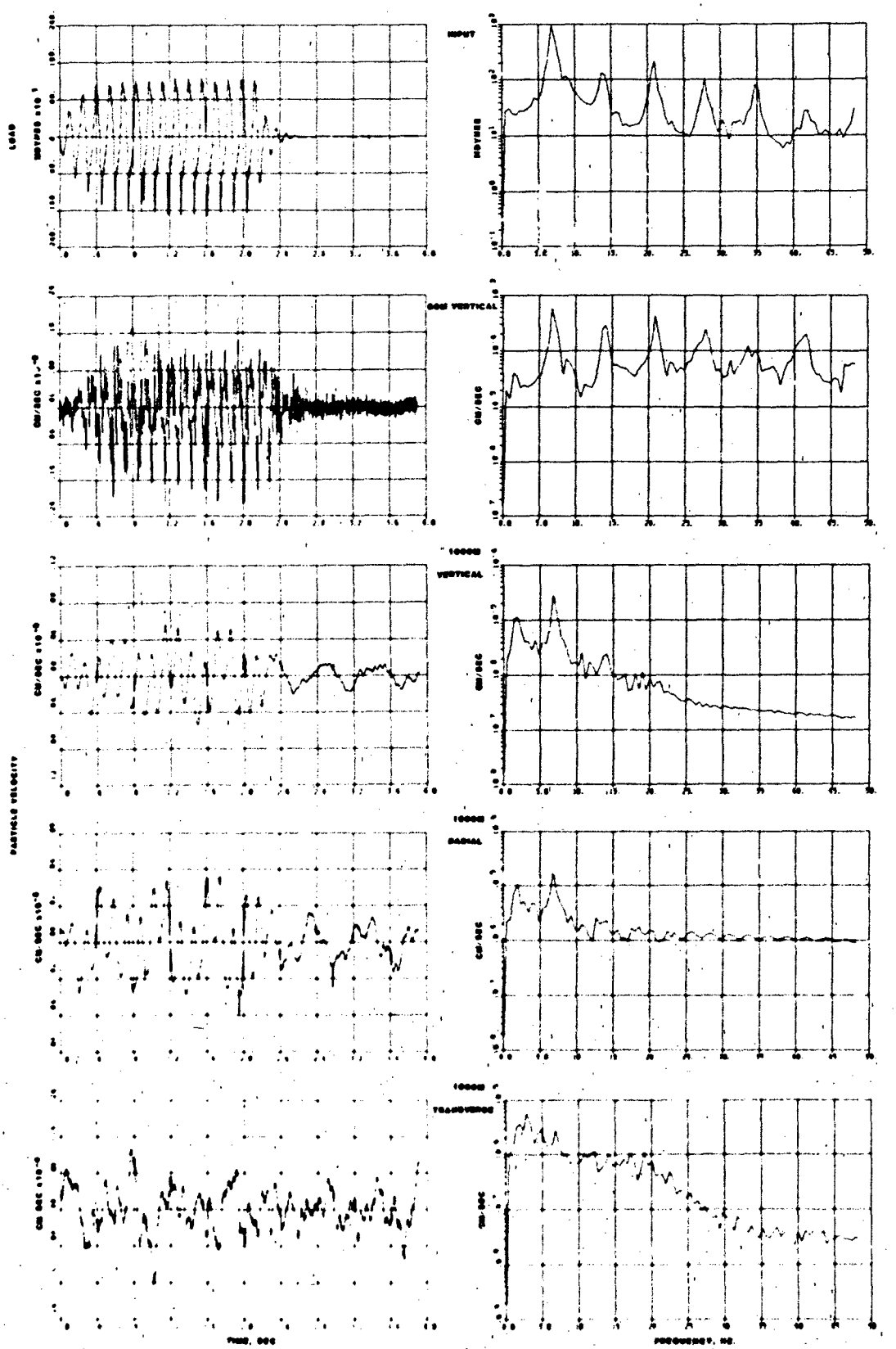

PLATE 74

TEST 103 7HZ SINE WAVE TONE BURST

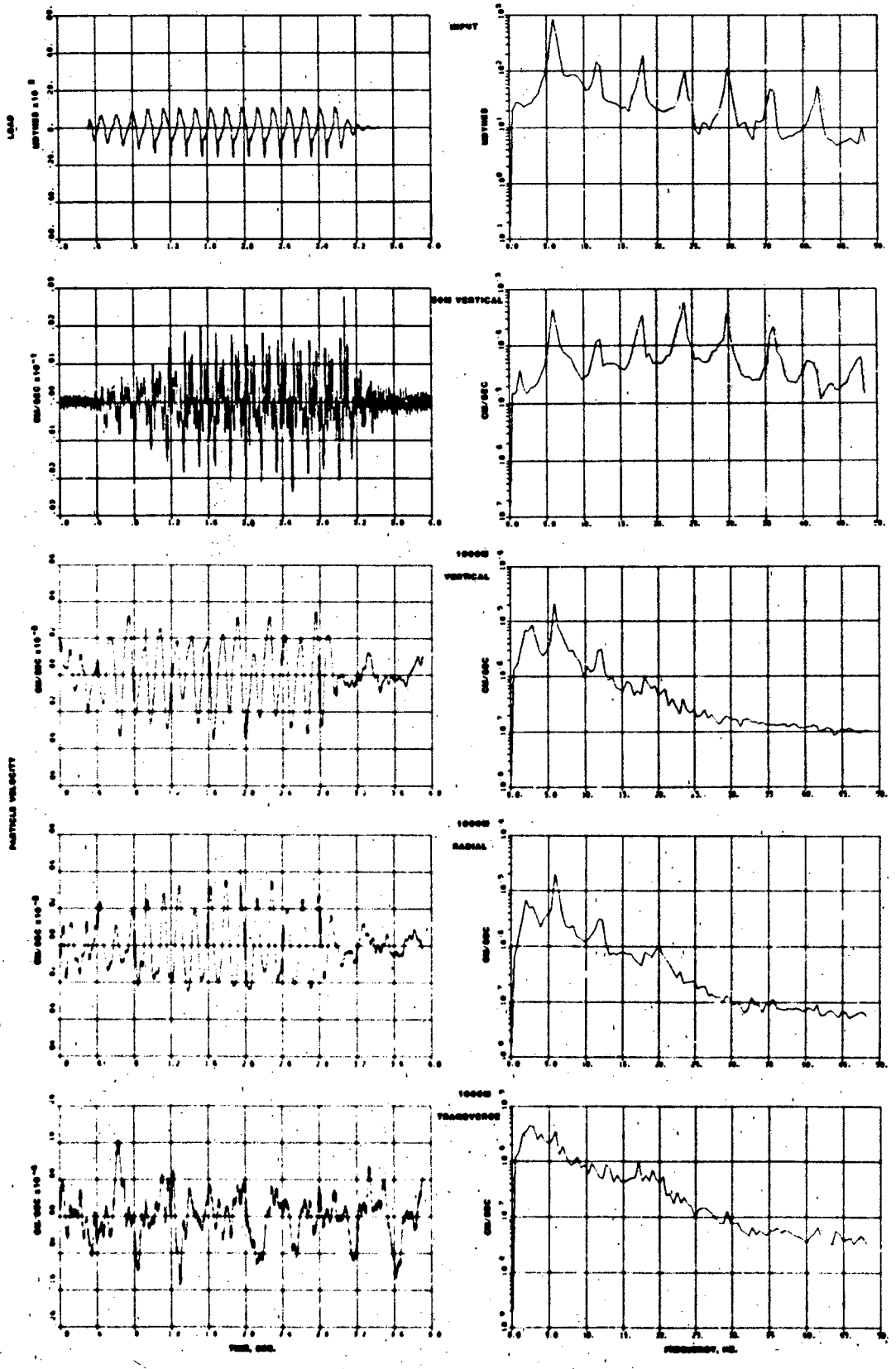

TEST 106 6HZ SINE WAVE TONE BURST

PLATE 75

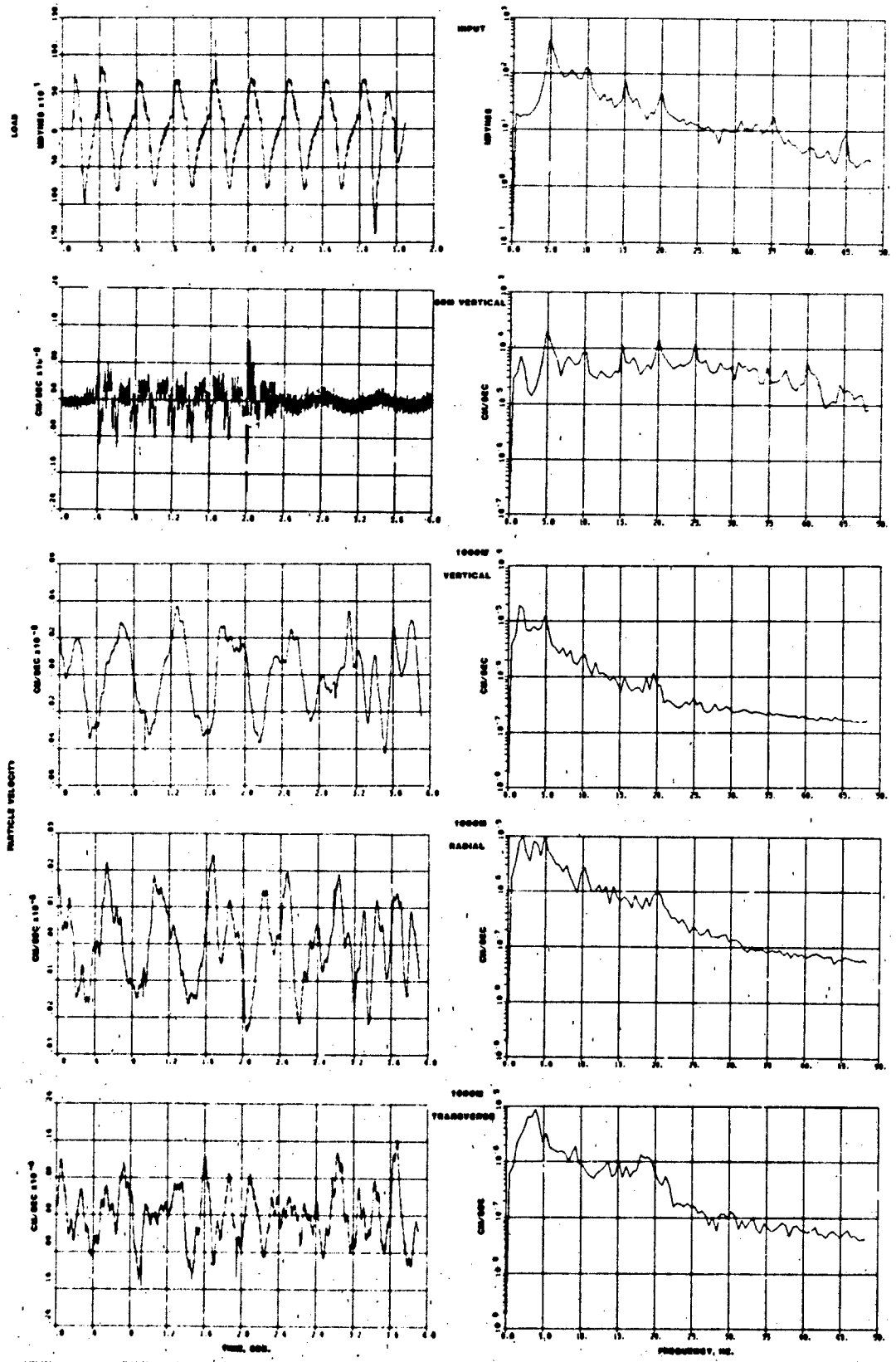

PLATE 76

TEST 107 5HZ SINE WAVE TONE BURST

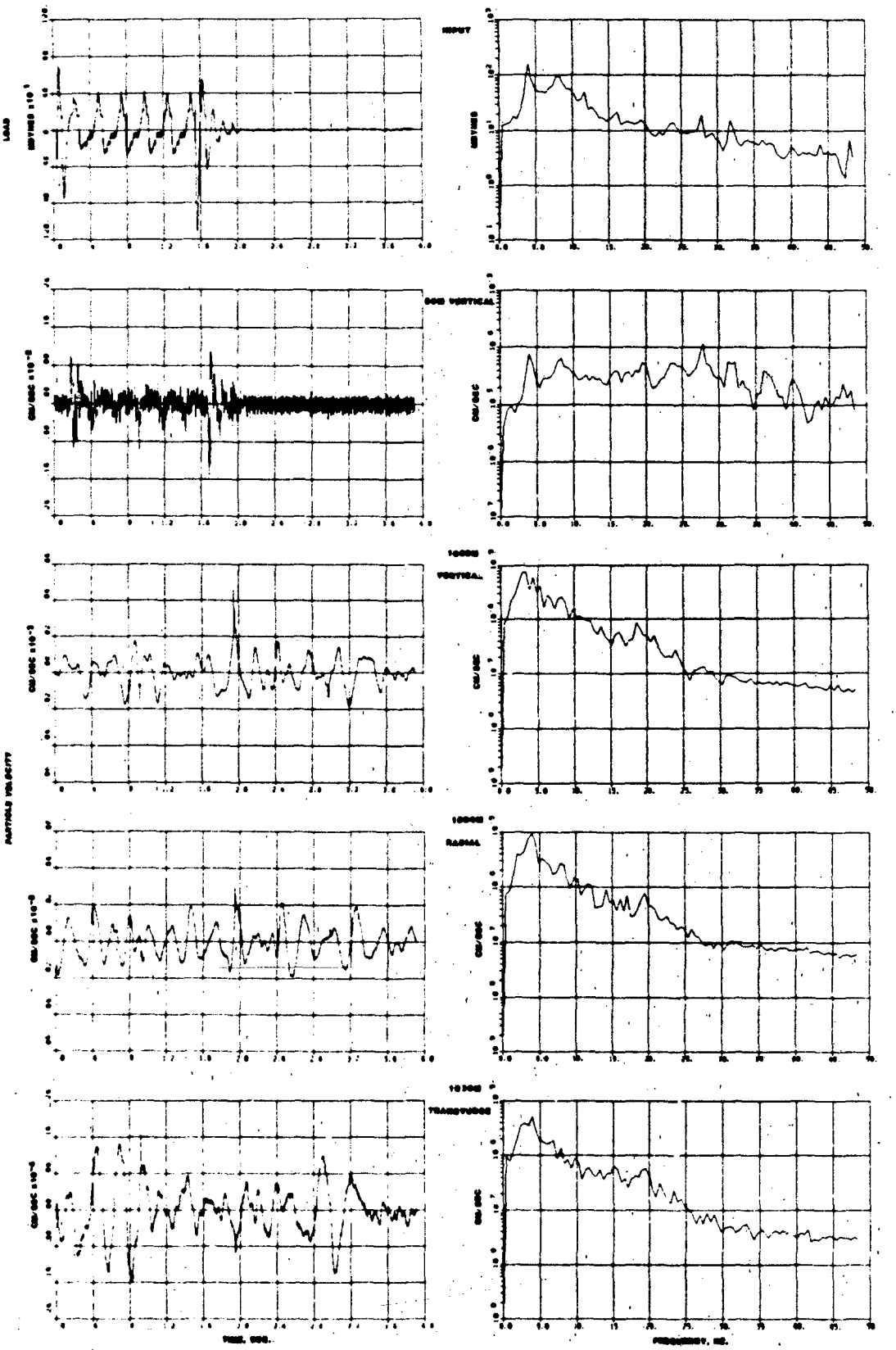

TEST 109 4HZ SINE WAVE TONE BURST

PLATE 77

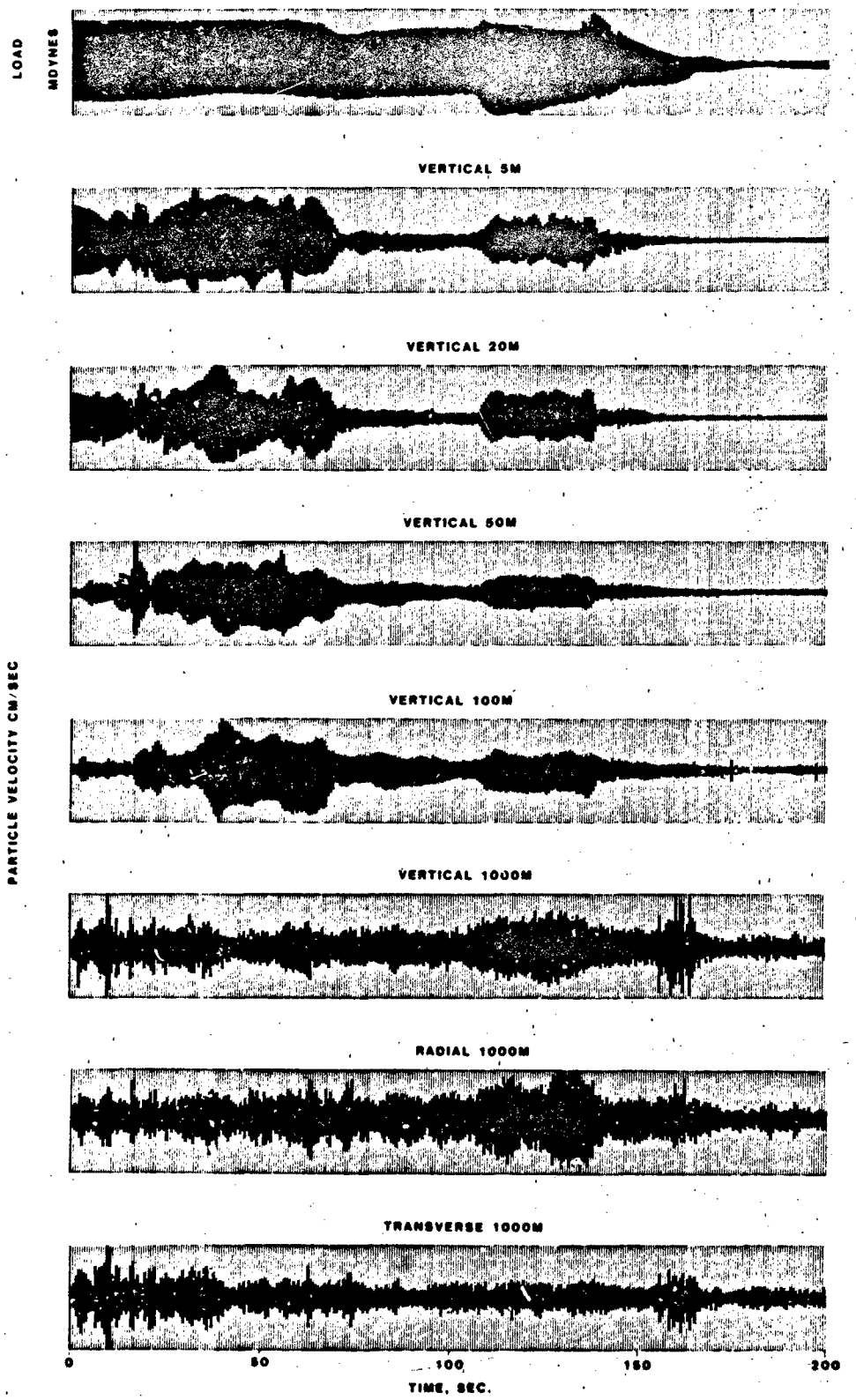

PLATE 78

TEST 91 50+1HZ SINE WAVE SWEEP TEST

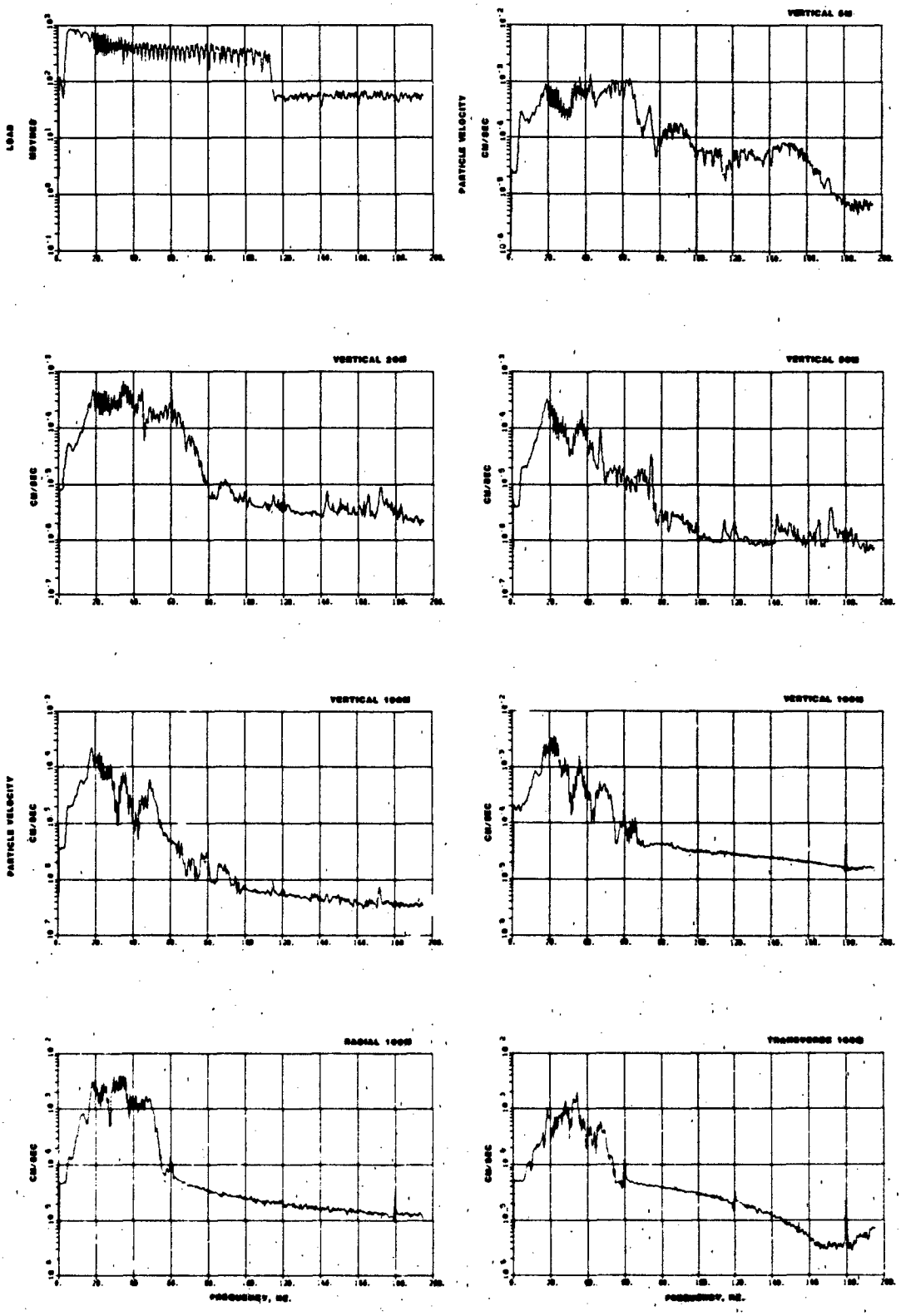

TEST 15 120±1HZ SINE WAVE SWEEP TEST

PLATE 79

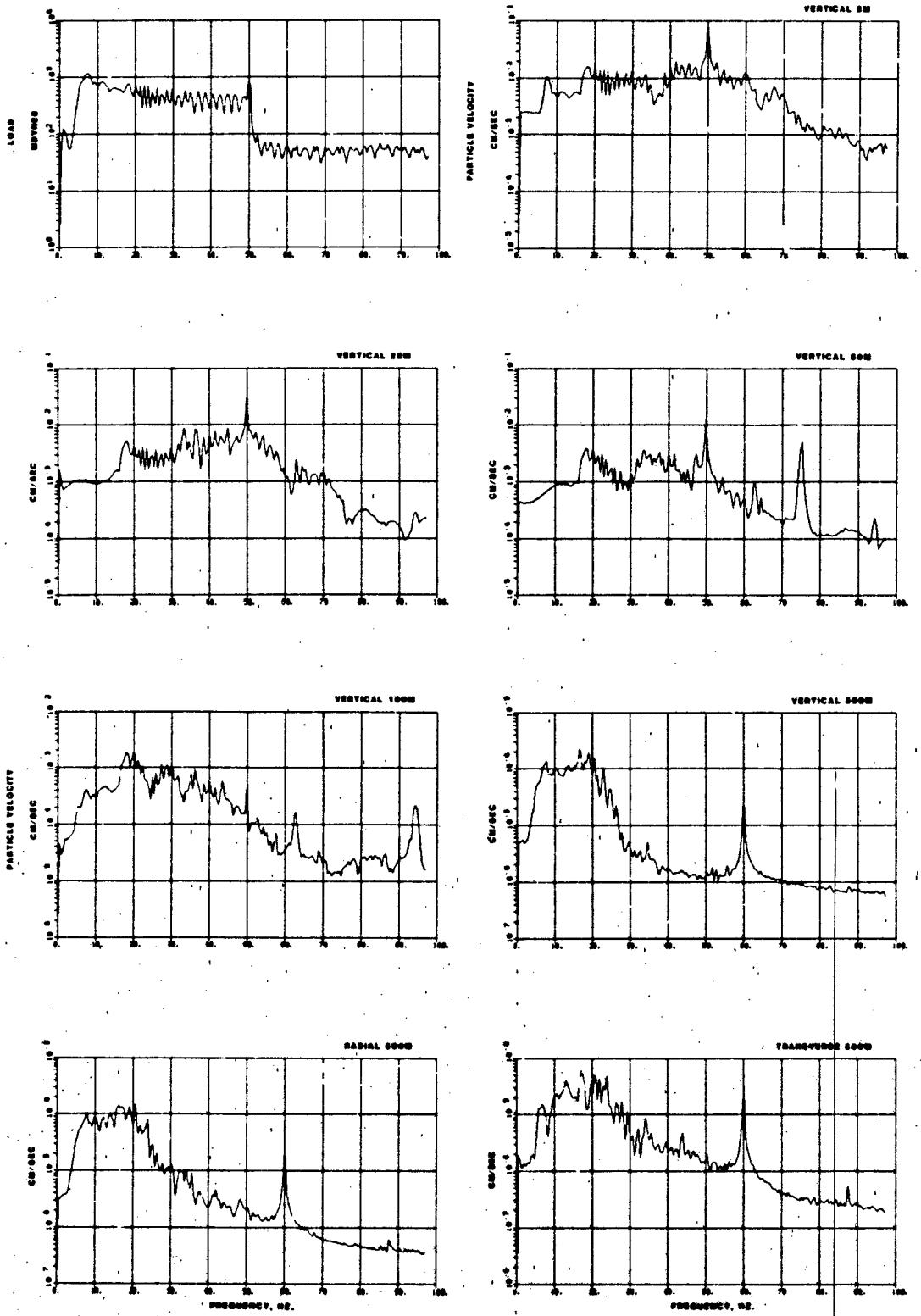

PLATE 80

TEST 53 50-1HZ SINE WAVE SWEEP TEST

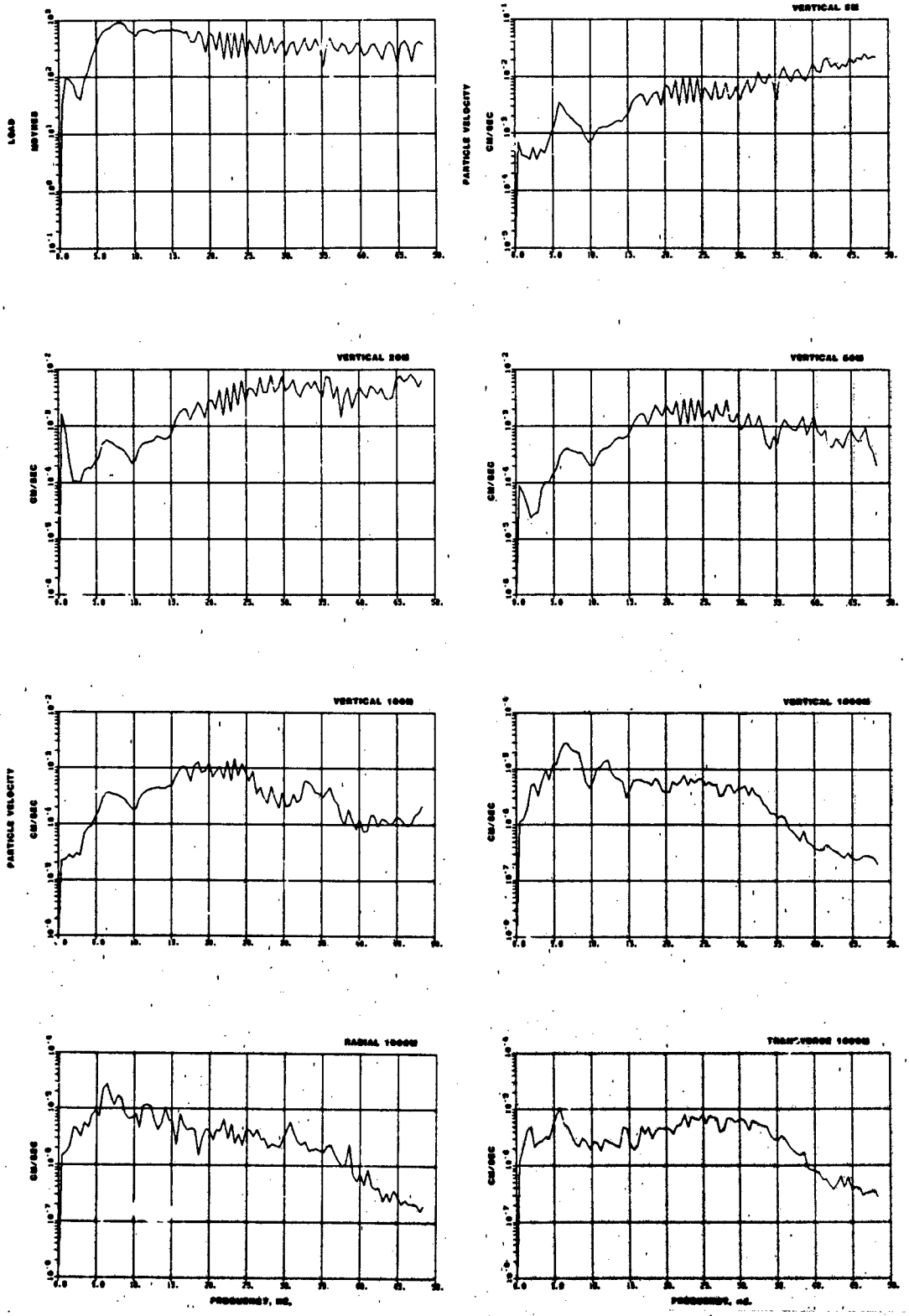

TEST 91 50-1HZ SINE WAVE SWEEP TEST

PLATE 81

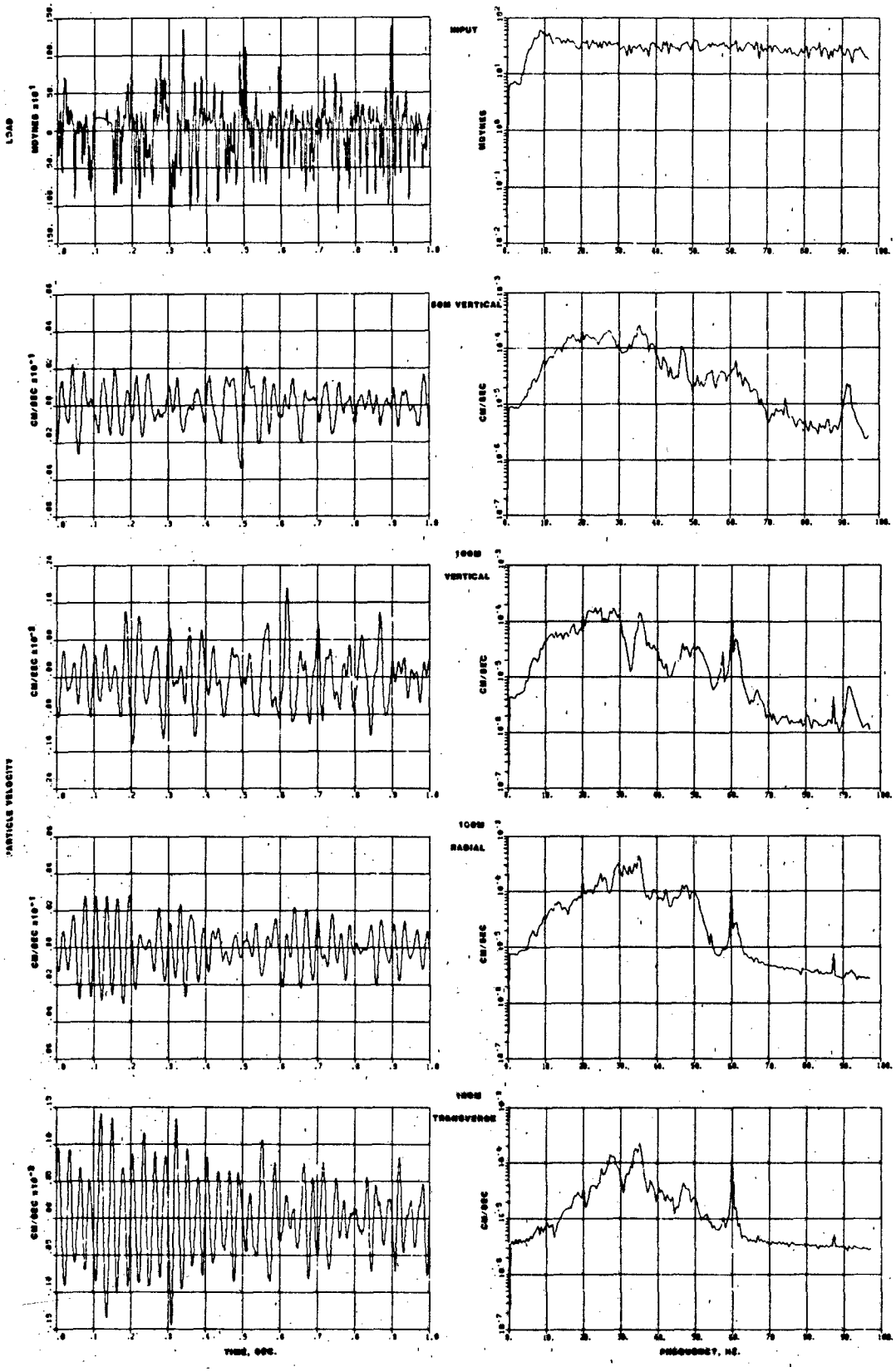

TEST 40 RANDOM NOISE

PLATE 82

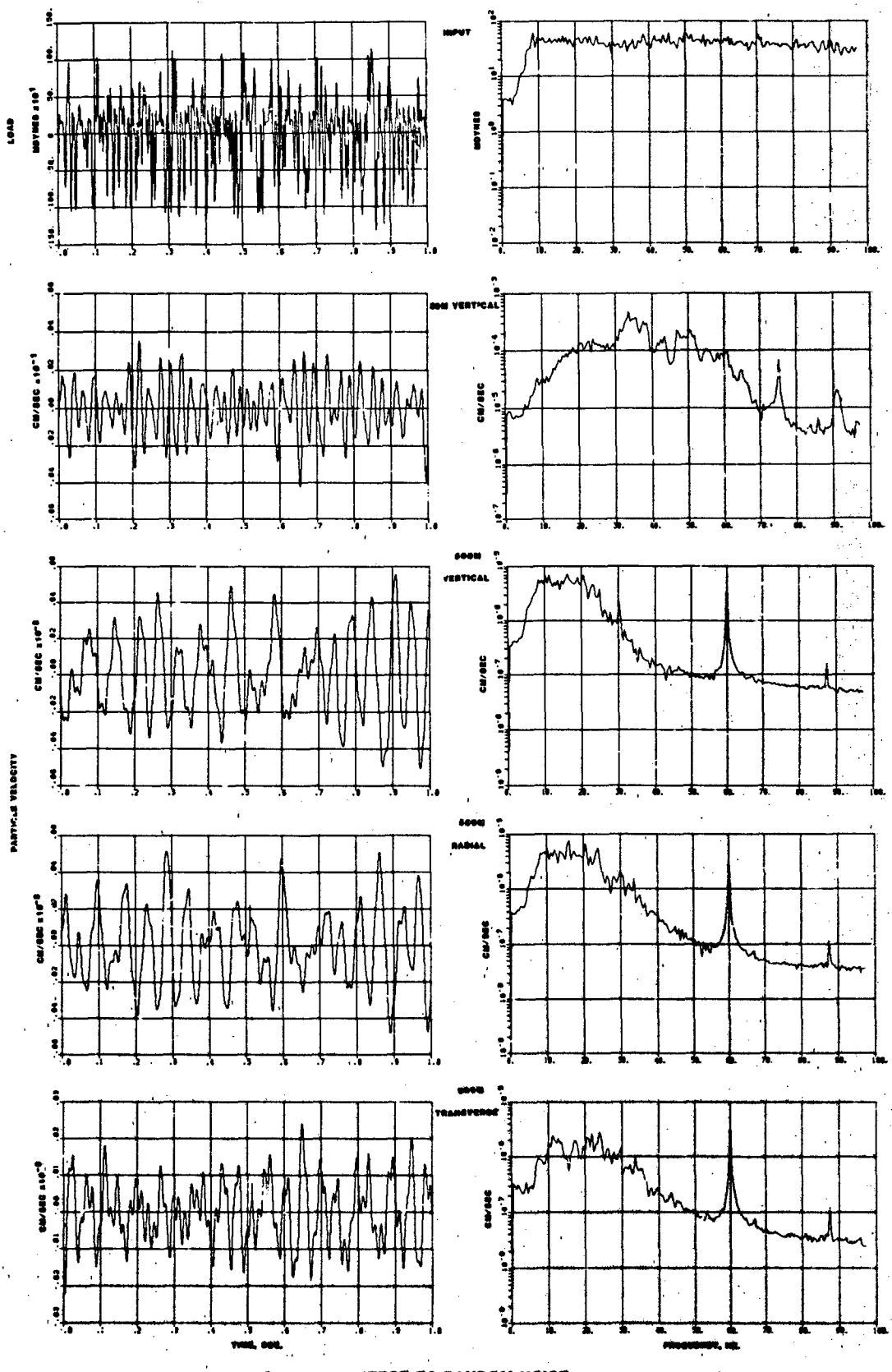

TEST 79 RANDOM NOISE

PLATE 83

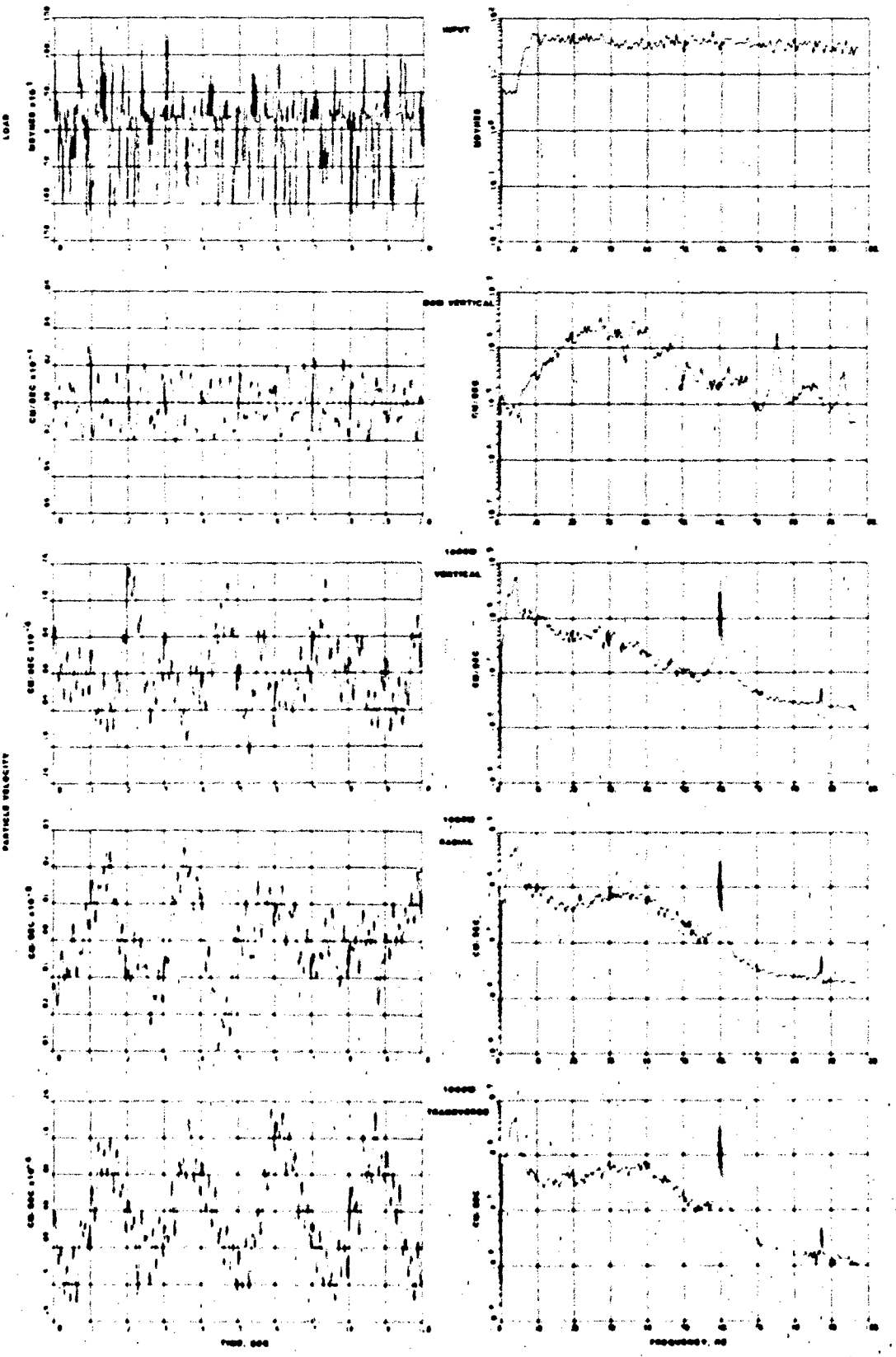

PLATE 84

TEST 112 RANDOM NOISE

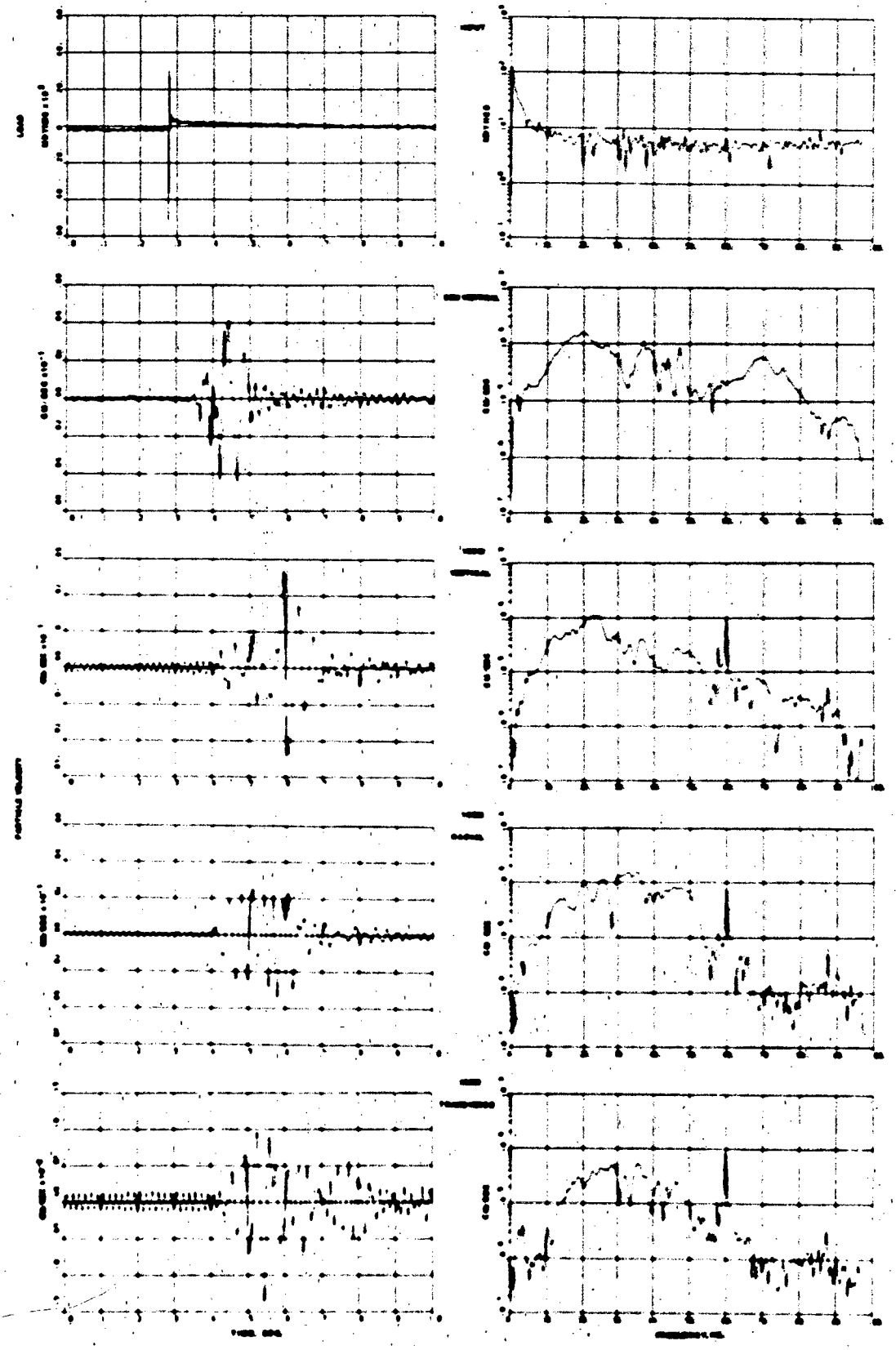

TEST 46 IMPULSE TEST

PLATE 85

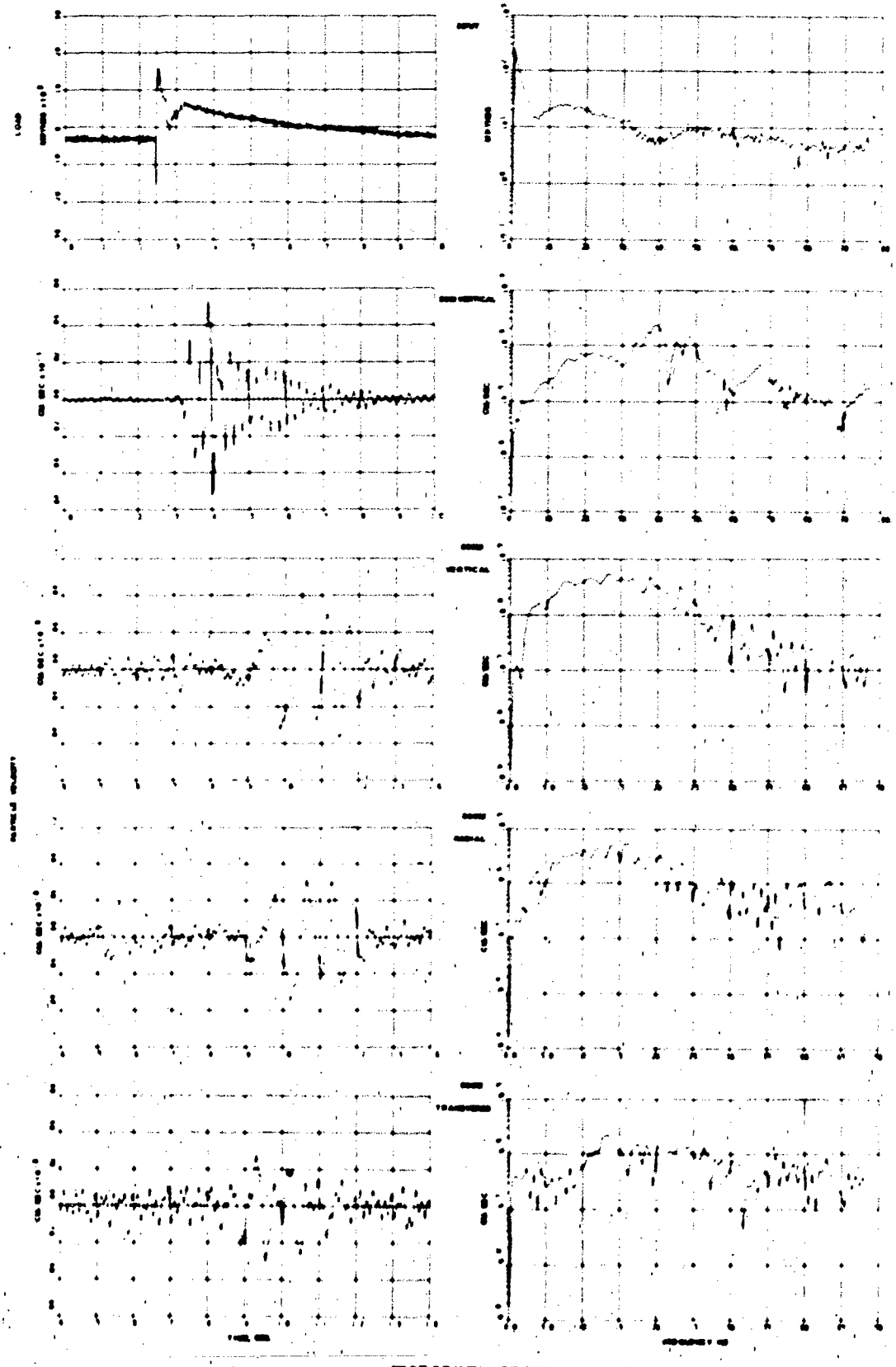

PLATE 86

TEST 87 IMPULSE TEST

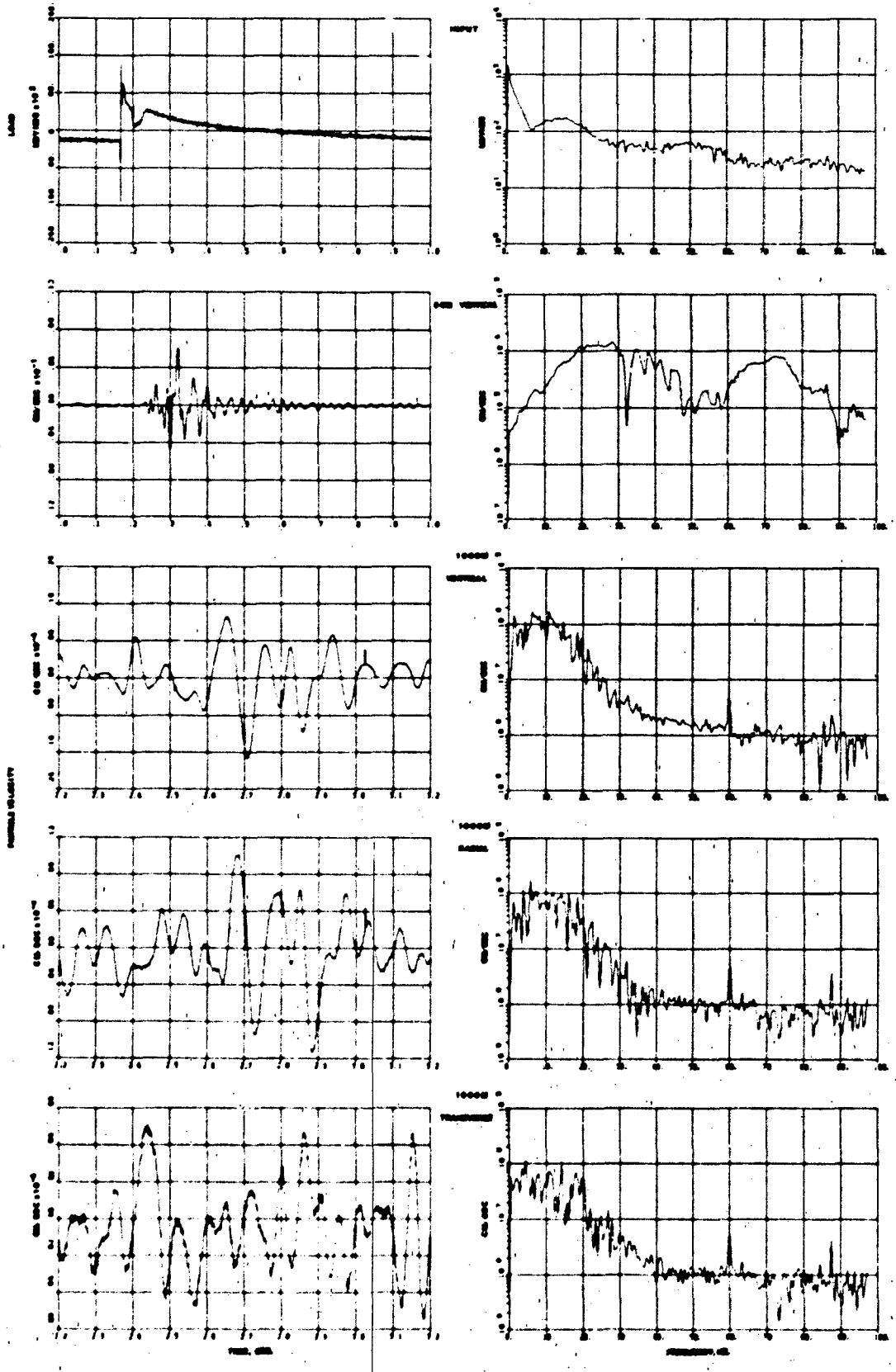

TEST 116 IMPULSE TEST

PLATE 87

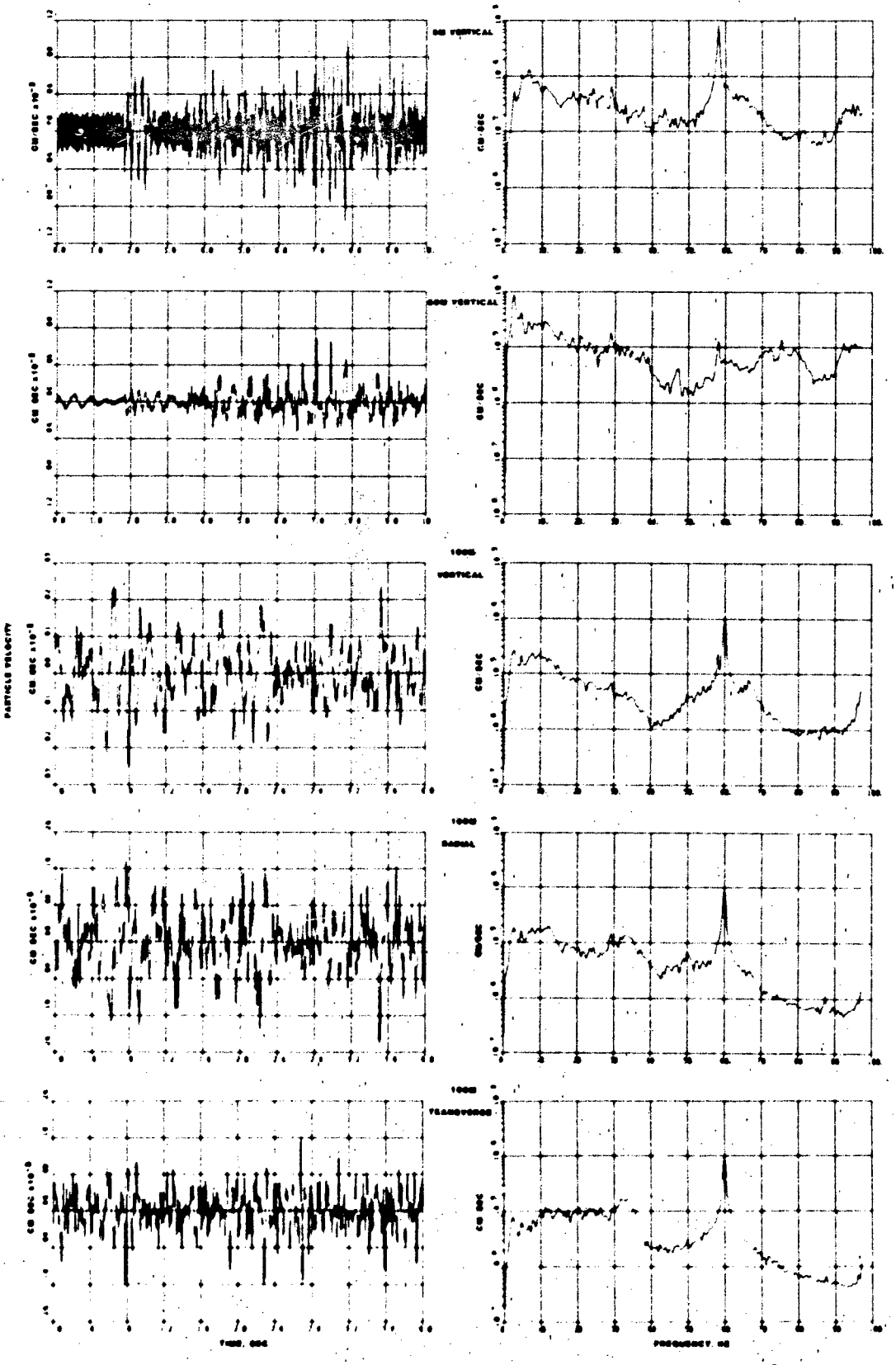

PLATE 88

TEST 47 VEHICLE TEST 8 KPH

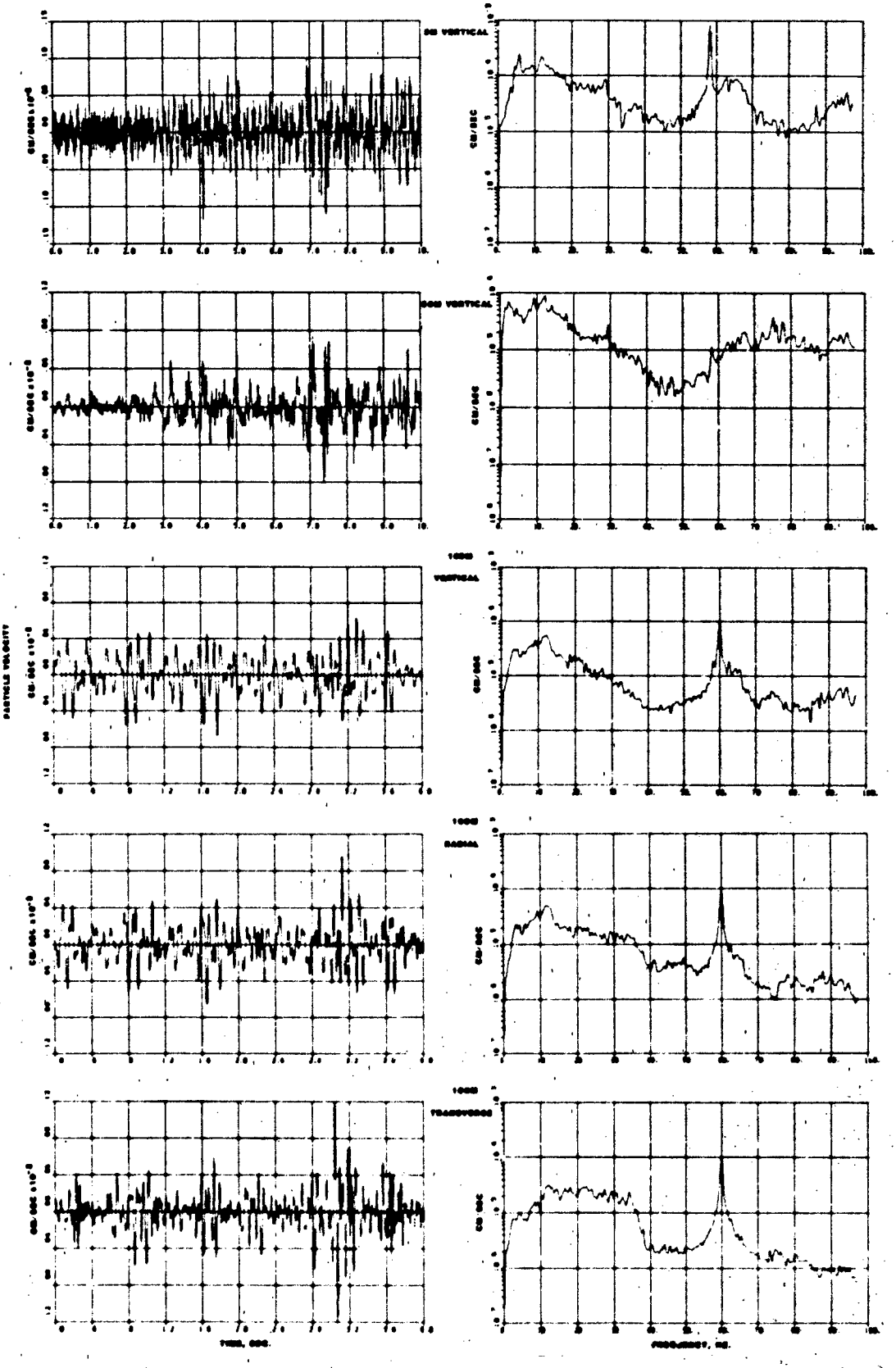

TEST 49 VEHICLE TEST 16 KPH

PLATE 89

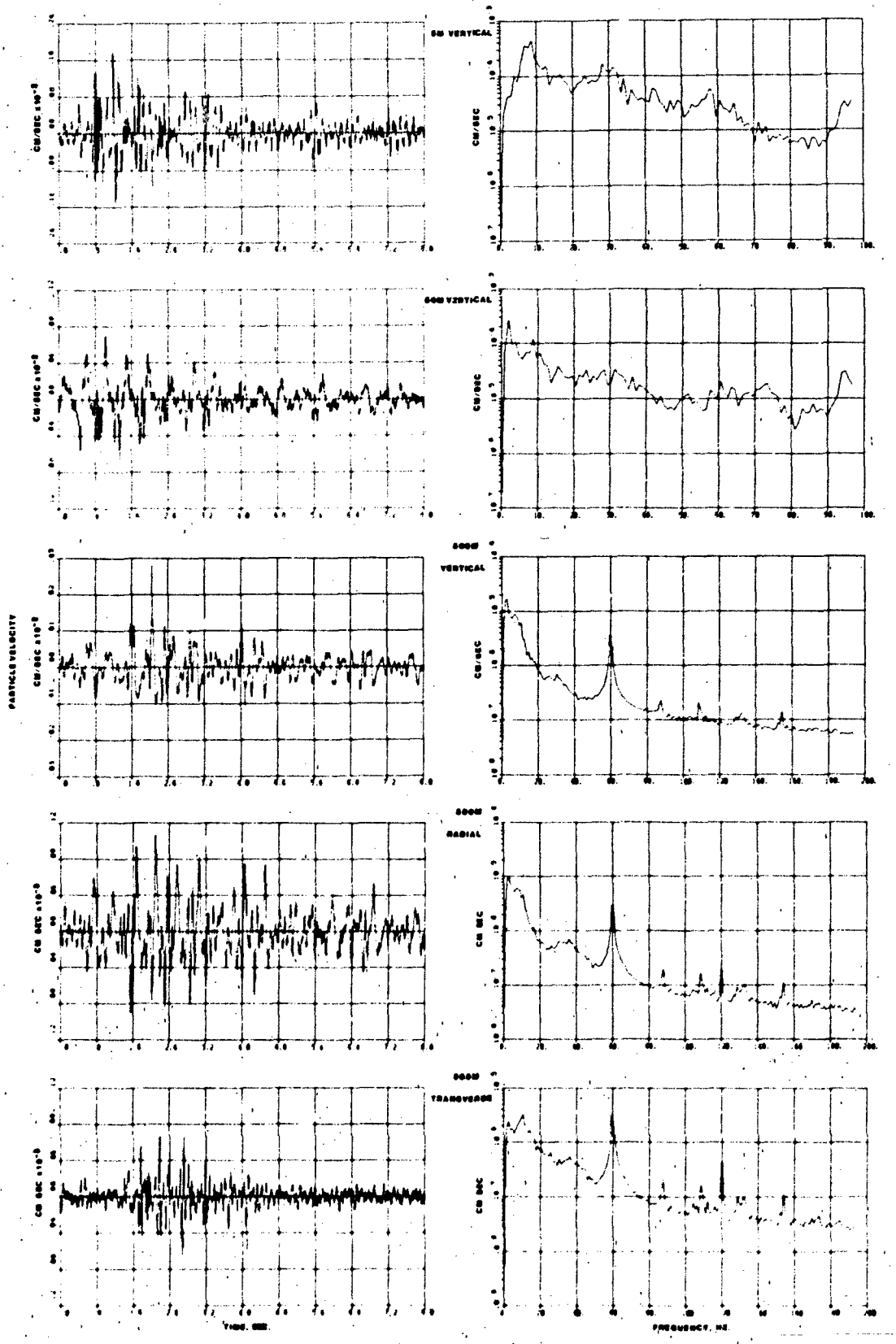

PLATE 90

TEST 81 VEHICLE TEST 8 KPH

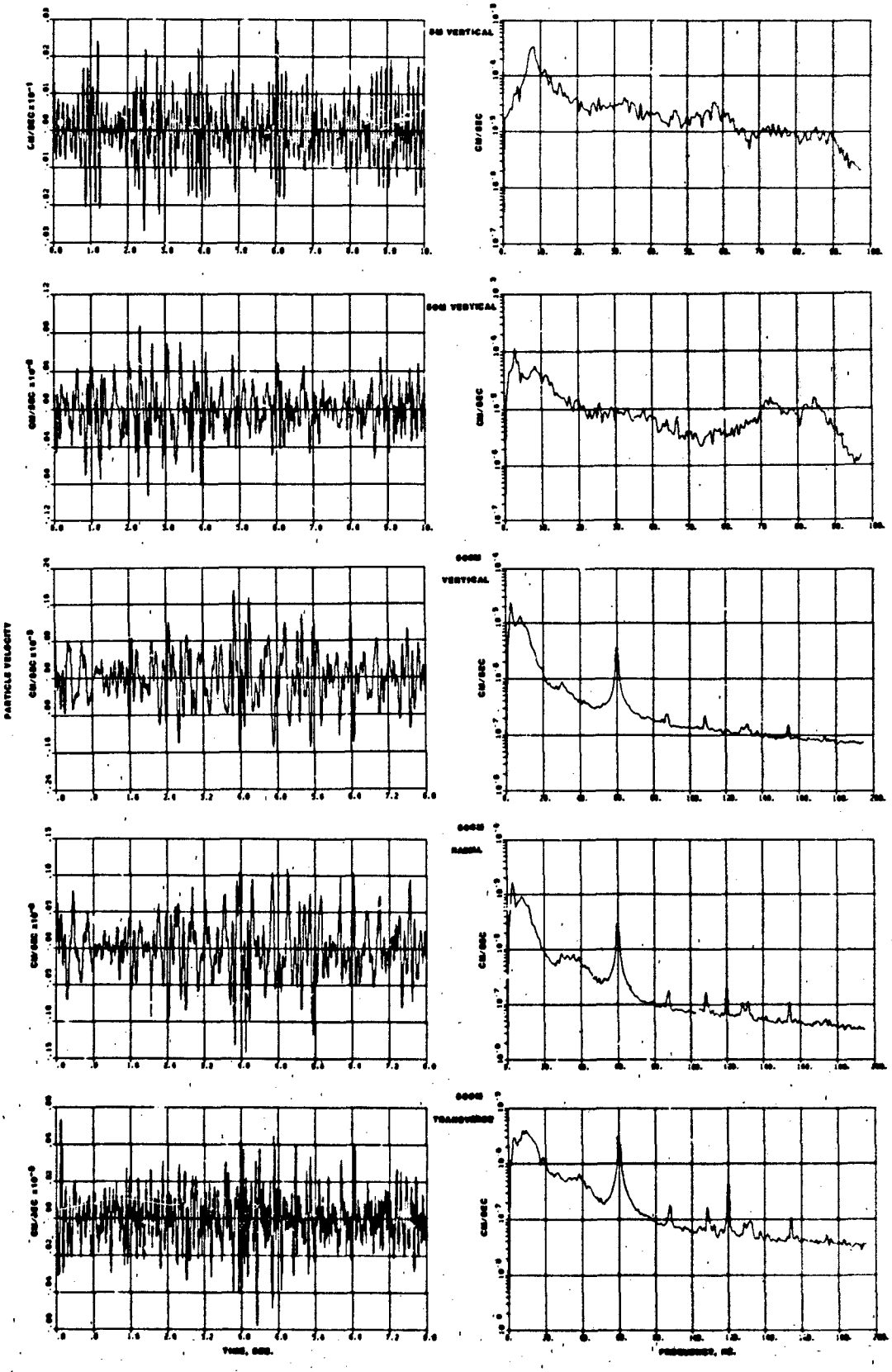

TEST 83 VEHICLE TEST 16 KPH

PLATE 91

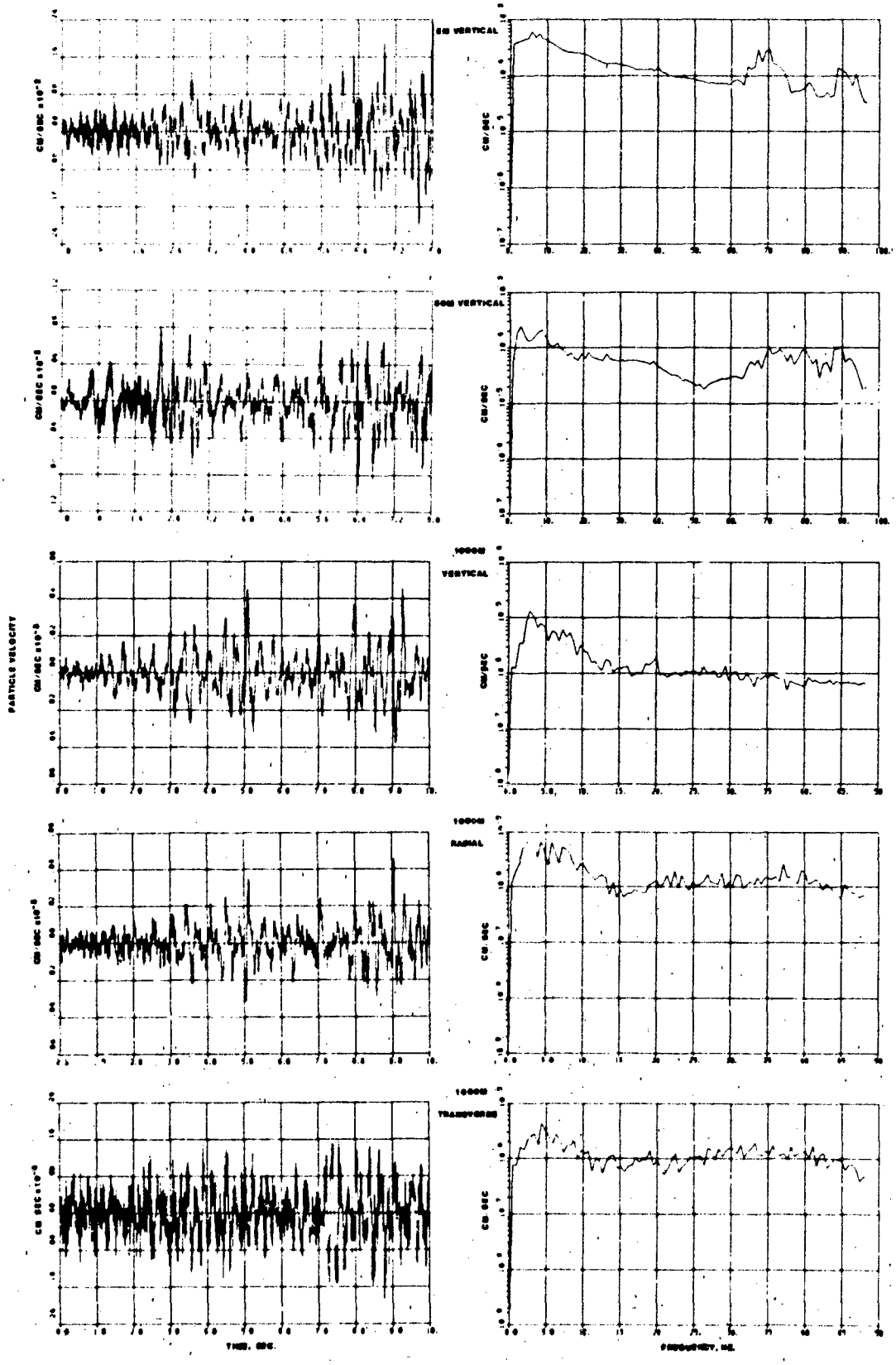

TEST 119 VEHICLE TEST 8 KPH

PLATE 92

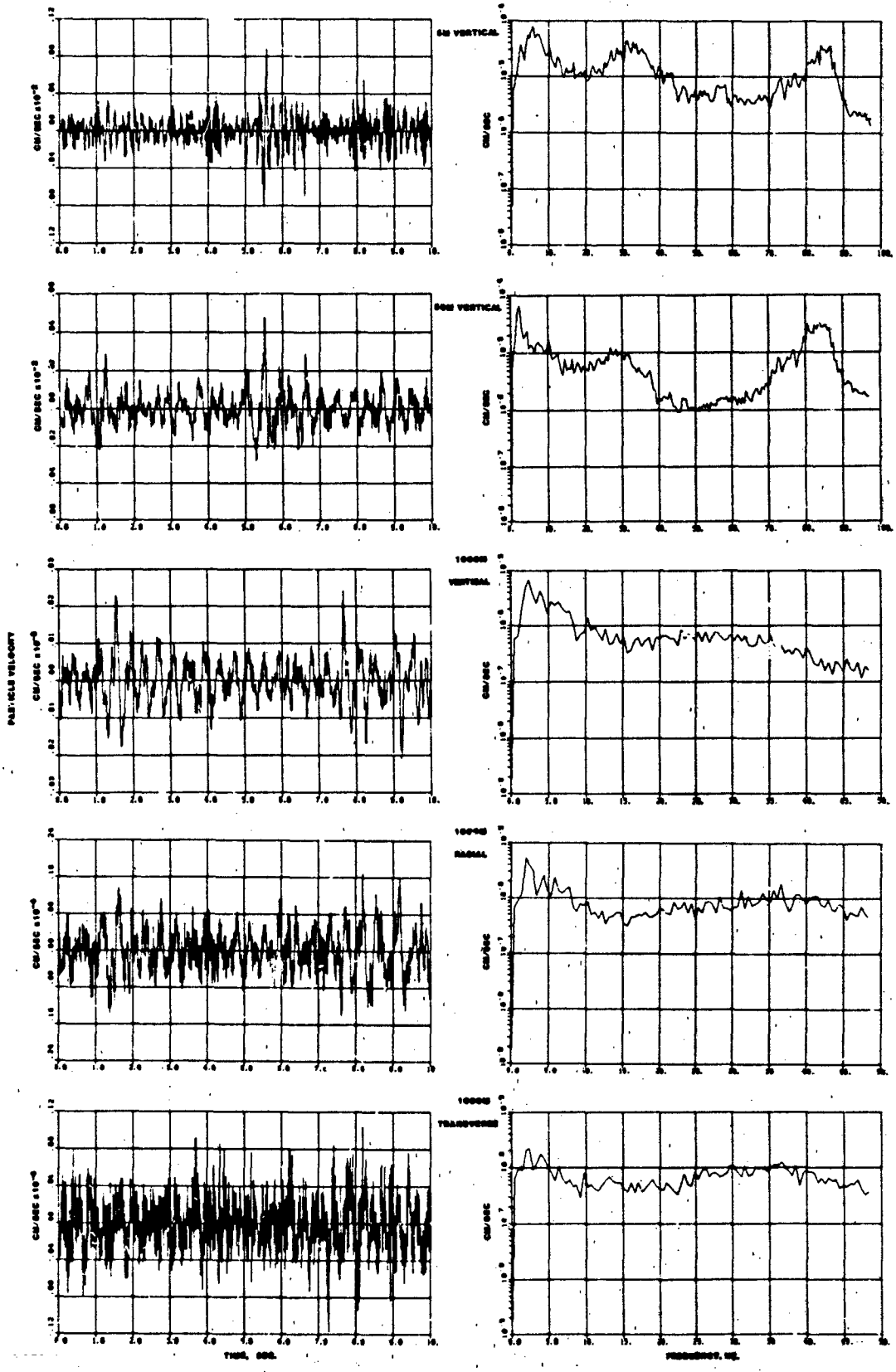

TEST 121 VEHICLE TEST 16 KPH

PLATE 93

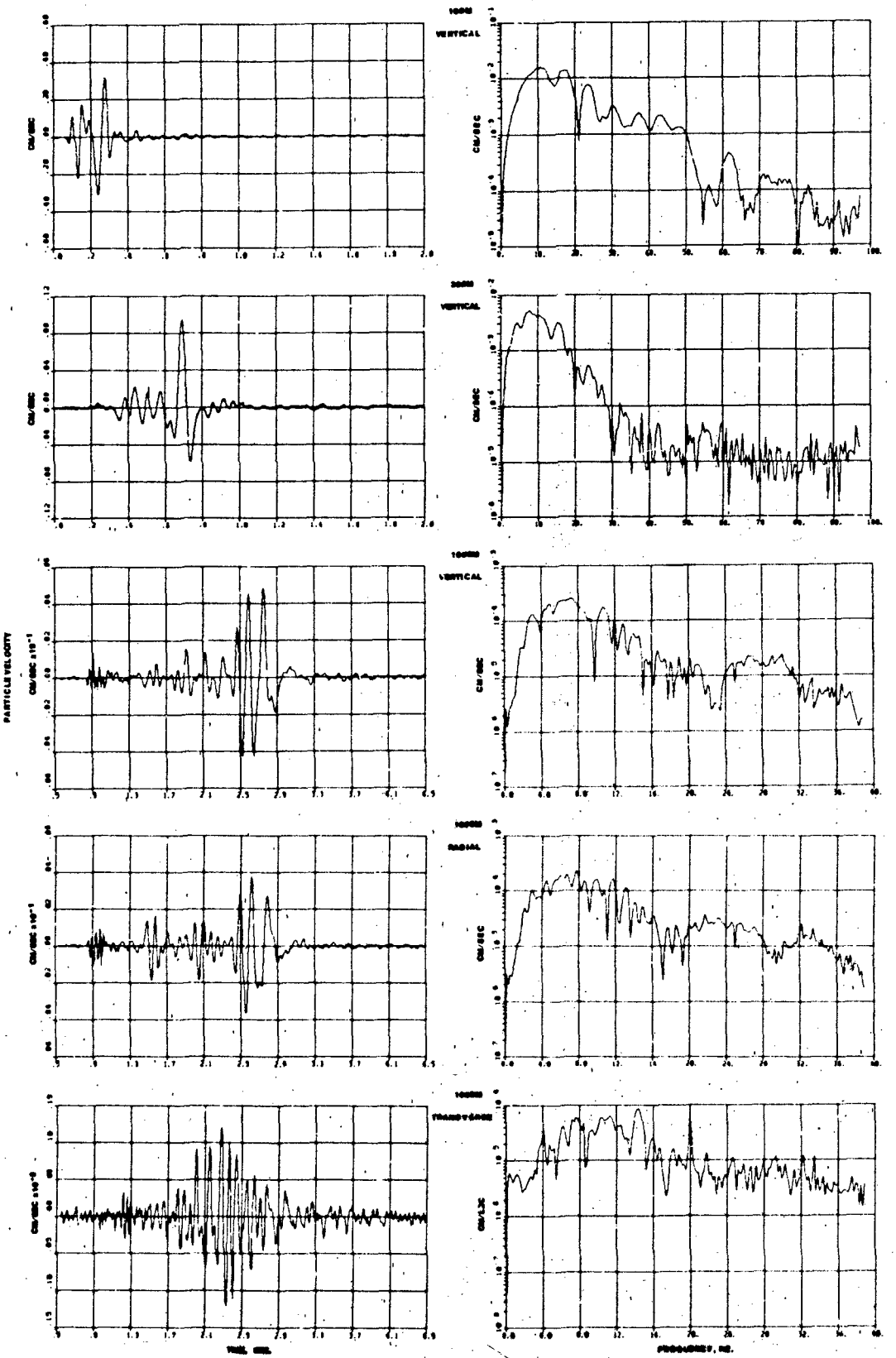

PLATE 94

TEST 133 EXPLOSIVE SOURCE AT 1 KM

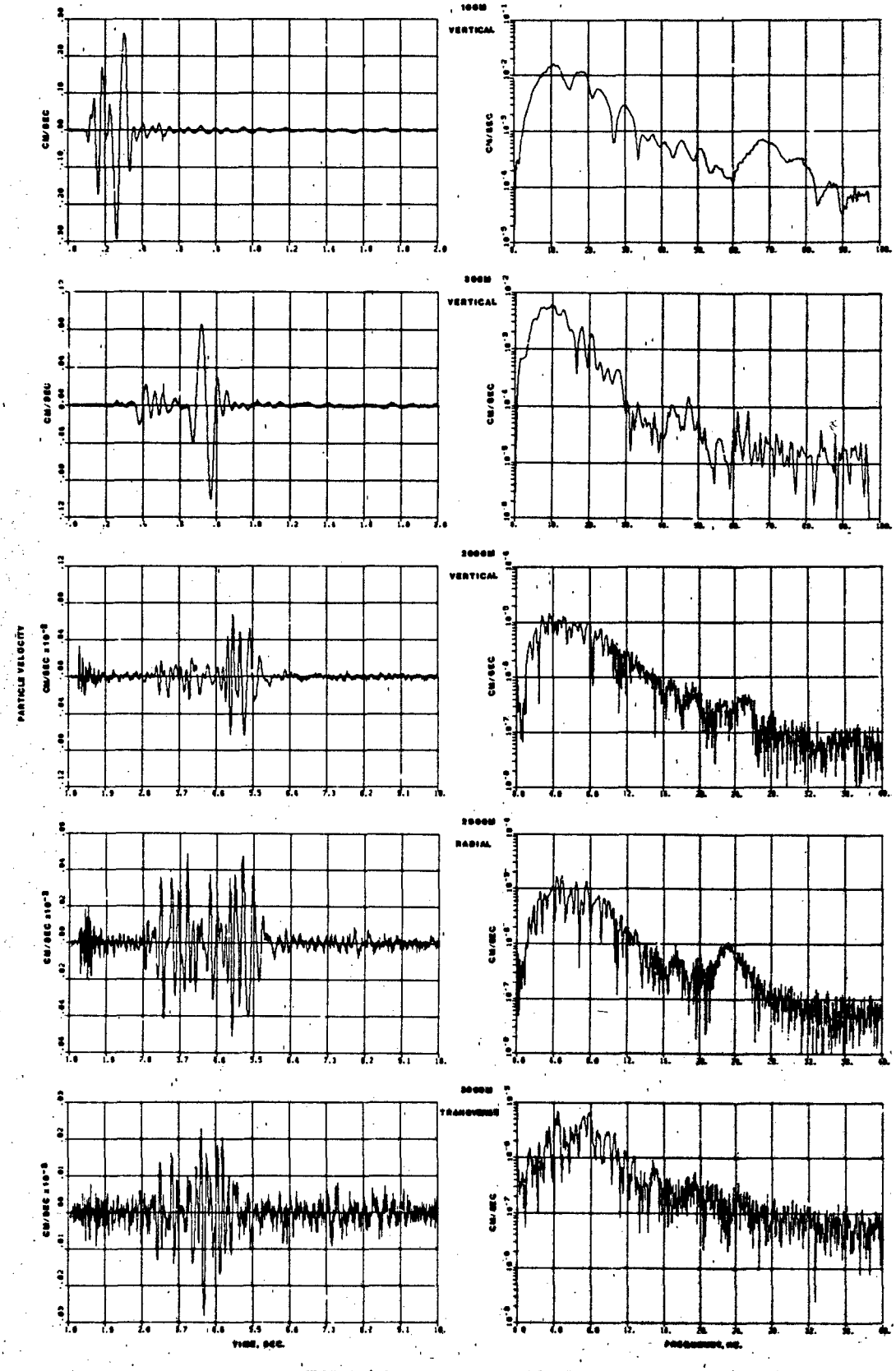

TEST 132 EXPLOSIVE SOURCE AT 2 KM

PLATE 95

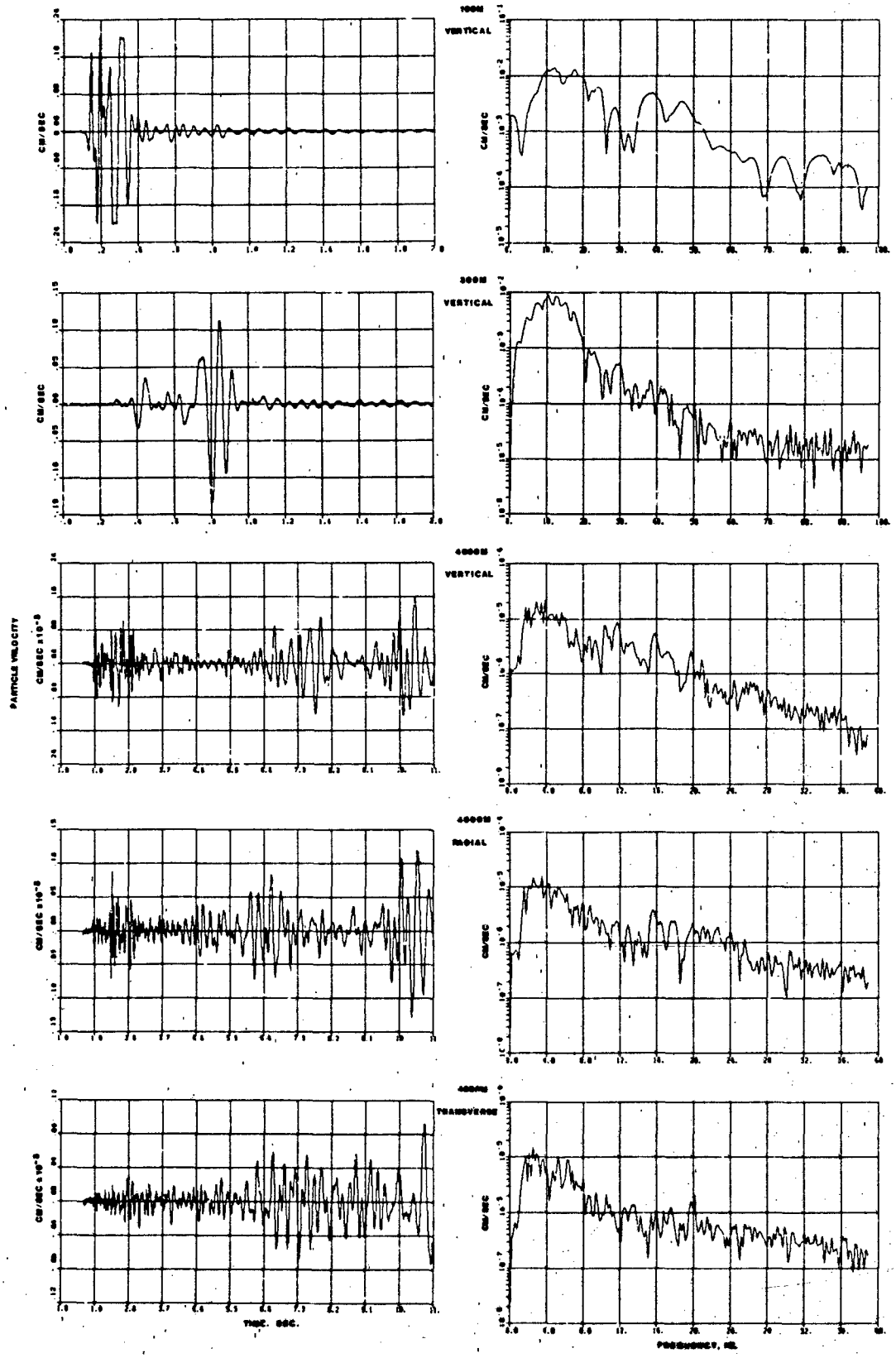

TEST 131 EXPLOSIVE SOURCE AT 4 KM

PLATE 96

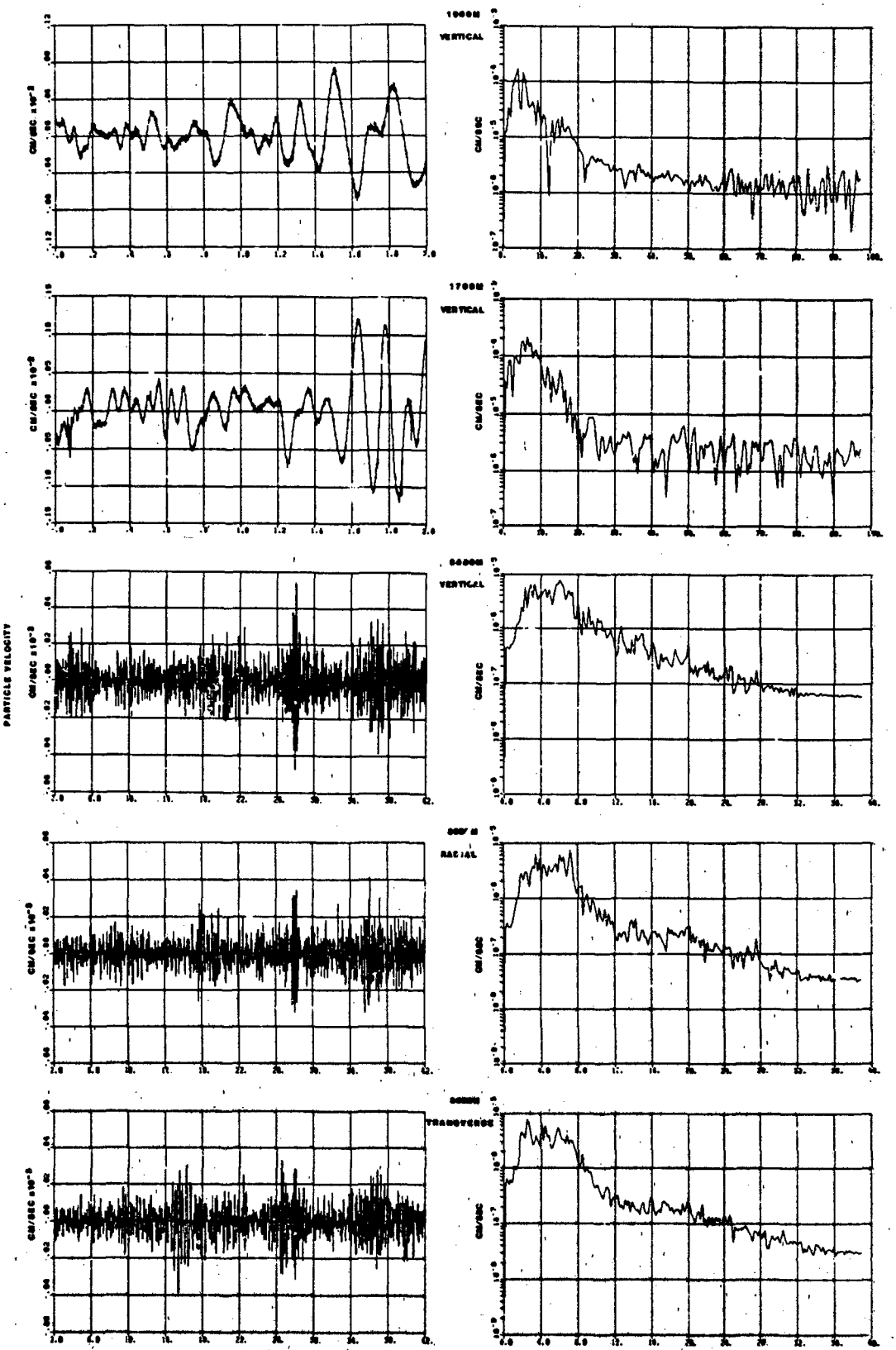

TEST 135 EXPLOSIVE SOURCE AT 8 KM

PLATE 97

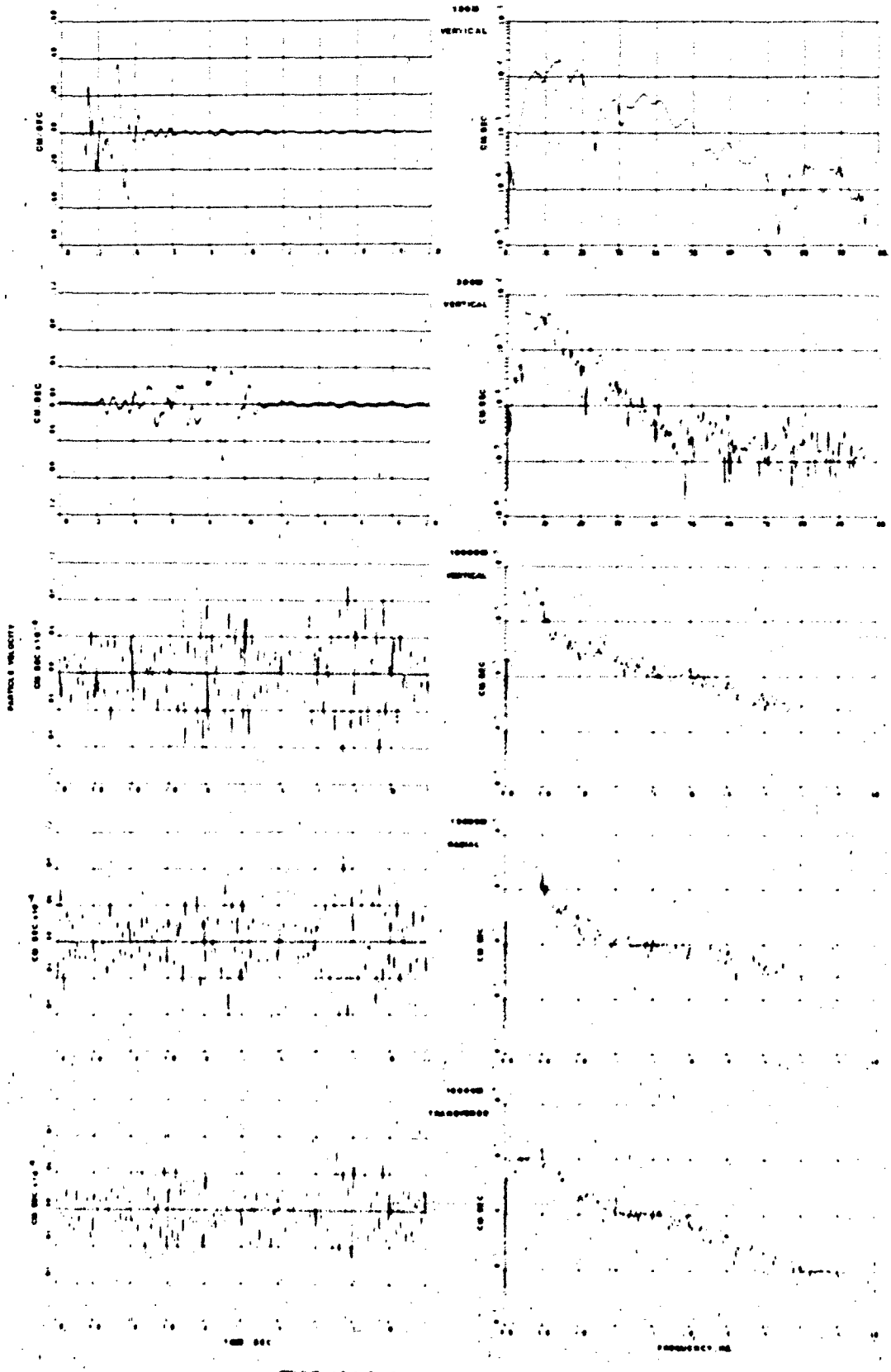

PLATE 98

TEST 134 EXPLOSIVE SOURCE AT 10 KM

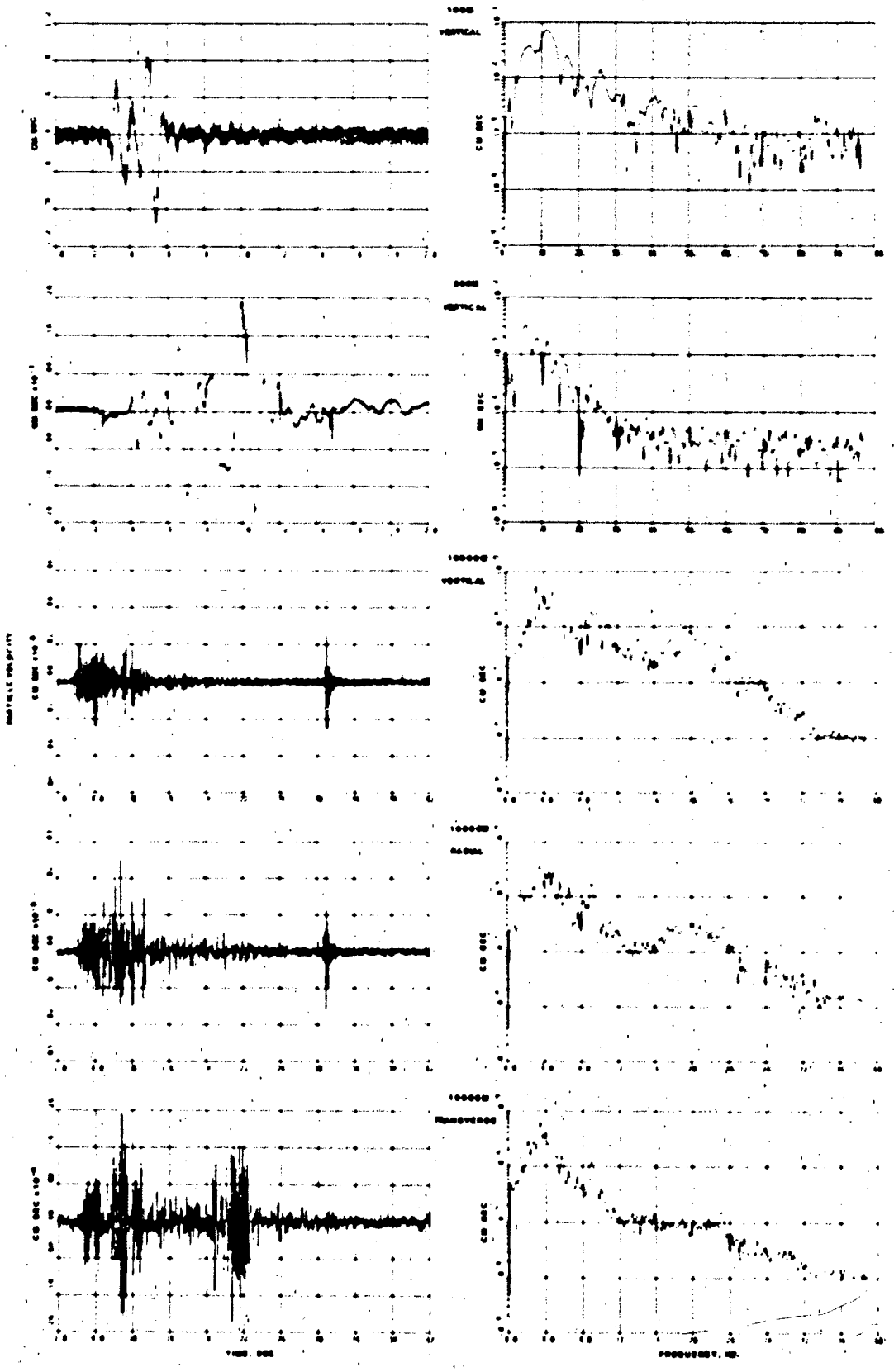

TEST 136 EXPLOSIVE SOURCE AT 10 KM

PLATE 99

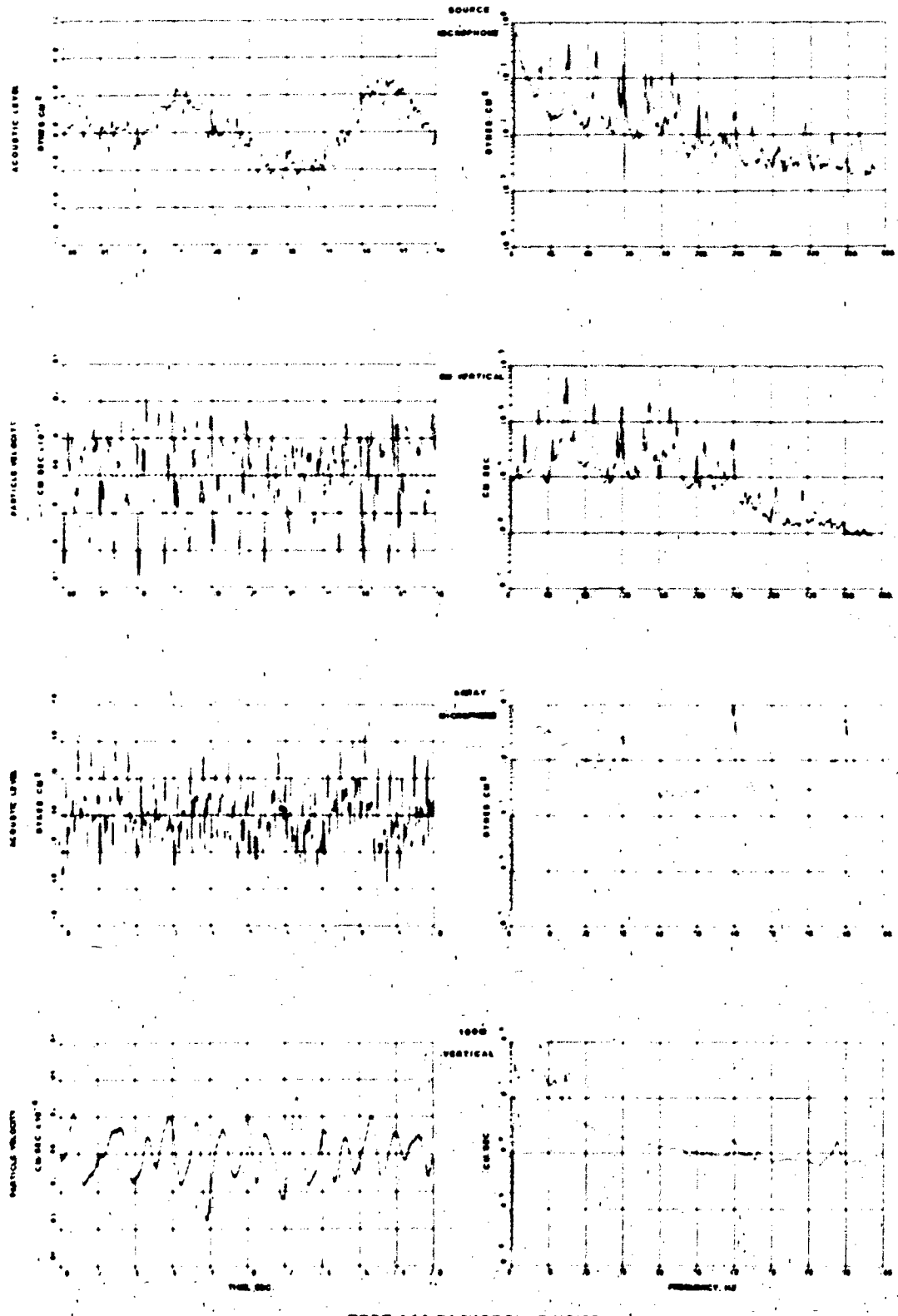

PLATE 100

TEST 14A BACKGROUND NOISE

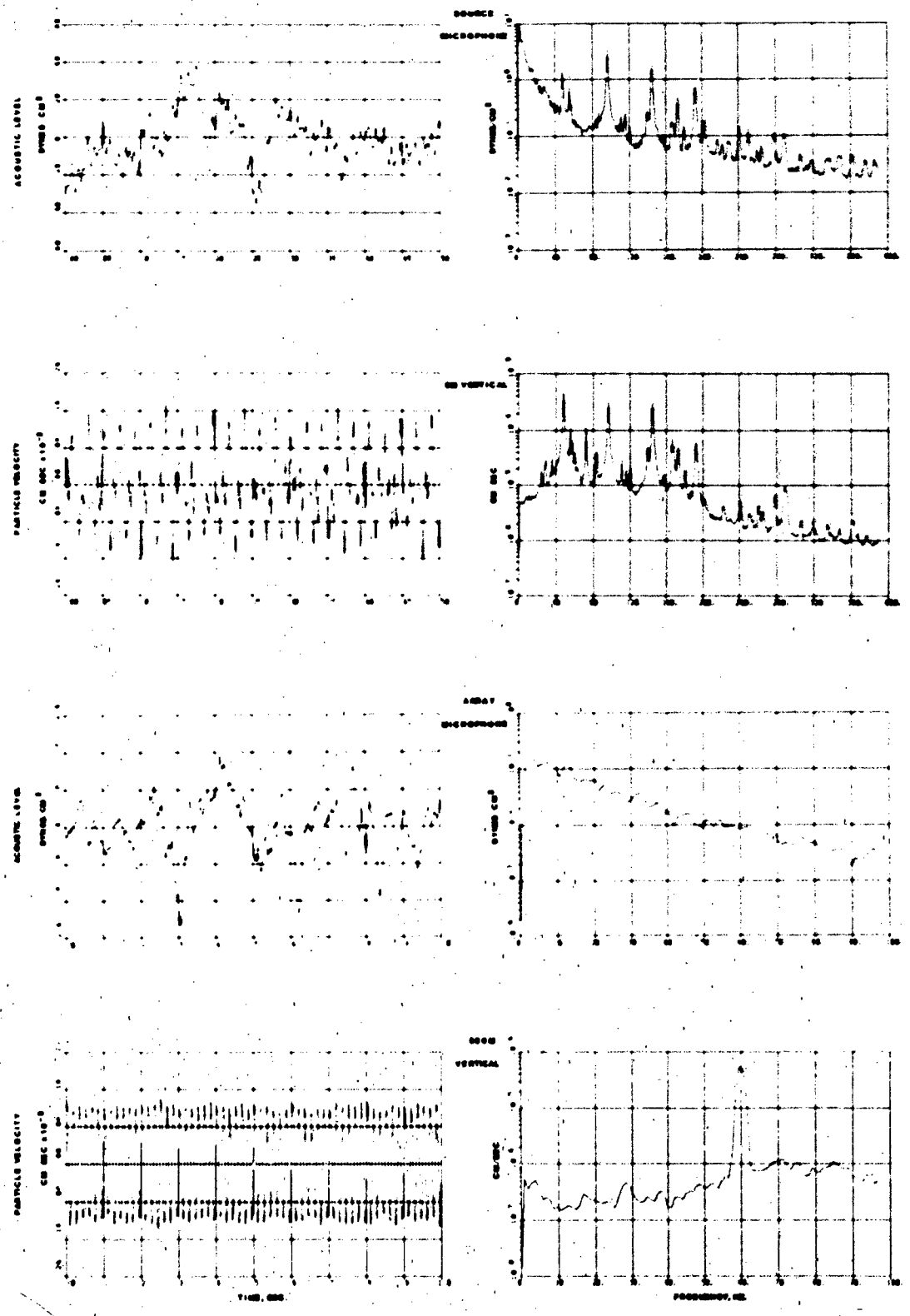

TEST 89A BACKGROUND NOISE

PLATE 101

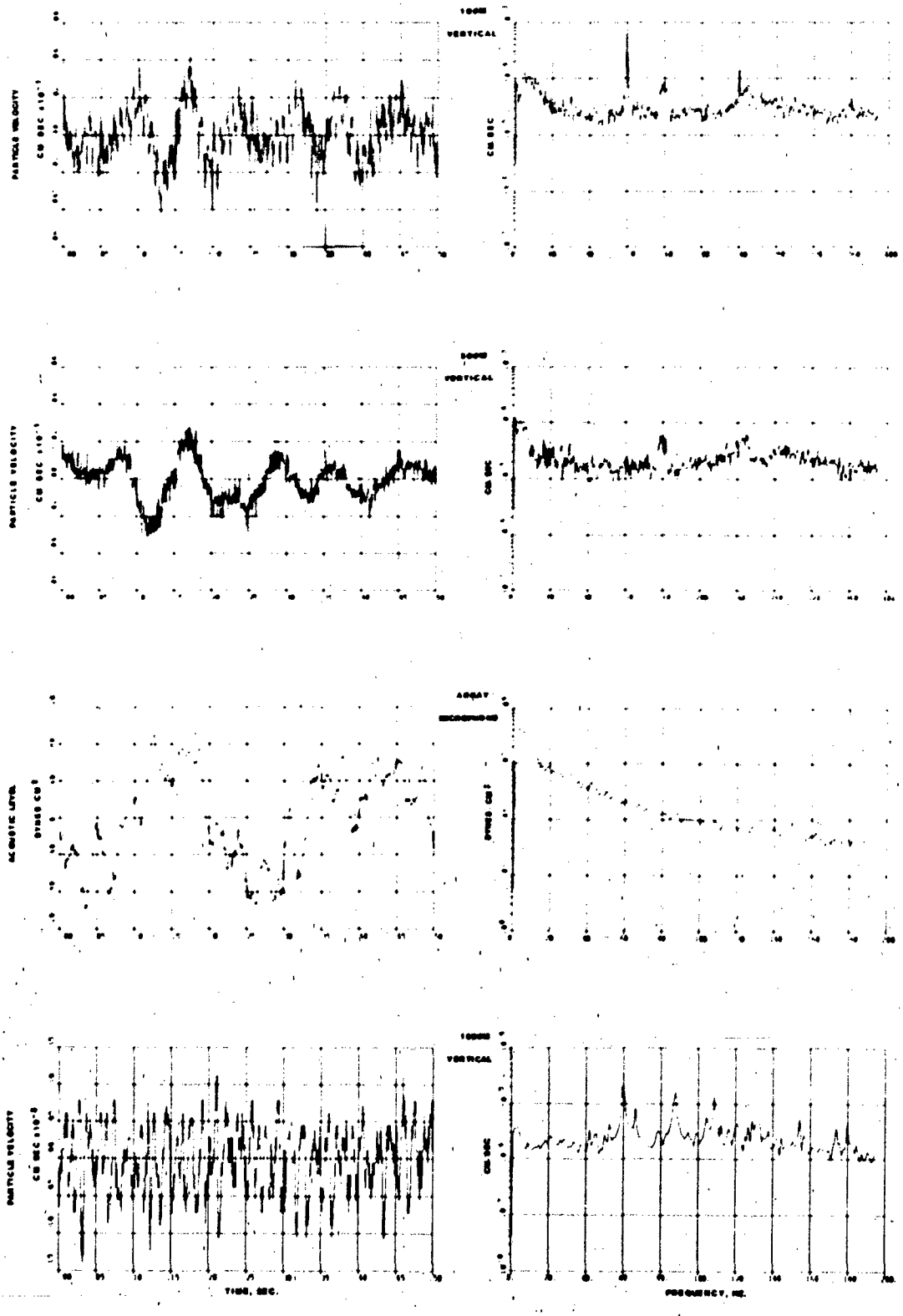

TEST 133A BACKGROUND NOISE

PLATE 102

APPENDIX A: SEISMIC ATTENUATION TEST PROGRAM

Introduction

Background

1. Seismic tests have been conducted at sites all over the continental United States by the US Army Engineer Waterways Experiment Station (WES) to characterize site conditions. Nondestructive seismic tests such as those which measure wave refraction are valuable, easy-to-run field experiments that provide quantitative engineering information on surface and subsurface soil and rock. Experience has shown that seismic and acoustic signals are affected by a number of environmental source variables which can cause large differences in measured seismic response. However, there has been little correlation of these differences, and the effects of environmental constraints on seismic wave propagation cannot be predicted with confidence unless these source variables are properly documented.

Purpose

2. The purpose of this test plan is to establish a series of experiments that will:

a. Determine the relative efficiencies that seismic signals from impulsive and continuous wave sources propagate in natural terrain.

b. Determine the resolution and fidelity of multiple frequency signals propagating in natural terrain.

c. Supplement an existing database that in turn will be used to validate theoretical models of seismic wave propagation in natural terrain.

Approach

3. The project will be conducted by WES personnel. Based on existing data, a site with appropriate physical, seismic, and environmental properties will be selected. The experimental array will be laid out at the site, and the site will be characterized physically and seismically to confirm its properties. An instrumentation system including geophone, microphone, and meteorological sensors will be emplaced and monitored while seismic sources are moved from station to station along the experimental array. Measured data will be verified on site and then processed and analyzed at WES. Background noise will be monitored during the tests and characterized. The final data

will be used to verify theoretical model calculations and will be extrapolated to a range of conditions through model analysis.

Site Selection

Requirements

4. The site will be selected to meet the general characteristics listed in Table A1 below. Some tentative areas have been located at the White Sands Missile Range (WSMR), New Mexico, shown on Tularosa Quadrangle topographic map distributed by the US Geological Survey (USGS). These areas provide commercial power and easy access, as well as properties similar to those required.

Table A1

Site Characteristics

Property	Description
Topography	Flat/rolling
Vegetation	Sparse/no trees
Weather	Relatively dry
Soil, surface	Silt to sand - dry
Soil, subsurface	Silt/sand - cemented
Bedrock	Sedimentary - D > 45 m
Water table	D > 45 m
Seismic-compression wave velocity	300 m/sec (surface) - 5000 m/sec (bedrock)
Location	Remote - no obvious seismic sources

Site layout

5. The site will be laid out in the array specified in paragraph 10. The actual location of the site will be established by survey after an on-site inspection and preliminary characterization. The site will be laid out to facilitate ease of testing and movement of equipment. It will be necessary to drive to each source location with the vibrators and instruments. Power will be required for the instrumentation equipment at the sensor array, and cannot be furnished by generator because of acoustic and seismic noise.

Site Characterization

Seismic

6. Seismic refraction and vibratory tests will be made at the array and at most source locations on the test layout (Figure A1). These tests will include measurement of compression and shear wave velocities with a geophone package emplaced over a 200-m length. This will provide a seismic profile down to not less than 50 m. The seismic signals will be measured with a standard seismic refraction geophone (see paragraph 16).

Environmental

7. Each of the seismic source locations will be characterized using quantitative environmental data describing the substrate (i.e., soils, underlying rock, etc.), topography, vegetation, and meteorology. The environmental data will consist of those factors that may have significant effects on the generation and propagation of microseismic waves. Relevant environmental characteristics are as follows:

a. Soil.
   (1) Soil moisture content, percent.
   (2) Soil mass (or wet) density, g/cm^3.
   (3) Soil type (Unified Soil Classification System (USCS)).
   (4) Atterberg limits.
   (5) Soil particle sizes, percent finer by weight.
   (6) Cone penetration resistance, kPa.
   (7) Plate loading test.

b. Topography. Ground profile along the array-source line will be surveyed. (The general topography will also be documented by USGS topographic maps.)

c. Vegetation.
   (1) Type.
   (2) Height, cm.
   (3) Density, $stems/cm^2$.

d. Meteorology (history and test conditions at the array point).
   (1) Air temperature, deg C.
   (2) Wind speed, m/sec.
   (3) Wind direction, deg.

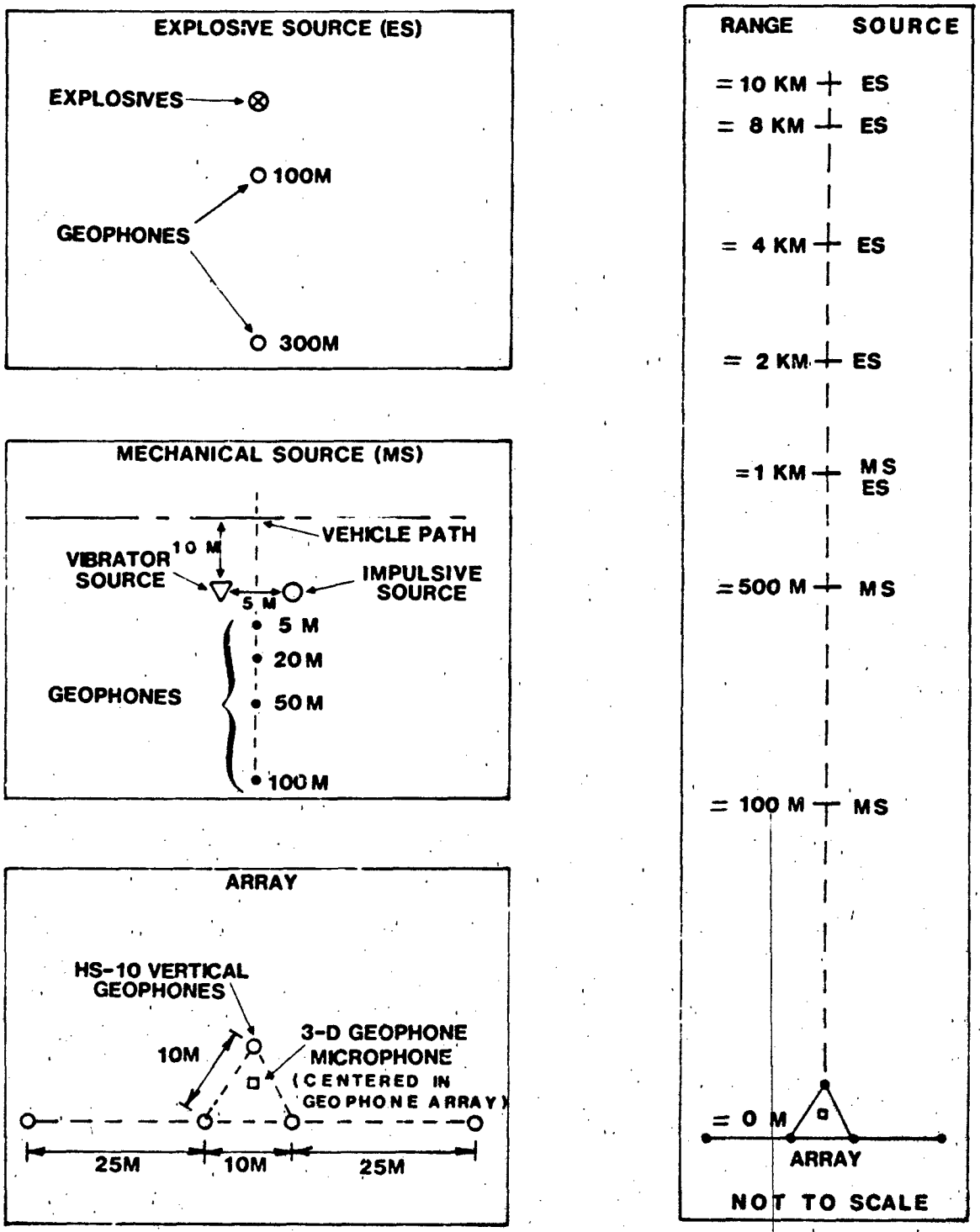

Figure A1. Layout of sources and array

(4) Precipitation (rainfall, snowfall), cm.

(5) Relative humidity.

8. Soil samples for describing the substrates will be obtained by igging a pit (when possible) to a depth of 1.0 m and hand-augering a hole pproximately 10 cm in diameter from the bottom of the pit to a total depth of m (from the original surface). Soil samples from which moisture content and et density can be determined will be obtained at the surface and at 50-cm ntervals to a depth of 2 m. Bulk samples will be taken at various depths (as pecified by the field engineer) to obtain USCS classification for each iden-ifiable soil layer. In addition to the soil samples, cone penetrometer read-ngs will be obtained at the array and at each source location along the eference line at the surface and at 7.5-cm increments to a depth of 45 cm.

9. Topography (ground surface configuration) will be obtained by sur-eying a detailed profile along the source-array line. The vegetation sur-ounding the site will be described by determining the plant type, height, and ensity of stems per unit area. In addition, the dominant and codominant lants will be determined. Weather conditions will be measured on-site, and ecords from the nearest official weather station (e.g., Holloman Air Force ase) will be provided.

Seismic Data Collection

est geometry

10. The tests will be conducted in the array shown in Figure A1. The rray of calibrated geophones capable of measuring 1-200 Hz will be emplaced t the beginning point of the test line. The array will include five vertical eophones, one three-dimensional geophone, and one outdoor microphone unit. his will be called the array geophone system. Four calibrated vertical geo-hones will be emplaced near the source to measure input and close-in attenua-ion. Also, a load cell will measure input load from the vibrator, and a icrophone will be used to measure noise. These will be called the source eophone system. In addition, a portable triaxial geophone package will be mplaced at other locations on bedrock or on a rigid substratum to give an ndication of signal characteristics at a high-contrast interface. This will e called the lateral geophone system. (The geophones, microphone, and

instrumentation packages are described further in paragraphs 16-18. Tests using several seismic sources will be conducted at each of eight ranges (at the array, 100 m, 500 m, 1 km, 2 km, 4 km, 8 km, and 10 km). However, when a particular test no longer produces signals at the array, that test will be omitted from the remaining ranges. (The source signatures are described in paragraphs 13 and 14.) The tests are listed and described in Table A2.

Table A2

Summary of Seismic Test Sources

No.	Description	Length
1	Vibrate discrete frequency sine waves of 1, 2, 3, 4, 5, 6, 7, 10, 15, 20, 30, 50, 100, 120 Hz at maximum force output	~30 sec each test
2	Frequency sweep, vibrator at maximum force output, 1-200 Hz	
3	Vibrate discrete frequency sine waves of 2, 15, 50, and 200 Hz and vary frequency by 1 to 10%	
4	Vibrate with tone bursts (approximately 8 cycles of each frequency in no. 1)	~30 sec w/dead time
5	Vibrate with random input (white noise) source; limited bandpass 1-200 Hz	~30 sec
6	Impact tests: 5 impacts to seat plate and calibrate; then dead time, followed by 5 impacts (explosives will be used as an impact source if necessary, to obtain data on the far-range tests)	~30 sec dead time between impacts
7	M-35 Truck: normal - modified	~15 sec 10 mph

Spectral array data

11. The tests listed in Table A2 will provide an extensive amount of data relating wave propagation and attenuation to input frequency and loading. By varying the range and the input loading, resulting data will show the effect of the natural terrain on seismic wave propagation. The vehicle test will provide realistic data for comparison. All data will be processed for spatial information by calculating pointing angles for waves propagating across the array. The pointing angle variations with frequency and range will be correlated with site physical features (e.g., topography, vertical

cuts, subsurface variations, etc.), so that similar results can be extrapolated to other site conditions. Note that for spatial array analysis, geophones from both the fixed array and the movable source will be combined to form aperatures of various geometry as range is varied.

Background noise data

12. The seismic motions resulting from both ambient and natural noises and those caused by the testing equipment will be recorded periodically during and between testing. Specific tests to be conducted include a 24-hr test, recording data for 5 min of each hour, and a spatial array test in which data are recorded for approximately 5 min at 30 locations across the site. Thus, background noise will be characterized both with time and space to allow extrapolation to other sites.

Seismic Sources

13. The WES trailer-mounted shaker unit is a self-contained electrohydraulic vibrator consisting of a hydraulic system and shaker assembly driven by a gasoline engine. The programmable function system has a maximum force output of 0.91 metric ton between 15 and 200 Hz (output drops below 15 and above 200 Hz). The load is distributed through a 76.2-cm-diam base plate which limits soil stress to about 20.7 kPa. Shaker output can be in continuous sine waves at discrete frequencies and controlled force output, frequency-sweep sine waves at controlled force output, pulsed discrete frequencies, and random signals. The shaker was fabricated at WES using a controller and actuator manufactured by Zonic.

14. The impulse loader is a Dyna Source portable seismic energy source made by EG&G Geometrics. The system provides a mechanical energy source powered by a gasoline engine. The system has a piston weighing 39 kg that drops 1.8 m, using a vacuum to prevent rebound. The cycle time for the system is 15-20 sec. Should the impulse load be attenuated before reaching the array on any range, explosives will be substituted for the impulse load.

15. An M-35 Army 2.5-ton truck will also be used as a source of seismic signals. It provides a complex forcing function composed of both impulsive and multiple-frequency components. Several runs will be made at each range on a smooth road path and a modified path (i.e., path roughness increased to provide larger amplitude forcing function).

Sensors

16. The seismic refraction geophones will be Mark Products Model L-10, a standard vertical geophone used for seismic refraction. The Model L-10 has a natural frequency of 8.0 Hz.

17. The geophones to be used in the seismic tests are Geospace HS-10-1 calibrated vertical geophones with a natural frequency of 1 Hz, a response of 1-200 Hz, damped at 70 percent of critical, and a sensitivity of 2.95 V/cm/sec. The triaxial (three mutually perpendicular velocities) geophone will be a Mark Products Model L-4C-3D with a natural frequency of 1 Hz, damped 70 percent of critical, a response of 1-200 Hz, and a sensitivity of 2.35 V/cm/sec. These geophones will be emplaced according to the following specifications:

a. Dig a hole approximately the same size and shape as the geophone that is to buried. The best results will be obtained with the bottom of the hole flat and the soil disturbance kept to a minimum.

b. Place the geophone in the hole with the device base in firm contact with the bottom of the hole.

c. Take care in backfilling the hole. The excavated material should be replaced at as near in situ conditions as possible. The seismic signal undergoes reflection and refraction at each interface. This condition causes some of the seismic energy to dissipate. If the soil is backfilled exactly as the soil in situ, the number of interfaces between the source and sensor will be reduced by one. Since this is not altogether possible, the purpose is to approach this homogeneous state, which keeps the properties on each side of the interface similar and the energy decay to a minimum.

18. The microphone to be used in the array is a Bruel and Kjaer (B&K) Model 4921 outdoor microphone unit with a frequency of 10-20,000 Hz and a dynamic range of 140 db. This unit has a built-in electrostatic calibrator giving 90-db sound pressure level at 1000 Hz.

Instrumentation

Systems

19. The array geophone instrumentation system will record data at the array. The system will operate on 120-V power, which cannot be provided by a portable generator because of the noise in the array area. The source

)hone system will be portable, will always have the same orientation to the :ce, and will move to each new source location. This system will be :ery powered for convenience. A schematic of a basic instrumentation sys- is shown in Figure A2. Both systems described above are similar to the ving, except the array system would have a microphone added to the input as l as a low-pass filter between the amplifier and the recorder. The lateral)hone system (paragraph 10) is battery powered and has only three channels. ls a completely self-contained system with amplifier and analog tape re- ler. Its frequency response is 1-200 Hz; its natural frequency is 1 Hz ı a sensitivity of 2.35 V/cm/sec.

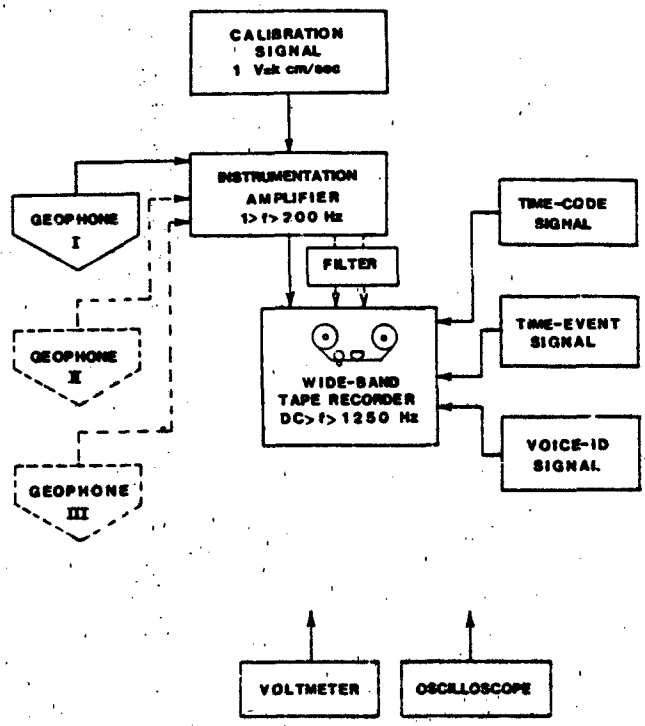

Figure A2. Block diagram of the major components in a typical seismic analog recording system

orders

20. Signals from the array geophone system will be recorded on a gamo Model 3500 14-track analog tape recorder, recording at 3-3/4 in. 5 cm)/sec FM-mode, which will give a frequency response of DC to 1250 Hz. s recorder requires 120 V AC power. The source geophone recorder will be a al Model STORE 7DS, seven-channel analog tape recorder operated in FM mode

at 3-3/4 in. (9.5 cm)/sec (DC to 1250-Hz frequency response). This recorder will be battery powered, operating on 24 V DC.

Amplifiers

21. The array system will employ Ithaca Model 456 amplifiers, with a bandwidth of 1-100,000 Hz and 100-db gain range in 1-db steps, which operate at 120-V AC. The source system amplifiers will be WES-made units, with a bandwidth of DC to 5000 Hz and a continuous gain range from 0 to 60 db, which operate at 12-V DC.

Filters

22. The array system will use Krohn-Hite Model 3323 filters which have the option of being low-pass, high-pass, or band-pass. These filters have a frequency range of 0.01 to 100,000 Hz and an attenuation rate of 24 db per octave outside the pass-band. It is not planned to filter the source geophones since the signals at the source will be quite strong compared to background noise.

Calibrators

23. Substitution sine-wave calibrations will be used as an alternate input to the amplifiers during system calibration. The sine-wave calibration signal will be monitored with a precision voltmeter and frequency counter. The sine-wave calibration voltage will be compared to the known geophone sensitivities to calculate the recording system sensitivity in velocity units. A time standard, IRIG B, will be recorded on both tape recorders for time of day and common timing on both tape recorders.

Spectrum analyzer

24. The spectrum analyzer will be used with the array instrumentation system to determine what and how background noise data can be filtered from actual signals. The analyzer to be used is a Hewlitt-Packard 3582, which has a frequency response of DC to 20,000 Hz and a dynamic range of 70 db. The system also has a plotting capability for permanent records made in the field.

Test Operations

Schedule

25. A schedule of activities for the period prior to the field tests, the actual field operations, and the data analysis period is given in Table A3.

Table A3

Schedule

Description	Time Frame	Personnel*	Remarks
Complete preparation of plan	21 Jan 83	EL/GL/ISD	
Approval of plan	Feb 83	US Air Force	Approx. 30 days
Preliminary site survey	28 Feb-4 Mar 83	EL/GL	WSMR
Site layout	14-19 Mar 83	EL	
Site characterization (physical)	14-19 Mar 83	EL	
Site characterization (seismic)	28 Mar-2 Apr 83	GL/EL/ISD	
Testing	28 Mar-16 Apr 83	GL/EL/ISD	
Signal processing	18 Apr-30 Apr 83	ISD	
Model calculations	1 Feb-14 May 83	EL	
Analysis	18 Apr-14 May 83	EL/GL	
Report draft	21 May 83	EL	

* WES organizations:
EL - Environmental Laboratory.
GL - Geotechnical Laboratory.
ISD - Instrumentation Services Division.

Site operations

26. All operations on site will be done in accordance with WES and WSMR safety standards. Contact will be kept with Range Control at all times. It is not anticipated that explosives will be used in all tests, but it may be necessary to generate measurable signals in the 2- to 10-km ranges. If explosives are used, all operations will be performed according to an Explosives Safety Plan submitted to WSMR, and timing and firing will be coordinated with Range Control. No damage is anticipated to the site other than a few small holes, and these will be filled upon completion of the tests.

Signal Processing

Real time

27. One method available to examine data as they are measured is an oscillograph record to reproduce time histories of the recorded data. In

addition, the spectrum analyzer provides a "quick look" processing capability, both of real time and recorded data, by displaying on a CRT screen amplitude spectrum data and phase spectrum data. It will also plot displayed data on an x-y plotter. Once the data are examined, changes can be made to compensate for deficiencies in recording the source input.

Post-test analysis

28. WES/ISD currently have the capability of performing time and frequency domain analysis over the entire length of a test. Time history, auto correlation, cross correlation, and impulse response will be calculated and plotted in the time domain. Fourier transform coefficients, power spectral density, phase, cross-power spectra, transfer function, and coherence will be calculated for selected records and plotted in the frequency domain. These frequency domain signals are acquired by time averaging Fast Fourier Transform ensembles of 512 points over any desired length of a test. A Hanning window will be applied to frequency domain data. Either axis can be plotted linearally or on 1-5 log cycles. The test number; tape number; channel number; and mean, root mean square, maximum, and minimum values are printed above each plot.

29. Utility software to scale and reduce any test to a new file starting at any selected sample is available. These data will also be plotted or listed for examination prior to the signal processing phase. Utility software will also be used to synchronize data recorded on different tapes that have a common event on each tape. The data will be digitized at a maximum through-put of 50,000 samples/second, using a 12-bit, ±5-V ADC.

Modeling Analysis

Description

30. The WES seismic model simulates the generation, coupling, propagation, and transfer of the seismic signal from the target to the sensor. Figure A3 illustrates these phenomena. Stress from a target (vibrator, moving vehicle, etc.) applied over a finite time causes the surface of the ground to deflect. This "forcing function" coupled to the ground initiates particle motion which, in turn, generates a seismic wave. Seismic waves can propagate in a number of modes and show a decrease in amplitude due to geometric attenuation and viscous damping. The seismic wave amplitude may be further reduced

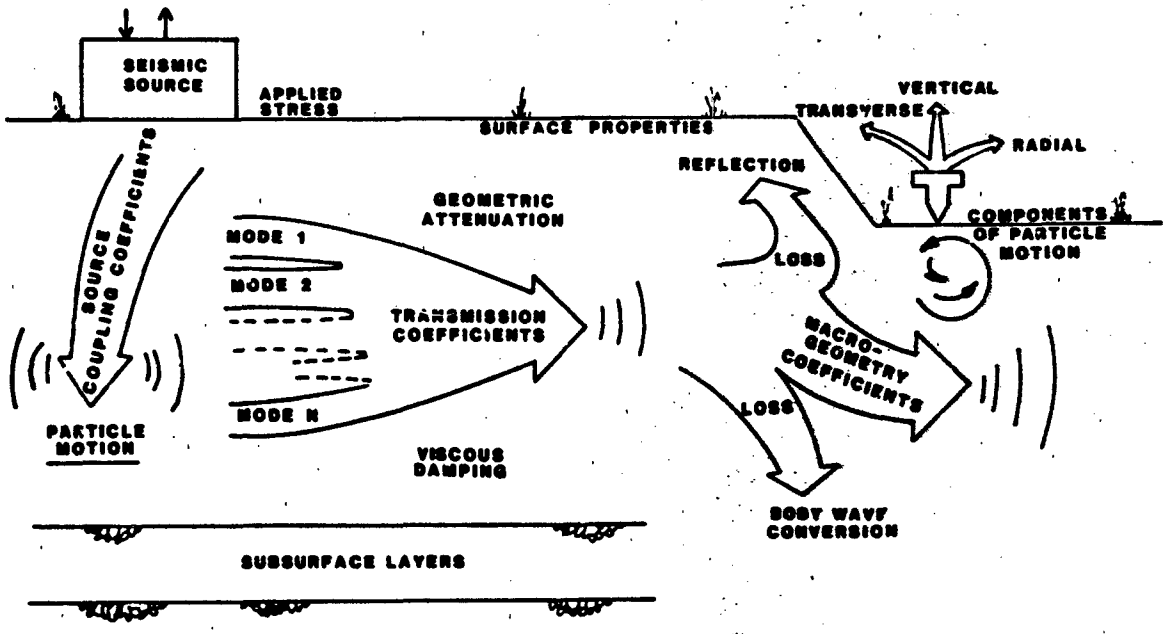

Figure A3. Seismic wave propagation

if the wave travels near the surface of a macrogeometry feature. For example, macrogeometry features such as trenches, wedges, or steps in elevation can cause part of the wave traveling along the surface to be reflected in a new direction of travel or converted to body waves, which may or may not travel in the same direction as the original wave. The waves finally arrive at a measurement point (a geophone) in a pattern entirely different from their initial pattern. This change is a function of site properties and range and path of propagation.

31. To develop the mathematics to simulate the phenomena in Figure A3, it is convenient to consider the earth as a homogeneous medium, but such a generalization does not allow a prediction of seismic waves comparable to those observed on seismic records measured in the field. A more realistic and useful assumption is one in which the earth is considered to be a layered medium with each layer considered homogeneous. The approach taken in the WES seismic model is one that attempts to develop the mathematics within the framework of theoretical mechanics to simulate the phenomena described above.

Pretest predictions

32. The WES seismic model will be used to predict the signals to be measured by the array geophones. The model will use site characteristics to be determined in the preliminary site characterization tests, with the source

loadings described in Table A2 to predict the signals. These predictions will be used to set gains on amplifiers and other pretest calibrations which must be done to receive signals above system noise levels and within the dynamic range of the instruments.

Post-test analysis

33. The WES seismic model will be used to relate input loading to measured output. This will be accomplished by the following:

a. Establish the forcing functions for the input loads. For the vibrator and impulse sources, the forcing function will be measured directly from the load cells. For a complex vehicle source, the forcing function will be computed using the AMC mobility model vehicle dynamics module (see Figure A4 for simplified diagram of this model for an M-35 truck).

b. After establishing site characteristics, the model can predict signals in both time and frequency domains for comparison to measured signals similar to those shown in Figures A5 and A6.

c. One purpose of the tests and model calculations is to calculate a transmission coefficient which, when multiplied by the source coupling coefficient, will produce a site transfer function. This process can be seen in Figures A7-A10. Once a site transfer function is completed, signals for any source can be calculated.

d. When the calculations are complete for the specified site, other site conditions can be input to the model for extrapolations of the basic phenomena to other areas.

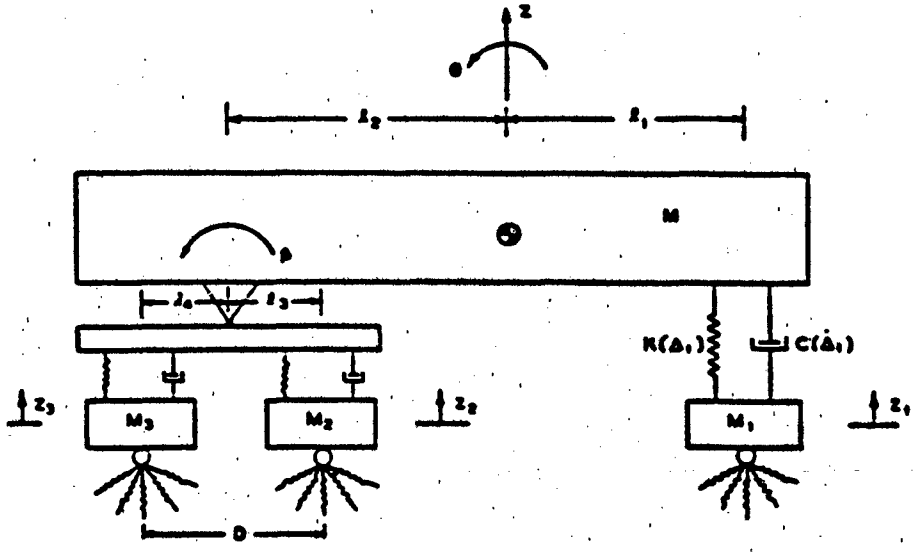

Figure A4. Schematic used to calculate forcing function for the M-35 truck

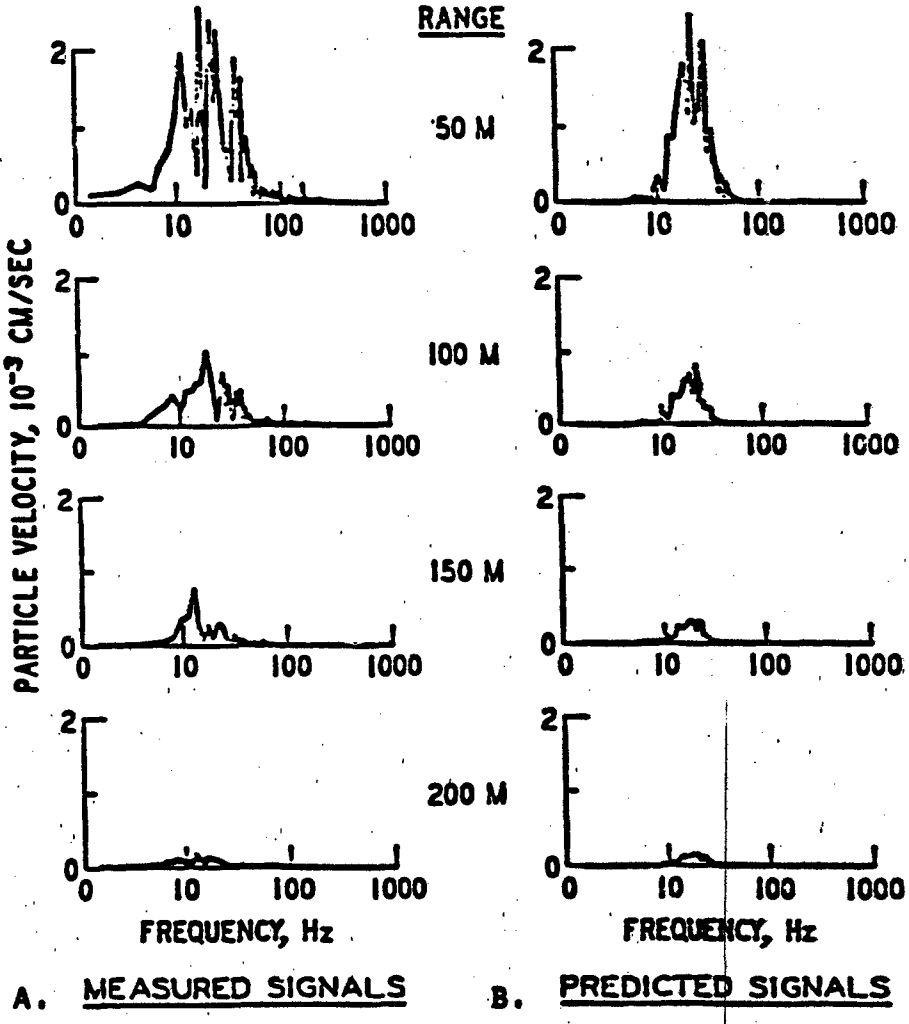

Figure A5. M-151 (jeep) signals, 32 km/hr, frequency domain

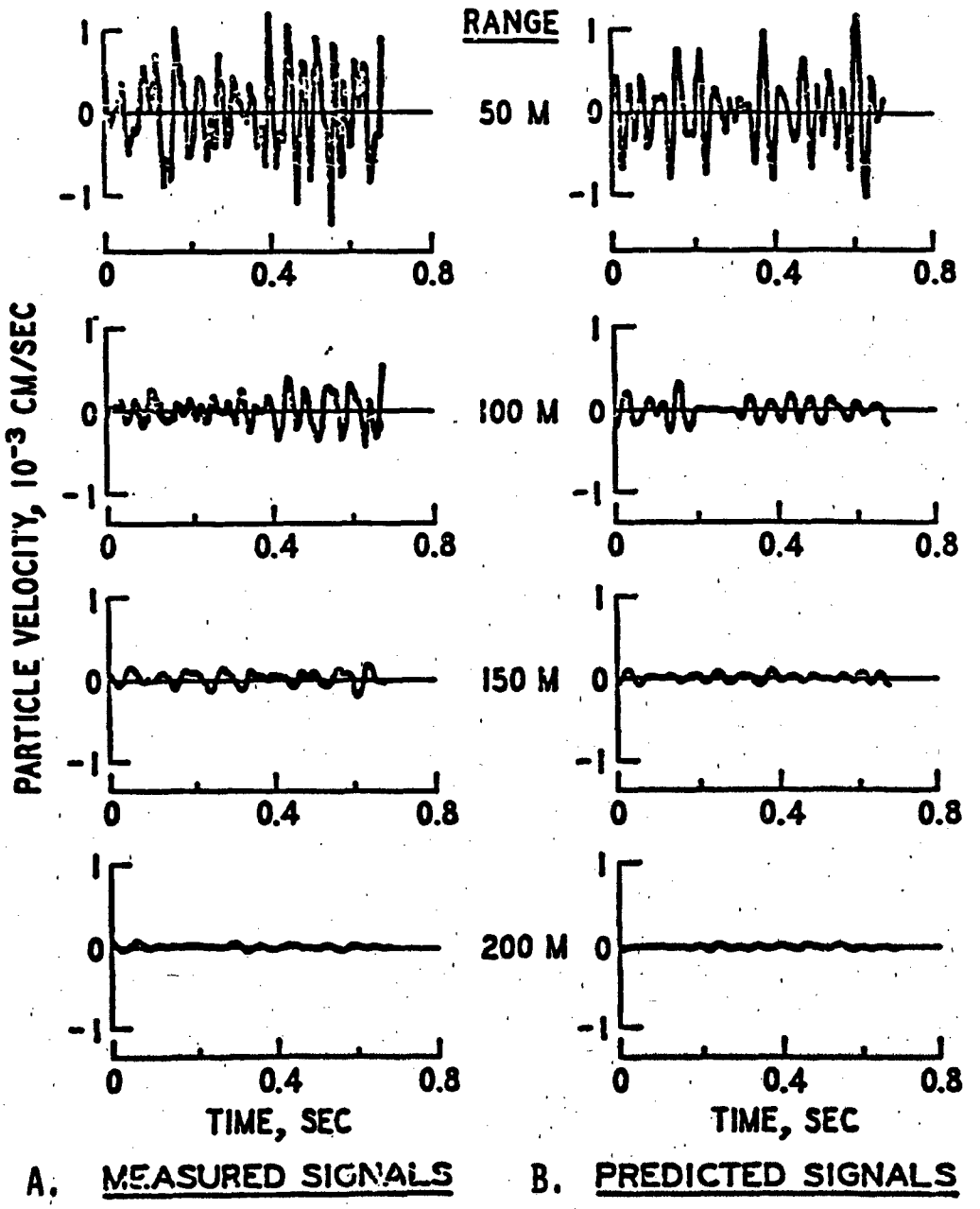

Figure A6. M-151 (jeep) signals, 32 km/hr, time domain

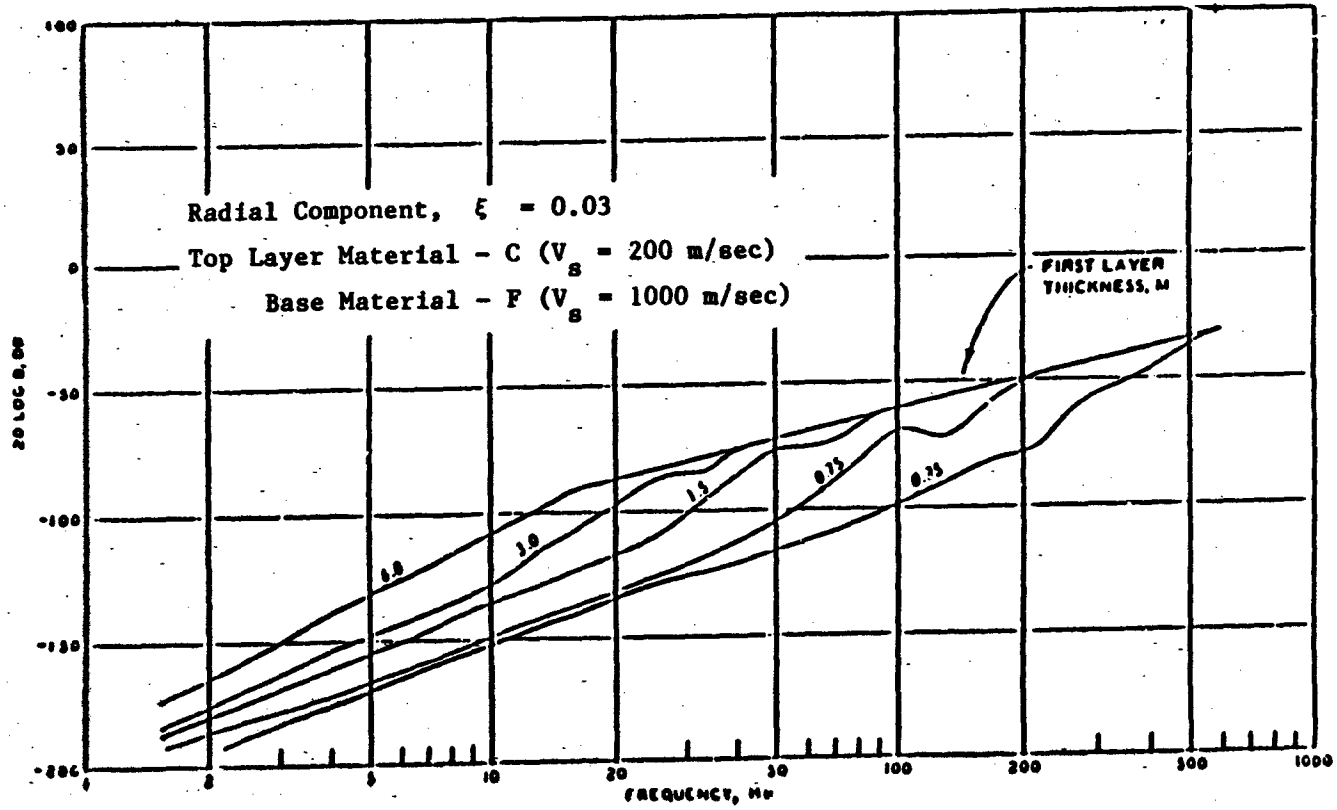

Figure A7. Source coupling coefficient, B

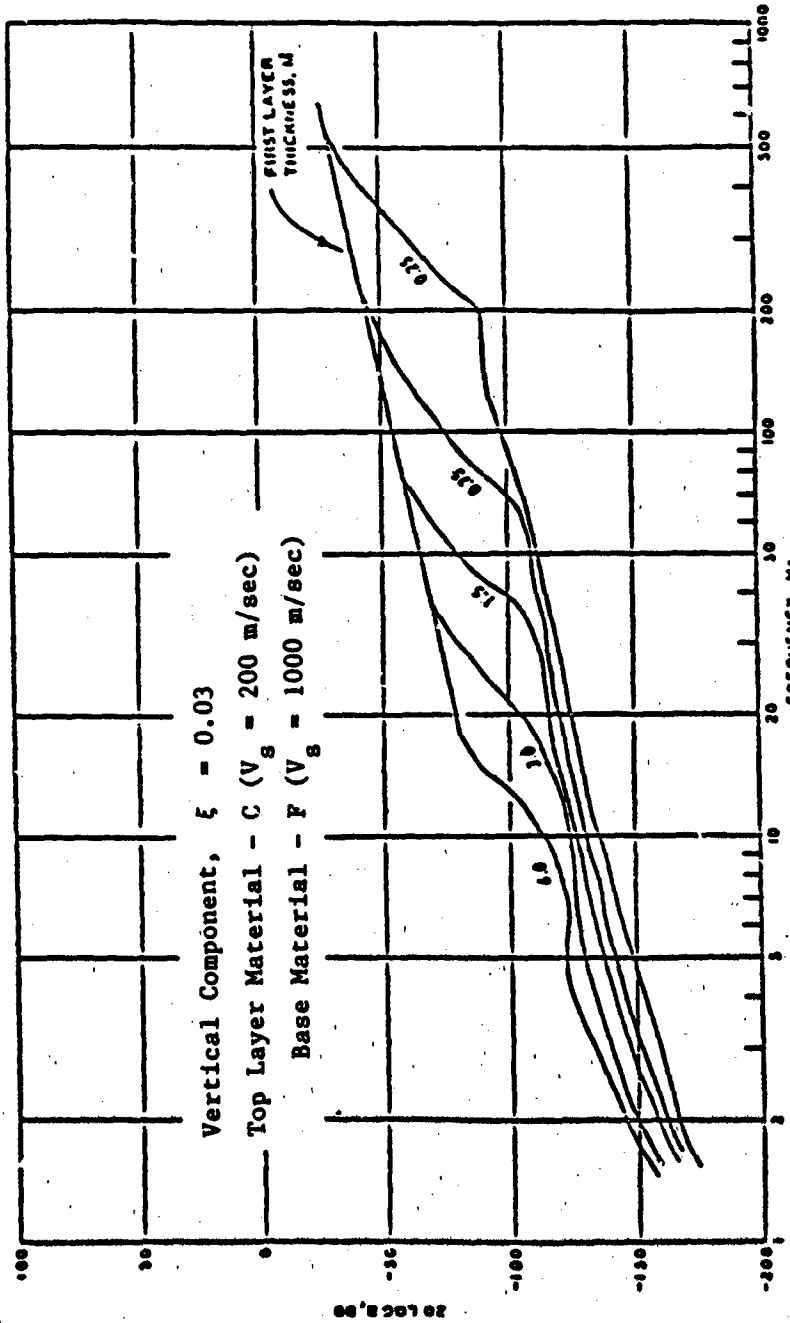

Figure A8. Source coupling coefficient, B

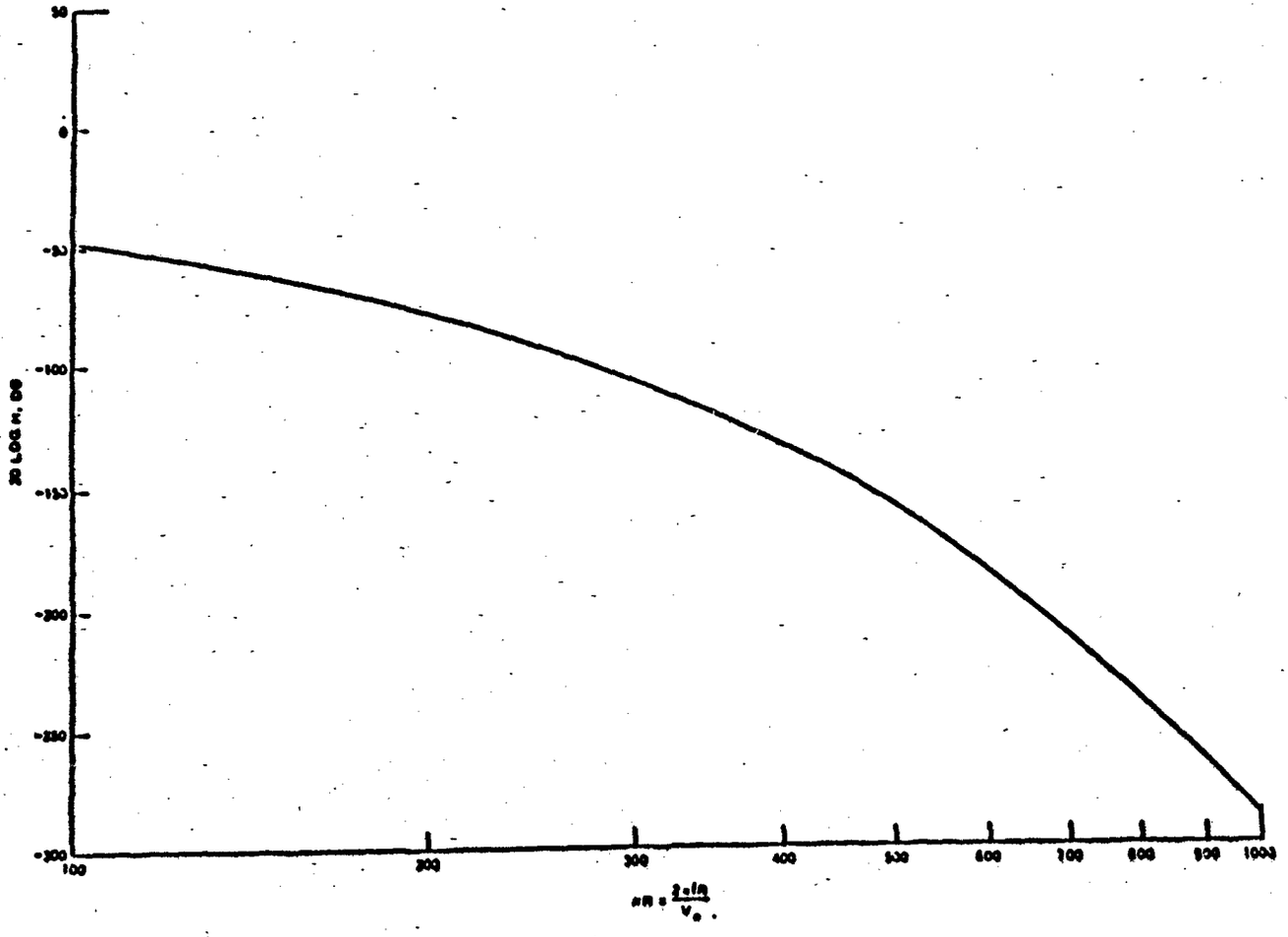

Figure A9. Transmission coefficient, H
ξ = 0.03. KR:100 - 1000

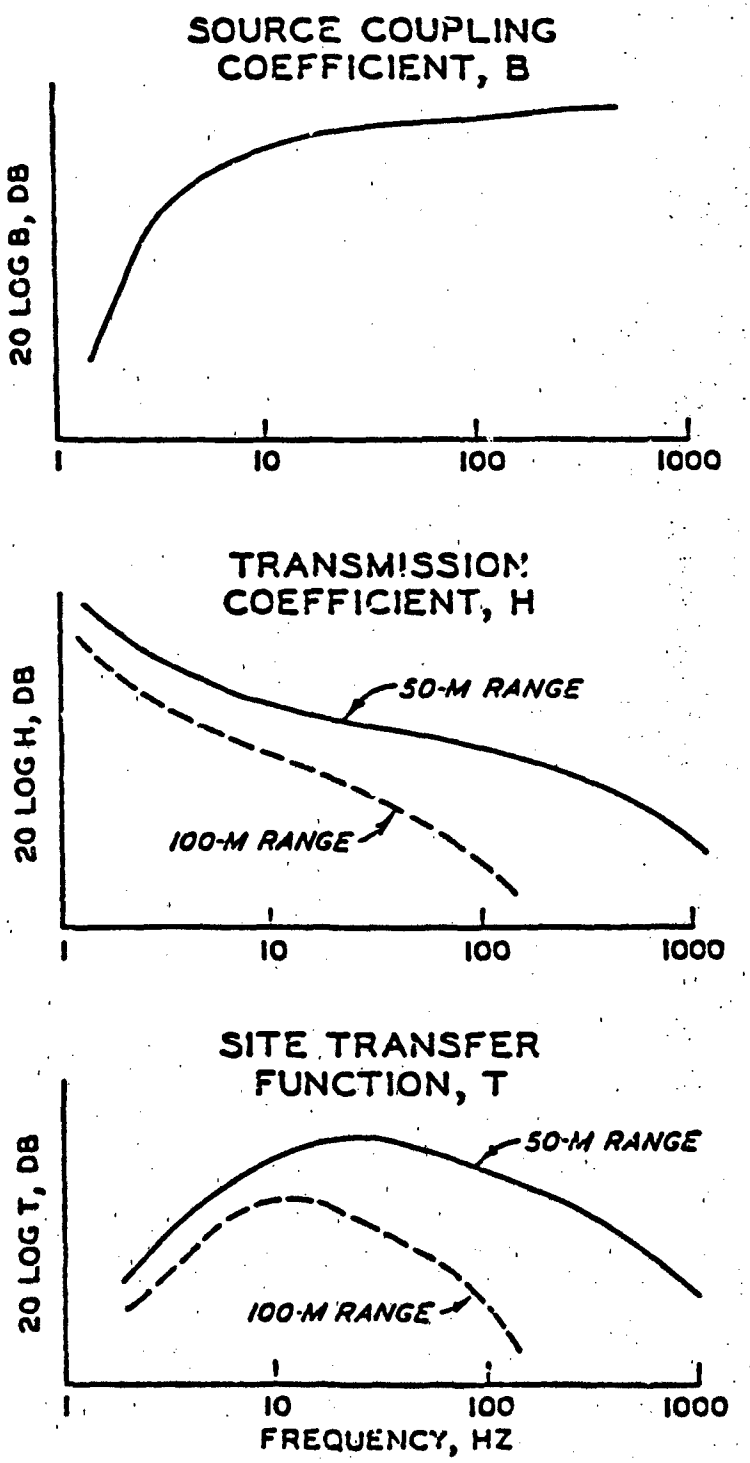

Figure A10. Derivation of the site transfer function

APPENDIX B: SEISMIC REFRACTION STUDY

Background

1. This study was conducted by the Earthquake Engineering and Geophysics Division (EEGD) to determine the compression (P-wave) velocity versus depth characteristics of a test site located at the White Sands Missile Range (WSMR), New Mexico. The work was performed in the period 3-15 April 1983 by Messrs. S. S. Cooper and S. G. Sanders. In this study, it was desired to model a typical alluvial valley environment having the following general characteristics:

a. Seismic (P-wave) profile:

Depth, ft*	P-Wave Velocity, ft/sec
0-20	1500 to 2400
20-140	2700 to 4300
140-250	5300 ± 200
250-600	5800 ± 100

b. Depth to water table of about 150 ft.

c. Reasonable uniformity in subsurface conditions over a planned test distance of 6.21 miles (10 km).

2. Information developed from earlier site selection studies had identified certain locales within the WSMR as having the general characteristics desired. The WSMR lies within the Mexican Highland Section of the Basin and Range Province, which is characterized by a series of tilted fault blocks forming asymmetric ridges or mountains and broad intervening basins. The area of primary interest for this study was the Jornado del Muerto Basin near the Trinity Site, where the test line was located as shown in Figure B1. In general, overburden in the alluvial fans and aprons closer to the Oscura Range can be expected to contain sand and rock fragments that grade coarser with depth, as well as minor amounts of silts and clays. Near-surface caliche deposits and conglomerates are also found in those areas. Toward the center of the basin, the overburden typically consists of thin-bedded fine material interbedded with occasional layers of coarse sand. The above conditions are

---

* To convert feet to metres, multiply by 0.3048.

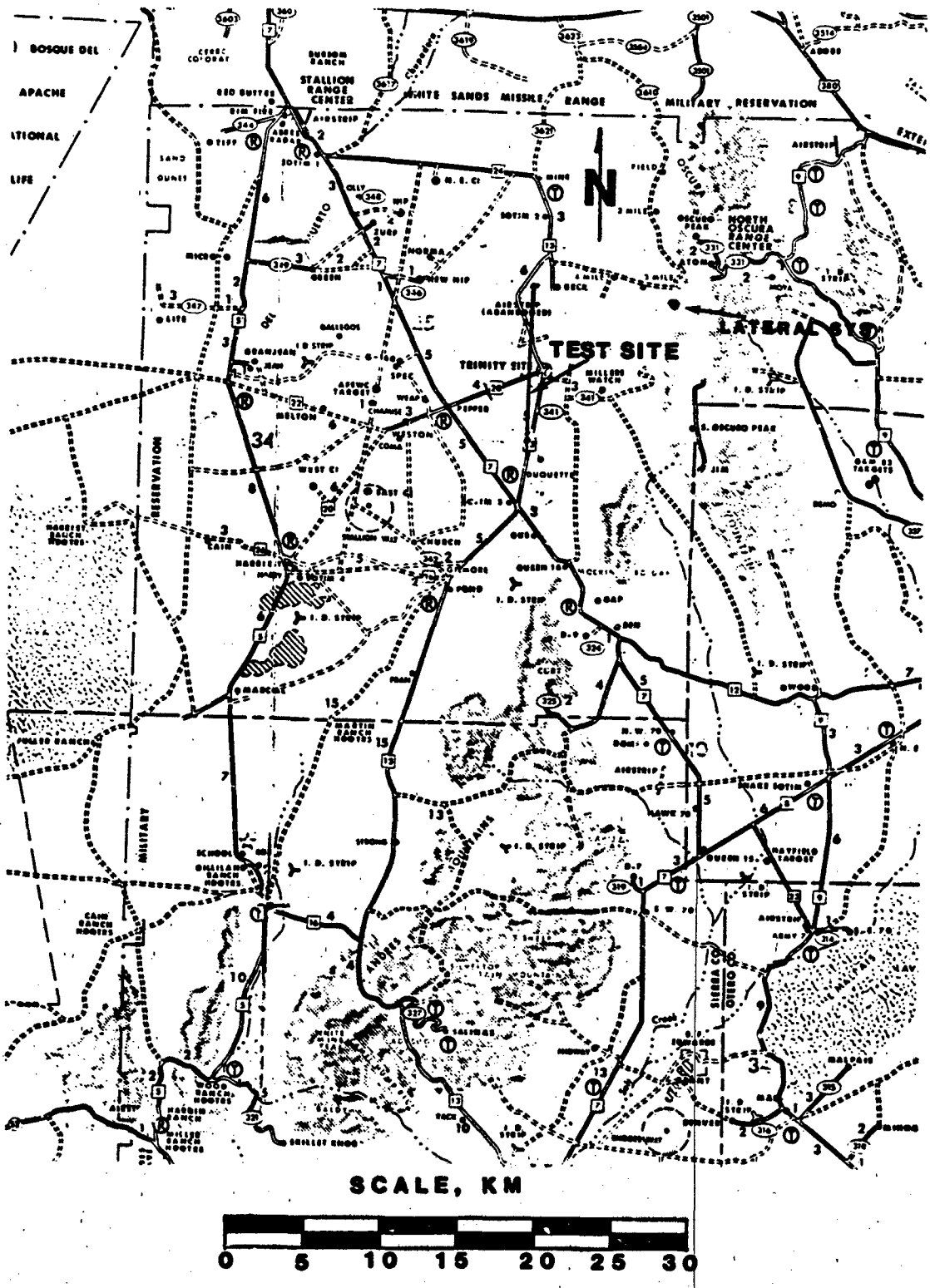

Figure B1. Site location map

considered to be generally representative of the typical alluvial valley environment.

3. In planning for the investigation, it was realized that time and funding constraints would not permit continuous refraction seismic coverage over the entire 6.21-mile (10-km) length of the test line, so it was decided to conduct one or more seismic surveys at each measurement location along the test line. Also, it was planned to use field data acquired from buried sensor arrays used in another phase of this study, i.e., source and main arrays, to derive a field attenuation plot of peak-to-peak maximum particle velocity versus range. This field-derived plot would assist in predicting ground motion response to explosive charges detonated at various ranges from the main sensor array, and would also provide a rough index of uniformity of ground motion response, hence site conditions, over the length of the test line.

Scope

4. This appendix documents the refraction seismic and special explosive tests conducted, describes how the various seismic refraction calculations were carried out, and presents results of the seismic investigation/site characterization.

Refraction Seismic Tests

5. It was recognized that refraction seismic survey lines up to 1200 ft in length would be required to reach depths of investigation on the order of 300-400 ft. The EEGD has a 24-channel SIE seismic unit, with two 12-channel spread cables having 50-ft geophone spacings; this equipment was used in the investigation. A 100-ft-long spread cable with 10-ft geophone spacings (12 channels) was also used to acquire near-surface P-wave data. A 16-lb (7.3-kg) sledgehammer and striker plate were used as the energy source for the near-surface (10-ft spacing) refraction surveys, but explosives were used as the source for longer geophone lines using 50-ft spacings. For reasons of safety and minimum restrictions on transport, a two-component mix of Kinepak explosive was used together with an explosive bridge wire (EBW) detonator and compatible FS-10 firing system. The Kinepak components are not classed as explosive until mixed on site, and the EBW firing system is insensitive to

accidental detonation from external influences such as static, powerline radiation, radios, etc. It had been decided that relatively long line refraction seismic surveys would be run at the main receiver array location and at ranges of 2.48 miles (4 km) and 6.21 miles (10 km). Near-surface (10-ft geophone spacing) refraction surveys would be used at intermediate measurement locations along the test line. The layout of the refraction survey lines at the main sensor array, and at the 2.48-mile and 6.21-mile locations, is shown in Figure B2. Time versus distance plots of refraction seismic results from the various surveys conducted are shown in Figures B3-B10. Shown in these plots are the calculated depths to interfaces between layers, the apparent P-wave velocity for each layer encountered, and the computed true velocity of each layer. Also indicated on each plot is the direction in which the survey was run, i.e., N-S indicates that the shot point was at the north end of the line and the geophone spread was toward the south. Unless otherwise noted, the center of the seismic survey was positioned over the survey stake identifying the test line measurement location.

6. A refraction seismic computer program, developed by Dr. H. M. Mooney, University of Missouri, was used to calculate the depth to interfaces and the apparent and true velocities of each refraction (layer). Hand calculations were also performed to validate the computer results, using both time/distance and time intercept formulas. Examples of the quick-check hand-calculation formulas are as follows:

$$\text{First Layer, } D_1 = \frac{X_1}{2} \sqrt{\frac{V_2 - V_1}{V_2 + V_1}}$$

$$\text{Second Layer, } D_2 = \frac{3}{4} D_1 + \frac{X_2}{2} \sqrt{\frac{V_3 - V_2}{V_3 + V_2}}$$

$$\text{Third Layer, } D_2 = \frac{1}{6} D_1 + \frac{3}{4} D_2 + \frac{X_3}{3} \sqrt{\frac{V_4 - V_3}{V_4 + V_3}}$$

where

D_2 = depth to layer

X_n = distance along x axis of plot to the point where the velocity (slope) changes due to presence of a new refractor

V_n = P-wave velocity of the refractors above and below an interface

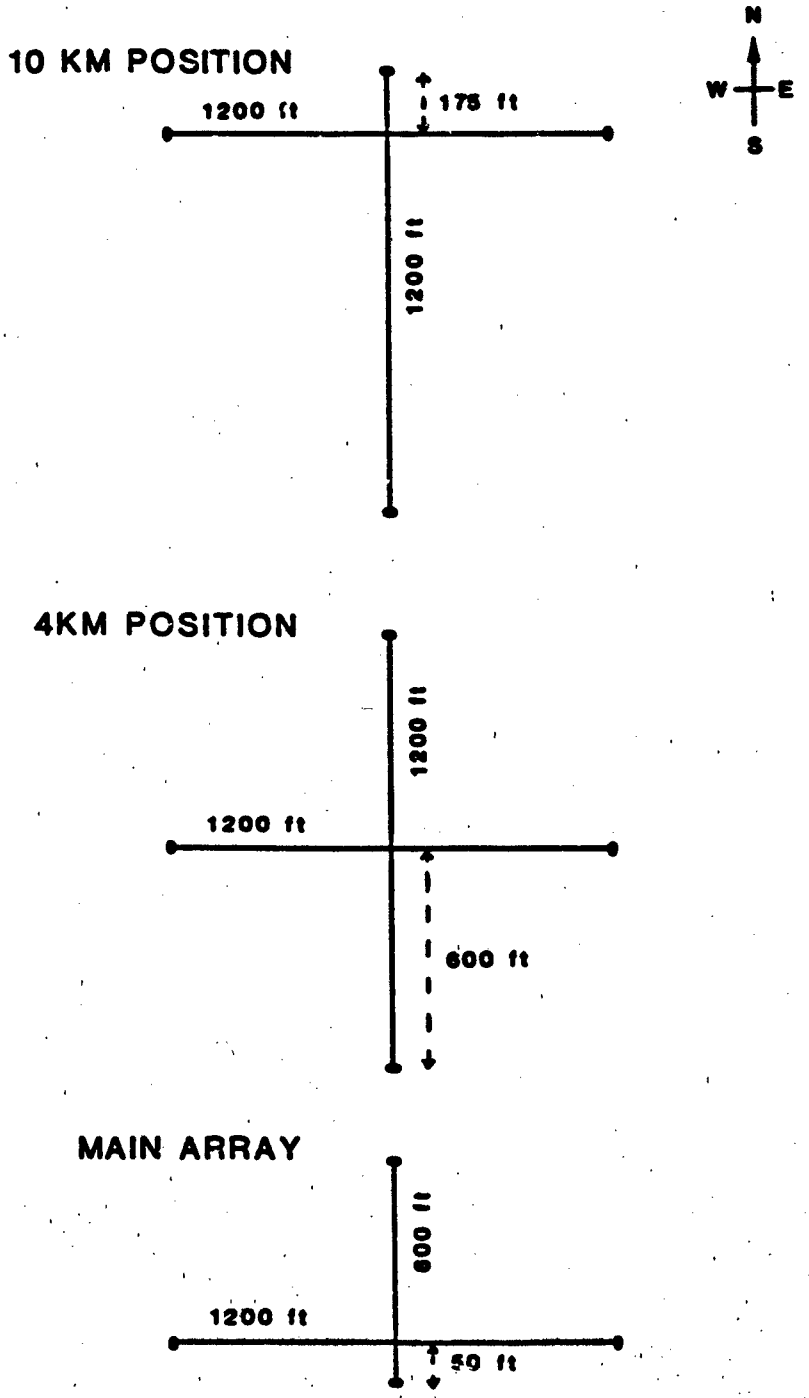

Figure B2. Seismic refraction survey line layout

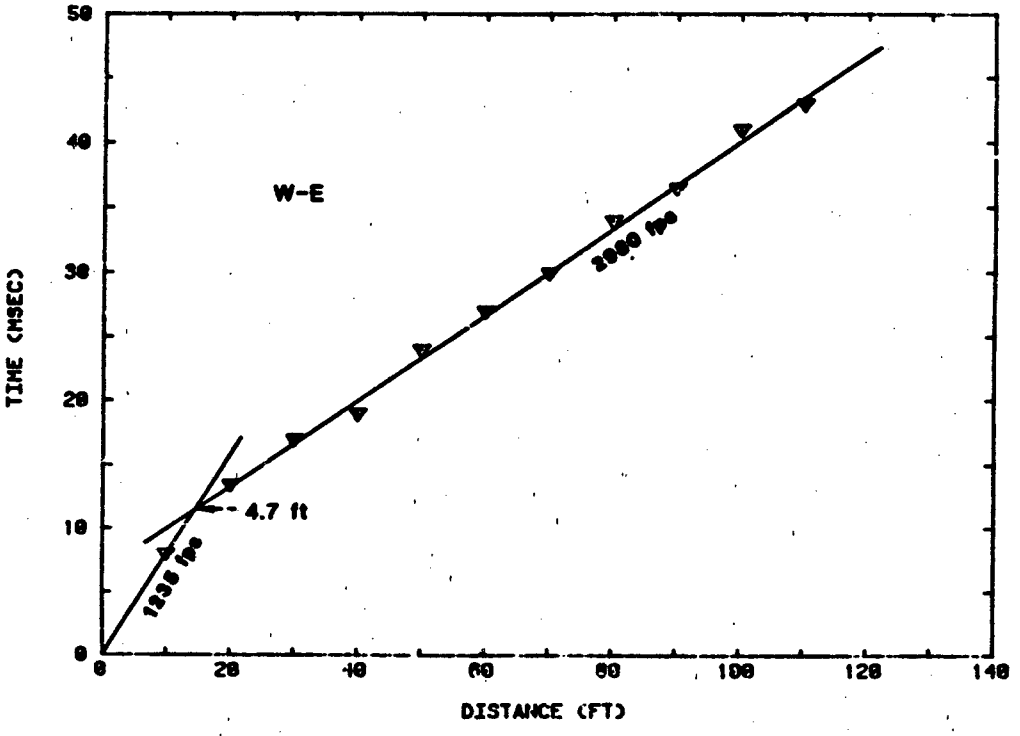

Figure B3. Main array, overburden test

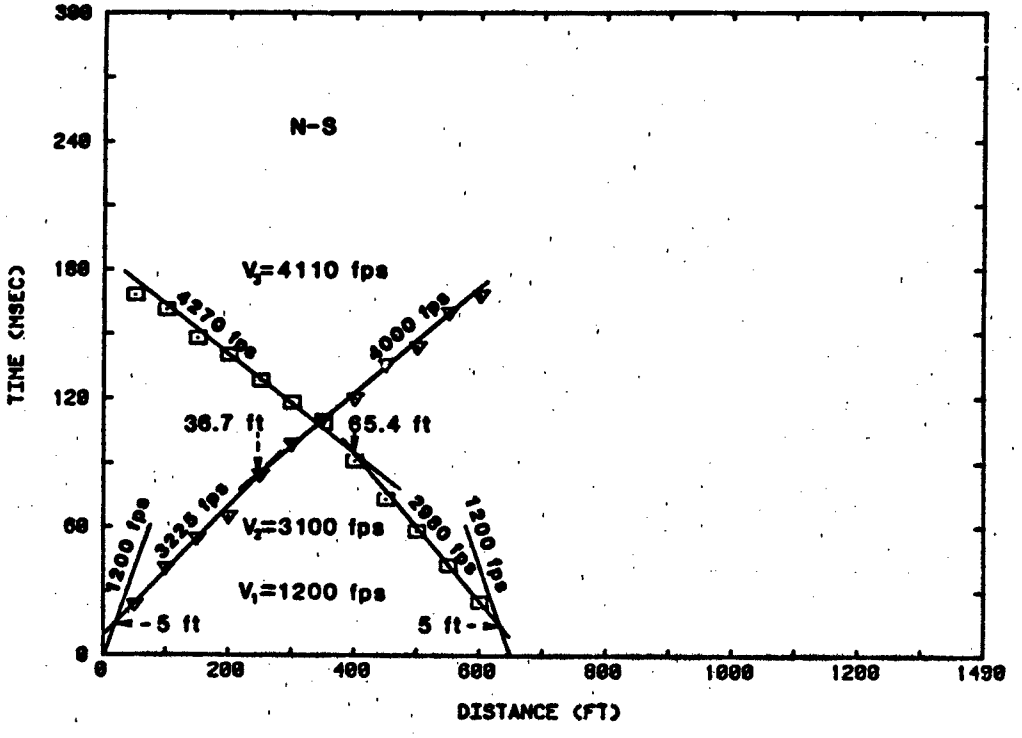

Figure B4. Main array (from previous geophysical survey)

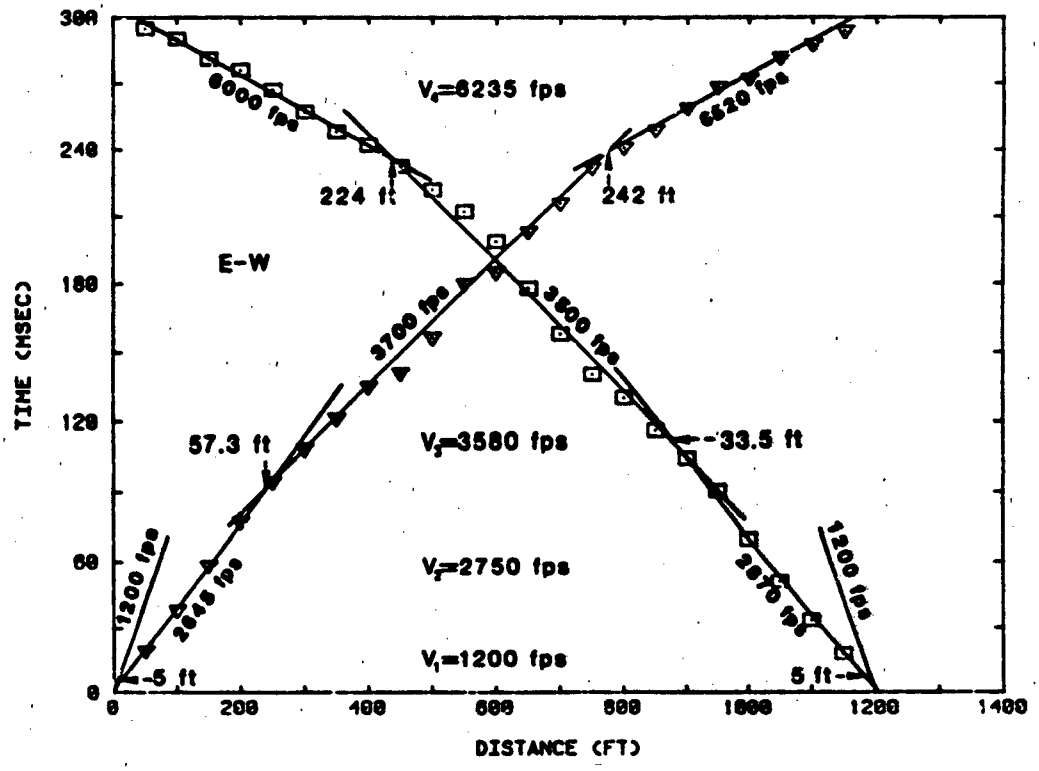

Figure B5. Main array

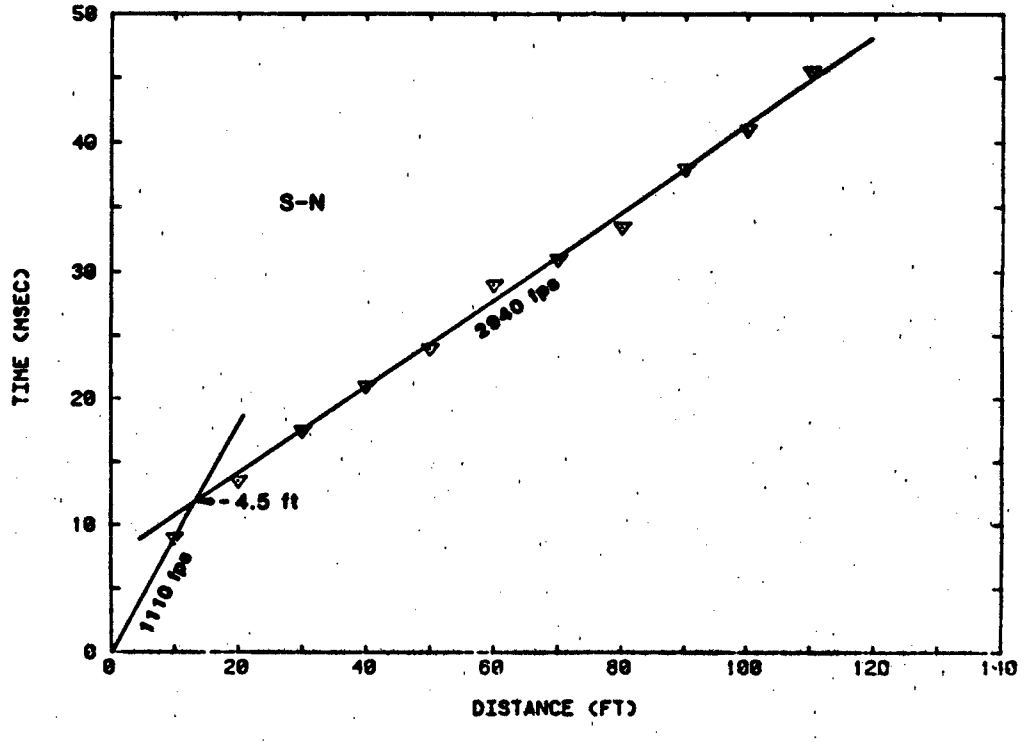

Figure B6. 2-km position, overburden test

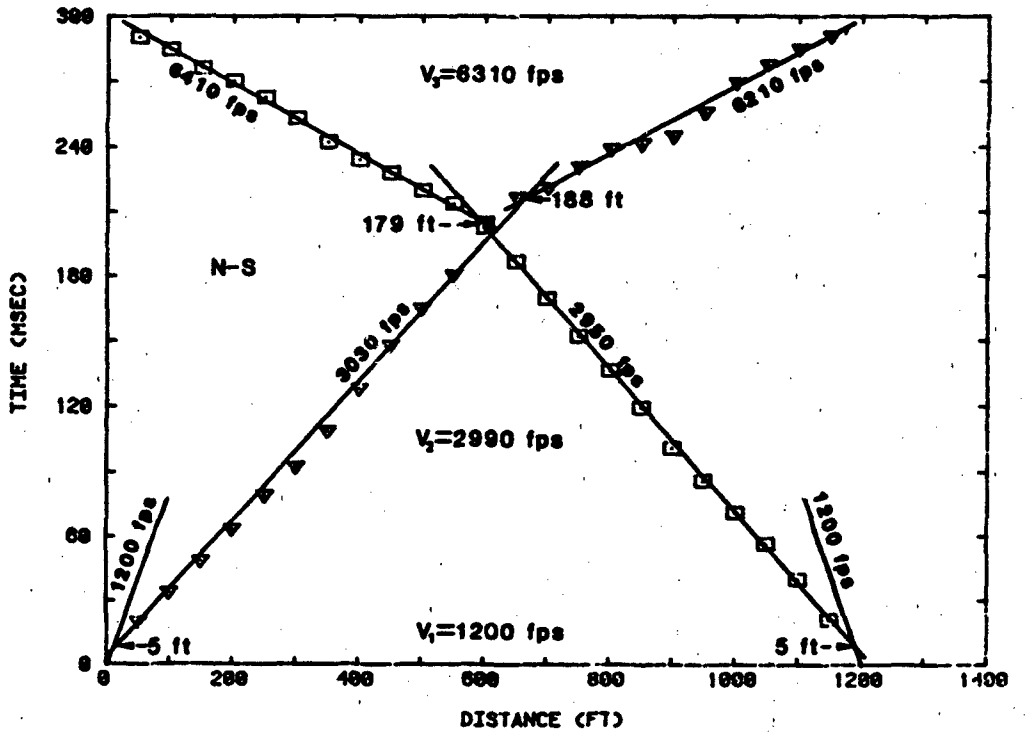

Figure B7. 4-km position, N - S

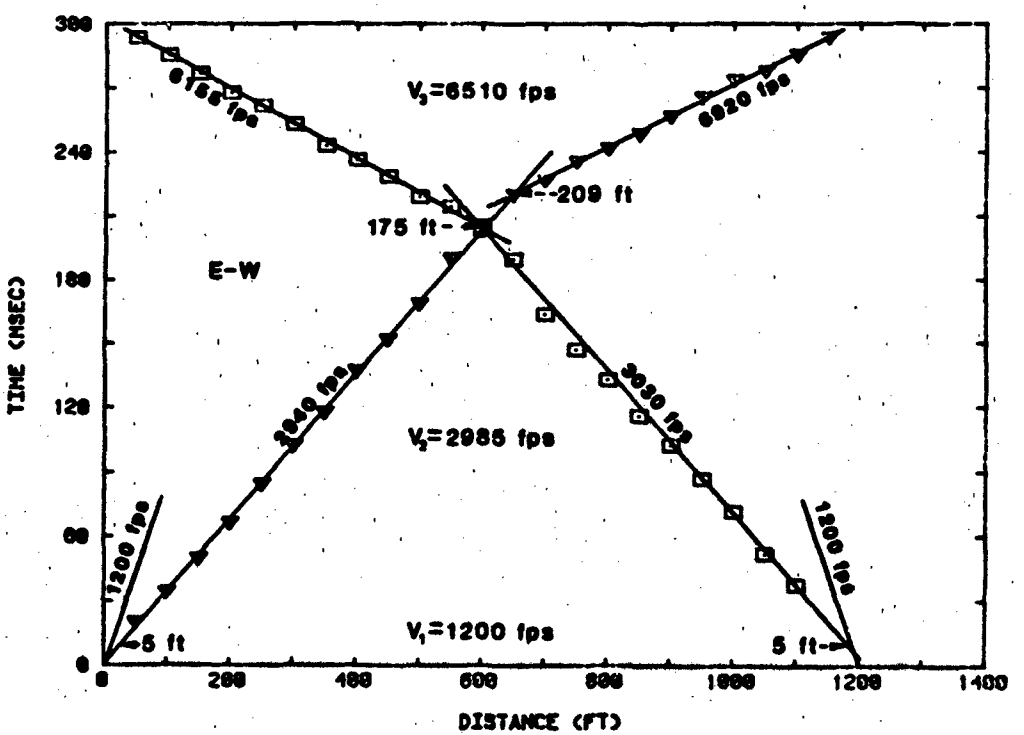

Figure B8. 4-km position, E - W

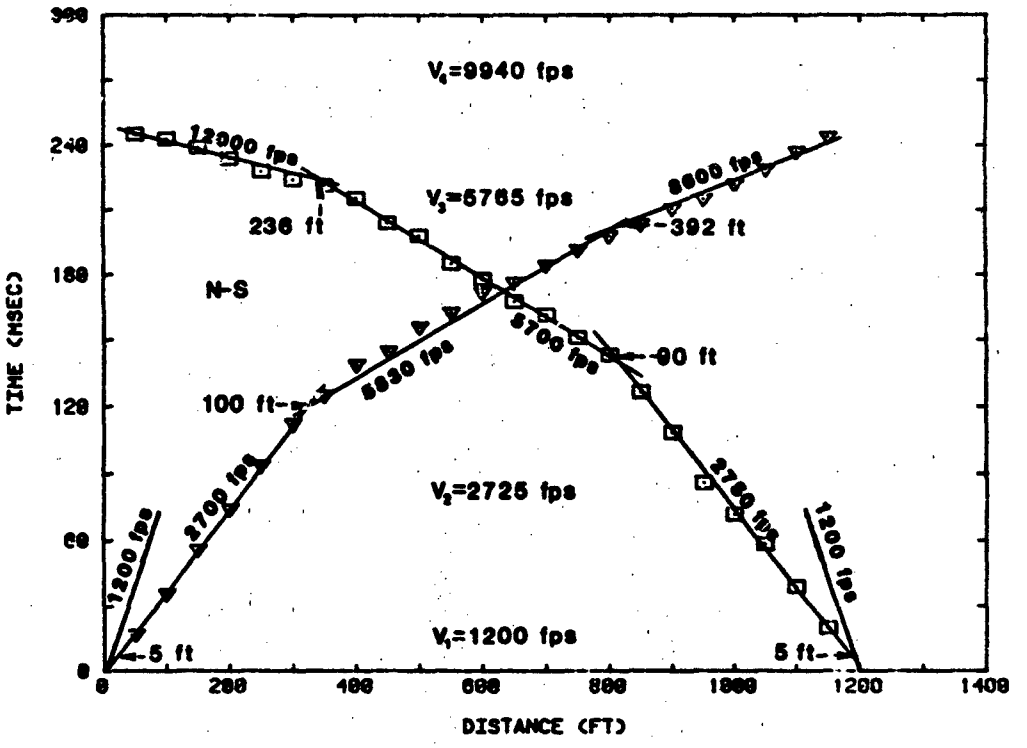

Figure B9. 10-km position, N - S

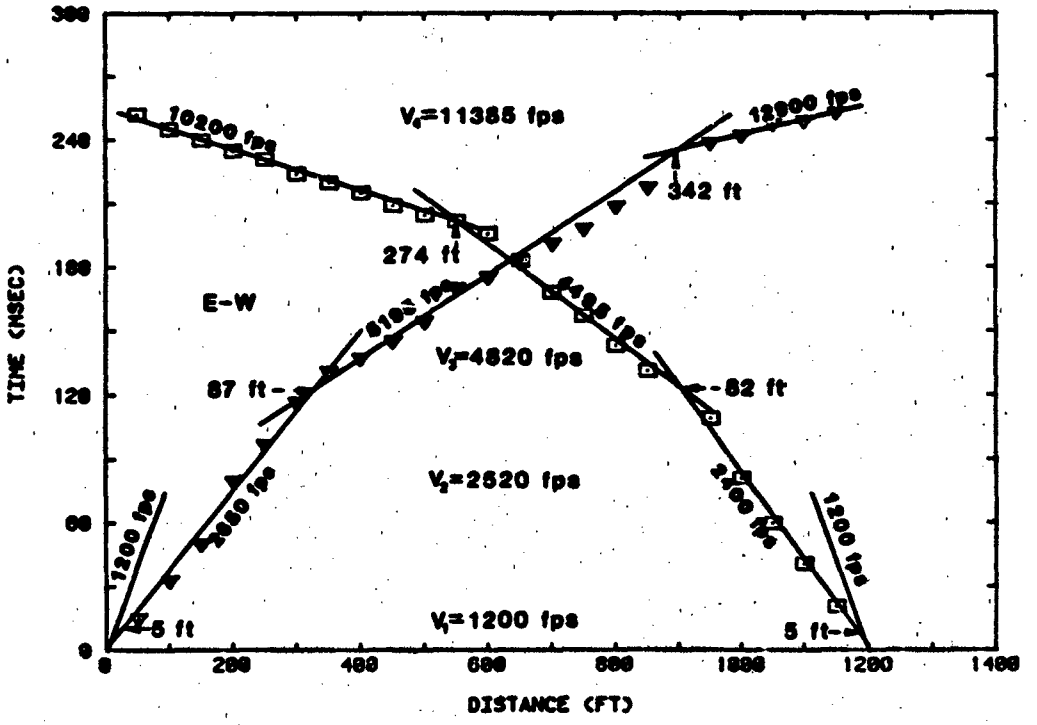

Figure B10. 10-km position, E - W

7. The P-wave velocities so calculated represent apparent rather than true velocities. To determine true velocity when dipping strata are encountered, it is necessary to shoot forward and reverse seismic profiles so that the dip and true velocity of the layers can be calculated. The true layer velocity is determined from the expression

$$V_T = \frac{2V_Y V_D}{V_u + V_d}$$

where

V_T = true layer velocity

V_U = apparent P-wave velocity up-dip

V_D = apparent P-wave velocity down-dip

8. The above calculations are of a simplified nature; however, the computer program used is much more sophisticated since it considers all the variables postulated by Snell's law of refraction, i.e., critical angle of incidence, velocity contrast, layer dip, etc. A more detailed description of these matters is available from the literature (Herland 1963; Headquarters, Department of the Army 1979); further discussion would be inappropriate for this study.

9. Also shown, in Figures B11-B16, are P-wave velocity profiles developed from the refraction seismic results presented. These plots depict the layer dips calculated by the computer program as well as the computed true velocity of each layer.

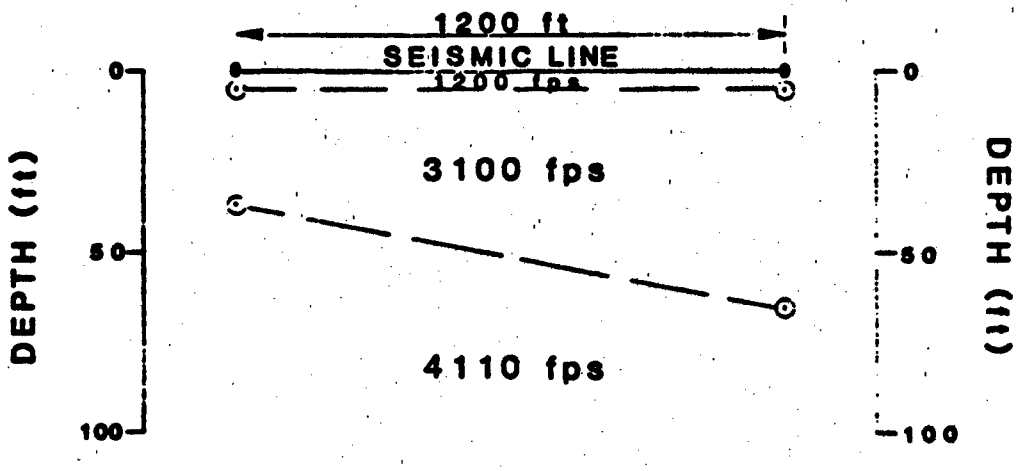

Figure B11. Main array (N - S)

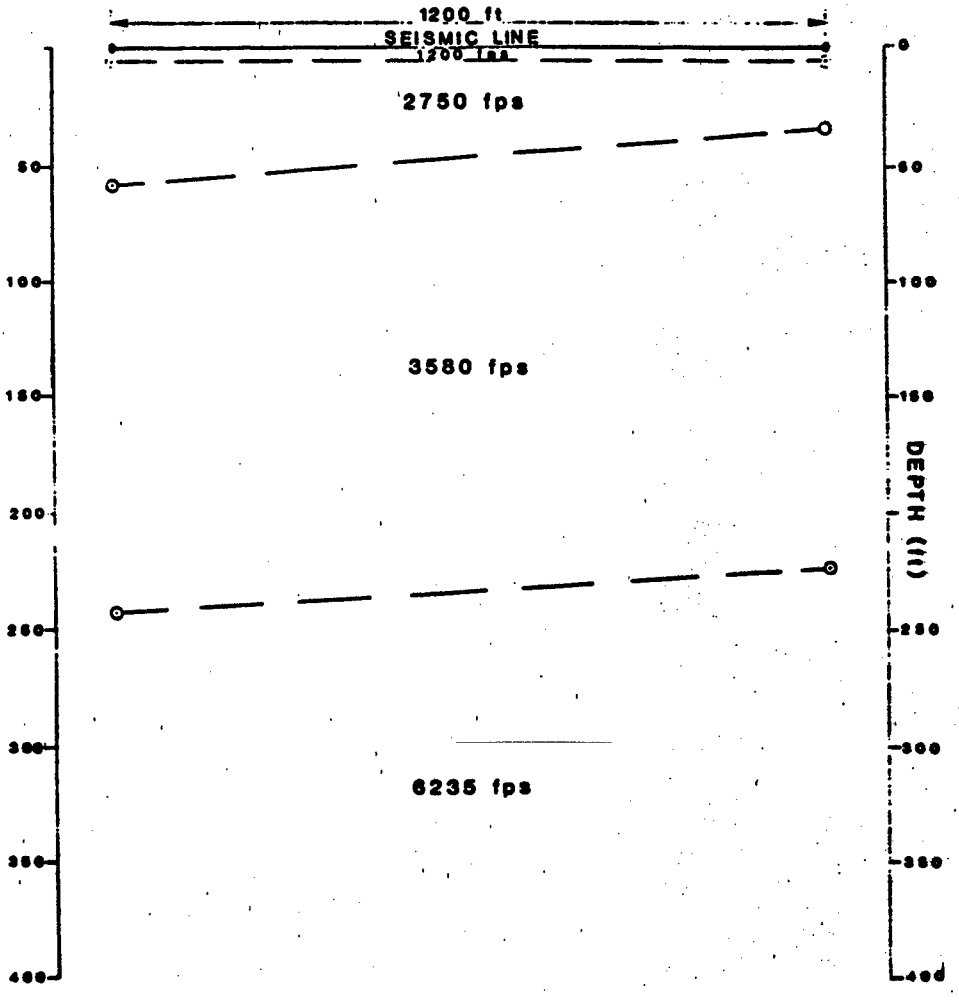

Figure B12. Main array (E - W)

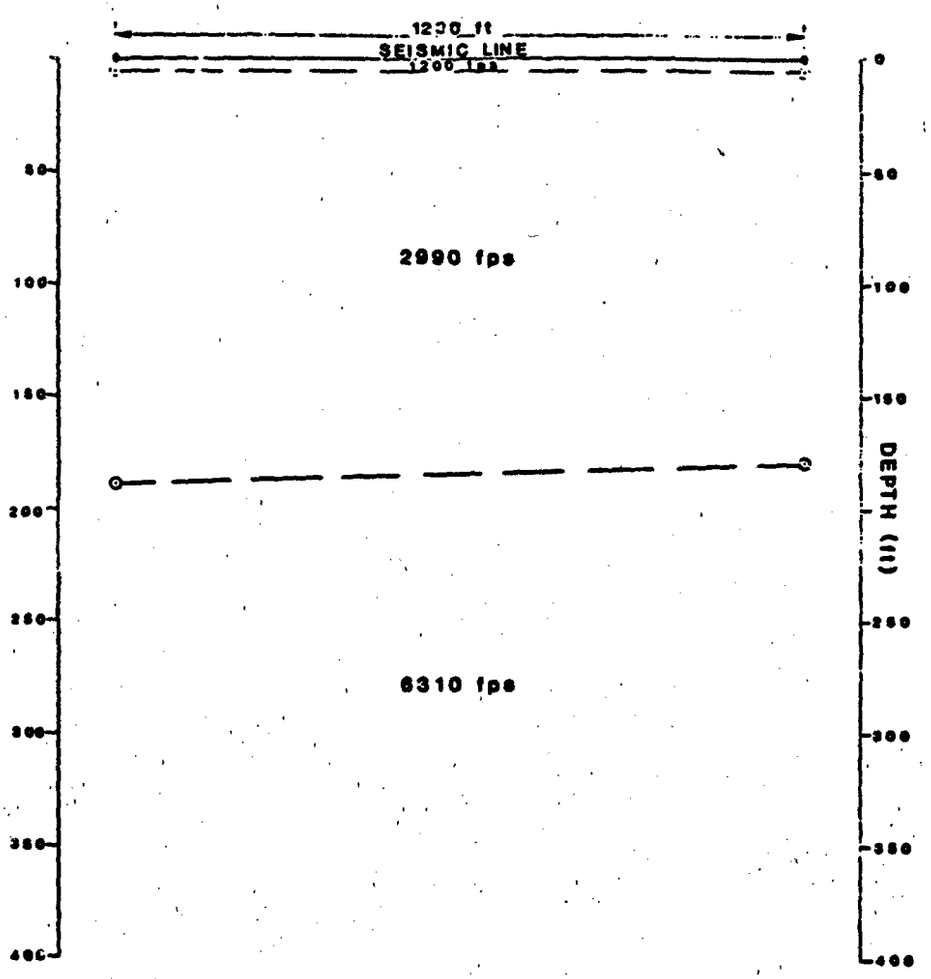

Figure B13. 4-km position (N - S)

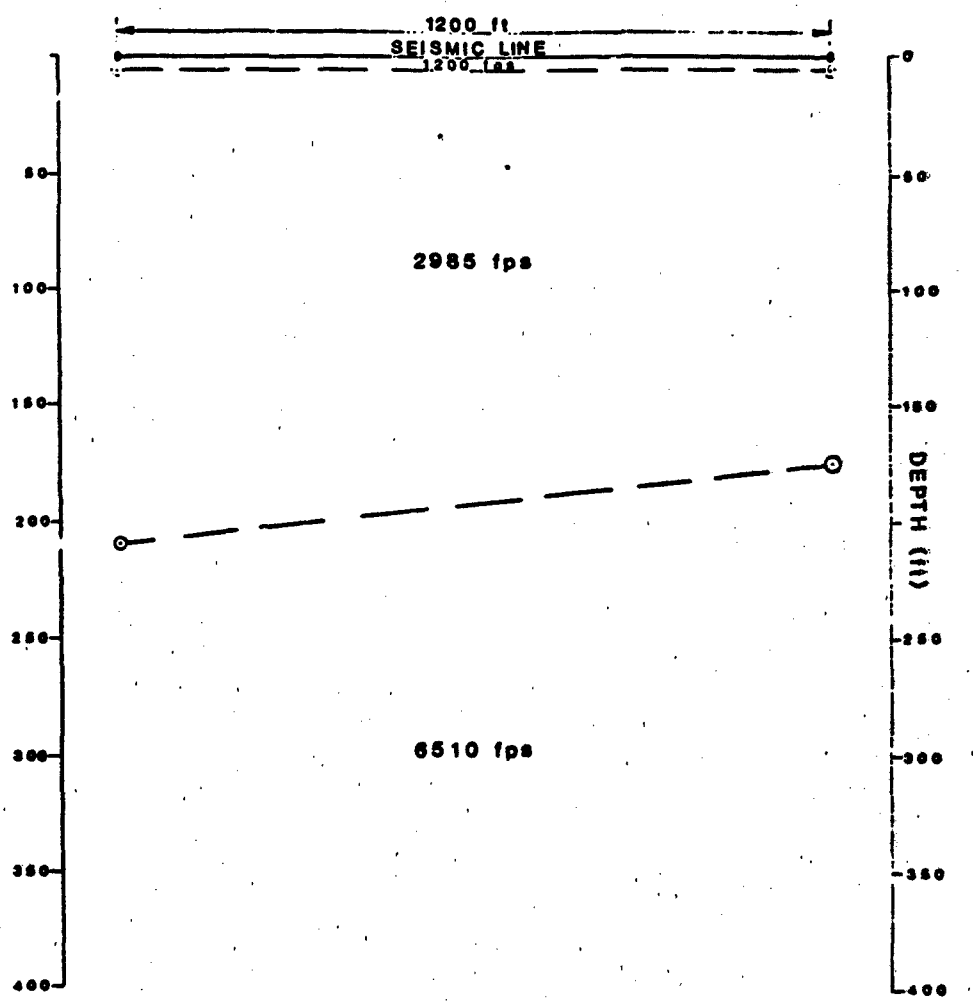

Figure B14. 4-km position (E - W)

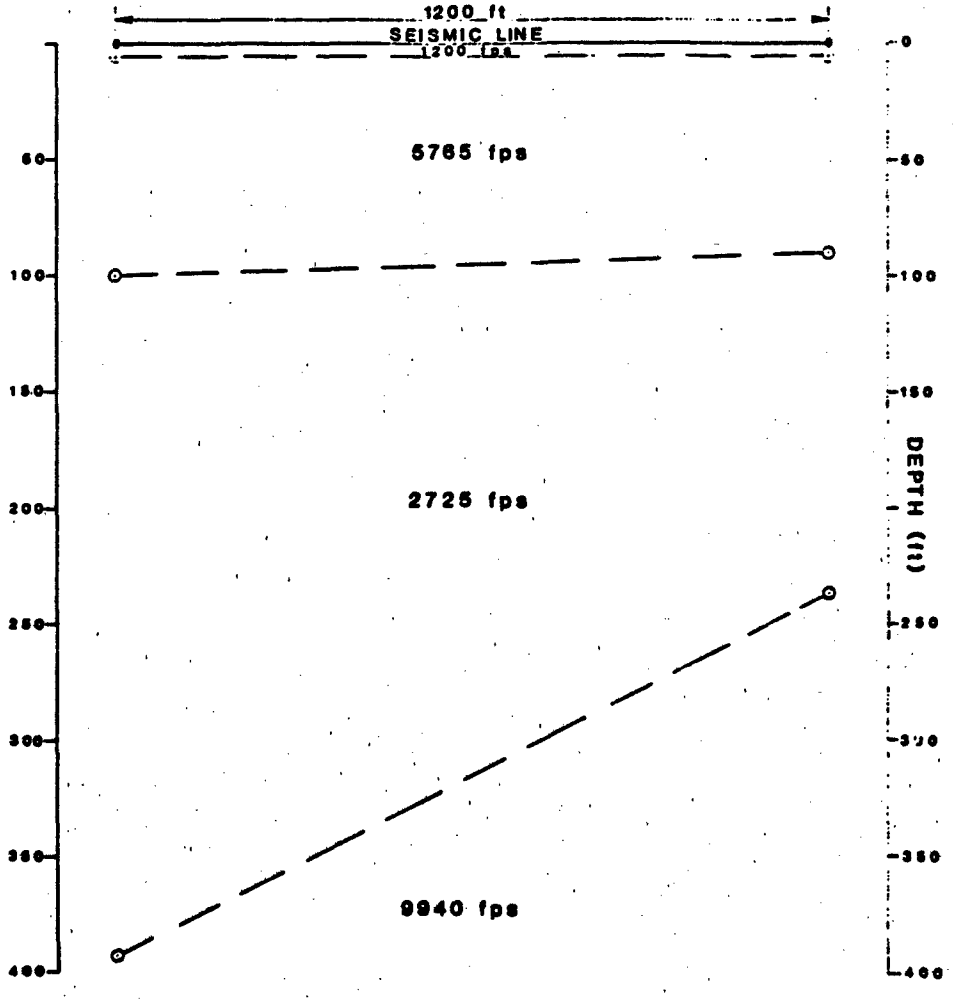

Figure B15. 10-km position (N - S)

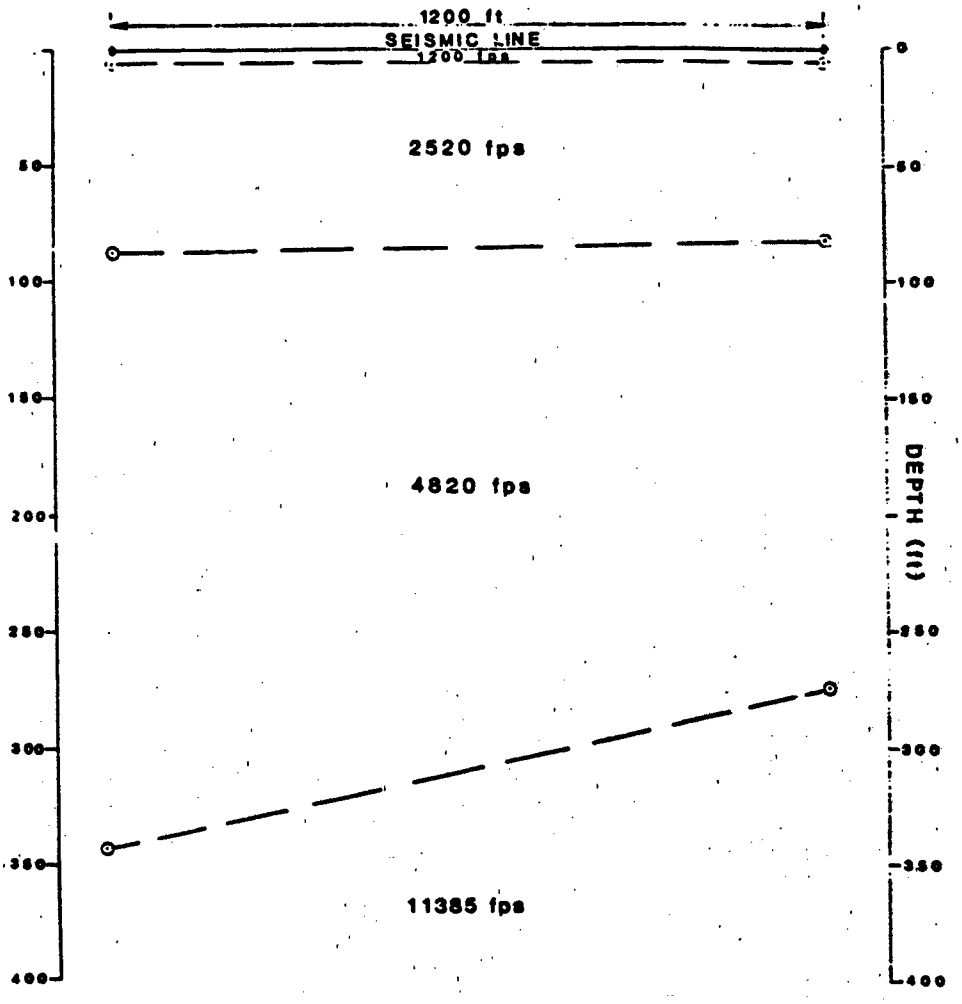

Figure B16. 10-km position (E - W)

Special Explosive Tests

10. In one phase of this study, it was necessary to detonate explosives at ranges of 0.62 mile (1 km), 1.24 miles (2 km), 2.48 miles (4 km), and 6.21 miles (10 km) north of the main sensor array. Ground motion data were obtained at two locations near the explosive source (at distances of 0.06 mile (100 m) and 0.18 mile (300 m) from the source), as well as at the main sensor array. These data were checked in the field and were used to develop the maximum peak-to-peak particle velocity attenuation versus range plot shown in Figure B17. From this plot it is seen that the attenuation versus range characteristics were reasonably uniform in character and that no severe aberrations in ground motion response were observed over the length of the test line. Of course, much more sophisticated computer analyses of these data are now being performed.

Summary of the Refraction Seismic/Site Characterization Results

11. As a preliminary assessment of desired versus actual modeling of site seismic characteristics, one can consider the composite P-wave velocity versus depth plot shown in Figure B18. This plot shows the desired seismic profile and the average depth and true seismic P-wave velocities computed from the field data obtained in this study. The match between desired and actual P-wave velocity profiles is considered to be reasonably good for purposes of this investigation.

12. Another summary of conditions along the test line is shown in Figure B19, where average layer depth and computed true P-wave velocity are shown with respect to position along the test line. Considerable license was taken in preparing this plot since continuous refraction seismic coverage could not be accomplished, for reasons discussed earlier. Water tables were estimated from available data (U. S. Department of the Interior 1965). The plot shown is considered to be in good agreement with desired site conditions since the velocity variations recorded to about 180 ft in depth are relatively subtle, and local variations in P-wave velocity should not have a significant influence on shear or Rayleigh waves that typically propagate at much lower frequency and much longer wavelengths over distances greater than 0.6 mile (1 km).

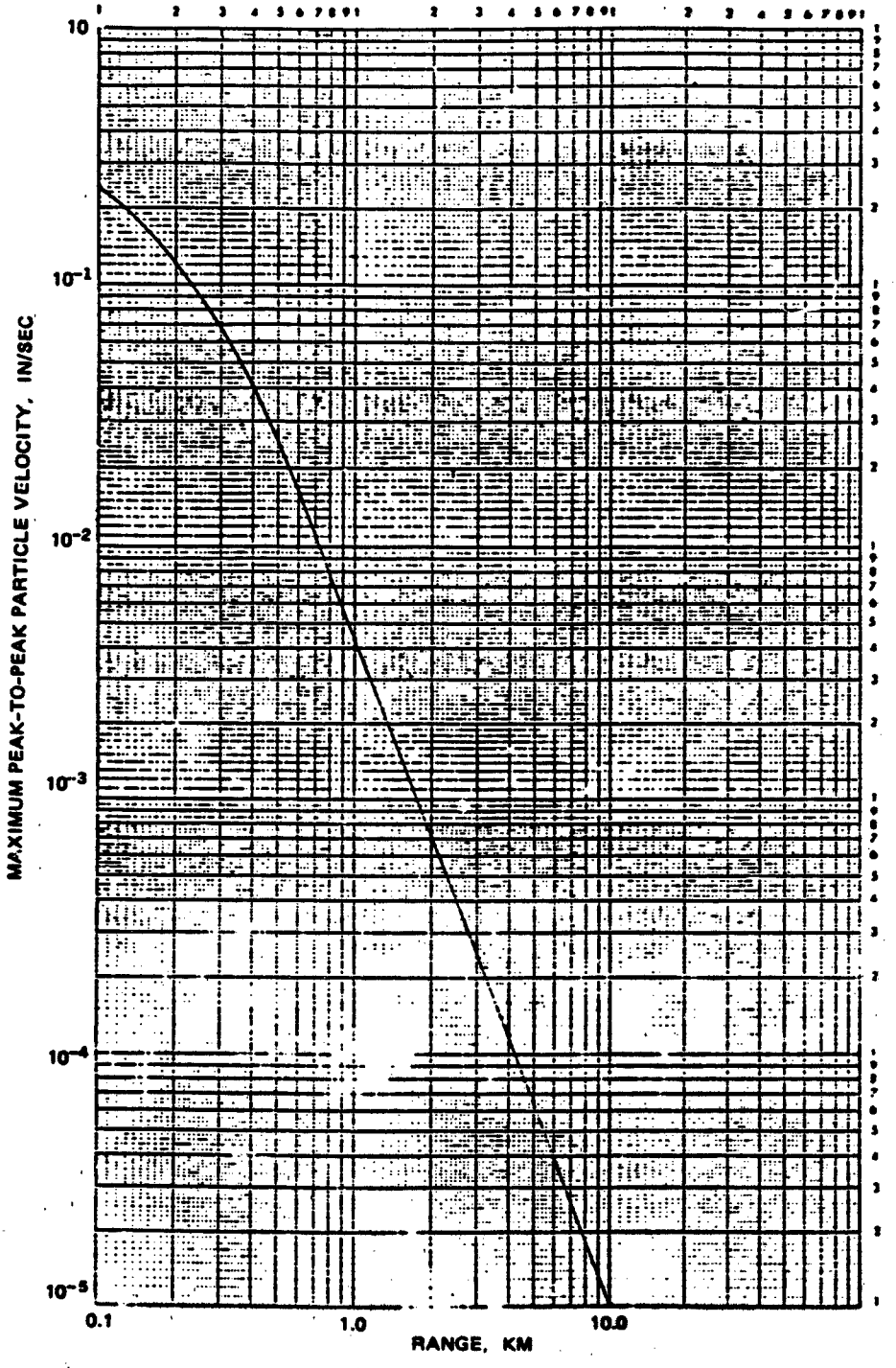

Figure B17. Maximum peak-to-peak particle velocity attenuation versus range

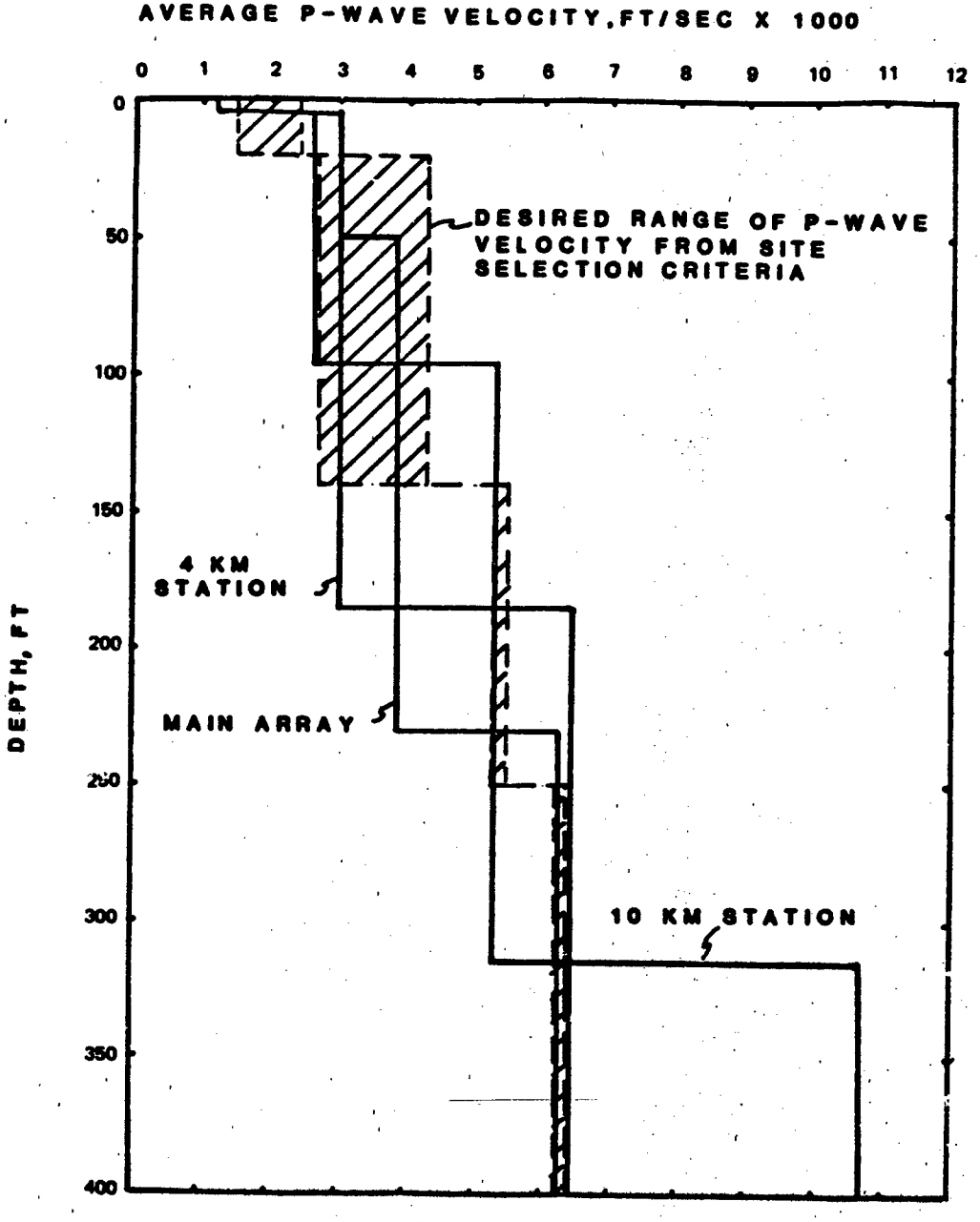

Figure B18. Composite P-wave velocity versus depth

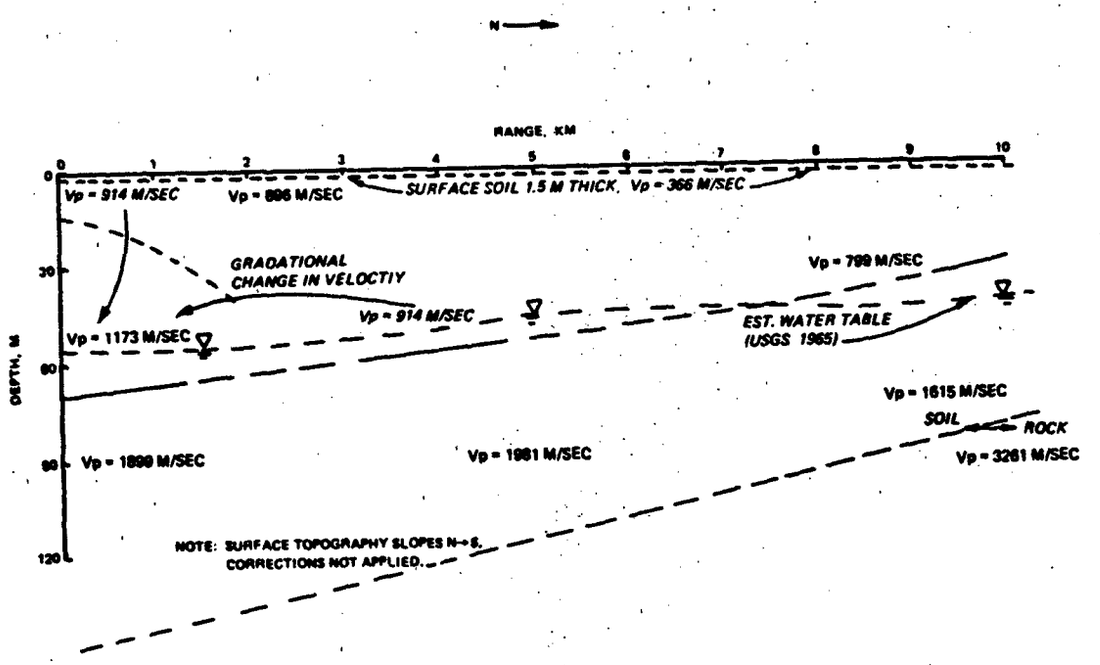

Figure B19. Seismic profile of test site

13. Finally, the fact that no major variations were observed in the plot of maximum peak-to-peak particle velocity attenuation versus range, shown in Figure B17, is evidence that subsurface conditions are reasonably consistent over the 6.21-mile (10-km) test line. Had this not been the case, these stations would have anomalous ground motion responses due to major subsurface discontinuities or features. It is concluded that the site chosen conforms reasonably well with the selection criteria and otherwise meets the objectives of the study. It is also concluded that the results obtained should be applicable to other alluvial valley sites having similar site conditions.